

ADVERTIMENT. L'accés als continguts d'aquesta tesi queda condicionat a l'acceptació de les condicions d'ús establertes per la següent llicència Creative Commons:  <https://creativecommons.org/licenses/?lang=ca>

ADVERTENCIA. El acceso a los contenidos de esta tesis queda condicionado a la aceptación de las condiciones de uso establecidas por la siguiente licencia Creative Commons:  <https://creativecommons.org/licenses/?lang=es>

WARNING. The access to the contents of this doctoral thesis it is limited to the acceptance of the use conditions set by the following Creative Commons license:  <https://creativecommons.org/licenses/?lang=en>

THE ROLE AND MODULATION OF PERINEURONAL NETS IN THE HEALTHY AND INJURED SPINAL CORD

Presented by
Judith Sánchez Ventura

ACADEMIC DISSERTATION

To obtain the degree of PhD in Neuroscience by the Universitat
Autònoma de Barcelona

March 2023

Thesis supervisor
Dr. Esther Udina Bonet

Academic Tutor
Dr. Xavier Navarro

Group of Neuroplasticity and Regeneration,
Institut de Neurociències

This study was funded by:

- The *Secretaria d'universitats i recerca* from *La Generalitat de Catalunya* by means of a predoctoral FI-DGR grant to Judith Sánchez Ventura, co-funded by the European Social Funds.
- The *Fundació La Marató-TV3* through the TV3-201736-30-31 grant “Modulation of perineuronal nets by physical exercise after spinal cord injury in animal models: Plasticity versus stability of the neuronal circuits” to Dr. Esther Udina.

Als meus pares.

INDEX

I. Summary.....	9
II. Articles produced in this thesis	13
III. Abbreviations.....	17
IV. Introduction.....	21
1. <i>Spinal cord</i>	23
1.1. Spinal cord organization and morphology	23
1.2. Spinal connectivity	29
1.3. Plasticity and stability processes in the spinal cord.....	34
2. <i>Perineuronal nets</i>	35
2.1. Composition and structure	35
2.2. Distribution.....	37
2.3. Development: PNN formation.....	39
2.4. Mature nervous system: PNN function and modulation.....	41
2.5. Insults in the central nervous system	43
3. <i>Spinal cord injury</i>	44
3.1. Classification.....	44
3.2. Pathophysiology.....	44
3.3. Plasticity events below the level of the injury. Experimental studies.....	46
3.4. Therapeutical approaches.....	49
V. Hypothesis and objectives.....	55
VI. Study design and methodologies.....	59
VII. Results.....	71
<i>Chapter I</i>	73
<i>Chapter II</i>	113
<i>Chapter III</i>	145
<i>Chapter IV</i>	171
<i>Annex</i>	193
VIII. General discussion.....	213
IX. Conclusions	223
X. References.....	227

I. Summary

Despite Camilo Golgi described perineuronal nets (PNNs) in the 19th century, the interest in this structure was tempered until a few years ago. Initially, its discovery was controversially discussed and finally dismissed by Ramón y Cajal, who argued that PNNs were an artefact of Golgi's preparation. Consequently, PNN research was ceased until histological techniques improved and enabled researchers to visualize, again, PNNs. These advances help to understand PNNs composition, but it was not until the 21st century that the role of PNNs in plasticity-stability regulation was reported. Afterwards, the interest in PNNs exponentially increased and, in 20 years, PNNs have been linked to many other functions in the healthy and diseased brain. Nevertheless, PNNs located in the spinal cord are quite unknown, and many questions are still unanswered.

Thus, the present doctoral thesis pretends to understand the role of spinal PNNs not only in normal conditions but also after spinal cord injury (SCI) and their implication in functional recovery. We hypothesize that the proper functioning of the spinal cord strongly depends on the stability of spinal circuits and therefore, PNNs' preservation is crucial. Indeed, we believe that alterations of spinal PNNs after a SCI can mediate some of the maladaptive plasticity observed after injury. Thus, reverting those PNN's changes through activity-dependent therapies, maladaptive plasticity might be shaped into functional recovery. Hence, we first deciphered the role of spinal PNNs in motor function characterizing transgenic mice with aberrant PNNs (*Crtll* KO mice). We observed that aberrant PNNs disrupted excitatory synapses and changed the physiological properties of motoneurons, overall increasing the excitability of spinal circuits and leading to motor impairment. Then, we wanted to know whether spinal PNNs were affected after a spinal cord injury, evaluating PNNs around disconnected cervical and lumbar spinal circuits. Interestingly, while PNNs around phrenic motoneurons increased their thickness after the injury, PNNs around lumbar motoneurons reduced it. These differences could be caused by the different plastic mechanisms initiated after injury in each circuit. In the thoracic SCI study, lumbar PNNs' reduction was accompanied by hyperalgesia and hyperreflexia. An intense activity-dependent rehabilitation not only compensated PNNs' reduction but also promoted better functional recovery. The correlation between PNN alterations and maladaptive plasticity was eventually explained as a cause-effect relationship. After applying a thoracic SCI to WT and *Crtll* KO mice, we observed that the hyperalgesia and hyperreflexia found in WT-injured mice were already present at basal levels in transgenic mice. This finding suggested that altered PNNs are enough to mimic the functional outcomes observed after SCI in WT mice.

Collectively, the results of this thesis enhance the current knowledge of PNNs. This new data could facilitate the development of more targeted strategies to treat SCI and other neurological disorders, where both protection of synaptic integrity and controlled plasticity are needed.

II. *Articles produced in this thesis*

Research papers

- Sánchez-Ventura J, Giménez-Llort L, Penas C, Udina E (2021). Voluntary wheel running preserves lumbar perineuronal nets, enhances motor functions and prevents hyperreflexia after spinal cord injury. *Exp Neurol.* 336:113533.
- Sánchez-Ventura J, Canal C, Hidalgo J, Penas C, Navarro X, Torres-Espin A, Fouad K, Udina E (2022). Aberrant perineuronal nets alter spinal circuits, impair motor function, and increase plasticity. *Exp Neurol.* 358:114220.

Review

- Sánchez-Ventura J, Lane MA, Udina E (2022). The role and modulation of spinal perineuronal nets in the healthy and injured spinal cord. *Front. Cell. Neurosci.* 16.
 - Part of the introduction and discussion is extracted from this review.

Peer reviewed publication

- Sánchez-Ventura J, Lago N, Penas C, Navarro X, Udina E. Link protein 1 is involved in the activity-dependent modulation of perineuronal nets in the spinal cord.

In preparation

- Sánchez-Ventura J, Schardien KA, Fortina TA, Zholudeva LV, Lane MA, Udina E. Perineuronal net changes reveal a distinct right and left spinal phrenic circuit.
- Sánchez-Ventura J, Badia C, Herrando-Grabulosa M, Udina E. Do spinal perineuronal nets participate in motoneuron degeneration?

III. Abbreviations

- 5-HT: 5-hidroxytryptamine; serotonin
- ADAMTs: A disintegrin and metalloproteinase with thrombospondin motifs
- BDA: biotinylated dextran amine
- BMS: basso mouse scale
- BSA: bovine serum albumin
- BPI: brachial plexus injury
- ChABC: chondroitinase ABC
- ChAT: choline acetyltransferase
- CrtlI: cartilage link protein I
- CMAP: compound muscle action potential
- CNS: central nervous system
- CSPGs: chondroitin sulfate proteoglycans
- CST: corticospinal tract
- DI: discrimination index
- DPI: days post-injury
- EE: enriched environment
- ECM: extracellular matrix
- GAG: glycosaminoglycan
- GFAP: glial fibrillary acidic protein
- Hx: hemi-section
- IB4: isolectin IB4 biotin
- Iba1: ionized calcium binding adaptor molecule 1
- Ip: intraperitoneal
- KCC2: potassium-chloride transporter
- KO: knock-out
- LFB: luxol fast blue
- MEP: motor evoked potential
- MN: motoneuron
- MMP: matrix metalloproteinase
- MU: motor unit
- NORT: novel object recognition test.
- Neo: neomycin
- ON: overnight
- PB: phosphate buffer
- PBST: phosphate buffer saline Triton
- PFA: paraformaldehyde
- PhMN: phrenic motoneuron
- Propul: propulsion
- PRV: pseudorabies virus
- PNN: perineuronal net
- RDD: rate-dependent depression
- ROI: region of interest
- RMS: root mean square
- RT: room temperature
- SCI: spinal cord injury
- SED: sedentary
- SEM: standard error of the mean
- Sema3A: semaphorin 3A
- SMUA: single motor unit action potential
- TB: True Blue Chloride
- TR: forced treadmill running
- VGlut1: vesicular glutamate transporter 1
- VGAT: vesicular GABA transporter
- WR: voluntary wheel running
- WT: wild type

IV. Introduction

1. Spinal cord

The nervous system is divided into two main parts: the central and the peripheral nervous system. The central nervous system (CNS) is made up of the brain and the spinal cord, whereas the peripheral nervous system is composed of nerves that branch off from the spinal cord and extend to all parts of the body.

As the major link between the brain and the body, the **spinal cord** transmits motor, sensory and autonomic information bidirectionally. On the one hand, the spinal cord relays signals from the brain and brainstem to activate the muscles. On the other hand, it also receives sensory information from the body and sends it to upper centers for processing.

Additionally, the spinal cord can independently respond to sensory inputs and coordinate its own networks to produce motor reflex responses (Watson and Kayalioglu, 2009).

1.1. Spinal cord organization and morphology

The human spinal cord extends from the medulla oblongata to the lower back (lumbar 1-2 vertebrae), where it terminates as the conus medullaris. It is protected by the vertebral column and enclosed by three membranes called meninges: the dura mater, the arachnoid mater, and the pia mater (Murray, 2014).

From a transversal view, the spinal cord shows two distinct parts (Figure 1): a butterfly-shaped **gray matter** in the center, surrounded by **white matter** on either side. Moreover, from each side of the spinal cord, a **spinal nerve** comes out to innervate specific areas of the body (Watson and Kayalioglu, 2009; Silva et al., 2014).

1.1.1. Spinal nerves

From each side of the spinal cord, two pairs of nerve roots extend from each segment of the spinal cord (Figure 1). Ventral roots contain efferent fibers from motoneurons (MNs) that carry motor information from the CNS to the periphery. Dorsal roots contain afferent fibers from sensory neurons that transmit sensory information from the periphery to the CNS. Along each dorsal root, cell bodies of sensory neurons are clustered in a structure called the dorsal root ganglion (DRG) (Silva et al., 2014).

Shortly after leaving the cord, the dorsal and ventral roots from each side eventually combine forming the spinal nerve. Thus, spinal nerves are mixed since they

contain both sensory and motor information from and to the periphery, respectively. The spinal nerve's nomenclature depends on the spinal segment from which they exit: cervical (C1-C8), thoracic (T1-T12), lumbar (L1-L5), sacral (S1-S5) and coccygeal (Co1) (Watson and Kayalioglu, 2009; Silva et al., 2014).

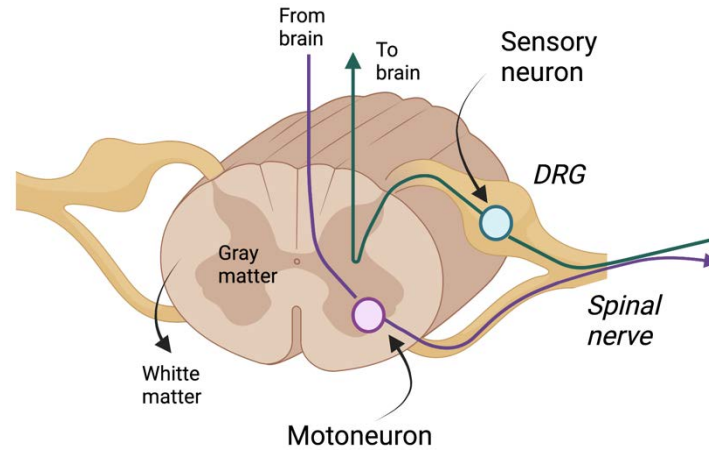


Figure 1. A transversal section of a spinal cord segment. On the left side of the spinal cord, it is represented the gray and the white matter. On the right side, it is shown how sensory neurons (located in the DRG) convey sensory information from the periphery to the CNS, whereas motoneurons (located in the ventral horn) integrate motor information from upper centers to elicit a muscle contraction. DRG: dorsal root ganglia. Individual images obtained from Biorender.

1.1.2. Gray matter

The gray matter contains the cell bodies of interneurons, MNs and glial cells. Macroscopically, is divided into dorsal and ventral parts (Figure 2). The dorsal region or **dorsal horn** is the sensory portion of gray matter, where pain, temperature and proprioception nuclei are located. The ventral arms are called the **ventral horns** and are considered the motor portion where somatic MNs are found. Between both horns, there is a region called the intermediate gray matter (Watson and Kayalioglu, 2009; Murray, 2014; Silva et al., 2014). Microscopically, the gray matter can be divided into ten layers of cells called the Laminae of Rexed (Figure 2). Each lamina is composed of different types of neurons according to their structure and function (Rexed, 1954).

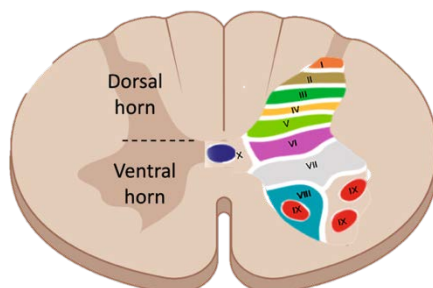


Figure 2. A transversal view of a spinal cord segment. On the left side of the spinal cord, the different parts of the gray matter are represented: the dorsal and the ventral horn. On the right side, the different Laminae of Rexed are shown. Individual images were obtained from Biorender.

1.1.2.1. Spinal interneurons

Spinal interneurons, as the name suggests, connect sensory neurons with MNs. In the spinal cord, they are widely distributed along all the gray matter. They can be excitatory or inhibitory, which confers them a vast range of properties and functions (Zholudeva et al., 2021). Spinal interneurons can be divided into two different types: propriospinal neurons, with ascending and descending projections; and local interneurons with ipsilateral projections or projections that cross the midline of the spinal cord (commissural) (Lane, 2011; Zholudeva et al., 2018).

1.1.2.2. Spinal motoneurons

Despite spinal MNs can be divided into visceral and somatic MNs, this doctoral thesis is focused on somatic ones. **Somatic MNs** are cholinergic neurons located in the ventral horn, specifically in the IX lamina, that project their axons to skeletal muscles (Watson and Kayalioglu, 2009). They can be divided into α or γ -MNs (Figure 3). They differ in the morphology and connections established outside and within the spinal cord. Morphologically, α -MNs are the most abundant type and have a larger cell body and a thicker axon, which produces a faster conduction velocity, compared to γ -MNs. α -MNs innervate force-generating extrafusal muscle fibers, leading to muscle contraction. In contrast, changes in the activity of γ -MNs do not modify the total length of the muscle. Instead, they innervate intrafusal fibers or muscle spindles, which are sensory receptors that detect muscle length. Considering the type of input, α -MNs received c-boutons and Ia-derived proprioceptive sensory inputs, while γ -MNs do not (Witts et al., 2014).

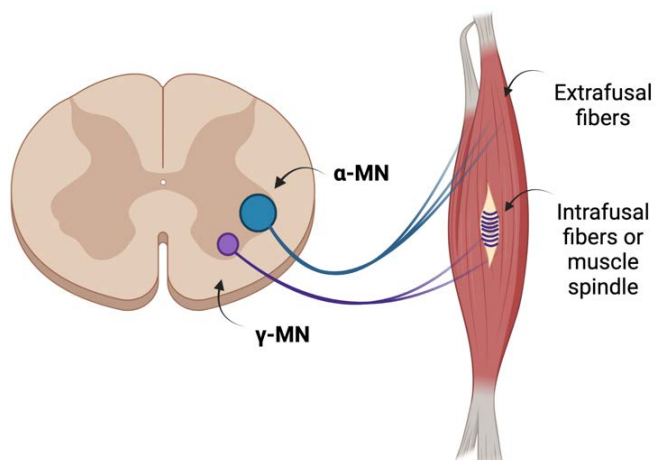


Figure 3. Schematic overview of the different somatic MNs and their muscle innervation. While α -MNs innervate extrafusal fibers of the muscle, γ -MNs innervate intrafusal fibers or muscle spindles. MN: motoneuron. Individual images were obtained from Biorender.

α -MNs can be further divided into three subtypes depending on the extrafusal fiber type they innervate: slow fatigue-resistant MNs (SFR), fast fatigable-resistant MNs (FFR) and fast fatigable MNs (FF) (Burke et al., 1973). Specifically, they differ in size,

excitability and firing pattern. SFR MNs have a smaller cell body and consequently fewer ion channels on the membrane. This confers a high input resistance which means that small amount of synaptic current will be enough to reach the firing threshold. Thus, SFR MNs are recruited first during muscle contraction. Besides, they are more resistant to fatigue than FF MNs. FF MNs have a larger cell body and are recruited after SFR, giving extra strength to the activated muscle. Considering conduction velocity, MNs innervating fast fibers are faster than SFN (Burke et al., 1973). Lastly, FFR physiology is quite unknown. It is believed that presents intermediate properties between SFN and FF MNs (Stifani, 2014).

1.1.3. White matter

The white matter includes axonal projections and their associated glial cells. These axons longitudinally run through the cord and are organized into specific groups depending on their origin, termination and information transmitted, forming the so-called **spinal tracts** (Murray, 2014). Based on the direction of the information carried, tracts can be divided into ascending or descending. While ascending tracts arise from sensory neurons from the DRG and transmit sensory information up, descending tracts usually relay motor information from the cortex and subcortical structure down. However, there are also sensorial descending pathways, such as those involved in pain modulation (Watson and Kayalioglu, 2009).

1.1.3.1. Ascending tracts

Ascending tracts can transmit two types of afferent information: exteroceptive and proprioceptive. Exteroceptive information comes from the environment, external to the body and includes nociception, temperature, and touch. In contrast, proprioceptive information comes from the inside of the body, informing from the state of muscles and joints (Watson, 2012).

All ascending pathways are made up, at least, of three different types of neurons: the **first-order** neuron (the soma lays in the DRG and projects sensory information from the periphery to the dorsal horn of the spinal cord), the **second-order** neuron (the intermediate relay) and the **third-order** neuron (the cell body lays in subcortical areas and sends its axons to the cerebellar or cerebral cortex) (Wolfe et al., 2006).

There are 3 types of ascending pathways (Table 1, Figure 4):

- **Spinocerebellar.** It transmits unconscious proprioceptive signals from the muscle and joints. The receptors that process this information are the muscle spindles and Golgi tendon organs found in the muscles.
- **Spinothalamic.** It processes touch, pressure, pain, and temperature. The receptors that process this information are usually non-specialized or free nerve endings, such as low threshold mechanoreceptors (gross touch), nociceptors (pain), and thermoreceptors (temperature).
- **Dorsal column-medial lemniscal (DCML).** It transports information about vibration, fine touch and proprioception. The receptors that process touch and vibration are mechanoreceptors in the skin, whereas proprioception is processed by muscle spindles and Golgi tendon organs. Axons of 1st order neurons ascend through the homolateral dorsal column and relay in the gracilis or cuneatus nuclei, depending on whether the information comes below or above T6-T8, respectively). This determines the division of the tract in fasciculus gracilis (FG) and cuneatus (FC). (Wolfe et al., 2006).

Table 1. Anatomical location of neurons in the ascending pathways

	1 st order	2 nd order	3 rd order	Destination
Spinocerebellar	DRG	Ipsilateral dorsal horn	Cerebellar peduncle	Cerebellum
Spinothalamic	DRG	Contralateral dorsal horn	Thalamus	Primary sensory cortex
Dorsal column-medial lemniscal	DRG	Medulla oblongata	Thalamus	Primary sensory cortex
		FG: gracilis nuclei		
		FC: cuneate nuclei		

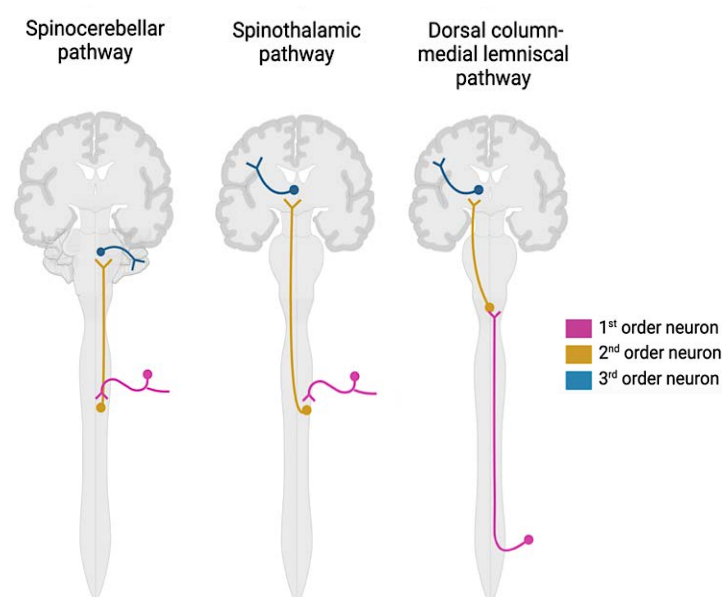


Figure 4. Schematic representation of ascending tracts. Individual images obtained from Biorender.

1.1.3.2. Descending tracts

Most of the descending tracts transmit motor orders that are generated in the brain or the brainstem to α -MNs (Figure 5). The motor tracts are classically defined as a two-neuron system: an **upper** MN found in the brain or brainstem and a **lower** MN found in the ventral horn of the spinal cord (or exceptionally in the brain stem for cranial nerves) (Table 2). The upper MN sends its axon to the spinal cord to synapse with the lower MN (Watson and Kayalioglu, 2009). However, it is currently accepted that upper MNs usually relay the information to lower MN through spinal interneurons, at least at the lumbar level (Witts et al., 2014). Finally, the lower motoneuron innervates the skeletal muscle.

There are two general descending systems, the lateral and the medial system.

- The lateral descending system contains the **corticospinal** and **rubrospinal** tracts, being the corticospinal one the main descending system for the control of voluntary movements.
- The medial descending system contains the **vestibulospinal** and **reticulospinal** tracts. They mediate balance and posture.

Table 2. Anatomical location of neurons in the descending pathways

	Upper MN	Lower MN
Corticospinal tract	Primary, secondary motor cortex	α and γ spinal MNs
Rubrospinal tract	Red nucleus (midbrain)	
Vestibulospinal tract	Vestibular nuclei (medulla)	
Reticulospinal tract	Reticular formation (pons and medulla)	

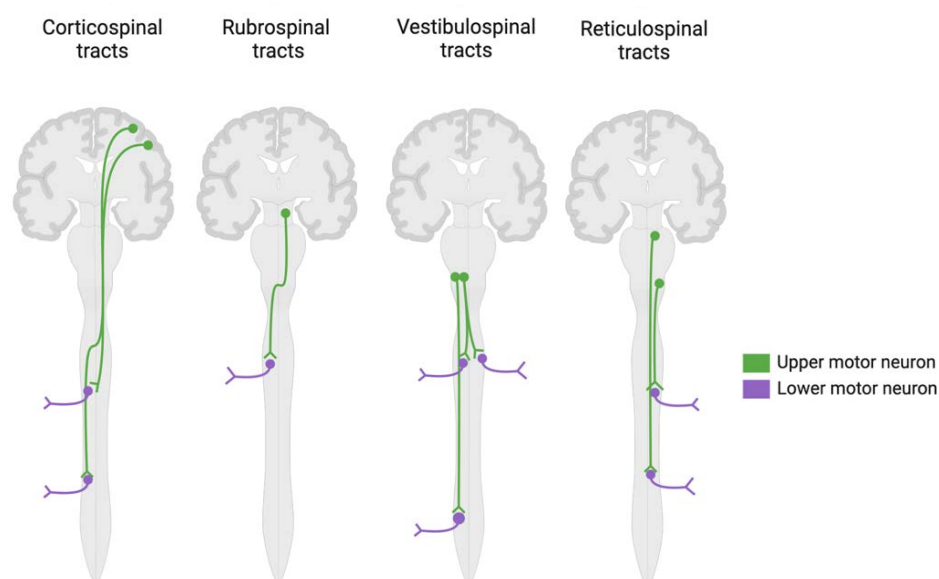


Figure 5. Schematic representation of descending tracts. Individual images obtained from Biorender.

There are other descending pathways that are not involved in motor control but rather modulate pain perception. These descending modulatory pathways are originated in higher centers such as the periaqueductal gray (PAG) and the rostral ventromedial medulla (RVM), among others. These higher areas control pain perception by either inhibiting or facilitating the transmission of nociceptive inputs at the level of the dorsal horn. These modulatory effects are mainly mediated by monoaminergic pathways including serotonin, norepinephrine or dopamine (Kwon et al., 2014).

1.2. Spinal connectivity

The spinal cord is generally considered a highway of communication through the well-characterized spinal tracts. However, the spinal cord is capable of much more than only supplying signals to and from the brain. Indeed, it has autonomous circuits that can work independently. These circuits are implicated in the generation of motor behaviors that range from vital breathing movements to limb muscle contraction for locomotion. These networks, known as **central pattern generators (CPGs)**, are composed of excitatory and inhibitory interneurons that generate rhythmic and patterned motor outputs (Grillner, 2006). Nevertheless, this basic motor response needs to be modulated considering the changing environment. Thus, close communication between the CPGs and other neural structure (the cortex, the brainstem, the cerebellum, and the spinal cord) are required for producing meaningful movements (Jordan and Sławińska, 2014).

In this thesis, the motor behaviors studied are respiration and locomotion. Both movements are rhythmic, unconscious, and generated by a specific CPG located in the brainstem or spinal cord, respectively. Both rhythmic motor patterns are constantly modulated by internal and external sensory information provided by sensorimotor inputs. Of particular interest for this thesis is the sensory input these CPGs receive from the spinal cord. While the sensory modulation of the respiratory circuitry is mainly provided by individual spinal interneurons, the locomotor one is mainly regulated by spinal reflexes.

1.2.1. Respiratory circuit

Breathing is a three-phase rhythmic movement – inspiration, post-inspiration, and expiration – orchestrated by neurons found in the brainstem. Specifically, it is controlled by the respiratory center, a group of 4 nuclei distributed along the pons and

the medulla: the apneustic and pneumotaxic centers are found in the pons, whereas the dorsal and ventral respiratory groups (DRG and VRG, respectively) are bilaterally located in the medulla. The VRG nuclei can be further subdivided into 4 subnuclei, being the Bötzing and the pre-Bötzing complex the most relevant ones. Indeed, the interaction between the pre-Bötzing and Bötzing complexes generates the **principal respiratory rhythm**: excitatory neurons from the pre-Bötzing complex produce the spontaneous and rhythmic pattern of respiration, whereas the inhibitory neurons from the Bötzing complex switch from inspiration to expiration (Ghali, 2018). These structures establish the rhythmogenesis required for normal motor pattern generation. Nevertheless, this respiratory pattern is not static and can be adjusted to the internal and external milieu (chemical, mechanical and emotional afferences). Thus, the rest of the structures of the respiratory center as well as spinal interneurons are involved in the final respiratory response produced by MNs. In the present thesis, we are going to focus on the modulation performed by spinal interneurons.

After the modulation provided by higher structures, the DRG and VRG send a monosynaptic and ipsilateral excitatory (during inspiration) or inhibitory (during expiration) drive to spinal MNs. These MNs are found throughout the cervical, thoracic, and lumbar spinal cord to innervate the diaphragm, the intercostal and abdominal muscles respectively (Ellenberger and Feldman, 1988; Lane, 2011). Specifically, phrenic motoneurons (PhMN) located between C3-C6 innervate the diaphragm. Remarkably, these ipsilateral bulbospinal inputs are not the only inputs PhMNs receive (Cregg et al., 2017). Firstly, different works have revealed that some of these bulbospinal descending axons decussate at the brainstem and spinal cord to innervate contralateral PhMNs (Boulenguez et al., 2007; Lane et al., 2009). Secondly, direct cortical inputs from the corticospinal tract (CST) can modulate the voluntary control of breathing (Gandevia SC and Rothwell JC, 1987). Finally, spinal interneurons located in cervical, thoracic and lumbar segments seem to participate in breathing too. The cervical ones are pre-phrenic interneurons located in C1-C2 and C3-C6 (near the phrenic nucleus). Several studies have shown that they can integrate the phrenic network on each side of the spinal cord and with other respiratory networks, for instance, coordinating phrenic and intercostal motor output. Besides, propriospinal interneurons can also modulate PhMN excitability sending excitatory and inhibitory inputs and thus, shaping the pattern of respiratory motor output (Lane et al., 2009; Lane, 2011; Zholudeva et al., 2018). This is because afferents rarely project directly to PhMN, instead, project to interneurons from the dorsal

or intermediate laminae. The afferents that spinal interneurons receive include group Ia (muscle spindles that sense stretch) Ib (Golgi tendon organs, that sense tension) and group III and IV (that sense fatigue). Compared to the limb or intercostal muscles, the diaphragm has a very low proportion of muscle spindles, suggesting that Ia fibers rarely contribute to PhMN excitability (Corda et al., 1965; Jammes et al., 2000).

Overall, breathing is possible due to the contraction and relaxation of the diaphragm and other respiratory muscles produced by the synaptic integration of the respiratory center and spinal interneurons.

1.2.2. Locomotor circuit

Locomotion is a rhythmic movement that requires the coordination of a group of extensor and flexor muscles. This coordination is possible due to the dynamic interaction between MNs, the CPG and feedback mechanisms (Côté et al., 2018). The locomotor CPG is located at the lumbar level and generates the rhythmic locomotor pattern that would activate MNs. Although this motor pattern is generated independently from descending and afferent inputs, they are critical in adapting the operation of the CPG in the real environment, performing rapid postural and movement corrections (Rossignol et al., 2006; Jordan and Sławińska, 2014). Finally, MNs integrate all the information and transform it into a precise and coordinated activation of muscles. The feedback mechanisms are exposed below:

Descending tracts. There are excitatory and inhibitory descending tracts that can modulate the locomotor response. On the one hand, excitatory tracts activate the spinal locomotor network to initiate, stop and steer locomotion. For instance, reticulospinal and vestibulospinal pathways are relevant in initiating locomotion and postural control, respectively. Corticospinal and rubrospinal tracts are important in voluntary and goal-directed aspects of locomotion (Rossignol and Frigon, 2011). On the other hand, other descending pathways regulate the amount of pre-synaptic inhibition that Ia sensory afferents received and thus, adjust spinal circuits such as the stretch reflex (Faist et al., 1994).

Afferent inputs. Most of the afferent information that modulates the locomotor response comes from the proprioceptors located in the skeletal muscle and nociceptors found in the skin. Considering proprioceptors, they detect the length of the muscle (muscle spindles), the tension of the ligaments and tendons (Golgi tendon organs) and inform the CNS to shape the motor output (Pearson, 2004). All the sensory signals are

transmitted to the spinal cord, where they are integrated into **spinal reflexes** to eventually modulate ongoing movements.

1.2.2.1. Spinal reflexes

Spinal reflexes are one of the most studied spinal circuits due to their relevance in posture and locomotion. All spinal reflexes are formed, at least, by 4 elements: a somatic receptor, a sensory (afferent) neuron, a MN (efferent neuron) and the skeletal muscle. For more complex reflexes, an interneuron is included in the circuit. Indeed, spinal reflexes can be classified considering their complexity in **monosynaptic** and **polysynaptic** reflexes.

Monosynaptic reflexes consist of two neurons (sensory and motor) and a single synapse between them. In contrast, in polysynaptic reflexes, one or more interneurons participate, meaning that the sensory neuron and the MN establish indirect communication. These interneurons can be excitatory or inhibitory. Hence, one transmitted input to the interneuron can generate a great diversity of responses (contract or relax a muscle or group of muscles) at the same time. The typical method to evaluate spinal reflex is using electromyography recordings (EMG).

A clear example of the monosynaptic reflex is the **stretch reflex** (Figure 6A). Firstly, information related to proprioception (stretching of the muscle) is transduced in the muscle spindles (receptor) and processed by the sensory neuron located in the DRG. This sensory neuron projects its axon (Ia sensory group) to the spinal cord, through the dorsal horn. The Ia afference directly synapses to the α -MN. Finally, the axon of the MN synapse with the extrafusal fibers muscle to contract it, proving monosynaptic feedback from muscle spindles in the same muscle it innervates (Ira Fox, 2003).

During contraction, the Golgi tendon organ registers this tension and becomes excited (Figure 6B). When this occurs, another spinal reflex becomes active, specifically a disynaptic one called the inverse stretching reflex. After the activation of the Golgi tendon organ, its afferent fibers activate an inhibitory interneuron located in the gray matter of the spinal cord. This interneuron informs that the muscle tension is too high. Thus, it sends inhibitory inputs to the same α -MN that innervates the contracted muscle to relax it and restore the muscle length (Ira Fox, 2003).

Another example of polysynaptic reflex is the **withdrawal reflex**, produced after a painful stimulus, and mediated by nociceptors of the skin (Figure 6C). It is a complex response that requires coordination of different muscles, and thus, is mediated by

interneurons at different spinal segments. Firstly, the nociceptor becomes active and its fibers synapse with an interneuron. This interneuron activates the ipsilateral MN of the flexor muscle, and at the same time, inhibits the ipsilateral MN that innervates the extensor muscle. Besides, this same interneuron sends collaterals to the contralateral side of the spinal cord. There, it activates and inhibits the MN that innervates the contralateral extensor and flexor, respectively (Clarke and Harris, 2004).

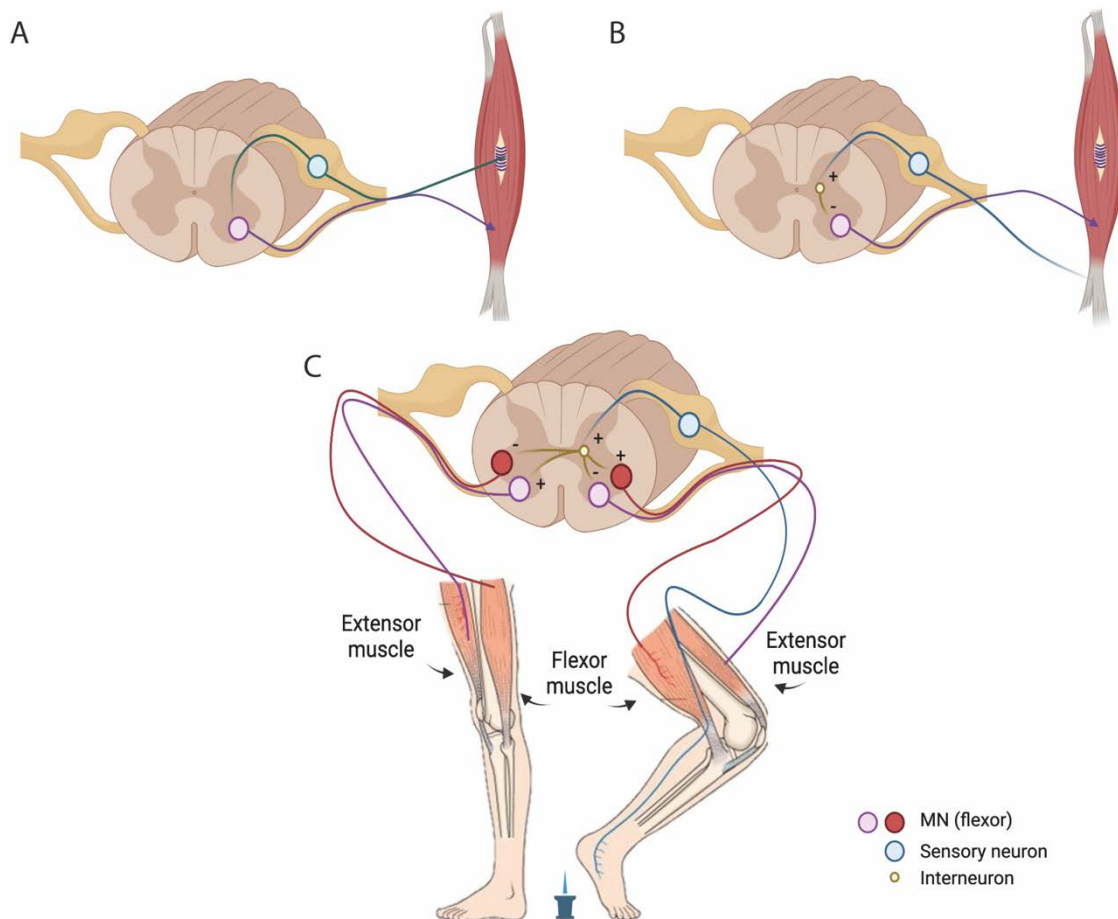


Figure 6. Schematic representation of spinal reflexes. The stretch reflex (A), inverse stretching reflex (B) and the withdrawal reflex circuits are shown. MN: motoneuron. Individual images obtained from Biorender.

This tight muscle coordination is also observed during locomotion, in which synergistic and antagonistic muscles are controlled under inhibitory and excitatory signals. Specifically, once synergistic muscles become active, the antagonistic ones must be inhibited (Côté et al., 2018). This pattern is possible due to the reciprocal inhibition also produced by interneurons (Ira Fox, 2003).

Finally, sometimes it is necessary to decrease the sensory feedback before it reaches the motoneuron. Presynaptic inhibition allows it, and it is mediated by interneurons that

are controlled by descending inhibitory tracts, that would directly synapse to Ia afferents, decreasing their input (Faist et al., 1994).

1.3. Plasticity and stability processes in the spinal cord

Rather than being a static highway of information with rigid circuitry, the spinal cord presents a degree of plasticity that varies throughout life. Indeed, its proper functioning depends on a balance between plasticity and stability processes. During development, this balance leans towards plasticity, favoring the formation of new synapses and fine-tuning spinal neuron properties. However, in the mature nervous system, the balance mainly tips towards stability despite plasticity is also needed. Thus, a balance between plasticity and stability needs to be dynamically controlled in adulthood (Takesian and Hensch, 2013). Clear examples of this plasticity-stability trade-off are the locomotor and respiratory circuits. Both spinal circuits produce stable and synchronized synapses to ensure the generation of a motor output: walking or breathing. Hence, stability is required to sustain their CPGs, generated during development, throughout life. Nevertheless, considering the environmental challenges that can perturb normal locomotion and respiration, a degree of flexibility is also needed to constantly reorganize the system to changing physiological demands and environmental stimuli, without leading to instability. This synaptic regulation is complex and not only requires the interplay of neurons and glial cells, but also the extracellular matrix (ECM), establishing the so-called tetrapartite synapse (Dityatev and Schachner, 2003; Dityatev and Rusakov, 2011). Particularly, there is a specialized and highly condensed ECM called the perineuronal net (PNN) that surrounds some neurons in the central nervous system (CNS) with a widely known role in synaptic stabilization. However, instead of being a stable scaffold, PNNs are a dynamic extracellular matrix that can rearrange their structure in an activity-dependent manner, and thus, promote plasticity or stability (Kalb and Hockfield, 1988; Dityatev et al., 2007). They have been extensively studied in the brain and associated with neuroprotection, ionic buffering, and neural maturation. However, their biological function in the spinal cord remains elusive.

2. Perineuronal nets

2.1. Composition and structure

2.1.1. Composition

PNNs are condensed ECM rich in chondroitin sulfate proteoglycans (CSPGs) that surround the soma and the proximal dendrites of some neurons in the CNS (Celio et al., 1998). PNNs are composed of hyaluronan (HA), CSPGs (aggrecan, brevican, neurocan and versican), link proteins and tenascin-R (tn-R) (Kwok et al., 2011). Their composition makes them different from the diffuse ECM, widely present throughout the CNS. Although both types of ECM contain HA, tn-R and some CSPGs, the diffuse matrix lacks link proteins.

Among all PNNs components, link proteins are crucial for their formation. *In vitro*, the lack of the *Crtll* gene, which encodes the link protein 1, prevents PNNs formation around PNN-bearing cells (Kwok et al., 2010). *In vivo*, it generates attenuated PNNs in the visual cortex (Carulli et al., 2010). Another important element in PNNs structure is aggrecan (Rowlands et al., 2018), the most abundant CSPGs. While mice deficient for other CSPGs such as neurocan (Zhou et al., 2001) or brevican (Brakebusch et al., 2002) present organized PNNs, aggrecan-deficient mice show altered PNNs (Giamanco et al., 2010). The importance of tn-R in PNNs formation is observed in the tn-R knock out (KO) mouse whose PNNs structure is affected in both development and adulthood (Weber et al., 1999; Brückner et al., 2000; Haunsoø et al., 2000).

Most PNNs components, including aggrecan, HAS and link proteins (Matthews et al., 2002) are produced by neurons, although astrocytes and oligodendrocytes also contribute to PNNs formation through synthesizing neurocan (Jones et al., 2003) and tn-R (Galtrey et al., 2008), respectively.

2.1.2. Structure

PNNs components are highly organized in a ternary stable structure (Figure 7). Firstly, PNNs are anchored to neurons by the enzyme hyaluronan synthase (HAS), which produces a hyaluronan polymer chain on the neuronal surface, constituting the backbone of PNNs. In the spinal cord, HAS 3 is expressed in PNN-enwrapped neurons (Galtrey et al., 2008). Then, HA provides a scaffold for the binding of CSPGs. CSPGs are the major

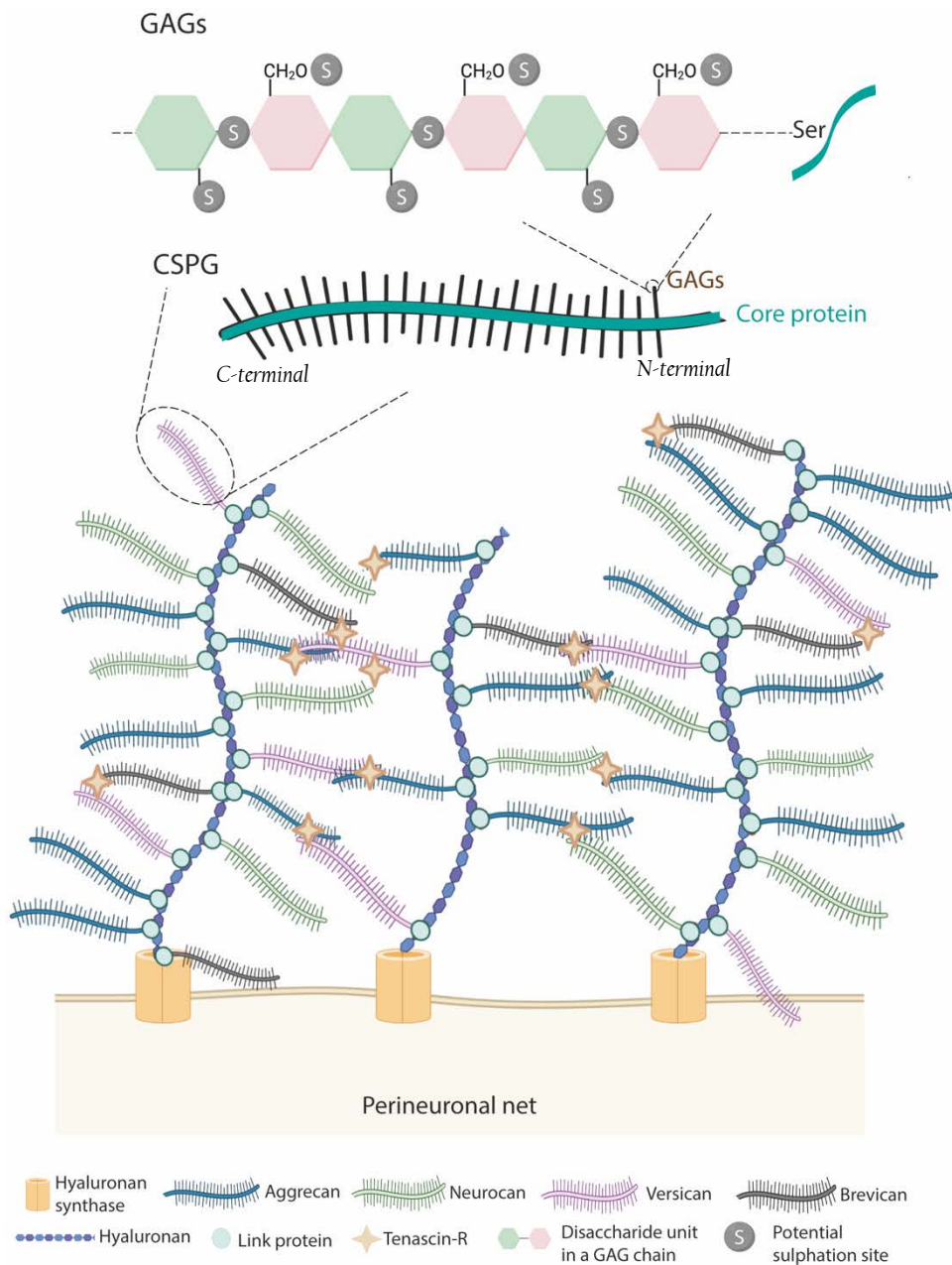


Figure 7. Structure of PNNs. PNNs are composed by hyaluronan, link proteins, CSPGs and tenascin-R. Hyaluronan, secreted by the HAS, binds to members of the lectican family of CSPGs (aggrecan, brevican, versican and neurocan) via link proteins. Then, tenascin-R further cross-links lecticans generating a lattice-like structure. CSPGs are formed by a core protein in which GAGs are covalently attached through serine residues. GAGs are composed of disaccharide units of chondroitin sulfate chains, which can be sulfated at the 2, 4 and 6th positions. CSPG: chondroitin sulfate proteoglycan, GAG: glycosaminoglycan. Individual images were obtained from Biorender.

components of PNNs representing only 2% of all the CSPGs of the nervous system (Fawcett, 2015). Among CSPGs, aggrecan is the major constituent of spinal PNNs, and the three other CSPGs (brevican, neurocan and versican) are present in PNNs in variable degrees. All types of CSPGs are composed of two parts: a core protein and a variable number of glycosaminoglycans (GAG) chains. The core proteins are a tridomain

structure formed by a N- and C-terminal globular domain, necessary for the binding of HA and tn-R, respectively and a central region (Yamaguchi, 2000). In the N-terminal, the interaction between HA and CSPGs is maintained by link proteins (HAPLN family genes). Although HAPLN1, 2 and 4 are found in the nervous system, in the spinal cord only HAPLN1/Crtll and HAPLN4/Bral2 are described in PNN-bearing neurons (Galtrey et al., 2008). Tn-R binds to the C-terminal of the CSPGs, and thanks to its trimeric structure, facilitates the cross-link between HA and CSPGs (Lundell et al., 2004). In the central region, GAGs are covalently attached to the core protein through serine residues.

Although PNNs disposition is quite preserved, slight changes in CSPGs conformation contribute to PNNs heterogeneity. Their heterogeneity arises from the type of core protein found (aggrecan, neurocan, brevican, versican) (Dauth et al., 2016) and/or the number and sulfation pattern of GAG chains (Miyata and Kitagawa, 2017). The GAGs can be sulfated at different positions including the 4th (CS-A), 6th (CS-C), 2nd-6th (CS-D) and 4th-6th (CS-E). Changes in this sulfation pattern can modify CSPGs' charge and thus, provide binding properties to PNNs, a characteristic that also differs from the diffuse ECM (Carulli et al., 2006). Interestingly, CS-A and CS-C have different characteristics: while CS-A is inhibitory to axon growth and suppresses plasticity, CS-C is permissive to axon growth and increases plasticity (Wang et al., 2009; Miyata et al., 2012). Furthermore, antibodies against different CSPGs core proteins and sulfation patterns have shown a different distribution compared to the brain and spinal cord sections (Galtrey et al., 2008). When spinal PNNs were stained with Wisteria floribunda lectin (WFA), a marker that detects the non-sulfated GAlNAc residues (Nadanaka et al., 2020), a low percentage of detection was found compared to cortical ones (Irvine and Kwok, 2018).

2.2. Distribution

PNNs have been described in various mammals, including rodents (Kalb and Hockfield, 1988; Galtrey et al., 2008), cats (Hockfield and McKay, 1983), dogs (Atoji et al., 1997), sheep (Härtig et al., 2017), primates (Mueller et al., 2016), humans (Jäger et al., 2013)) and non-mammal species such as fish (Takeda et al., 2018), birds (Balmer et al., 2009), frogs (Gaál et al., 2014) and chickens (Morawski et al., 2009)). Among all of them, spinal PNNs have been characterized in fish, rodents, cats, primates, and humans.

This mesh-like structure is irregularly distributed throughout the brain (Brückner et al., 1996) and spinal cord (Vitellaro-Zuccarello et al., 2007). In the brain,

they mainly ensheath fast-spiking GABAergic parvalbumin (PV) interneurons (*reviewed in* (Härtig et al., 1992; van 't Spijker and Kwok, 2017)). However, PNNs also surround pyramidal neurons in the hippocampus (Carstens et al., 2016), visual, somatosensory, and motor cortex (Hausen et al., 1996; Alpár et al., 2006), PV-positive and negative neurons in the striatum (Lee et al., 2012), and excitatory neurons in the amygdala and deep cerebellar nucleus (Carulli et al., 2006; Morikawa et al., 2017).

Along the spinal cord, PNNs surround MNs and spinal interneurons. Remarkably, there are differences in the proportion of PNN-enwrapped neurons throughout the spinal laminae (Figure 8). In the dorsal horn, 20% of neurons present PNNs and specifically, none in the laminae I and II (Galtrey et al., 2008). The lack of PNNs in those laminae correlates with the grade of synaptic plasticity found in that region after injury, which is related to neuropathic pain development (Woolf et al., 1992). In contrast, in laminae VII and VIII, 50% of neurons have PNNs. This proportion has been associated with spinal interneurons including both PV and calbindin-positive cells (Renshaw cells) (Vitellaro-Zuccarello et al., 2007). Finally, in contrast to the brain, PNNs located in the ventral horn surround large neural somas: spinal MNs (Vitellaro-

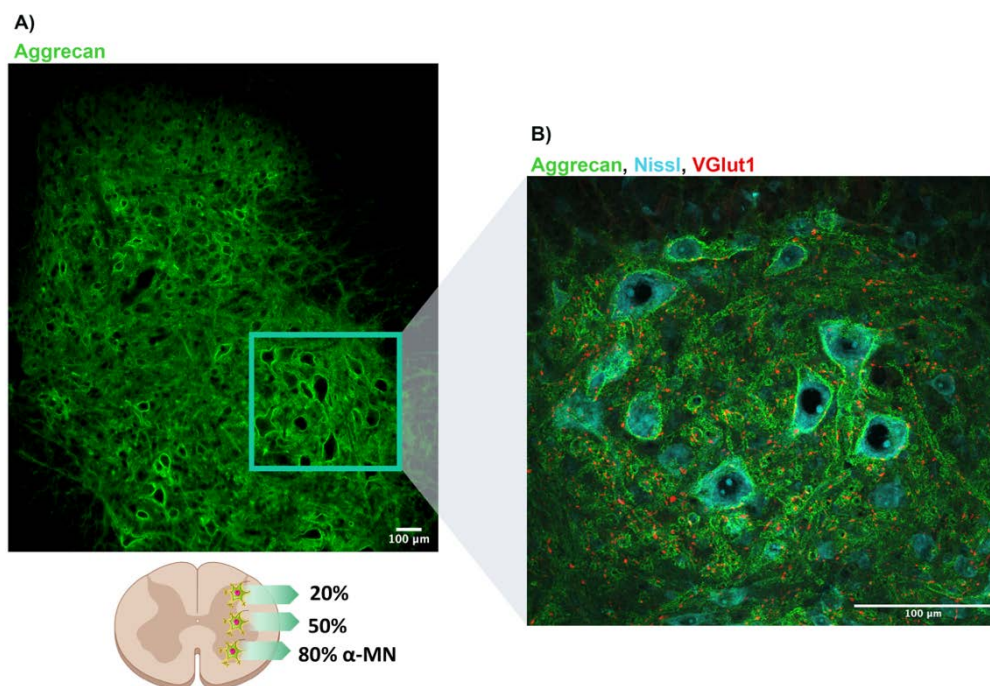


Figure 8. PNNs distribution along the dorso-ventral axis of the lumbar spinal cord. A) PNNs are labelled by aggrecan (in green) and observed along the whole lumbar spinal cord. B) Schematic representation of the distribution of PNNs in the spinal cord: 20% of neurons in the dorsal horn present PNNs, whereas 50% of neurons located in the intermediate column are wrapped by PNNs. Considering α -MN, around 80% are surrounded by PNN. C) Magnification of the region of the ventral horn where most of MNs are localized. Neurons are labelled in blue (Nissl) and proprioceptive afferents (VGlut1) that typically project to MN are labelled in red. Scale bar: 100 μ m. MN: motoneuron.

Zuccarello et al., 2007; Galtrey et al., 2008). Notably, only α -MNs present PNNs in the spinal cord, unlike γ -MNs (YD et al., 2020). Considering the percentage of α -MNs enwrapped by PNNs, it was initially thought that only 30% of α -MNs had PNNs when they were stained with WFA (Galtrey et al., 2008). Nonetheless, selectively staining for the expression of aggrecan offers a different perspective on spinal PNNs, detecting around 80% of α -MNs with dense aggrecan-positive PNNs in rat (Irvine and Kwok, 2018) and 76% in primates (Mueller et al., 2016). These results certainly reinforce the physiological relevance of spinal PNNs.

2.3. Development: PNN formation

During postnatal development, there is a window of plasticity, called the critical period, during which neural circuits are sensitive to environmental stimuli (Hubel and Wiesel, 1970; Berardi et al., 2000). These stimuli increase neuronal activity resulting in a boost of plasticity that favors synaptic wiring and fine-tunes spinal neuron properties (Kalb and Hockfield, 1994; Cameron and Núñez-Abades, 2000). During the critical period, excitatory circuits predominate over inhibitory ones, as the high Cl^- levels within immature GABAergic neurons result in depolarizing responses. This excitatory environment favors some intracellular and extracellular changes that progressively occur parallelly. On the one hand, it gradually lowers Cl^- levels inside GABAergic neurons, switching from depolarizing to hyperpolarizing actions (Ben-Ari et al., 2012). The developmental upregulation of the K^+/Cl^- cotransporter (KCC2) also contributes to this shift (Rivera et al., 1999). On the other hand, there is a progressive increase in the expression of some CSPGs that generates a diffuse structure around immature neuron (Galtrey et al., 2008). Once the CSPGs' expression reaches a peak, the link protein I is upregulated and condensed PNNs appear (Carulli et al., 2010). At the same time, there is also an increase in the sulfation CS-A/CS-C ratio of PNNs' CSPGs (Carulli et al., 2006; Miyata et al., 2012). In the spinal cord of rodents, PNNs formation occurs in the second postnatal week (Kalb and Hockfield, 1988; Galtrey et al., 2008) (Figure 9), and it is comparable among the three spinal regions, although it appears earlier in the cervical segment than in the thoracic and lumbar one (Takiguchi et al., 2021). PNNs appearance marks the end of the critical period and their digestion by the enzyme chondroitinase ABC (chABC) reopen this window of plasticity (Pizzorusso, 2002; Pizzorusso et al., 2006). Indeed, the GABAergic shift occurs at the end of the critical period too (Berardi et al., 2000; Frischknecht et al., 2009; Takesian and Hensch, 2013). A negative correlation

between PNNs intensity and intracellular Cl^- levels was reported and further confirmed after digesting PNNs and measuring increased intracellular Cl^- levels (Glykys et al., 2014).

Once PNNs are fully formed, they mold the new connections generated into a meaningful manner to prepare the circuitry for adulthood: while active neurons would be wrapped by PNNs to strengthen their connections, their absence around unused synapses would lead to their pruning (*reviewed in* (Murakami et al., 1992)). In the spinal cord, around 50% of synapses are lost during development (Ronnevi and Conradi, 1974). Interestingly, transgenic mice lacking *tn-R*, neurocan and brevican also exhibited an increase in excitatory synapses around cortical neurons (Gottschling et al., 2019). Therefore, an adequate synaptic balance in mature neurons depends on the presence of proper PNNs.

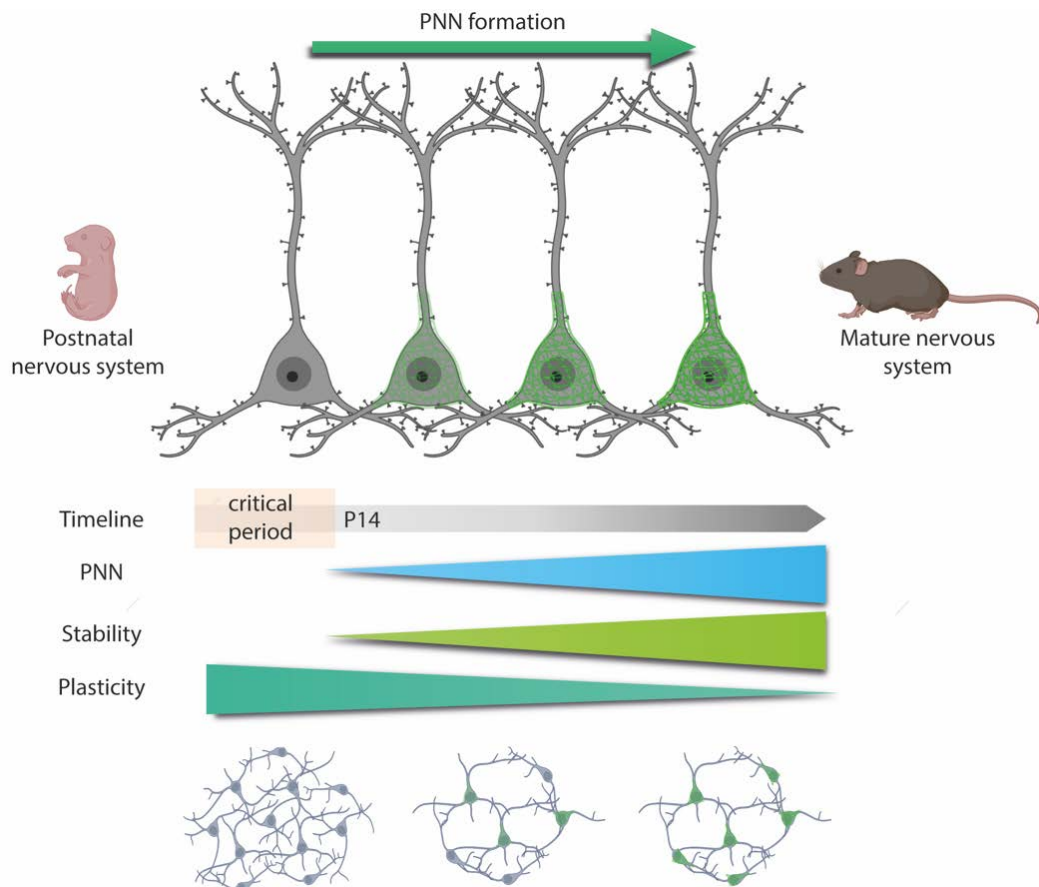


Figure 9. Developmental PNNs formation. PNNs first appear during development, specifically at the end of the critical period – P14 in the spinal cord –. The critical period is a plastic phase in which neurons increased their activity and generate new synaptic contacts. Once PNNs appear, they would wrap active neurons and stabilize these new connections formed. However, the absence of PNNs around unused synapses would lead to their pruning. Thus, along with PNNs formation, the plasticity of the CNS decreases while stability increases. PNN: perineuronal net. Individual images were obtained from Biorender.

Thus, the formation of PNNs is activity-dependent and coexists with the end of the critical period and the maturation of the CNS in which synaptogenesis, synaptic refinement and neural maturation occur (Pizzorusso, 2002; Carulli et al., 2006; Galtrey et al., 2008). Alterations in developmental activity of MN can produce changes in their morphology, connectivity, and electrophysiological properties. In the spinal cord, all the excitatory drive that MNs received during development is provided by proprioceptive and supraspinal inputs (Kalb and Hockfield, 1994). Hence, sciatic nerve injury or thoracic hemisection before PNNs deposition, suppresses MN activity and disrupts aggrecan expression (Kalb and Hockfield, 1988).

Overall, PNNs are instrumental in the transition from a permissive to a restricted milieu in the adult. The GABA potential shift and PNNs formation contribute to the well-known inhibitory environment found in the mature nervous system.

2.4. Mature nervous system: PNN function and modulation

2.4.1. PNN modulation

Once the critical period ends and PNNs have fully emerged, plasticity is not permanently lost, but rather regulated more rigorously under the dynamic control of PNNs. This dynamism is explained by the activity-dependent modulation of PNNs still present in the adult: changes in the activity of mature neurons would structurally rearrange PNNs and consequently, plasticity would be restricted or facilitated (Smith et al., 2015; Favuzzi et al., 2017). This modulation is mediated by endogenous and exogenous mechanisms. Exogenous mechanisms are mainly used in experimental studies and consist in the application of degrading enzymes like chABC and hyaluronidase (Pizzorusso, 2002; Massey et al., 2006; Pyka et al., 2011; Starkey et al., 2012). Endogenous mechanisms are the main physiological modulators of PNNs, adjusting the synthesis and degradation of the different PNNs components. This constitutive remodeling is controlled by several protease families such as metalloproteases (MMP) and ADAMTS (A Disintegrin and Metalloproteinase with Thrombospondin motifs) (Cawston and Young, 2010). Furthermore, the sulfation of CSPGs is another endogenous way through which activity can alter PNNs condensation and conformation (Miyata et al., 2012).

2.4.2. PNN function

The regular turnover of PNNs persists throughout life and it is crucial for many physiological processes. Although PNNs are widely known for their role in plasticity inhibition and synaptic stabilization, other functions have been attributed to cortical PNNs such as ionic buffering, neuroprotection, and neural maturation (*extensively reviewed in* (Kwok et al., 2011; van 't Spijker and Kwok, 2017; Lorenzo Bozzelli et al., 2018; Fawcett et al., 2019)). Remarkably, PNNs' functions are tightly related to the structural properties of their CSPGs. Hence, manipulation of PNN's CSPGs has a direct impact on the function of PNNs and the neuron surrounded (Gama et al., 2006). The highly negative charge of GAGs is one of the most important factors determining PNNs functions (Brückner et al., 1993), and this can be considered in several different ways:

- PNN's negative charges provide a suitable microenvironment around fast-firing neurons due to their buffering capacity of local ions. PNNs can control the diffusion of ions serving as a fast cation exchanger to provide rapid neuronal responses (Hartig et al., 1999). Besides, in the brain (Hartig et al., 1999; Carulli et al., 2006) and the dorsal and intermediate zone of the spinal cord (Deuchars et al., 2001), there is a good correlation between the expression of the potassium channel Kv3.1b, a marker of fast-firing neuron, (Rudy and McBain, 2001) and PNNs. Interestingly, this is not the case for spinal MNs.
- The negative charges of GAGs can buffer cations produced after oxidative stress or toxic metal ions, conferring neuroprotective capabilities to PNNs (Morawski et al., 2010; Suttikus et al., 2014).
- The negative milieu, provided by the charge, around neurons determines the membrane capacitance, which affects neural excitability (Tewari et al., 2018). Indeed, Glykys *et al.* found a negative correlation between PNNs intensity and internal Cl⁻ concentration, suggesting that PNNs are involved in setting the local Cl⁻ levels (Glykys et al., 2014). Indeed, PNNs degradation resulted in increased neural excitability (Hayani et al., 2018).
- Negative charges can, directly and indirectly, inhibit neural regeneration. Although the mechanisms used by CSPGs to inhibit neural regeneration are not completely understood, the GAG chains generate a steric hindrance for regrowth. This is observed in the fibro-glial scar formed after a SCI (McKeon et al., 1999) and overcome after chABC application (Bradbury et al., 2002). Indirectly, their inhibitory properties can also be triggered after interacting with specific

receptors (Shen et al., 2009; Lang et al., 2015). Moreover, GAGs chains disulfated at the 4th–6th position (CS-E) facilitate the binding of the repulsive guidance molecule semaphorin 3A (Sema3A), which inhibits neural outgrowth and regeneration (Dick et al., 2013; Vo et al., 2013).

Importantly, the sulfation pattern can contribute to other neural functions such as maturation. After the binding to PNNs through CS-E chains, the Otx2 protein can translocate into neurons and facilitate parvalbumin positive-neurons maturation (Sugiyama et al., 2008; Beurdeley et al., 2012). PNNs components also interact with ion channels and receptors and thus, regulate synaptic activity and membrane current. Tn-R binds to GABA receptors (GABA_R) through the HNK-1 motif (Saghatelyan et al., 2000). This PNN component also interacts with subunits of voltage-gated Na⁺ channels (Xiao et al., 1999), while brevican interacts with K⁺ channels and AMPAR (Favuzzi et al., 2017). Consequently, their removal can alter the excitatory/inhibitory balance. Furthermore, the lateral mobility of some receptors is also restricted by PNNs. ECM digestion with chABC increases the mobility of AMPAR (Frischknecht et al., 2009).

Overall, while PNNs have been classically defined as a barrier for plasticity, they also regulate numerous neuronal functions. These functions that appear to be crucial to neural development may play an important role in pathological conditions.

2.5. Insults in the central nervous system

The malleability of PNNs maintains the nervous system in equilibrium. Nonetheless, its imbalance, in any direction, can have broad implications in terms of neurological diseases. Excessive proteolytic processing of PNNs can lead to excessive plasticity as well as increased vulnerability to neurotoxic stimuli, which can trigger neurological disorders mainly studied in the brain. Indeed, cortical PNNs alterations have been linked with seizures (Tewari et al., 2018), CNS infection (Belichenko et al., 1997), traumatic brain injury (Hsieh et al., 2017) and stroke (Hobohm et al., 2005), among others. Nonetheless, very few studies have evaluated whether changes in PNNs can lead to pathological conditions in the spinal cord.

To better understand the possible implication of spinal PNNs in the functional outcomes after a spinal cord injury, we must first understand this pathological condition.

3. Spinal cord injury

Despite the spinal cord is protected by the vertebral column, it can be damaged. A spinal cord injury (SCI) is defined as a neurological damage on the spinal cord that causes motor, sensory and autonomic dysfunctions, directly impacting the quality of patients' life (Lima et al., 2022). Unfortunately, there are no currently reparative treatments to reverse the damage on the spinal cord.

3.1. Classification

SCI can be divided into different classifications depending on the etiology and extent and level of the lesion. Etiologically, SCI can be traumatic (90%) or non-traumatic (10%). Non-traumatic SCIs occur due to acute or chronic illnesses such as tumors, infections, or degenerative diseases. In contrast, common causes of traumatic SCI include traffic accidents, falls, sports or violence. Traumatic SCIs occur most frequently at the cervical level (59%), followed by thoracic (32%) and lumbosacral (9%) (Ahuja et al., 2017).

Regarding the severity of the lesion, patients can present complete or incomplete injuries. In an incomplete injury, the spinal cord can still transmit some information to and from the brain. However, in a complete injury, there is no axonal communication below the level of the trauma. Altogether, this doctoral thesis is focused on **incomplete traumatic SCI**.

The clinical outcome depends on the level and severity of the injury. Considering movement and sensation, patients can experience paraplegia or tetraplegia depending on the level of the injury. **Paraplegia** is defined as the impairment of sensory and/or motor function in lower extremities while **tetraplegia** affects all four limbs. Additional common features of SCI symptoms are neuropathic pain, spasticity, and loss of bladder, bowel, respiratory and sexual functions (Alizadeh et al., 2019).

3.2. Pathophysiology

SCI develops with primary and secondary pathophysiological mechanisms (Zhou et al., 2014). The primary injury corresponds to the initial damage produced by the mechanical trauma, which disrupts the vertebral column and compresses the spinal cord. This focal damage produces acute hemorrhage, blood-spinal cord barrier disruption and local cell death within minutes to hours (Ahuja et al., 2017). Together, they initiate a

cascade of events – secondary injury – that further exacerbates the neurological damages through vascular, biochemical, and cellular changes (calcium and glutamate excitotoxicity, vascular damage, ionic imbalance, ROS production, lipid peroxidation, inflammation, and apoptosis) (Hausmann, 2003; Oyinbo, 2011; Anjum et al., 2020). The overactivation of the immune system produces a persistent pro-inflammatory microenvironment, which contributes to cell death and changes the architecture of the spinal cord (Figure 10) (Ahuja et al., 2017). Regarding cell death, neuronal damage in the gray matter and oligodendrocyte loss in the spinal tracts disconnect the spinal cord from the rest of the nervous system and periphery. Considering the architecture of the spinal cord, a cystic cavity and a fibro-gliar scar appear at the level of the injury (Alizadeh et al., 2019). The fibro-gliar scar is produced by an up-regulation of CSPGs at the injury site. Specifically, there is a significant increase in lecticans such as neurocan, versican, phosphacan, NG2 and brevican but not aggrecan (Lemons et al., 2001; Jones et al., 2003; Buss et al., 2009). These CSPGs persist in the glial scar (Silver and Miller, 2004) and are remodeled by MMP, which expression significantly increases after injury (de Castro et al., 2000; Zhang et al., 2011). Apart from CSPGs up-regulation, selective changes in the sulfation pattern of GAGs have been reported. Following SCI, a large increase in the 4-sulfated (CS-A) GAG chains in the injury site have been observed (Wang et al., 2009; Hussein et al., 2020).

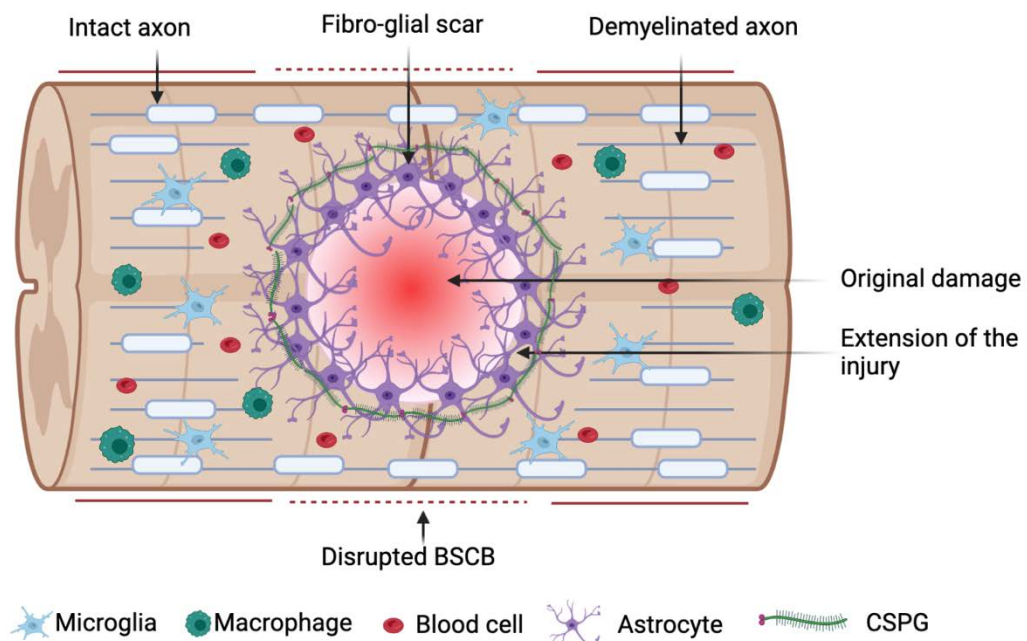


Figure 10. Representation of some of the events that contribute to the secondary damage after SCI. The disruption of the blood-spinal cord barrier (BSCB) induces the infiltration of macrophages and the activation of resident glial cells. Astrocytes generate the fibro-gliar scar. CSPG: chondroitin sulfate proteoglycan. Individual images were obtained from Biorender.

The glial scar cannot be simply defined as beneficial or detrimental to CNS repair since it walls the injured area, but also forms a barrier for axonal regeneration (Fawcett and Asher, 1999; Sofroniew, 2010). Lots of effort has been made to find an effective strategy to overcome the inhibitory influence of GAGs and thus, promote regeneration. A clear example is the enzyme chABC (*see 3.4, below*).

Finally, at chronic stages, the persistent inflammation, the glutamate excitotoxicity, and the poor regeneration capacity led to maladaptive changes in the spinal cord that eventually generate neuropathic pain and spasticity.

3.3. Plasticity events below the level of the injury. Experimental studies

Most spinal cord injuries are anatomically incomplete. The spared neural pathways can contribute to the spontaneous anatomical and functional plasticity that can favor recovery but also lead to maladaptive plasticity. To better understand the controversial outcomes produced by these automatic plastic events, animal models have been developed to understand the complexity of SCIs. Small rodents are the most frequently used animals in this field (Alizadeh et al., 2019). In the following section, some examples of adaptive or maladaptive plasticity generated below the injury are explained.

3.3.1. Respiratory recovery. High cervical spinal cord injury

Injuries at the high or mid-cervical level are the most common and devastating SCIs, producing tetraplegia and dysfunctional breathing. In fact, breathing impairment is the greatest cause of morbidity and mortality after a traumatic SCI (Hoh et al., 2013). Compromised breathing is not only produced by the disconnection from the higher respiratory center but also by the direct damage of the phrenic motor circuitry, which controls the main respiratory muscle, the diaphragm. Finally, paralysis or paresis of the diaphragm leads to respiratory deficits that often necessitate ventilator support.

Despite these devastating consequences, there is evidence of spontaneous respiratory plasticity at the injured spinal cord that led to some limited functional improvement (Porter, 1895). To better understand these neuroplasticity processes, researchers have used many preclinical models. One of the most studied models is the lateral hemisection at the second cervical spinal level (C2Hx) (Boulenguez et al., 2007; Komnenov et al., 2016; Zholudeva et al., 2017; Satkunendrarajah et al., 2018). Rodents receiving a C2 hemisection show acute paralysis of the ipsilateral hemidiaphragm and

decrease ventilation due to the interruption of axons from the medulla that monosynaptically project onto ipsilateral PhMNs. Besides, an increased contralateral response of the uninjured hemidiaphragm is also observed as a compensatory mechanism (Zholudeva et al., 2017, 2018; Sunshine et al., 2020).

Nonetheless, some weeks post-injury, some recovery in the ipsilateral spinal cord has been reported. This recovery can be attributed to two main factors:

- Activation of **contralateral (spared) axons** from the medulla and other respiratory-related supraspinal areas that cross the spinal midline below the injury. These axons provide glutamatergic and serotonergic inputs, essentials for restoring plasticity. These contralateral pathways are normally latent but become active after the lesion (Minor et al., 2006). Interestingly, their activation can be accelerated and potentiated through the application of respiratory challenges as a therapy such as hypoxia – reduced levels of O₂ –or hypercapnia – changes in the concentration of CO₂ (Devinney et al., 2016; Randelman et al., 2021).
- Activation of **spinal interneurons**. PhMNs not only receive glutamatergic inputs from supraspinal projections but also from propriospinal interneurons. After injury, spinal interneurons contribute to anatomical plasticity facilitating motor recovery (Cregg et al., 2017). They can be recruited into novel circuits to restore the connectivity between supraspinal neurons and spinal segments caudal to the lesion. Besides, below the site of the injury, they can change the connectivity of a specific circuitry, increasing the input to the spinal phrenic network. The glutamatergic V2a spinal interneurons are an example since their silence attenuates functional recovery (Zholudeva et al., 2017).

3.3.2. Spasticity and neuropathic pain. Thoracic spinal cord injury

After a low thoracic SCI, patients develop paraplegia observed as motor, sensory and autonomic alterations in the trunk, legs, and pelvic organs. The injury disconnects specific ascending and descending spinal tracts, generating motor and sensory impairment. Below the level of the injury, some plastic reorganization of the spinal cord can occur spontaneously. This disorganization altered the equilibrium between excitatory and inhibitory networks that facilitate the development of **spasticity** and **neuropathic pain**, affecting 60% and 70% of individuals living with SCI, respectively (Finnerup, 2017; Nees et al., 2017).

Spasticity is defined as a motor disorder characterized by a velocity-dependent increase in muscle tone, with exaggerated stretch reflexes (Navarro and Udina, 2009). Neuropathic pain is defined as a lesion of the somatosensory nervous system that leads to allodynia (painful sensation due to a stimulus that does not normally produce pain) and/or hyperalgesia (increased response to a stimulus that is normally painful) (Nees et al., 2017). Despite their apparent differences, these two pathological conditions share common features, such as their late onset following SCI and a spinal excitatory-inhibitory dysregulation. Indeed, the increased prevalence of spasticity in SCI patients with neuropathic pain suggests a mechanistic link between them. The underlying mechanisms that contribute to their development have been studied using animal models, being the contusive one the most clinical-relevant one. Some of them are shown below.

3.3.2.1. Spasticity

The loss of descending inputs from supraspinal structures alters the function of spinal circuits. In spinal reflexes such as the stretch reflex, the absence of descending inhibitory signals facilitates neuronal activity and increases the excitability of the circuitry. This increased stretch excitability can be produced by either a reduction of the threshold needed to elicit a response or an increased magnification of the stretch reflex (D'Amico et al., 2014). For instance, presynaptic inhibition, which normally controls the amount of afferent information that arrives to MNs (Faist et al., 1994), is no longer under the control of descending inhibitory input leading to an uncontrolled motoneuron fire rate. Changes in membrane receptors can also change the responsiveness of MN to respond to a specific input. In normal conditions, the KCC2 receptor regulates the intracellular concentration of Cl⁻ in adult neurons. After SCI, its downregulation decreases the GABAergic tone of neurons, producing excitatory inputs after inhibitory signals, increasing spinal hyperexcitability (Boulenguez et al., 2007). Besides, the huge release of glutamate during the secondary injury exacerbates the excitatory response overactivating glutamate receptors and downregulating glutamate transporters.

Spasticity can be indirectly evaluated by the electrophysiological study of the stretch reflex. The H wave is the electrophysiological analogue of the stretch reflex, thus, changes in its amplitude after a single or consecutive stimulus informs us about the excitability of the circuit (Lee-Kubli et al., 2018).

3.3.2.2. Neuropathic pain

The loss of descending modulatory sensory projections and disruption of ascending sensory tracts contribute to altered sensory perception after SCI. Similar to spasticity, there is a loss of inhibitory control that increases the responsiveness of sensory neurons to normal afferent and nociceptive inputs. This loss of inhibitory control is due to the loss of GABAergic interneurons, the upregulation of ionic channels and the reduction of GABAergic receptors and the KCC2 cotransporter in the dorsal horn (Kakinohana et al., 2006).

Besides, some of the primary nociceptive afferents that have lost their synapse can sprout into deeper laminae of the dorsal horn, contributing to neuropathic pain development (Nees et al., 2017). Neuroinflammation, including the activation of microglia and astrocytes, favors the maintenance of neuropathic pain (Costigan and Woolf, 2000). In experimental models, hyperalgesia can be evaluated using algometry tests (Hargreaves et al., 1988).

3.4. Therapeutical approaches

3.4.1. ChABC

Chondroitinase ABC is an enzyme that can degrade the sugar chains of CSPGs. Its application in the fibro-glial scar is one of the most successful strategies to overcome the inhibitory influence of GAGs and consequently, promote regeneration (McKeon et al., 1991). The effectiveness of chABC in degrading CSPGs has been tested *in vitro* and *in vivo* (Lee et al., 2010). *In vivo*, chABC has demonstrated huge potential in promoting regeneration of dopaminergic (Moon et al., 2001) and sensory axons (Shields et al., 2008), as well as inducing sprouting of both intact and injured serotonergic (Tom et al., 2009), corticospinal (Barritt et al., 2006; García-Alías et al., 2009) and sensory fibers (Massey et al., 2006). However, controversial results do appear in the literature, too. When CST regeneration was compared in hemisection and contusion models, chABC injections only enhanced regeneration of the CST in the hemisection model (Iseda et al., 2008). Accordingly, chABC's effect may depend on the severity and location of the lesion, in addition to the number of spared tissue and the time of the chABC injection.

Although axonal growth (regeneration or sprouting) is typically necessary for recovery, it is not always sufficient. Despite some studies have demonstrated improved motor, sensory and bladder function after chABC application (Bradbury et al., 2002;

Caggiano et al., 2005; Massey et al., 2006; Cafferty et al., 2008), many others found limited results. The main limitation of chABC application is that the plasticity that promotes needs an appropriate interaction with its target to make functional networks (García-Alías et al., 2009; Tom et al., 2009; Harris et al., 2010; Alilain et al., 2011; Wang et al., 2011). In this last step, activity-dependent therapies are a useful tool.

3.4.2. Activity-dependent therapies

Rehabilitative training is currently one of the most successful approaches promoting functional recovery following a SCI in animal models and clinical studies. This non-invasive treatment provides repetitive sensory inputs that reactivate and reorganize spinal cord circuits, in absence of descending inputs (Fouad and Tetzlaff, 2012; Torres-Espín et al., 2018). Such activity-dependent reorganization produces changes in neuronal function and connectivity that can be accompanied by functional recovery (de Leon et al., 1998; Battistuzzo et al., 2017). Although the mechanisms that underlie these activity-mediated improvements are not well known, a lot of literature have described some molecular and anatomical changes. Briefly, rehabilitation produces changes in the expression of genes related to cell survival, neuronal excitability, synaptic plasticity, and axonal plasticity (Molteni et al., 2004). Specifically, it upregulates the expression of neurotrophic factors such as brain-derived neurotrophic factors (BDNF) and neurotrophin 3 (NT-3) in the spinal cord and skeletal muscle (Gómez-Pinilla et al., 2002). It also enhances intracellular levels of Ca²⁺ and cyclin adenosine monophosphate (cAMP) and reduces inflammation. Besides, it restores the concentration of KCC2 expression on the MN's membrane (Côté et al., 2014). Overall, activity-dependent therapies are neuroprotective, promote regeneration and reduce maladaptive plasticity such as neuropathic pain and spasticity (Nees et al., 2016). Nevertheless, there is some controversial literature regarding the effects of the different activity-dependent protocols applied. Variations in duration, intensity, and type of training protocol may contribute to these discrepancies.

Considering the moment when rehabilitation should start, some studies have indicated that it is more effective when applied within the first 2 weeks. After that, there is a decline in the window of plasticity that prevents an effective recovery. *Detloff et al.* demonstrated that the application of a treadmill protocol 5 days after the injury prevented neuropathic pain development (Detloff et al., 2014), whereas the same protocol applied at 14 or 28 days after the injury was unable to reduce this maladaptive

plasticity already present (Detloff et al., 2016). Contrarily, other works demonstrated that treadmill training initiated 6 weeks post-injury resulted in a partial amelioration of pain (Sliwinski et al., 2018).

Intensity is another important factor to consider. Sometimes, non-trained animals exhibit self-training in their home cage (movement linked to their daily living) (Fouad et al., 2000). If the intensity of the protocol training is negligible in comparison to the self-training of non-trained animals, no effects produced by the training protocol would be observed.

Finally, the type of exercise protocol is also important. Rodent models of rehabilitation after SCI can be classified into voluntary and forced paradigms. Voluntary training involves enriched environment (EE) and wheel-running while forced training encompasses treadmill running, bicycling, or swimming. The pros and cons of each type of activity-dependent therapy are explained below.

Forced treadmill. It is one of the most common methods to provide locomotor rehabilitation in SCI in both pre-clinical and clinical studies. Nevertheless, the degree of recovery seen with this exercise protocol has been variable, specifically after incomplete SCI. In fact, it is believed that the effect of forced treadmill depends on the severity of the injury (Ichiyama et al., 2009). Thus, its limited effect after incomplete injuries in rodents could be due to spontaneous recovery of both trained and untrained groups (Battistuzzo et al., 2016). For instance, *Multon et al.* found that daily treadmill training started a day after a compression injury resulted in improved locomotor function (Multon et al., 2003), whereas *Fouad et al.* did not find beneficial effects on locomotor recovery after a dorsal hemisection in rats (Fouad et al., 2000). Some beneficial effects on modulating neuropathic pain have been also published (Nees et al., 2016).

The main advantage of forced treadmill is that the intensity can be controlled and changed depending on the study requirements. However, the main drawback is caused by a negative impulse provided, which is usually a shocking stimulus with low levels of electric current. This negative impulse can increase distress values, depressive behavior, and inflammatory reactions (Svensson et al., 2016). The most common protocol is based on running 30-60min/day with a frequency of 5-7 days/week.

Voluntary wheel. Wheels are installed inside the home cage to provide free access to trained animals. They are connected to recording devices that count the number of revolutions and/or the total time of running activity. To avoid animal isolation, animals can be housed in pairs, a group size that ensures that both animals could run at the same

time. In fact, this is the main drawback of voluntary wheel running training, since individual differences among the pair of mice are difficult to identify. Nevertheless, compared to forced treadmill exercise, voluntary wheel running presents some advantages: the running pattern is like natural running behavior, it is performed under non-stress conditions and does not require direct interference from the research which makes it an attractive method for long-term studies. Besides, since researchers do not directly participate, the training does not interfere with the normal nocturnal-diurnal rhythmicity of animals. In fact, activity is mainly accomplished during the dark phase of the 12/12h light-dark cycle (Manzanares et al., 2019).

Mice run a total distance of 4 to 20 km per day and a total activity time of 3 to 7h a day, which supposes a higher exercise dose than forced treadmill protocols. This increased amount of activity favors functional recovery in SCI models (Engesser-Cesar et al., 2005, 2007; Perreau et al., 2005). However, other studies did not find this positive effect (Erschbamer et al., 2006).

Enriched environment (EE). It refers to house conditions that facilitate enhanced sensory, cognitive, and motor stimulation. It can also include social stimulation through a larger number of animals per cage (van Praag et al., 2000). There are some aspects that differ from the rest of activity-dependent therapies. One of them is the novelty factor, which is achieved by changing the objects and their position. Another one is that it provides broader and more general training through great levels of sensory stimulation and associated physical activity (Nithianantharajah and Hannan, 2006). Indeed, *Hutson et al.* demonstrated increased regeneration after exposing mice in an EE, which enhanced their propriospinal activity (Hutson et al., 2019). In that work, their EE includes free access to a running wheel, therefore combining also voluntary wheel running.

3.4.2.1. Activity-dependent therapies and PNN

Interestingly, activity differently modulates PNNs depending on their anatomical location (Smith et al., 2015). In the cerebellum, an EE reduced the synthesis of PNNs components and enhanced their degradation by increasing the activity of MMP2 and MMP9 (Foscarin et al., 2011). In contrast, in the spinal cord, *Wang et al.* (Wang et al., 2011) were the first to demonstrate that activity, in terms of rehabilitation, increased spinal PNNs in a SCI model. This specific finding – the impact of physical activity on spinal PNNs— did not receive much attention, despite clearly demonstrating that activity

differentially modulates spinal and encephalic PNNs. Afterwards, two studies corroborated that physical exercise increased PNNs around intact spinal motoneurons (Arbat-Plana et al., 2015; Smith et al., 2015). Thus, the same physical activity that decreases PNNs' thickness around neurons located in the brain, increases PNNs' thickness in the spinal cord (Smith et al., 2015). This differential activity-dependent modulation could have a biological significance, as most spinal cord functions rely on the stability of spinal circuits, whereas plasticity is essential for most brain functions.

V. Hypothesis and objectives

Hypothesis

The proper functioning of the spinal cord strongly depends on the stability of spinal circuits. Thus, we hypothesize that PNN preservation is crucial to guarantee this stability. Indeed, considering that PNNs control plasticity and stability processes, we believe that the maladaptive plasticity observed after a SCI could be linked to changes in spinal PNNs. Since PNNs are modulated by activity, we propose that the application of different activity-dependent therapies would compensate PNNs' changes after injury and consequently, shape maladaptive plasticity into functional recovery.

Objectives

The general objective of this doctoral thesis is to study the biological function and modulation of spinal PNNs in the healthy and injured spinal cord. To address it, the thesis has been divided into four different chapters with the following specific objectives:

Chapter I. Aberrant perineuronal nets alter spinal circuits, impair motor function, and increase plasticity

- To decipher the role of mature spinal PNNs in motor function using transgenic mice that lack the cartilage link protein 1.
- To determine the involvement of mature spinal PNNs in the plastic potential of the corticospinal tract.

Chapter II. Voluntary wheel running preserves lumbar perineuronal nets, enhances motor functions and prevents hyperreflexia after spinal cord injury

- To assess the changes produced in lumbar PNNs after a thoracic SCI and different activity-dependent therapies.
- To correlate PNN changes with functional recovery.
- To evaluate PNN changes in the dorsal column nuclei and compared them with those observed at the lumbar level.

Chapter III. Link protein 1 is involved in the activity-dependent modulation of perineuronal nets in the spinal cord

- To investigate whether the link protein 1 is implicated in the activity-dependent modulation of PNNs.

- To compare the maladaptive plasticity observed after a spinal cord injury with the phenotype of the *Crtll* KO mice.

Chapter IV. Perineuronal net changes reveal a distinct right and left spinal phrenic circuit

- To study the changes that PNN suffer after injuring another spinal circuit, the spinal phrenic circuit.
- To characterize the structural plasticity in the right and left spinal phrenic system.

Annex. Do spinal perineuronal nets participate in motoneuron degeneration?

- To appraise the role of spinal PNNs in motoneuron survival using an injury model of motoneuron death.

VI. Study design and methodologies

General considerations for PNNs study

The study of PNNs was performed in WT and transgenic mice. While WT mice were used for assessing PNN changes in different experimental conditions (cervical or thoracic SCI and activity-dependent therapies), transgenic mice were required to evaluate the repercussion of PNN dysfunction and, thus their role, in the different situations (healthy and injured spinal cord). Our transgenic mice lack the cartilage link protein 1 (*Crtll* KO mice), which is implicated in PNNs assembly (Carulli et al., 2010). In these mice (Figure 11), the expression of the *Crtll* gene was disrupted by the addition of a Neomycin cassette in the exon 4 of the gene. As the link protein 1 is also implicated in cartilage formation, the *Crtll*^{-/-} mice had skeletal malformations that were countered by overexpressing the gene in the cartilage. Briefly, a vector containing the gene and a cartilage-specific promoter was generated and introduced in fertilized egg cells. The resulting *Crtll*^{-/+} mice were intercrossed with *Crtll*^{-/-} mice until a *Crtll*^{-/-/+} was achieved. In these newly generated mice, the *Crtll* gene was expressed in the cartilage and depleted in the rest of the tissues (Czipri et al., 2003; Carulli et al., 2010). To simplify, the *Crtll*^{-/-/+} would be named *Crtll* KO mice during the rest of the manuscript.

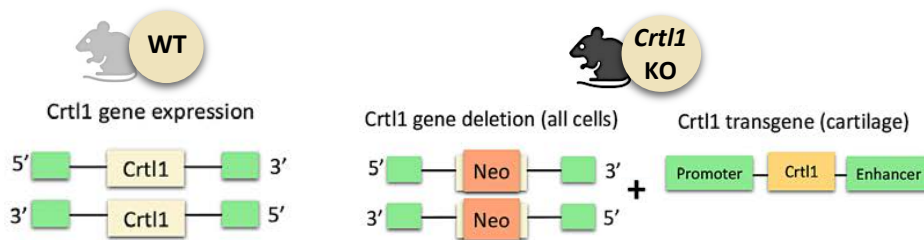
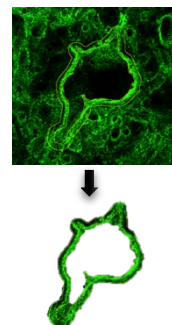


Figure 11. Diagram describing the genotype of the mice models used in this thesis. Individual images are obtained from Biorender.

Since PNN analysis is performed in all chapters, a detailed explanation of how these nets were evaluated is needed. In other studies, PNN values are obtained by analyzing the intensity of the PNN marker in the whole picture (Alilain et al., 2011; Hirono et al., 2018). This method generates an inaccurate evaluation of PNNs because it includes the intensity of the diffuse extracellular matrix too. Thus, we have used a more specific approach. Here, we have just quantified the PNN marker within 4 μ m around the soma of the neuron of interest, thereby, excluding the diffuse extracellular matrix (Figure 12).

Figure 12. Schematic representation of the quantification of PNN intensity.



Chapter I. Aberrant perineuronal nets alter spinal circuits, impair motor function, and increase plasticity

To elucidate the role of PNNs on motor function and plasticity in the spinal cord, two sets of experiments were carried out.

In the first part of the study, the role of spinal PNNs on motor function was assessed by submitting *Crtll* KO mice and their WT littermate into a battery of functional tests (shown in the table found on the next page). Then, a histological assessment of the lumbar spinal cord, the motor cortex and the tibialis anterior muscle were performed.

In the second part, we wanted to evaluate the plastic potential of the corticospinal tract, one of the most important motor pathways involved in locomotion. Hence, *Crtll* KO and WT mice suffered a dorsal hemisection at the left cervical 4 level (C4) to injure that motor tract. 21 days after the injury, the sprouting of the spared and contralateral corticospinal pathway was evaluated due to the injection of an anterograde tracer (BDA) in the left motor cortex (Figure 13).

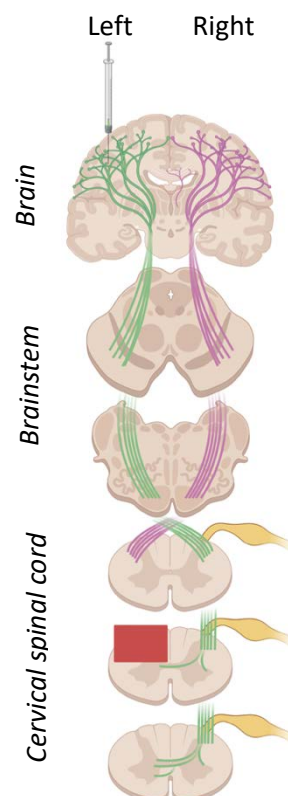
















Figure 13. Image representing the left and right corticospinal tracts. The dorsal hemisection was performed at the left C4 level. Considering that the corticospinal tract crosses the midline before reaching the spinal cord, the BDA tracer was injected at the left motor cortex to trace the contralateral axons. Individual images were taken from Biorender.

Experimental design	
Animal model	<i>Crt11</i> KO mice (🐭) WT littermates (🐭)
Background	C57BL6/J
Age	Adult (8-12 weeks)
Sex	♀ ♂
Experimental design	<p>1. <i>Crt11</i> KO mice characterization (n=62) <u>Groups:</u></p> <div style="display: flex; justify-content: space-around; align-items: center;"> <div style="border: 1px solid black; padding: 5px; text-align: center;">WT mice (n=35) 🐭</div> <div style="border: 1px solid black; padding: 5px; text-align: center;"><i>Crt11</i> KO mice (n=27) 🐭</div> </div>
	<p>2. Sprouting study (n= 34) <u>Injury:</u> C4 dorsal hemisection (dHxC4) 🐭 <u>Tracer:</u> BDA anterograde tracer (7 days post-injury) ○ Injection: motor cortex <u>Follow-up:</u> 3 weeks <u>Groups:</u></p> <div style="display: flex; justify-content: space-around; align-items: center;"> <div style="border: 1px solid black; padding: 5px; text-align: center;">WT sham (n=6) 🐭</div> <div style="border: 1px solid black; padding: 5px; text-align: center;">WT dHxC4 (n=12) 🐭</div> <div style="border: 1px solid black; padding: 5px; text-align: center;"><i>Crt11</i> KO sham (n=10) 🐭</div> <div style="border: 1px solid black; padding: 5px; text-align: center;"><i>Crt11</i> KO dHxC4 (n=6) 🐭</div> </div>
Functional evaluation	
1. <i>Crt11</i> KO characterization	<u>Behavioral tests:</u>
	<ul style="list-style-type: none"> - Open Field - Novel Object recognition test
	<u>Locomotor tests:</u>
	<ul style="list-style-type: none"> - Pole test - Adapted rotarod - DigiGait - Maximal velocity running
	<u>Strength test:</u> Grip test
	<u>Electrophysiological test:</u> H _{max} /M _{max} , RDD, withdrawal reflex.
2. Sprouting study	-
Histological analysis	
1. <i>Crt11</i> KO characterization	<u>Spinal cord</u> (lumbar): PNNs, synaptic markers, ionic transporter
	<u>Brain</u> (motor cortex): PNNs
	<u>Tibialis anterior muscle:</u> Collagen type IV
2. Sprouting study	<u>Spinal cord</u> (cervical): BDA tracer

Chapter II. Voluntary wheel running preserves lumbar perineuronal nets, enhances motor functions and prevents hyperreflexia after spinal cord injury

To investigate the activity-dependent modulation of PNNs in the context of SCIs and physical rehabilitation, WT mice received a thoracic SCI followed by different activity-dependent therapies and their lumbar PNN were studied. The evaluation of PNN was performed at two different time points to assess PNN dynamics. In a short-term study (5 weeks), a functional evaluation and histological analysis were conducted (found in the table on the next page). The functional recovery of each group was correlated with their PNN levels. In the long-term study (11 weeks), only a histological evaluation was performed.











Experimental design			
Animal model	WT mice (🐭)		
Background	C57BL6/J		
Age	Adult (8 weeks)		
Sex	♀		
Experimental design	PNN changes after SCI and activity-dependent therapies		
	<p>1. Short-term study (n=28) <u>Injury</u>: Moderate thoracic (T11) spinal cord contusion  <u>Activity-dependent therapies</u>: - Enriched environment (EE)  - Voluntary wheel (W)  - Treadmill (TR)  <u>Follow-up</u>: 5 weeks <u>Groups</u>:</p> <div style="display: flex; justify-content: space-around; align-items: center;"> <div style="border: 1px solid black; padding: 5px; text-align: center;">Sham (n=5) </div> <div style="border: 1px solid black; padding: 5px; text-align: center;">SCI SED (n=5) </div> <div style="border: 1px solid black; padding: 5px; text-align: center;">SCI EE (n=6) </div> <div style="border: 1px solid black; padding: 5px; text-align: center;">SCI W (n=7) </div> <div style="border: 1px solid black; padding: 5px; text-align: center;">SCI TR (n=5) </div> </div>		
	<p>2. Long-term study (n=26) <u>Injury</u>: Moderate thoracic (T11) spinal cord contusion  <u>Activity-dependent therapies</u>: treadmill (TR)  <u>Follow-up</u>: 11 weeks <u>Groups</u>:</p> <div style="display: flex; justify-content: space-around; align-items: center;"> <div style="border: 1px solid black; padding: 5px; text-align: center;">Sham (n=10) </div> <div style="border: 1px solid black; padding: 5px; text-align: center;">SCI SED (n=8) </div> <div style="border: 1px solid black; padding: 5px; text-align: center;">SCI TR (n=8) </div> </div>		
Functional evaluation			
1. Short-term	Basso Mouse Scale (BMS)	Algesimetry tests (Thermal)	Electrophysiological test (H_{max}/M_{max} , RDD)
2. Long-term	-		
Histological analysis			
1. Short-term	<u>Spinal cord (thoracic: injury side)</u> : Myelin evaluation <u>Spinal cord (lumbar)</u> <ul style="list-style-type: none"> - Ventral horn (L4-L5): PNNs, synaptic markers, ionic transporter, inflammatory markers - Dorsal horn (L5-L6): inflammatory and nociceptive markers 		
	<u>Dorsal column nuclei (brainstem)</u> : PNNs, synaptic markers		
2. Long-term	<u>Spinal cord (lumbar)</u> : Ventral horn (L4-L5): PNNs, synaptic markers		

Chapter III. Link protein 1 is involved in the activity-dependent modulation of perineuronal nets in the spinal cord

To decipher the involvement of link protein 1 in the activity-dependent modulation of spinal PNNs, two different experimental sets were performed.








Firstly, *Crtll* KO mice were submitted to an activity-dependent condition that enhance neuronal activity: a voluntary-wheel running protocol of two weeks. In this part, histological analysis of PNNs and synaptic markers were performed.

Secondly, *Crtll* KO mice were submitted to an activity-dependent condition that reduced neuronal activity: a thoracic SCI. In this case, we followed the same functional and histological evaluation as in the previous chapter (shown in the table next page).

Experimental design				
Animal model	<i>Crt11</i> KO mice (🐭) WT littermates (🐭)			
Background	C57BL6/J			
Age	Adult (8-10 weeks)			
Sex	♀ ♂			
Experimental design	PNNs remodeling after different activity patterns 1. Evaluation of increased (↑) activity (n=23) Activity-dependent therapy: voluntary- wheel (W)  Follow-up: 2 weeks Groups: <div style="display: flex; justify-content: space-around; align-items: center;"> <div style="border: 1px solid black; padding: 5px; text-align: center;">WT SED (n=8) </div> <div style="border: 1px solid black; padding: 5px; text-align: center;">WT W (n=9) </div> <div style="border: 1px solid black; padding: 5px; text-align: center;"><i>Crt11</i> KO SED (n=6) </div> <div style="border: 1px solid black; padding: 5px; text-align: center;"><i>Crt11</i> KO W (n=10) </div> </div>			
	2. Evaluation of reduced (↓) activity (n=34) Injury: Moderate thoracic (T11) spinal cord contusion  Follow-up: 5 weeks Groups: <div style="display: flex; justify-content: space-around; align-items: center;"> <div style="border: 1px solid black; padding: 5px; text-align: center;">WT sham (n=10) </div> <div style="border: 1px solid black; padding: 5px; text-align: center;">WT SCI (n=8) </div> <div style="border: 1px solid black; padding: 5px; text-align: center;"><i>Crt11</i> KO sham (n=10) </div> <div style="border: 1px solid black; padding: 5px; text-align: center;"><i>Crt11</i> KO SCI (n=6) </div> </div>			
Functional evaluation				
1. ↑ activity	-			
2. ↓ activity	<table border="1" style="width: 100%; border-collapse: collapse;"> <tr> <td style="width: 25%;">Basso Mouse Scale</td> <td style="width: 25%;">Algesimetry tests: - Thermal - Mechanical</td> <td style="width: 50%;">Electrophysiological test (H_{max}/M_{max}, RDD)</td> </tr> </table>	Basso Mouse Scale	Algesimetry tests: - Thermal - Mechanical	Electrophysiological test (H_{max}/M_{max} , RDD)
Basso Mouse Scale	Algesimetry tests: - Thermal - Mechanical	Electrophysiological test (H_{max}/M_{max} , RDD)		
Histological analysis				
1. ↑ activity	Spinal cord (lumbar): - Ventral horn (L4-L5): PNN			
2. ↓ activity	Spinal cord (lumbar): - Ventral horn (L4-L5): PNNs, synaptic markers, inflammatory markers - Dorsal horn (L5-L6): inflammatory markers			






Chapter IV. Perineuronal net changes reveal a distinct right and left spinal phrenic circuit

To assess whether all spinal PNNs are equally modulated after injury, we studied cervical PNNs implicated in the breathing circuit. We performed a hemisection at the cervical 2 level to disrupt the spinal phrenic circuit. This injury was performed on both sides of the spinal cord to corroborate that the right and left phrenic circuits showed the same structural plasticity. PNN changes were evaluated in the whole spinal circuit due to the aid of a transsynaptic retrotracer called pseudorabies virus (PRV) (Fortino et al., 2022) that was topically applied in the hemidiaphragm of interest.

Experimental design	
Animal model	WT mice (🐁)
Background	C57BL6/J
Age	Adult (10-12 weeks)
Sex	♀
Experimental design	<p>PNN changes in the spinal phrenic motor system after SCI</p> <p>1. Assessment of PNN changes 7 and 14 dpi after C2Hx (n=43)</p> <p><u>Injury</u>: C2 cervical hemisection (HxC2) at the left (L) and right side (R) of the spinal cord. </p> <p><u>Tracer</u>: pseudorabies virus (PRV) transsynaptic retrotracer (72h before euthanizing)</p> <ul style="list-style-type: none"> - Injection: left and right hemidiaphragm <p><u>Follow-up</u>: 1 or 2 weeks</p> <p><u>Groups</u>:</p> <div style="display: flex; justify-content: space-around; align-items: center;"> <div style="border: 1px solid cyan; padding: 5px; text-align: center;">Sham (n=7) </div> <div style="border: 1px solid cyan; padding: 5px; text-align: center;">HxC2 L 7 dpi (n=16) </div> <div style="border: 1px solid cyan; padding: 5px; text-align: center;">HxC2 R 7 dpi (n=6) </div> <div style="border: 1px solid cyan; padding: 5px; text-align: center;">HxC2 L 14 dpi (n=14) </div> </div>
	<p>2. Phrenic motoneuron (PhMN) comparison (n=8)</p> <p><u>Tracer</u>: True Blue Chloride (TB) retrotracer</p> <div style="display: flex; justify-content: space-around; align-items: center;"> <div style="border: 1px solid orange; padding: 5px; text-align: center;">Left motor pool (n=7) </div> <div style="border: 1px solid orange; padding: 5px; text-align: center;">Right motor pool (n=8) </div> </div>
Functional evaluation	
1. HxC2	-
2. PhMN	-
Histological analysis	
1. HxC2	<p><u>Spinal cord (cervical)</u>:</p> <ul style="list-style-type: none"> - Dorsal horn, intermediate region, and ventral horn: PNNs and synaptic markers.
2. PhMN	<u>Spinal cord (cervical)</u> : TB retrotracer counting

Annex. Do spinal perineuronal nets participate in motoneuron death?

To study the role of spinal PNNs in neuroprotection, *Crt11* KO and WT mice suffered a left brachial plexus injury, which is a model of lesion to evaluate motoneuron death (Ruven et al., 2014). To localize the axotomized spinal cord region, the left triceps muscle was retrogradely traced. Finally, MN survival and PNN changes were evaluated in that spinal cord region.

Experimental design	
<i>Animal model</i>	<i>Crt11</i> KO mice (🐭) WT littermates (🐭)
<i>Background</i>	C57BL6/J
<i>Age</i>	Adult (8-12 weeks)
<i>Sex</i>	♀ ♂
<i>Experimental design</i>	<p>Study the role of spinal PNNs in motoneuron death (n=21)</p> <p><u>Injury</u>: Brachial plexus injury (BPI): C5-C8/T1. Left side. </p> <p><u>Tracer</u>: TB retrotracer</p> <p>- Injection: Left triceps muscle</p> <p><u>Follow-up</u>: 3 weeks</p> <p><u>Groups</u>:</p> <div style="display: flex; justify-content: space-around; align-items: center;"> <div style="border: 1px solid black; padding: 5px; text-align: center;"> WT sham (n=6)  </div> <div style="border: 1px solid black; padding: 5px; text-align: center;"> WT BPI (n=5)  </div> <div style="border: 1px solid black; padding: 5px; text-align: center;"> <i>Crt11</i> KO sham (n=4)  </div> <div style="border: 1px solid black; padding: 5px; text-align: center;"> <i>Crt11</i> KO BPI (n=6)  </div> </div>
Functional evaluation	
-	
Histological analysis	
<p><u>Spinal cord (cervical: C5-C8)</u></p> <p>- Ventral horn: MN counting, PNNs, inflammatory markers</p>	

VII. Results

Chapter I

Aberrant perineuronal nets alter spinal circuits, impair motor function, and increase plasticity

**Aberrant perineuronal nets alter spinal circuits, impair motor function,
and increase plasticity**

Sánchez-Ventura J¹, Canal C¹, Hidalgo J¹, Penas C¹, Navarro X¹, Torres-Espin A², Fouad
K³, Udina E^{1*}

Author affiliations:

¹Institute of Neuroscience, Department Cell Biology, Physiology and Immunology, Universitat Autònoma de Barcelona, and Centro de Investigación Biomédica en Red sobre Enfermedades Neurodegenerativas (CIBERNED), Bellaterra, Spain

²Weill Institute for Neuroscience, Brain and Spinal Injury Center (BASIC), Department of Neurological Surgery, University of California San Francisco, San Francisco, CA, USA

³Neuroscience and Mental Health Institute, Department of Physical Therapy, Faculty of Rehabilitative Medicine, University of Alberta, Edmonton, AB, Canada.

Abstract

Perineuronal nets (PNNs) are a specialized extracellular matrix that have been extensively studied in the brain. Cortical PNNs are implicated in synaptic stabilization, plasticity inhibition, neuroprotection, and ionic buffering. However, the role of spinal PNNs, mainly found around motoneurons, is still unclear. Thus, the goal of this study is to elucidate the role of spinal PNNs on motor function and plasticity in both intact and spinal cord injured mice. We used transgenic mice lacking the cartilage link protein 1 (*Crtll* KO mice), which is implicated in PNN assembly. *Crtll* KO mice showed disorganized PNNs with an altered proportion of their components in both motor cortex and spinal cord. Behavioral and electrophysiological tests revealed motor impairments and hyperexcitability of spinal reflexes in *Crtll* KO compared to WT mice. These functional outcomes were accompanied by an increase in excitatory synapses around spinal motoneurons. Moreover, following spinal lesions of the corticospinal tract, *Crtll* KO mice showed increased contralateral sprouting compared to WT mice. Altogether, the lack of *Crtll* generates aberrant PNNs that alter excitatory synapses and change the physiological properties of motoneurons, overall altering spinal circuits and producing motor impairment. This disorganization generates a permissive scenario for contralateral axons to sprout after injury.

Keywords: perineuronal nets, link protein 1, plasticity, locomotion, spinal cord injury

Introduction

Perineuronal nets (PNNs) are a dynamic extracellular matrix that surround neurons in the central nervous system (CNS) and play a key role in synaptic stabilization and plasticity inhibition (Wang and Fawcett, 2012). They are composed of chondroitin sulfate proteoglycans (CSPGs), hyaluronan and proteins such as tenascin-R, link proteins and Semaphorin 3A (Kwok et al., 2010). PNN formation is activity dependent and occurs at late postnatal stage, specifically at the end of the ‘critical period’ for plasticity which coincides with the maturation of neural circuits and the decline of neural plasticity (Berardi et al., 2000; Pizzorusso, 2002; Dityatev et al., 2007). In fact, the enzymatic breakdown of PNNs by chondroitinase ABC (chABC) reopens the plasticity window, demonstrating the implication of PNNs in this process (Pizzorusso, 2002). Among all PNN components, the cartilage link protein 1 (*Crtl1*) is crucial in PNN formation since its expression closely follows the assembly of PNNs (Carulli et al., 2010). *In vitro*, its absence prevents PNN formation around PNN-bearing cells (Kwok et al., 2010). *In vivo*, its genetic deletion confers increased levels of plasticity in the adult visual cortex and Purkinje cell terminals and also promotes regeneration into the denervated cuneate nucleus (Carulli et al., 2010; Foscarin et al., 2011).

In the mature CNS, the role of PNNs in regulating plasticity-stability processes has been extensively studied in the brain, demonstrated in the visual cortex (Pizzorusso, 2002), amygdala (Nadine et al., 2009), medial prefrontal cortex (Slaker et al., 2015), and the cerebellum (Carulli et al., 2020). Other functions have been attributed to cortical PNNs, such as ionic buffering (Brückner et al., 1993), neuroprotection (Suttkus et al., 2014), and synaptic refinement (Frischknecht et al., 2009). In contrast, little is known about PNNs’ function within the spinal cord even though they surround 80% of α -motoneurons (MNs) and many spinal interneurons (Irvine and Kwok, 2018).

Interestingly, spinal PNNs thickness is modulated by neuronal activity in the opposite direction of cortical PNNs, since activity reduces brain PNNs but increases spinal ones (Smith et al., 2015). Thus, decreased spinal motoneurons activity below a SCI reduces the thickness of their PNNs. This reduction is reversed by physical rehabilitation (Sánchez-Ventura et al., 2021), and depends on increased synaptic activity (Arbat-Plana et al., 2015; Smith et al., 2015). It is interesting to note that application of chABC at the injury site in SCI models, degrades CSPGs secreted by the fibro-glial scar, and attenuates the growth limiting properties of CSPGs (Barritt et al., 2006; Massey et al., 2006). However, the plasticity achieved by chABC only establishes meaningful connections and

translates into functional recovery when combined with rehabilitative motor training (García-Álías et al., 2009; Tom et al., 2009; Wang et al., 2011), to facilitate the formation and stabilization of functional connections. This synaptic stabilization is comparable to that found at the end of the developmental critical period in which PNNs participate.

Despite sound and promising evidence, most studies highlight the potential of chABC to boost plasticity in the spinal cord without properly evaluating the importance of modulating PNNs. Thus, the current study aims to describe the role of spinal PNNs on motor function by using transgenic mice lacking the Hyaluronan and Proteoglycan Link protein 1 (*Crtll*/HAPLN1) gene, which encodes the cartilage link protein1 (*Crtl* 1), a key element triggering PNN formation (Carulli et al., 2010). In previous research, *Crtll* KO mice were used to study PNNs' role in the cerebellum and brain (Carulli et al., 2010; Foscarin et al., 2011). Within the present study, our goal was to study the functional importance of PNNs in the motor system using behavioral, electrophysiological, and histological analysis in *Crtll* KO mice. Elucidating PNN function in the spinal cord will improve our understanding of its role in fine-tuning synaptic plasticity and stability.

Materials and methods

Experimental design

Transgenic mice (*Crtll* KO) used in this study were provided by Dr. Pizzorusso (Carulli et al., 2010) and maintained in the Animal Service of the Universitat Autònoma de Barcelona (UAB).

Their generation and phenotype are described by *Czipri et al* (Czipri et al., 2003). In brief, *Crtll* KO mice lack for the cartilage link protein 1, encoded by the *Crtll*/HAPLN1 gene, which is required for the proper assembly of PNNs (Figure 1). These *Crtll* KO mice are rescue transgenic mice, in which *Crtll* is expressed under the control of the type II collagen cartilage-specific promoter and enhancer, resulting in *Crtll* expression in cartilage but depletion in all tissues including the CNS (Carulli et al., 2010). This specific overexpression is produced to avoid skeletal malformations incompatible with life (Suppl. Figure 1). They are maintained in a C57BL6/J genetic background.

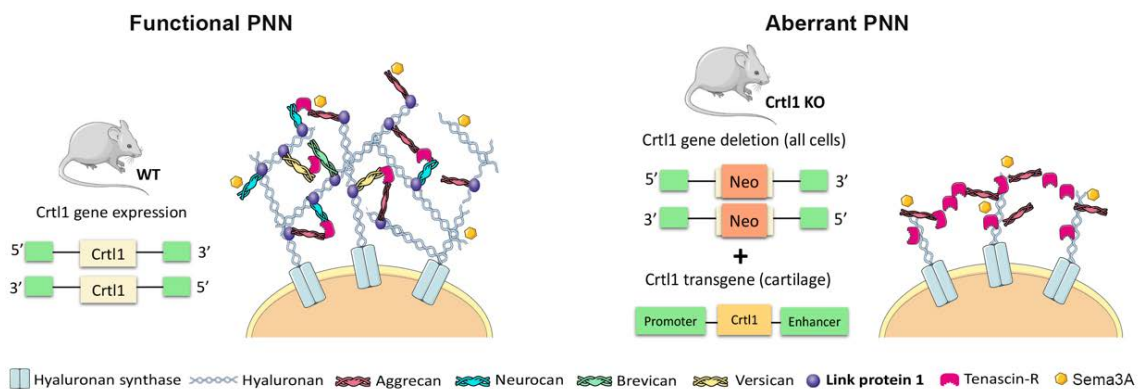


Figure 1. Schematic diagram illustrating the genetic differences between the *Crtll* KO and WT mice and their corresponding PNN structure. WT mice present highly organized and functional PNN. These nets are anchored to neurons by the enzyme hyaluronan synthase, which produces a hyaluronan polymer chain. This chain provides a scaffold for the binding of different types of CSPGs of the lectican family (aggrecan, neurocan, brevican and versican), whose interaction is stabilized by the link protein 1. Finally, the tenascin-R interconnects the different chains of CSPGs, generating a complex structure. The Sema3A protein can bind to the PNN's structure. In the *Crtll* KO mice, the expression of the *Crtll* gene is disrupted by the addition of a Neomycin vector in all cells. In the cartilage, there are normal levels of *Crtll* expression given that these mice overexpress the *Crtll* gene under the control of a cartilage-specific promoter. *Crtll* KO mice present disorganized PNNs due to the lack of the stabilizer link protein 1. Sema3A: semaphorin 3A; WT: wild type; KO: knock-out; PNN: perineuronal nets; *Crtll*: cartilage link protein 1; Neo: neomycin.

Ninety-six female and male adult (8-12 weeks of age) *Crtll* KO mice and their WT littermates were used. A total of 62 mice were used for characterization and 34 for

evaluating the role of link protein 1 in sprouting after SCI. From the 62 mice used for characterization, 20 were randomly chosen for histological analysis. Since no sex differences were detected (Suppl. Figure 2), data from both sexes was pooled. All experiments were blinded to genotype during behavioral testing and histological analysis.

The experimental procedures were approved by UAB Experimental Ethical Committee (CEAAH) and conducted following the animal welfare guidelines 2010/63/EC of the European Communities Council Directive. Mice were housed in groups, at 22 °C (\pm 2 °C), kept on a 12:12 light/dark cycle and received water and food *ad libitum*.

Genotyping

The genotype of mice (Table 1) was determined using mouse tail genomic DNA and 3 specific sets primers by PCR (Table 2).

Table 1. Genotypes generated.

	Neomycin	Crtll	MC59
WT (<i>Crtll</i> +/+)	-	+	-
Heterozygous (<i>Crtll</i> +/- <i>Crtll</i> -Tg +/0 or <i>Crtll</i> +/-)	+	+	+/-
KO (<i>Crtll</i> -/- <i>Crtll</i> -Tg +/0)	+	-	+

Table 2. Primer sequences and PCR conditions.

Gene	F/R	Sequence	PCR conditions
Crtll	F	5' TAATGACCTTTCCTGTCTCTCC 3'	94°C for 2 min, 35x (94°C for 15s, 60,5°C for 30s, 72°C for 5 min) and 72°C for 5 min.
	R	5' CCCAAAACCCGTTAGTTCC 3'	
Neomycin	F	5' CTTGGGTGGAGAGGCTATTCC 3'	95°C for 3 min, 35x (95°C for 30s, 60°C for 30s, 72°C for 45s) and 72°C for 2 min.
	R	5' AGGTGAGATGACAGGAGATC 3'	
Crtll cartilage (MC59)	F	5' CCTTTCAGACAGCTACACTCC 3'	94°C for 2 min, 30 x (94°C for 30s, 59°C for 30s, 72°C for 1 min) and 72°C for 5 min.
	R	5' AAACACTCGACCTTGATAGCC 3'	

Functional assessment

Animals were handled for 3 days and habituated for 15 minutes in the behavioral room before each test.

Open field test

Open field testing was used to measure general locomotor activity (Seibenhener and Wooten, 2015). Mice were individually placed into a white methacrylate box (56 x 36,5 x 31 cm) and allowed to explore for 5 minutes. Their exploratory behavior was recorded for automated assessment. The total distance, and the average speed travelled were analyzed from recorded footage with Ethovision XT version 11.5 (Noldus) software, whereas the number of rearings was annotated during the test session.

Novel object recognition test (NORT)

NORT was performed in the Open field arena. Mice were habituated during 3 consecutive days (10 minutes) to the arena. The familiarization phase started on the 4th day. During this session, two identical objects (A1 and A2) were placed in the middle of the arena and mice explored them for 10 minutes. Two hours after familiarization, short-term memory was tested by placing mice back into the arena for 10 minutes, where one of the familiar objects was replaced by a novel object (B). To test long-term memory, animals were put back in the box 24h after the familiarization phase, to explore the familiar object A and a second novel object C (10 minutes). The time spent with each object – when an animal sniffed or touched it – was measured. Finally, a discrimination index (DI) was calculated as the difference between the time spent with the novel or familiar objects divided by the total time spent with the two objects at 2, 5 and 10 minutes cumulatively. A higher DI reflects greater memory consolidation for the familiar object (Bevins and Besheer, 2006). All objects had similar sizes but different shapes and colors. Between trials, ethanol was applied to the objects to avoid the use of odor cues.

Pole test

The pole test is used to evaluate coordination and balance (Ogawa et al., 1985). A pole (50 cm high, 1 cm in diameter) was vertically placed on a soft platform, which contains the nesting material of the animal home cage to motivate the mouse to climb down. Following a brief period (30 seconds) of ground exploration, each mouse was placed on the top of the pole and the time required to turn head down (T-turn) and descend the pole (T-descend) was measured. A maximum of 120 seconds was allowed to complete the task. If the mouse fell from the top of the pole, this trial was discarded. Each mouse underwent 3 consecutive trials.

Adapted rotarod

Standard rotarod tests evaluate motor function and coordination (Shiotsuki et al., 2010). To also assess motor learning, the test was repeated during 4 consecutive days at a constant velocity of 10 rpm (Shiotsuki et al., 2010). The day before training sessions, mice were habituated to stay on the stopped rotarod for 3 minutes. This habituation protocol was repeated every test day for 1 minute, just before the training session started. In each session, mice were placed on the rotarod and the latency to fall was measured. Immediately after falling, mice were placed back on the drum up to 5 times. A fall was overlooked when the animal endured on the drum for 180 seconds. Finally, the total fall latencies of each day were summed and compared between the 4 days and groups. The habituation and the training session were performed at the same time of the day.

DigiGait and maximal velocity assessment

The maximal velocity that animals could reach was evaluated on a treadmill. Locomotion kinematics was evaluated through the DigiGait system (Mouse Specifics, Boston, MA) in which animals were placed onto the treadmill belt at 20 cm/s, based on previous results of our laboratory (Mancuso et al., 2011). Only those *Crtll* KO mice that could reach that velocity were included in the DigiGait analysis. A high-speed video camera (150 frames/second) located below the transparent belt was used to monitor around 10-12 strides/animal. Two trials were given to each animal to obtain an appropriate video for analysis, which was considered when mice walked straight ahead at a constant velocity. Then, each video was digitized, and the area of the paw was calculated with the DigiGait software. Mistakes of the imaging in which the paw area was not correctly detected were manually corrected. Parameters such as the percentage of duration of the stride phases, the ratio between the stance and the swing phase, the paw area at the stance phase and the dA/dT_{\max} and dA/dT_{\min} were evaluated.

Grip strength

The limb strength of all mice was determined using the grip strength test (Meyer et al., 1979). For three days, mice were placed on a grid strength apparatus so they could grab a small grid with their fore and both fore and hindlimbs. Afterwards, mice were slowly pulled away from the grid until they release it. The maximal peak force was measured using a sensor connected to the grip strength apparatus. Each day, five trials

of 15 seconds were performed and averaged. All the values were normalized using the body weight of each mouse.

Electrophysiological tests

To evaluate the state of spinal reflexes, electrophysiological tests were performed under anesthesia (ketamine 90 mg/kg and xylazine 10 mg/kg) since it has negligible effects on electrophysiological recordings (Ho and Waite, 2002).

For stretch reflex measurements, the sciatic nerve was stimulated by delivering a single electrical pulse of 0.02 ms at supramaximal intensity (Grass S88) by a monopolar needle inserted in the sciatic notch. The compound muscle action potential (CMAP) of the plantar muscle was recorded using a monopolar needle inserted in that muscle. In this recording, the maximal baseline to peak amplitude of the M wave (M_{max} : direct muscle response), initial and final M wave latencies, and the maximum amplitude of the H wave (H_{max} : monosynaptic reflex) were measured. Finally, the H_{max}/M_{max} was calculated as an index of the excitability of the Ia afferent synapses on spinal MNs (Thompson et al., 1992). While M wave values were obtained with supramaximal stimulations, the H_{max} was elicited after progressively increasing the intensity of the electrical stimulation until reaching the maximal amplitude of the H wave. The depression profile of the H wave or rate-dependent depression (RDD) was performed following the protocol previously described (Sánchez-Ventura et al., 2021).

Regarding the withdrawal reflex, the ipsilateral polysynaptic reflex was elicited by stimulating the sciatic nerve with a pulse of 0.1 ms at a supramaximal intensity and the potentials were recorded at the ipsilateral tibialis anterior muscle. The contralateral polysynaptic reflex was elicited by stimulating the left tibial nerve at the ankle and recorded at the right tibialis anterior muscle. The maximum amplitude, and the area under the curve (Root Mean Square; RMS) of the third component (C3) were evaluated, which is conveyed by C fibers and found in latencies between 18-55 ms (Valero-Cabré et al., 2004).

For motor units' evaluation, the mean amplitude of single motor unit activation potentials (SMUA) was assessed. From a subthreshold intensity, the sciatic nerve was stimulated with pulses that progressively increased their intensity and recorded in the plantar and tibialis anterior muscle. Increments higher than 50 μ V were considered as indicative of the recruitment of an additional motor unit. Finally, the mean amplitude of individual motor units was calculated as the average of consistent increases.

All recorded potentials were amplified and visualized on a digital oscilloscope (Tektronix 450S). LabChart Reader software was used for the analysis.

Spinal cord injury

To determine the potential of the corticospinal axons to sprout and grow after injury, a unilateral dorsal hemi-section at the C4 level (HxC4) was performed. Before the injury, the following experimental groups were randomly generated: WT sham (n=6); WT+ HxC4 (n=12); *Crtll* KO sham (n=10); *Crtll* KO + HxC4 (n=6).

For the surgical procedure, mice were anesthetized using an intraperitoneal injection (i.p.) of ketamine (90mg/kg) and xylazine (10mg/kg) in saline solution. After skin and muscle incision, a laminectomy of segment C3-C4 was performed to expose the spinal cord. Then, a unilateral dorsal hemi-section of the left C4 spinal cord was done, using small scissors, to a depth of 1.0 mm to completely sever the dorsolateral corticospinal tract. To ensure that the lesion was complete, the scissors were passed through the dorsal part of the spinal cord three times. After surgery, animals received 1 ml of saline solution subcutaneously. For pain management, subcutaneous injections of buprenorphine (0.1mg/kg) were administered. Mice were kept on a 38°C heating pad during the surgical procedure and until they were fully awake.

Biotinylated dextran amine tracing

To anterogradely label the axons of the corticospinal tract (CST), 1.5 µl of the neuronal tracer biotinylated dextran amine (BDA; 10000 MW; 10% in PB; Thermo Fisher) were injected in the left motor cortex. Briefly, 7 days after injury, mice were deeply anesthetized with ketamine/xylazine (see above) and placed in a stereotaxic device to perform the craniotomy and the injection of the tracer. The injection was set up in three points of the left motor cortex (ipsilateral to SCI): -1 mm lateral to the midline, at 0.5mm, -0.5mm and -1 mm from Bregma and at a depth of 0.7 mm ventral to the dura. A 10 µl Hamilton syringe fitted with a 33 G needle was used. Each injection delivered 0.5 µl of the tracer at a velocity rate of 0.25 µl/min and the syringe was left at the site of injection for 3 minutes before removal. Two weeks after injection, animals were euthanized.

Histological evaluation

Mice were euthanized (pentobarbital; *ip*: 200 mg/kg) and transcardially perfused with 4% paraformaldehyde (PFA) in 0.1M phosphate buffer (PB). Spinal cords, brains and tibialis anterior muscles were harvested. Spinal cords and brains were post-fixed in 4% PFA over 2h and overnight (ON), respectively. Afterwards, both tissues were cryoprotected in 30% sucrose solution in PB at 4 °C until tissue sank, while tibialis anterior muscles were directly cryopreserved in that solution.

For the *Crtll* KO histological analysis, lumbar spinal cords (L4-L5), motor cortices (Bregma 0.98 to 1.94) and tibialis anterior muscles were transversally cut on a cryostat (20 µm thick) and collected onto gelatin-coated glass slides. To study PNN components (L4-L5 spinal segment and motor cortex), synaptic markers (L4-L5 spinal segment) and muscle fibers, tissue sections were permeabilized with Phosphate Buffer saline Triton 0.3% (PBST 0.3%) except for the KCC2 marker, which was permeabilized with PBST 0.3%-Bovine Serum Albumin 3%. Then, nonspecific interactions were blocked with 10% Normal Donkey Serum for 1h at room temperature (RT). Afterwards, sections were incubated ON at 4 °C with primary antibodies (Table 3). After washes, immunoreactive sites were revealed using species-specific secondary antibodies (1:200; 2h RT; Table 3). For Neurocan and Semaphorin 3A (Sema3A) markers, the signal was amplified by streptavidin (1:200) and biotin tyramide (1:60; TSA Biotin System; Perkin Elmer NEL700001KT) for 1h and 3 minutes, respectively. Finally, sections were coverslipped using Fluoromount-G medium (Southern Biotech).

For sprouting evaluation, the C1 level of the spinal cord was cross-sectioned (20 µm), whereas the rest of the cervical spinal cord was longitudinally cut (25 µm). Both types of sections were immunolabeled to detect the BDA tracer. For BDA detection, sections were initially washed with TBS-Tween 0.1 and then, endogenous peroxidases were blocked for 10 minutes. Next, we incubated the streptavidin-HRP (1:200) for 1h at RT. After several washes, the signal was amplified incubating the biotin tyramide (1:50) for 7 minute and visualized with Alexa Fluor 488-streptavidin (1:200) after 1h at RT.

Table 3. List of primary and secondary antibodies used in the histological analysis.

Primary antibodies				Secondary antibodies		
Antibody	Dilution	Host	Reference	Antibody	Host	Reference
Aggrecan (Cat301)	1:100	Mouse	MAB5284- Sigma Aldrich	Alexa Fluor 488	Donkey x Mouse	A21202 - Invitrogen
Link protein I	1:100	Goat	AF2608-SP, R&D systems	Alexa 594	Donkey x Goat	All058- Invitrogen
Sema3A	1:400	Goat	OASG06564 - Aviva Systems biology	Streptavidin- Cys3		43-4315- Zimed
Neurocan	1:50	Sheep	AF5800- R&D systems	Streptavidin 488		S11223- Invitrogen
Tenascin-R	1:200	Goat	AF3865- R&D systems	Alexa Fluor 594	Donkey x Goat	All058- Invitrogen
VGlut1	1:300	Guinea Pig	AB5905- Millipore	Cys 3	Donkey x Guinea Pig	706-165-148- Jackson
VGAT	1:1000	Rabbit	131 002- Synaptic systems	Alexa Fluor 488	Donkey x Rabbit	A21206- Invitrogen
KCC2	1:400	Rabbit	07-432- Millipore	Alexa Fluor 594	Donkey x Rabbit	A21207- Invitrogen
ChAT	1:50	Goat	AB144P, Millipore	Alexa Fluor 488	Donkey x Goat	A 11055- Invitrogen
MMP9	1:200	Rabbit	ab38898, Abcam	Cys 5	Donkey x Rabbit	711-175-152- Jackson
Collagen IV	1:100	Mouse	M3F7, Hybridoma Bank	Alexa Fluor 594	Donkey x Mouse	A21203 - Invitrogen

Image analysis

To analyze PNN components and synaptic markers, images were taken from 4 spinal cord (L4-L5) or brain sections (motor cortex) using a confocal laser-scanning microscope (around 30 steps, z-step size of 0.5 μm , Leica TCS SP5) at 40x for each mouse. To quantify PNNs and synaptic changes, a minimum of 30 MNs (located within the ventral horn and presenting an area $> 350 \mu\text{m}^2$ (Friese et al., 2009)) were measured for each animal. PNN analysis was performed as described before (Sánchez-Ventura et al., 2021). In brief, the maximal projection of the z-stacks was performed and then, the background was corrected. Then, a band of 4 μm around the cell body of MNs was delimited to measure the integrated density of that region. For synaptic measurements, VGlut1 (vesicular glutamate transporter 1) and VGAT (vesicular GABA transporter) + synaptic boutons presented in a band of 4 μm around the selected MN were measured

by integrated density. Synaptic competition between proprioceptive afferents and C-boutons (Jiang et al., 2016) was assessed by counting the number of VGlut1 positive synaptic boutons and C-boutons positive dots presented in the whole photograph.

For spinal MN analysis, slides corresponding to L4-L5 spinal cord sections separated 200 μm each were stained using ChAT (choline acetyltransferase) and MMP9 (matrix metalloproteinase 9) antibodies. The number of lumbar MN was determined by counting the number of ChAT+ cells located in lamina IX of grey matter (bilaterally). The percentage of MMP9+ cells was then calculated from the total of ChAT+ neurons. To quantify KCC2 staining at the dorsal horn, confocal images were obtained at 40x and the integrated density of the whole immunoreactivity was measured. For the VGlut1 marker, images were captured at 20x and the integrated density of immunoreactivity was measured in a region of interest (ROI) of 0.175 mm^2 . After background correction, the threshold was defined for all the microphotographs of the same marker.

The estimated number of muscle fibers found in the tibialis anterior muscle was calculated counting the number of fibers – delimited by the collagen IV staining – in 5 regions of 0,8043 μm^2 (captured at 20x) in a single muscle section. Then, the total area of the muscle slice (captured at 4x) was used to estimate the total number of muscle fibers. Two tibialis anterior muscle sections were used in each animal and obtained results were averaged.

To evaluate the sprouting of contralateral axons induced by the cervical injury, we first estimated the number of traced axons of the CST. Images from C1 sections containing the BDA tracer were taken at 40x and the total number of traced axons of the CST was counted in two different sections and averaged. Longitudinal sections were captured at 10x and then, the count of CST collaterals was performed at C3-C6 over 14 sections (separated by 50 μm each), and thus, evaluating a total extension of 700 μm of the spinal cord. Finally, the number of traced axons at C1 was used to normalize the sprouting in each animal.

Image analysis was performed by Fiji software.

Statistical analysis

Data is analyzed using GraphPad Prism 7 software and shown as mean \pm standard error of the mean (SEM). Differences were considered significant when $p < 0.05$. Shapiro-Wilk test confirmed a normal distribution of each response variable/group. Thus, functional results were analyzed by Student's t-test (unpaired), since variables

presented equal variance except for the adapted rotarod, pole test, DigiGait analysis, grip strength and NORT which were analyzed by two-way ANOVA repeated measures followed by pairwise post-hoc contrast with Bonferroni adjustment of p values. Histological results were analyzed by Student's t-test except for the MN distribution and the VGlut1 analysis at the dorsal horn that were evaluated by two-way ANOVA with same post-hoc as above. Considering Student's t-test for histological analysis, those variables that did not present equal variance (PNN analysis) were evaluated by Welch t-test.

Results

The lack of link protein 1 altered PNN composition in the spinal cord

We first corroborated the absence of link protein 1 in the central nervous system of *Crtll* KO mice. Immunofluorescence of the link protein 1 was neither detected in the lumbar spinal cord (Figure 2A) nor the motor cortex (Figure 3A). Since link protein 1 is implicated in the assembly of PNNs, we next studied PNN components of the *Crtll* KO mice by immunolabeling aggrecan, neurocan, Sema3A and tenascin-R in lumbar spinal cord samples (Figure 2A). No significant differences in the intensity of aggrecan labeling between WT and *Crtll* KO mice were observed (Figure 2B). Nevertheless, the aggrecan distribution in *Crtll* KO mice seemed more diffuse than in WT animals, suggesting a less dense PNN. Moreover, aggrecan was only distributed around the soma, with almost no staining around dendrites (Figure 2A), consistent with the motor cortex (Figure 3A, B). In addition, Sema3A staining at lumbar levels was reduced although not significantly in *Crtll* KO compared to WT mice ($p=0.06$; Figure 2A, B). Finally, *Crtll* KO mice showed a marked reduction of neurocan ($p<0.001$) and increased tenascin-R ($p<0.001$) in the spinal cord (Figure 2B). Notably, the tenascin-R increase was also visible across the grey matter

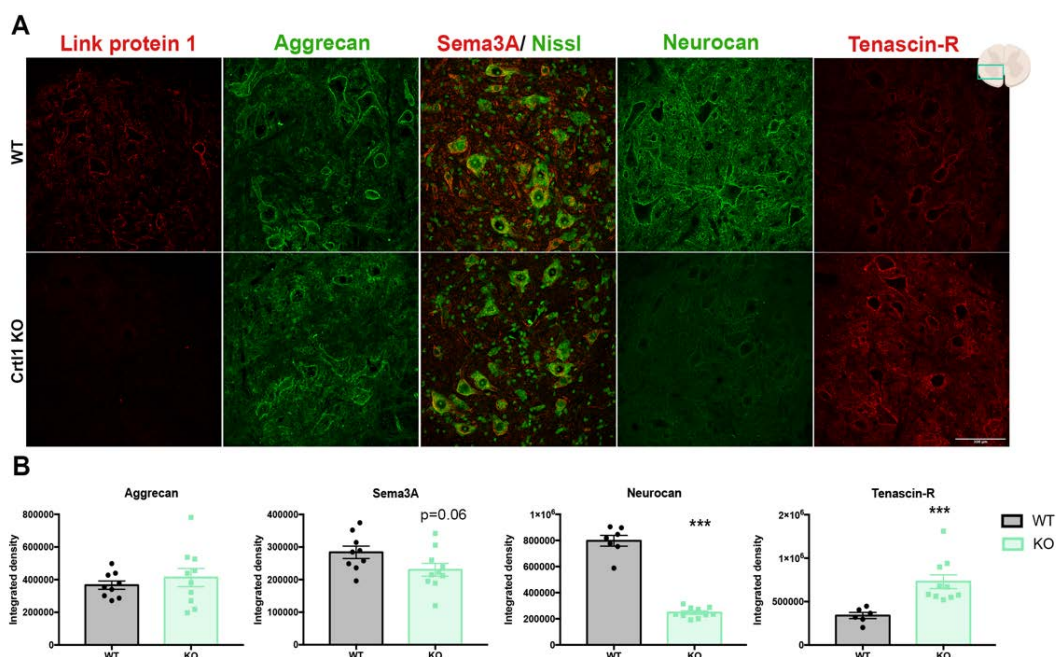


Figure 2. The lack of link protein 1 generates PNNs with altered proportion of their components in the lumbar spinal cord. A. Maximal projection of confocal images showing the expression of different components of PNNs around lumbar MNs: link protein 1 (red), aggrecan (green), semaphorin 3A (red) around Nissl positive-cells (green), neurocan (green) and tenascin-R (red). B. Quantification of the immunolabeling of PNN components. $N_{\text{total}}=19$ mice. Bar graphs are representing the mean values \pm SEM. Scale bar: 100 μm . ** $p<0.01$, *** $p<0.001$ by Welch t-test. *Crtll*: cartilage link protein 1; WT: wild type; KO: knock-out.

parenchyma (Figure 2A). In contrast, the expression of tenascin-R moderately decreased in cortical PNNs of *Crtll* KO mice, albeit not significantly (Figure 3B). Neurocan was not quantified in the motor cortex due to the faint staining observed in the WT group (Figure 3A).

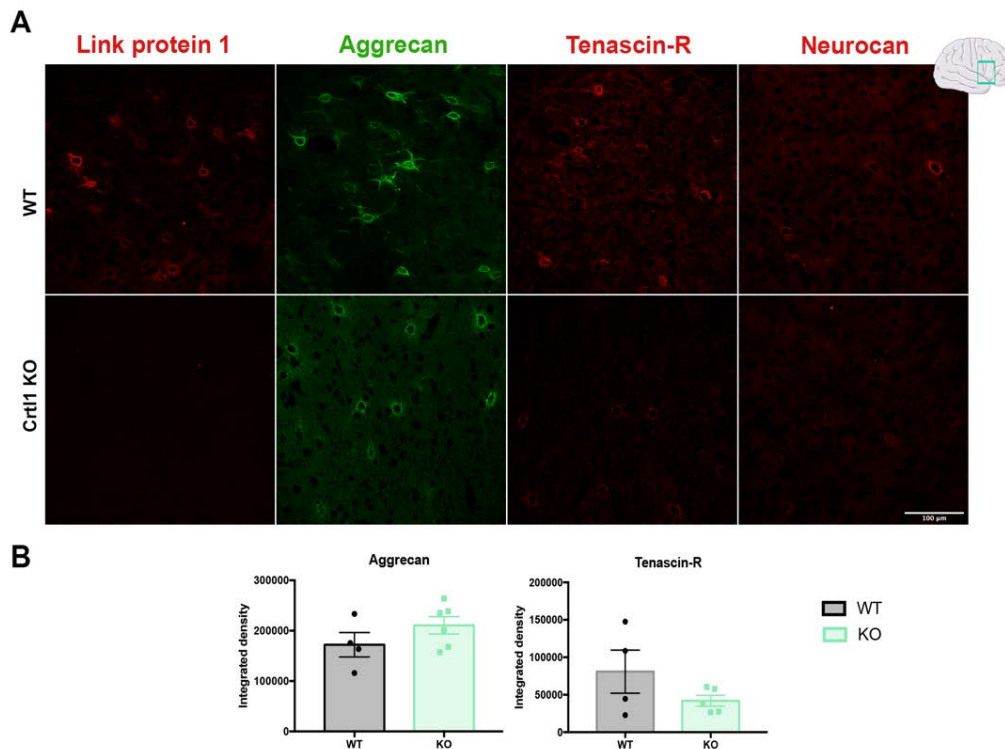


Figure 3. Characterization of PNN components in the motor cortex of the *Crtll* KO mice. A. Confocal images in which cortical PNN are stained against the link protein 1 (red), aggrecan (green), tenascin-R (red) and neurocan (red). B. Quantification of the immunolabeling of aggrecan and tenascin-R around neurons. Neurocan quantification is not shown due to the little staining found in the WT group. $N_{\text{total}}=10$ mice. Bar graphs are representing the mean values \pm SEM. Scale bar: 100 μ m. Significant differences were neither found by unpaired t-test (aggrecan) nor Welch t-test (tenascin-R). *Crtll*: cartilage link protein 1; WT: wild type; KO: knock-out.

Crtll KO mice presented reduced body weight and hypoactivity

Crtll KO mice of both sexes had significantly less weight compared to WT mice ($p<0.01$ in males and $p<0.001$ in females; Figure 4A). Evaluation of general overground locomotion (Open field arena) revealed that *Crtll* KO mice were hypoactive since their travel distance ($p<0.001$), locomotor velocity ($p<0.001$) and time locomoting ($p<0.001$) were reduced compared to WT mice. Similarly, *Crtll* KO mice showed reduced explorative behavior, with fewer rearings ($p<0.001$) (Figure 4B).

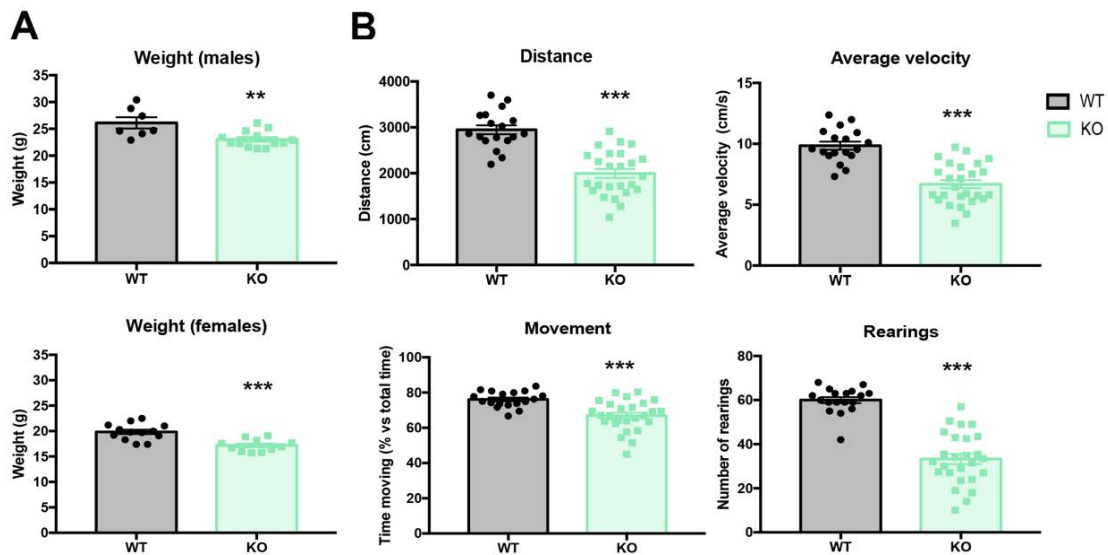


Figure 4. *Crtll* KO mice present reduced weight and hypoactivity assessed by Open Field test. A. Males and females *Crtll* KO mice presented reduced body weight. B. Open Field test revealed that *Crtll* KO present hypoactivity observed in the total distance traveled, average velocity, percentage of time in movement and number of rearing performed in 5 minutes. $N_{\text{total}} = 44$ mice. Bar graphs are representing the mean values \pm SEM. ** $p < 0.01$, *** $p < 0.001$ by unpaired t-test. WT: wild type; KO: knock-out.

Animals lacking link protein 1 displayed impaired locomotion, motor coordination and abnormal gait performance.

The observed hypoactivity prompted us to investigate whether it was caused by motor deficits. We addressed this using some complementary functional motor tests that allow us to evaluate motor coordination, locomotion, and motor learning. Animals lacking link protein 1 could not reach the maximum velocity values obtained by WT mice on a treadmill ($p < 0.001$, Figure 5A). Adapted rotarod gives us information about motor coordination and motor learning. We found that *Crtll* KO mice could not stay as long on the rotarod as WT mice (significantly different in the last two days of testing ($p < 0.001$; Figure 5B)). Performance of WT mice on the rotarod also improved over four consecutive days whereas *Crtll* KO mice exhibited limited improvement (interaction effect over time: $p < 0.001$; day 1 vs 2 WT and KO $p > 0.05$; day 2 vs 3 WT $p < 0.001$, KO $p > 0.05$; day 3 vs 4 WT $p < 0.01$, KO $p > 0.05$). During the pole test (also for motor coordination), WT mice turned 180° to orient themselves downward and descend the pole, whereas almost all *Crtll* KO mice failed to turn 180° and descended in a horizontal position (Figure 5C). The analysis showed that *Crtll* KO mice spend more time turning down (T-turn; 1st trial $p < 0.001$ and 2nd trial $p < 0.01$) and descending the pole (T-descend) (both trials $p < 0.001$) compared to WT mice (Figure 5D). In contrast, *Crtll* KO mice did not present alterations in the limb strength evaluated by the grip strength test compared to WT (Figure 5E; $p > 0.05$).

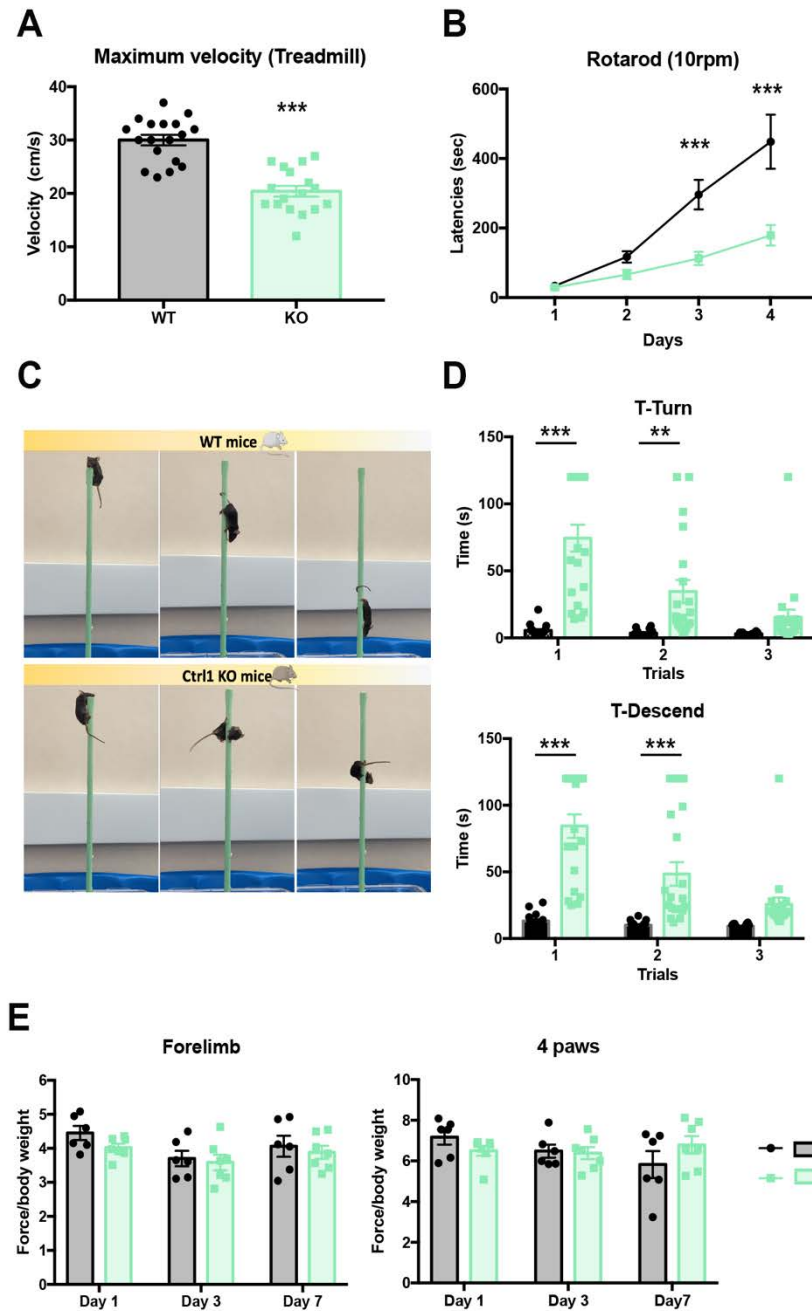


Figure 5. *Crtl1* KO mice displayed altered locomotor activity, coordination, and motor learning. A. Evaluation of the maximum velocity reached by *Crtl1* KO and WT mice on a treadmill. $N_{\text{total}} = 35$ mice. B. Quantification of the daily amount of time (latency) of *Crtl1* KO and WT mice sustained performance in the adapted rotarod during four consecutive sessions. $N_{\text{total}} = 30$ mice. C. Photographs representing the two possibilities to climb down the pole: turning 180° (WT mice) or climbing down in a horizontal position (*Crtl1* KO mice). D. Representation of the time required for the *Crtl1* KO and WT mice to turn down (T-turn) and descend the pole (T-descend) in three consecutive trials. $N_{\text{total}} = 38$ mice. E. Assessment of the grip strength of the forelimb and the 4 paws of *Crtl1* KO and WT mice for three days. $N_{\text{total}} = 14$ mice. Data are representing the mean values \pm SEM. *** $p < 0.001$ by unpaired *t*-test for the maximum velocity and ** $p < 0.01$, *** $p < 0.001$ by two-way ANOVA (*Adapted rotarod*: time $F_{3,123} = 53.72$, $p < 0.001$; group $F_{1,41} = 19.76$, $p < 0.001$; interaction $F_{3,123} = 12.66$, $p < 0.001$; *T-turn*: time $F_{2,72} = 24.63$, $p < 0.001$; group $F_{1,36} = 27.34$, $p < 0.001$; interaction $F_{2,72} = 20.82$, $p < 0.001$; *T-descend*: time $F_{2,72} = 27.79$, $p < 0.001$; group $F_{1,36} = 39.67$, $p < 0.001$; interaction $F_{2,72} = 20.93$, $p < 0.001$) followed by post hoc test with Bonferroni correction. *Crtl1*: cartilage link protein 1; WT: wild type; KO: knock-out.

Considering the marked motor discoordination observed, DigiGait was used for walking pattern analysis in both genotypes. Percentages of the stride phases in the *Crtll* KO mice were altered in both forelimb ($p < 0.001$ in brake and $p < 0.05$ in propulsion phase) and hindlimb ($p < 0.001$ in swing and propulsion phase) compared to WT mice. Consequently, these alterations decreased the stance/swing ratio in the hindlimb of *Crtll* KO mice compared to WT mice ($p < 0.001$). The plantar placement of the hindlimb of *Crtll* KO mice was also reduced, represented as a smaller paw area compared to WT mice. dA/dT_{\min} and dA/dT_{\max} refer to the maximal rate of change of paw area in contact with the treadmill belt during the propulsion and braking phase, respectively. Thus, dA/dT_{\min} shows how rapidly the animal can propel itself into the next step, while dA/dT_{\max} shows how quickly the limb is loaded during the initial period of stance (Figure 6B). Our data demonstrated that *Crtll* KO mice presented altered values in both parameters compared to WT mice (Figure 6C) in the forelimb ($p < 0.05$ in dA/dT_{\min} analysis) and hindlimb ($p < 0.01$ in the dA/dT_{\min} and $p < 0.001$ in the dA/dT_{\max}).

Since PNNs have already been described to have a role in memory consolidation (Nadine et al., 2009; Fawcett et al., 2019), we corroborated the altered functionality of PNNs in our *Crtll* KO mice by evaluating short- and long-term memory using the NORT (Suppl. Figure 3A). *Crtll* KO mice had a greater ability to recognize a new object in the short-term memory test ($p < 0.05$ at 2 minutes) but showed impaired long-term memory consolidation ($p < 0.01$ at 2 minutes; Suppl. Figure 3B).

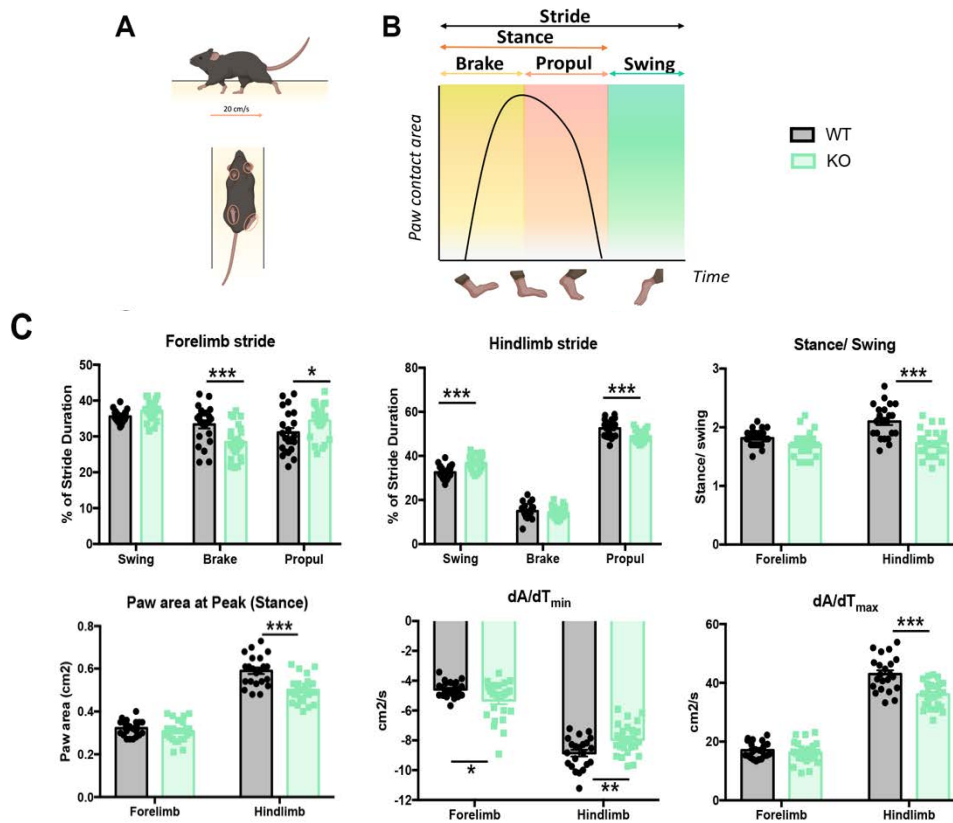


Figure 6. *Crtll* KO mice showed altered gait performance. A. Scheme of the experimental procedure in which mice run on a treadmill belt at 20 cm/s and their paws (marked in orange) are analyzed. B. Schematic representation of the different phases of the stride. The stride is divided into two parts: the swing and the stance phase, the latter is further divided into the brake and propulsion phase. The swing phase coincides when there is no paw contact with the treadmill belt. The brake phase includes from the initial paw contact to the maximum paw contact and the propulsion phase includes from the maximum paw contact to just before the swing phase starts. C. Gait analysis: representation of the % of duration of the different phases of the stride in both fore and hindlimb, the Stance/swing ratio, the maximum paw area at the peak, and the rate of change of paw area contact with the treadmill belt (dA/dT). $N_{total}=23$ mice. Bar graphs are representing the mean values \pm SEM. * $p<0.05$, ** $p<0.01$, *** $p<0.001$ by two-way ANOVA (Forelimb stride: time $F_{2,92}=13.12$, $p<0.001$; group $F_{1,46}=1.476$, $p=0.231$; interaction $F_{2,92}=8.03$, $p=0.006$; Hindlimb stride: time $F_{2,92}=10.96$, $p<0.001$; group $F_{1,46}=3.138e-010$, $p>0.99$; interaction $F_{2,92}=13.27$, $p<0.001$; Stance/swing: time $F_{1,46}=17.96$, $p<0.001$; group $F_{1,46}=20.74$, $p<0.001$; interaction $F_{1,46}=14.48$, $p=0.004$; Paw area at peak: time $F_{1,46}=12.39$; $p<0.001$; group $F_{1,46}=12.73$, $p=0.009$; interaction $F_{1,46}=32.52$, $p<0.001$; dA/dT_{min} : time $F_{1,46}=378.2$, $p<0.001$; group $F_{1,46}=0.147$, $p=0.703$; interaction $F_{1,46}=21.77$, $p<0.001$; dA/dT_{max} : time $F_{1,46}=15.99$; $p<0.001$; group $F_{1,46}=12.78$, $p<0.001$; interaction $F_{1,46}=29.06$, $p<0.001$) followed by post hoc test with Bonferroni correction. WT: wild type; KO: knock-out; Propul: propulsion.

Crtll KO mice presented increased excitability of spinal reflexes

Electrophysiological tests were used to assess if the motor impairments observed in the *Crtll* KO mice were linked to alteration in spinal networks. Stimulation of the sciatic nerve elicited a M wave with reduced initial ($p<0.05$) and final latency ($p<0.01$) in *Crtll* KO mice compared to WT mice (Figure 7B). Regarding the stretch reflex (or H-reflex), *Crtll* KO mice exhibited an increased H/M ratio compared to WT mice ($p<0.001$). Since the stretch reflex is a monosynaptic reflex in which only proprioceptive (Ia)

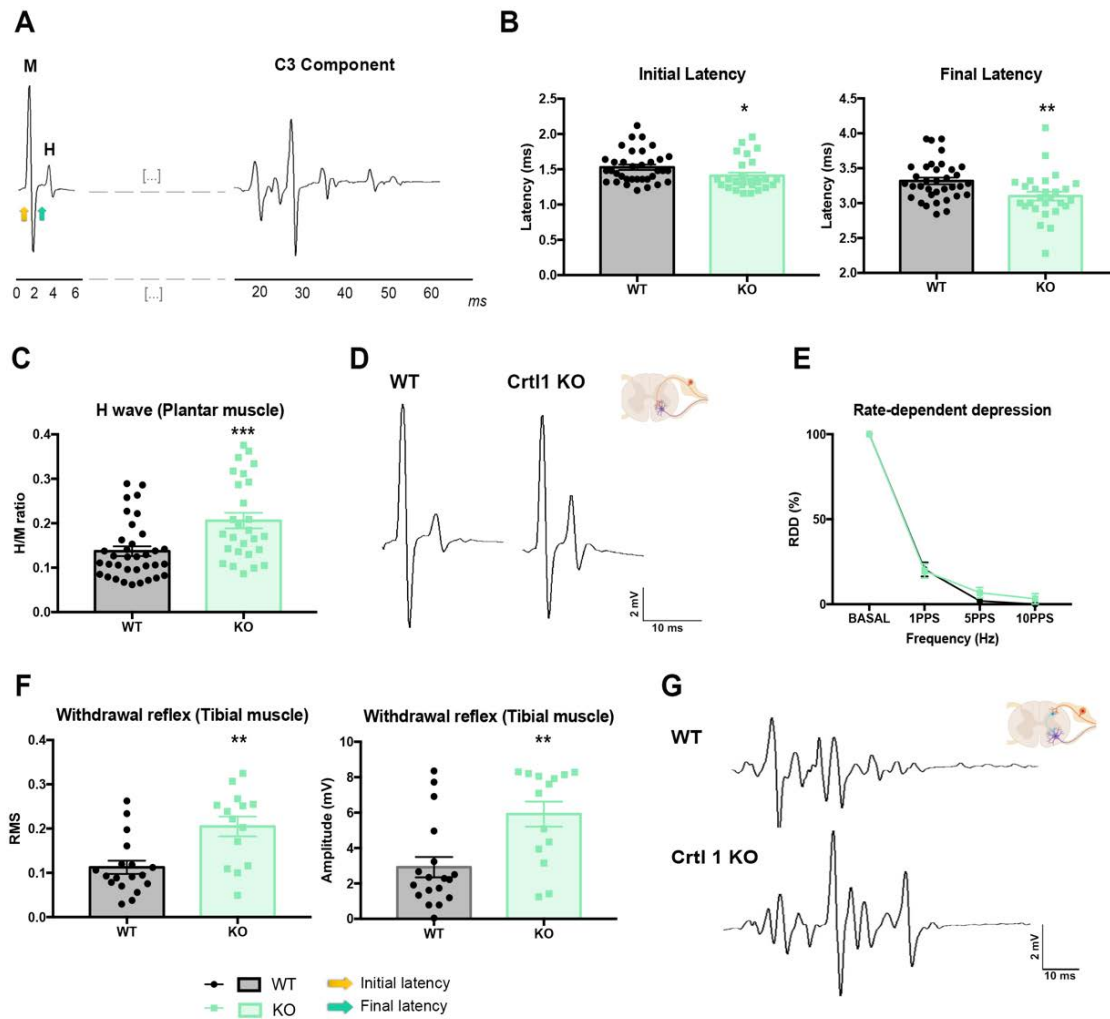


Figure 7. *Crt11* KO mice presented increased excitability of spinal circuits observed in both monosynaptic and polysynaptic spinal reflexes. A. Representative image of the recordings studied. At the left side of the image, it is represented the different components of the compound muscle action potential (CMAP): the M and the H wave. These waves are measured to evaluate the stretch reflex (monosynaptic). $N_{\text{total}} = 62$ mice. The colored arrows represent the onset (yellow) and final (green) latencies of the M wave. At the right side of the image, the C3 component of the withdrawal reflex is represented, whose maximum amplitude and the area under the curve are analyzed. B. Quantification of the onset and final latencies of the M wave studied in the plantar muscle. C. H/M ratio studied in the plantar muscle. D. Representative electromyographs showing the CMAP in the WT and *Crt11* KO mice. E. Depression profile of the H wave after consecutive stimulations at different frequencies. F. Evaluation of the area under the curve (RMS) and maximum amplitude of the C3 component of the withdrawal reflex, recorded at the ipsilateral tibialis anterior muscle. $N_{\text{total}} = 32$ mice. G. Representative electromyographs showing the C3 component of the withdrawal reflex in the WT and *Crt11* KO mice. Data are representing the mean values \pm SEM. * $p < 0.05$, ** $p < 0.01$, *** $p < 0.001$ by unpaired t-test. No significant differences were found in the depression of the H wave (RDD) analyzed by two-way ANOVA (time $F_{3,180} = 926.8$, $p < 0.001$; group $F_{1,60} = 0.514$, $p = 0.476$; interaction $F_{3,180} = 0.781$, $p = 0.506$) followed by a post hoc test with Bonferroni correction. *Crt11*: cartilage link protein 1; WT: wild type; KO: knock-out.

afferences and MNs participate, this hyperexcitability could be caused by an alteration of local circuitry between MNs and Ia afferences, or inhibitory descending pathways. These inhibitory descending pathways regulate the amount of pre-synaptic inhibition

that Ia afferents received and thus, indirectly adjust the stretch reflex (Faist et al., 1994). To elucidate the origin of this hyperexcitability, we studied the state of inhibitory descending pathways by evaluating the RDD of the H wave. Given that *Crtll* KO and WT mice presented a similar pattern of depression, we assumed that these descending pathways were unaffected (Figure 7E). Thus, the hyperexcitability observed in the H/M ratio may be caused by a change at the local MN circuitry. Next, the polysynaptic withdrawal reflex was evoked at the tibialis anterior muscle and assessed by C3 component evaluation (Figure 7G). Increased hyperreflexia in both the ipsilateral ($p < 0.01$; Figure 7F) and contralateral side (Suppl. Figure 4) was observed in transgenic animals compared to WT group, indicating a general hyperexcitability of the spinal reflex circuits in *Crtll* KO mice.

Mice with aberrant PNNs exhibited a general increase in excitatory but not inhibitory synapses

To complement the functional analysis and further study spinal circuits, we evaluated the composition of spinal synapses in *Crtll* KO mice. We found that lumbar MNs from *Crtll* KO mice received a greater number of excitatory (VGlut1), but not inhibitory (VGAT) inputs compared to WT mice (Figure 8A, B; $p < 0.001$ in the VGlut1 analysis). In contrast, however, KCC2, whose reduction is a hallmark of hyperexcitability (Boulenguez et al., 2010), was unaltered in the *Crtll* KO group (Figure 8A, B). Therefore, the hyperexcitability observed in the electrophysiological test could be caused by an increase in excitatory inputs. Consistent with this, the increased expression of VGlut1 was also notable in the dorsal horn of *Crtll* KO mice ($p < 0.001$). Of note, *Crtll* KO mice showed increased KCC2 staining in the dorsal horn ($p < 0.001$; Suppl. Figure 5).

Given that motoneurons from *Crtll* KO mice presented a high number of proprioceptive inputs (VGlut1), we wondered whether this increase could impact on the number of C-boutons (marked with ChAT) received (Figure 8C). We observed an increase of both VGlut1 and C-boutons in MNs from *Crtll* KO compared to WT mice ($p < 0.001$; Figure 8D), suggesting a general increase of excitatory synapses around MNs with aberrant PNNs.

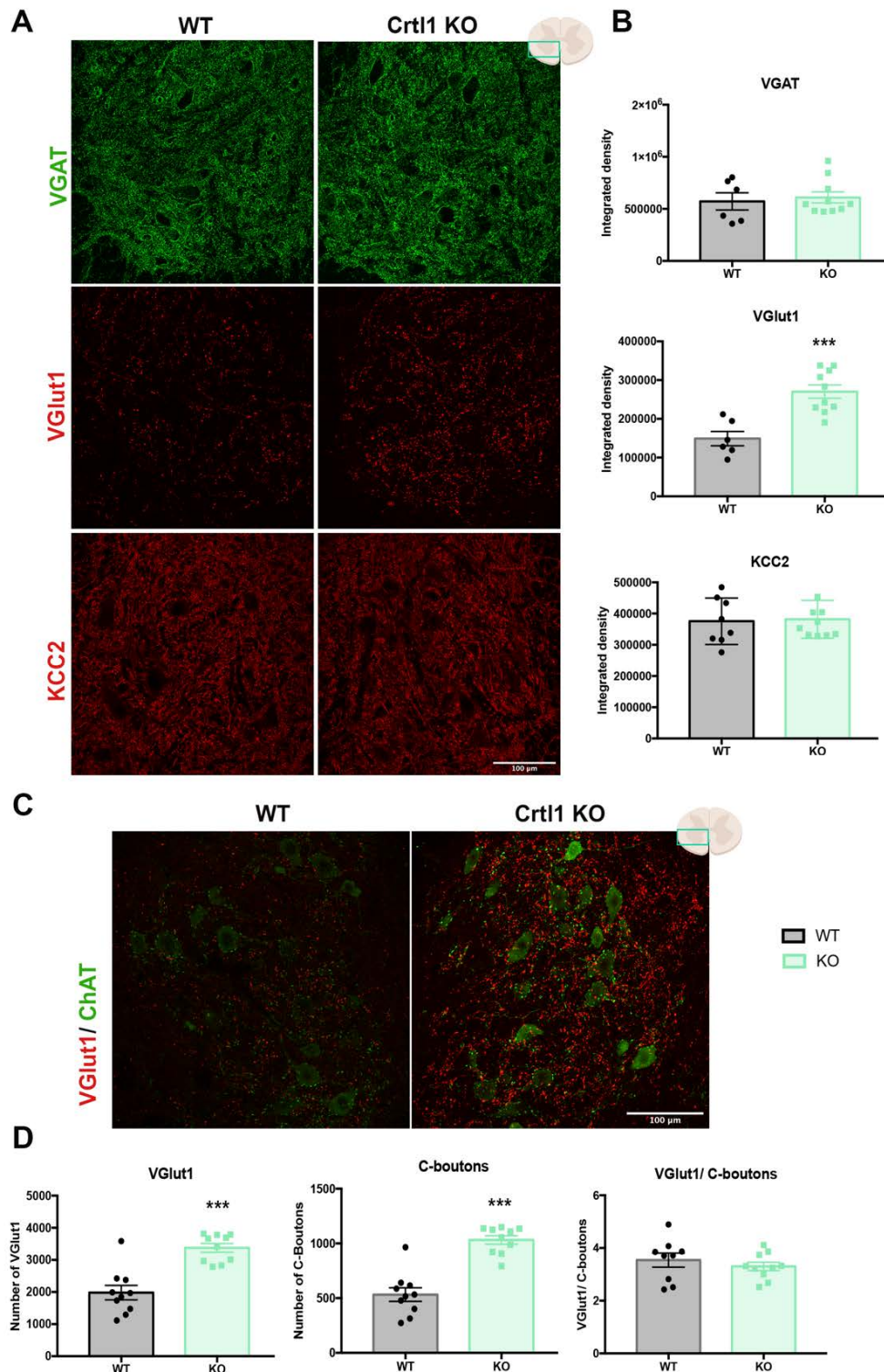


Figure 8. *Crt11* KO mice exhibited a general increase in excitatory synapses around lumbar motoneurons. A. Confocal images representing synapses around lumbar motoneurons (VGAT and VGlut1) and the KCC2 transporter anchored in motoneurons membrane. B. Quantification of the integrated density of the immunoreactive staining around lumbar motoneurons. C. Confocal images showing the amount of proprioceptive afferents (VGlut1) and C-boutons (ChAT) in *Crt11* KO and WT mice. D. Quantification of the number of VGlut1 and CHAT-positive dots and their ratio. Scale bar: 100 μ m. $N_{\text{total}} = 20$ mice. Bar graphs are representing the mean values \pm SEM. ** $p < 0.01$, *** $p < 0.001$ by unpaired t-test. VGlut1: vesicular glutamate transporter I; VGAT: vesicular GABA transporter; ChAT: choline acetyltransferase; *Crt11*: cartilage link protein I; WT: wild type; KO: knock-out.

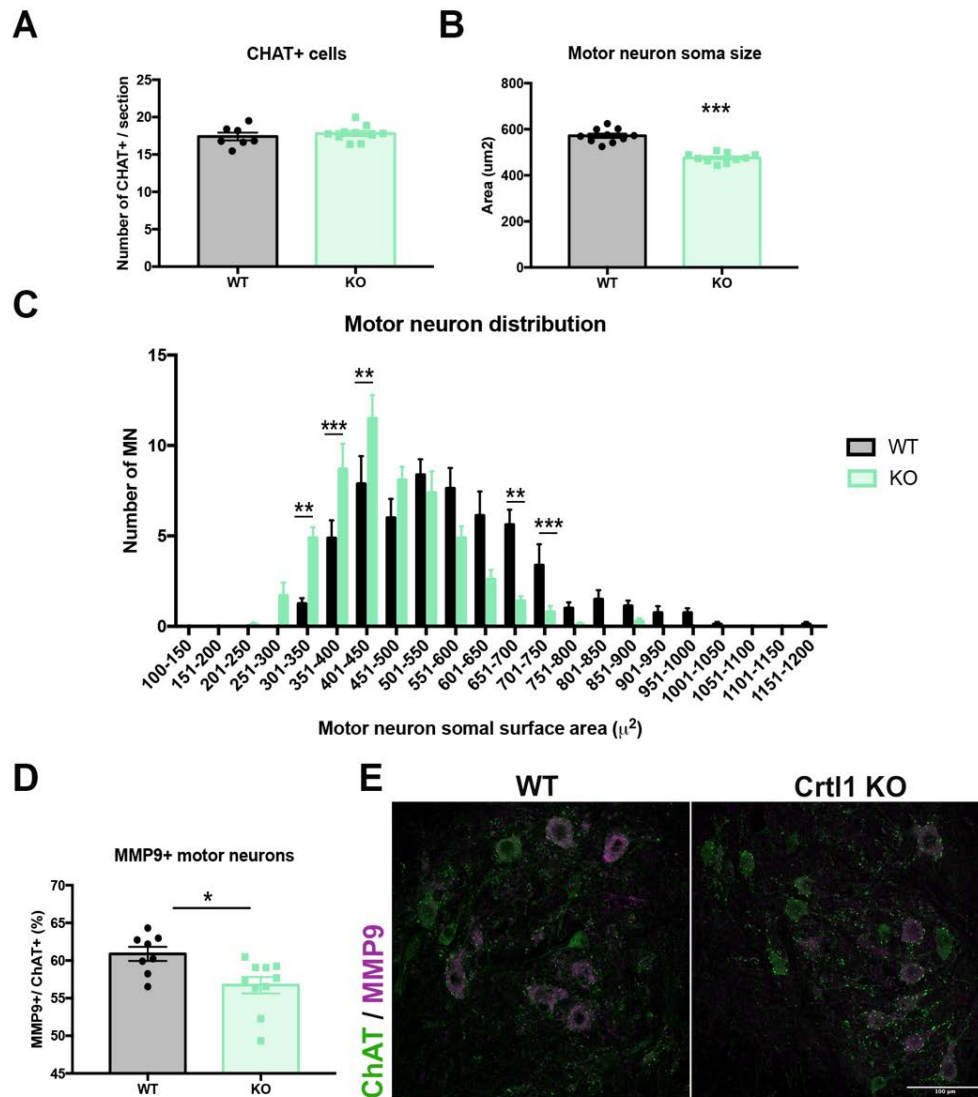
Altered PNNs modified the lumbar motoneuron size and motor unit properties

We discarded that the motor impairment was caused by MN loss as we did not find differences in the number of ChAT+ cells between groups (Figure 9A). However, we noticed a reduction in the mean area of motoneuron soma of *Crtll* KO compared to WT animals ($p < 0.001$; Figure 9B). This reduction could be mediated by a general reduction in the somatic area of all motoneurons or due to a decrease in the percentage of bigger neurons. Thus, we generated a distribution graph representing the number of MN found depending on their size. Figure 9C revealed a significant increase in the number of small MNs (between 300-450 μm) and a reduction in large MNs (between 650-750 μm) in *Crtll* KO compared to WT mice ($p < 0.01$, $p < 0.001$). To confirm whether this change in soma size is related to MN physiological properties, we stained MNs with anti-MMP9, a marker of MN from fast motor units (Kaplan et al., 2014) (Figure 9E). We found a reduction in the percentage of MMP9+/ChAT+ cells in *Crtll* KO compared to the WT group ($p < 0.05$; Figure 9D). Altogether, these results suggested that *Crtll* KO presents a shift in the lumbar MN pool composition, leading to an increase in slow motor units and a decrease in fast ones.

To evaluate the functional repercussion of this shift, motor unit recruitment and muscle properties were assessed (Suppl. Figure 6). *Crtll* KO mice presented a higher mean amplitude of their motor units (SMUA) compared to WT mice in both plantar ($p < 0.01$) and tibialis anterior muscle ($p < 0.001$). At the muscle level, *Crtll* KO mice showed a reduced number of muscle fibers in the tibialis anterior muscle ($p < 0.05$), as well as a reduction in the weight of the muscle studied ($p < 0.05$ in absolute values and $p < 0.001$ related to the body weight).

(Figure in the next page)

Figure 9. The lack of link protein 1 modified the properties of lumbar motoneurons. Quantification of the number of ChAT-positive cells/ section of the lumbar spinal cord (A) and the neuronal soma area (B). C. Motoneuron distribution of 55-70 motoneurons/animal based on the neuronal soma surface area. D. Percentage of ChAT-positive cells stained against the MMP9 marker. E. Representative microphotographs of the ventral horn of the lumbar spinal cord in which ChAT-positive (green) and MMP9-positive (purple) are shown. Scale bar: 100 μm . $N_{\text{total}} = 20$ mice. Data are representing the mean values \pm SEM. * $p < 0.05$, *** $p < 0.001$ by unpaired t-test. ** $p < 0.01$, *** $p < 0.001$ by two-way ANOVA (time $F_{21,336} = 47.31$, $p < 0.001$; group $F_{1,16} = 1.012$, $p = 0.329$; interaction $F_{21,336} = 5.684$, $p < 0.001$) followed by post hoc test with Bonferroni correction. ChAT: choline acetyltransferase, MMP9: matrix metalloproteinase 9; *Crtll*: cartilage link protein 1; WT: wild type; KO: knock-out.



Crt11 KO mice displayed increased corticospinal sprouting after spinal cord injury

To further evaluate the impact of cartilage link protein 1 on motor function, we next studied the corticospinal tract (CST) and its potential to sprout after SCI (Figure 10A). No significant differences were found in the number of fibers traced CST fibers between groups measured at C1 spinal level (Figure 10B, C). After unilateral dorsal hemisection at the C4 level, the contralateral CST of *Crt11* KO mice showed increased sprouting of spared axons below the injury level compared to WT mice ($p < 0.05$). Once contralateral axons reached the denervated side of the cord, a high density of small axons was found near the midline rather than observing long sprouts crossing the grey matter. No significant differences were observed in the percentage of contralateral projections between uninjured groups (Figure 10D, E).

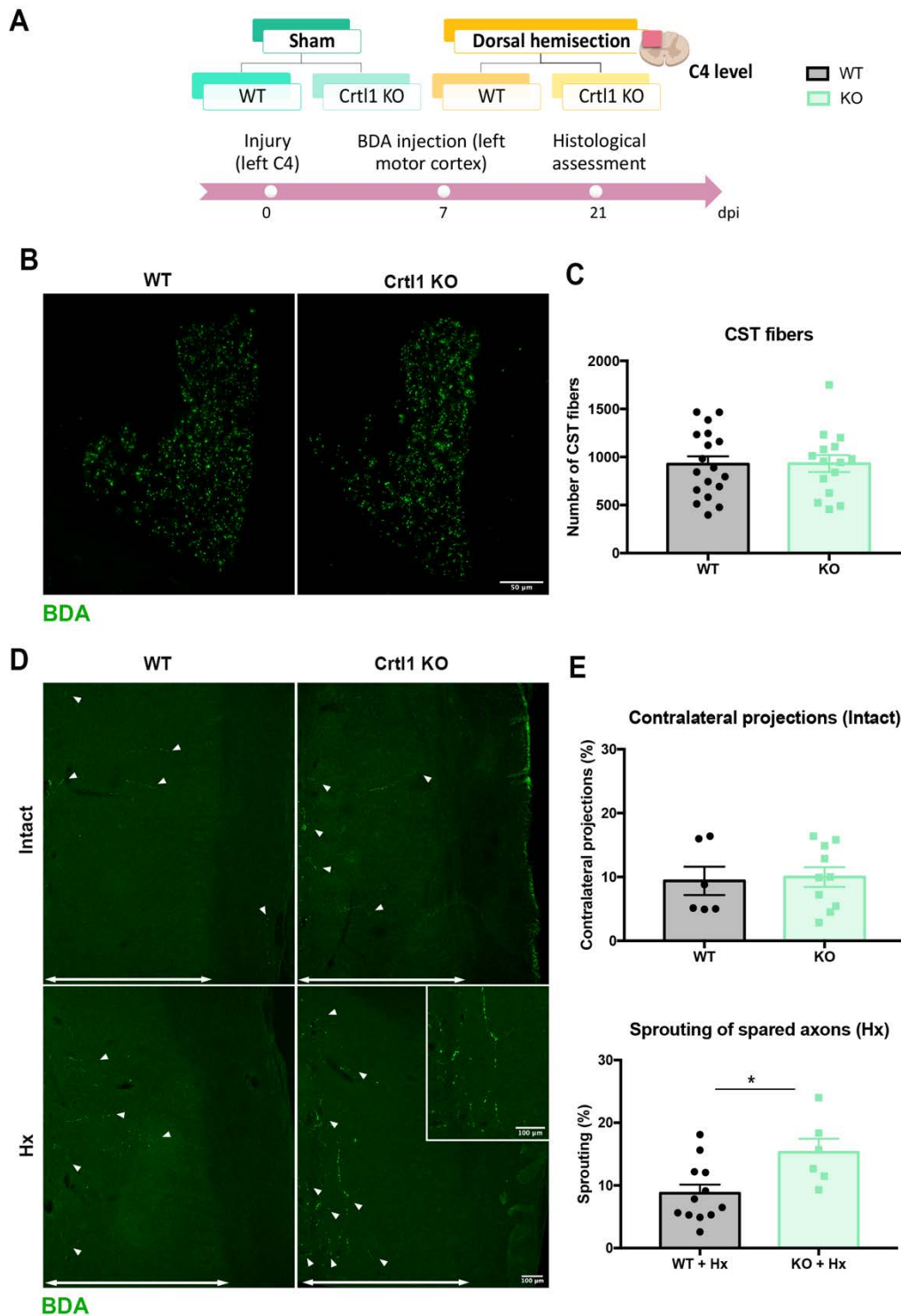


Figure 10. Sprouting of the intact CST after contralateral injury. **A.** Schematic representation of the experimental groups and the timeline of the experimental procedure. **B.** Representative cross-section images of the traced corticospinal axons using BDA (green) at C1 level. **C.** Quantification of the total number of traced axons of the corticospinal level at C1. **D.** Confocal images showing cervical longitudinal sections (C3-C6) in which contralateral projections are labeled with the BDA tracer (green) and sprouts are marked with white arrows. The arrows with two arrowheads delimitate the grey matter in each photograph while the part not included corresponds to the white matter. **E.** Percentage of CST collateral axons in the intact (above) and injured groups (below) based on the number of CST fibers counted at C1 level in each animal. Scale bar: 100 μ m. Data are representing the mean values \pm SEM. * $p < 0.05$ by unpaired t-test. Crt1l: cartilage link protein 1; WT: wild type; KO: knock-out; Hx: hemi-section.

Discussion

Although most spinal MNs are wrapped by PNNs, their functional role and the impact of their degradation remain largely unexplored. However, chABC application on the spinal cord has been used extensively in experimental models to promote axonal growth post-SCI (Bradbury et al., 2002; Fawcett, 2015). Thus, our goal was to assess the role of spinal PNNs on motor spinal networks.

Crtll KO mice show aberrant PNNs with an altered proportion of their components

To study the role of PNNs, we used *Crtll* KO mice as they lack the *Crtll/HAPLN1* gene, which encodes the cartilage link protein 1, crucial for PNNs formation during development. Once PNNs are formed, link proteins stabilize the interaction between CSPGs to the hyaluronan backbone in the net structure (Spicer et al., 2003). In the present work, we have found that aggrecan can still accumulate around the neuronal soma despite the lack of link protein 1, generating aberrant PNNs in these *Crtll* KO mice. Similar findings were reported by Carulli *et al* in the brain (Carulli et al., 2010). The presence of aggrecan allowed tenascin-R to attach to the remaining CSPGs and hence, contribute to this aberrant PNN deposition. In contrast, neurocan was almost absent in PNNs of *Crtll* KO mice. These altered PNNs were also found in neurons of the motor cortex. Thus, *Crtll* KO mice presented aberrant PNNs with disorganized morphology and altered proportion of their components.

Aberrant PNNs increase the excitability of spinal circuits

PNNs are highly organized structures that play a crucial role in stabilizing mature synapses initially formed during development. In our study, *Crtll* KO mice showed an increased number of excitatory, but not inhibitory synapses around lumbar MNs. One of the mechanisms that allow PNNs to restrict synapse formation is the expression of Sema3A (Vo et al., 2013). In our KO mice, we found a slight reduction of Sema3A in PNNs, which could partially facilitate synaptogenesis. The reduced levels of neurocan could also lead to this increased synaptic content since it contributes to neuronal outgrowth inhibition (Shen et al., 2009). This increased synapse formation was also observed in mice lacking different PNN components (Geissler et al., 2013) and after chABC injection (Pyka et al., 2011). Interestingly, chABC application modifies both inhibitory and excitatory neurotransmission. The lack of inhibitory inputs in our transgenic mice could

be attributed to the buffering role of PNNs conferred by the negative charge of their CSPGs. Both CSPG digestion and PNN reduction around denervated neurons after SCI change the transmembrane Cl^- gradient, altering GABAergic neurotransmission (Geissler et al., 2013; Hirono et al., 2018; Sánchez-Ventura et al., 2021). However, *Crtll* KO mice had CSPGs accumulating around the neuronal soma, whose negative charge can still have functional effects (Glykys et al., 2014). Similarly, the presence of the tenascin-R protein, which regulates GABA release (Saghatelian et al., 2000), can also contribute to the maintenance of inhibitory synapses in these transgenic animals. Thus, the altered composition of PNNs on *Crtll* KO mice produce an increased number of excitatory but not inhibitory synapses.

Specifically, we observed an increase of VGlut1-labeled boutons, corresponding to proprioceptive contacts (Alvarez et al., 2004). In fact, PNN breakdown has been associated with altered glutamatergic transmission (Frischknecht et al., 2009). We also observed an increased amount of C-boutons, corresponding to cholinergic interneurons (Witts et al., 2014). This finding is quite interesting since prior work has suggested that cholinergic and proprioceptive inputs compete for contact spinal MNs, dependent on neural activity. Thus, increased activity in proprioceptive terminals should correlate with fewer cholinergic inputs and *vice versa* (Jiang et al., 2016). Our findings suggest that this synaptic competition was absent in *Crtll* KO mice, where both VGlut1 and C-bouton inputs were increased, probably because MNs with altered PNNs have more synaptic space available. Nevertheless, these newly formed synapses might not be functional (Geissler et al., 2013).

The increase in excitatory synapses found in the ventral and dorsal horn can foster a more excitable milieu in the developmental spinal cord, that can affect MN maturation and motor circuitry function. *Crtll* KO mice showed an increased number of small MNs and a reduction of larger ones. The increased excitability found in the spinal cord of KO mice may affect the physiological properties of α -MNs during development, directing the maturation of MNs into a more excitable phenotype, compatible with smaller MNs (Martínez-Silva et al., 2018). In fact, fast and slow MNs have different excitability, and this can already be distinguished in the neonatal stage based on their firing pattern (Manuel and Zytynicki, 2019). Since PNNs can affect this firing pattern, and aberrant PNNs increase the membrane capacitance leading to excitable changes (Tewari et al., 2018), it is plausible that altered PNNs generate a slow MN-like firing pattern that increases the percentage of MNs maturing towards a slower profile. In fact, the role of

PNNs in neural maturation was already described in parvalbumin-positive cells (Sugiyama et al., 2008; Beurdeley et al., 2012). Overall, a correct PNN composition might be crucial for the function and identity of MNs, and their disorganization can affect the role and the connectivity of these neurons.

These changes in the properties of lumbar MNs have an impact on neuromuscular function. Indeed, the loss of fast MNs, which tend to innervate more and larger muscle fibers (Manuel and Zytnicki, 2019), can explain the decreased number of muscle fibers and the reduced weight of the tibialis anterior muscle. To compensate the loss of fast MNs, slow MNs would comparatively innervate more fibers than WT mice generating bigger amplitudes and thus, becoming larger than the ones from WT mice (Suppl Figure 6). However, these small changes did not have a functional repercussion on the muscle force assessment.

The disruption of spinal circuits leads to motor impairment

By electrophysiological tests, we evaluated monosynaptic and polysynaptic reflexes and we observed an increased excitability in the spinal circuits of *Crtll* KO mice. We also detected a reduction in both initial and final latencies of M wave in *Crtll* KO mice compared to WT. However, this reduction is unlikely to be related to altered nerve conduction velocity, since the formation of the nodes of Ranvier depends on link protein 2 expression (Bekku et al., 2010). Neurocan reduction could indirectly affect the structure of the node of Ranvier, which is also rich in CSPGs (Bekku and Oohashi, 2011), but we think that these shorter latencies can be easily explained by the reduced size of *Crtll* KO mice.

Moreover, *Crtll* KO mice presented hypoactivity and impaired motor function in the different functional tests performed. The hypoactivity observed could be explained by fewer fast MNs, which innervate rapidly contracting motor units (Olson and Swett Jr., 1969). The motor impairment was confirmed in the rotarod and pole tests, after observing that *Crtll* KO mice could not reach the maximum velocity obtained by WT, lasted a shorter time in the rotarod and needed more time to descend the pole. These results together with the gait abnormalities observed in the DigiGait analysis suggested impaired motor coordination in mice with altered PNNs. Similar functional outcomes were reported by Freitag et al. in animals with altered PNNs (Freitag et al., 2003). *Crtll* KO mice also present altered motor learning, assessed by the adapted rotarod. Learning and memory processes have been studied in the brain of animals with altered PNNs (Montag-

Sallaz and Montag, 2003) or after chABC administration (Hylin et al., 2013; Tsien, 2013). In our study, *Crtll* KO mice exhibited impaired memory consolidation, but improved ability to recognize a new object, as previously described (Romberg et al., 2013). However, this is the first time that motor learning has been assessed in the context of spinal PNNs.

Overall, the present work demonstrates the involvement of PNNs in motor function through properly wiring spinal circuits and determining the identity of lumbar MNs. Nevertheless, alteration of PNNs located in brain regions related to motor control, as well as the skeletal abnormalities described in these mice (Czipri et al., 2003), can contribute to this motor impairment.

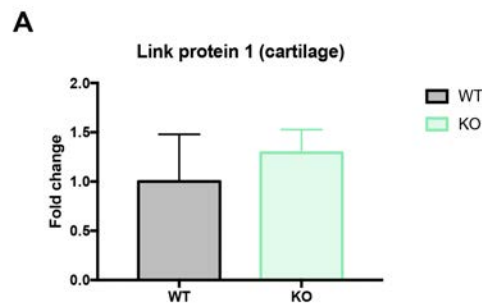
Aberrant PNNs increase sprouting after spinal cord injury

The role of PNNs in restricting plasticity has been known for decades (Pizzorusso, 2002). In fact, chABC application has been widely used to promote axon growth. When it is applied in a denervated sensory nucleus of the brainstem after a cervical SCI, an increased collateral sprouting is observed (Massey et al., 2006). Increased plasticity was also observed in our *Crtll* KO mice, shown by enhanced sprouting of spared contralateral axons after injuring the corticospinal tract. Therefore, alterations of PNNs generate a growth permissive environment for axons to sprout after injury. However, the application of chABC has a stronger impact on the sprouting of spared axons compared to our *Crtll* KO mice, based on the percentage of sprouting of contralateral axons below the injury (Starkey et al., 2012). This can be due to the incomplete loss of CSPGs around *Crtll* KO mice's neurons, that inhibits neural regeneration (Shen et al., 2009). Moreover, chABC acts on all CSPGs in the CNS, although only 2% are in PNNs (Fawcett, 2015), facilitating a more plastic milieu and hindering the distinction of the effects of modifying PNNs or the whole ECM. Hence, despite aberrant PNNs lead to detrimental effects at the locomotion level, they are beneficial promoting regeneration after a SCI. Thus, any therapeutical modulation of spinal PNNs must consider the balance between synaptic integrity and plasticity.

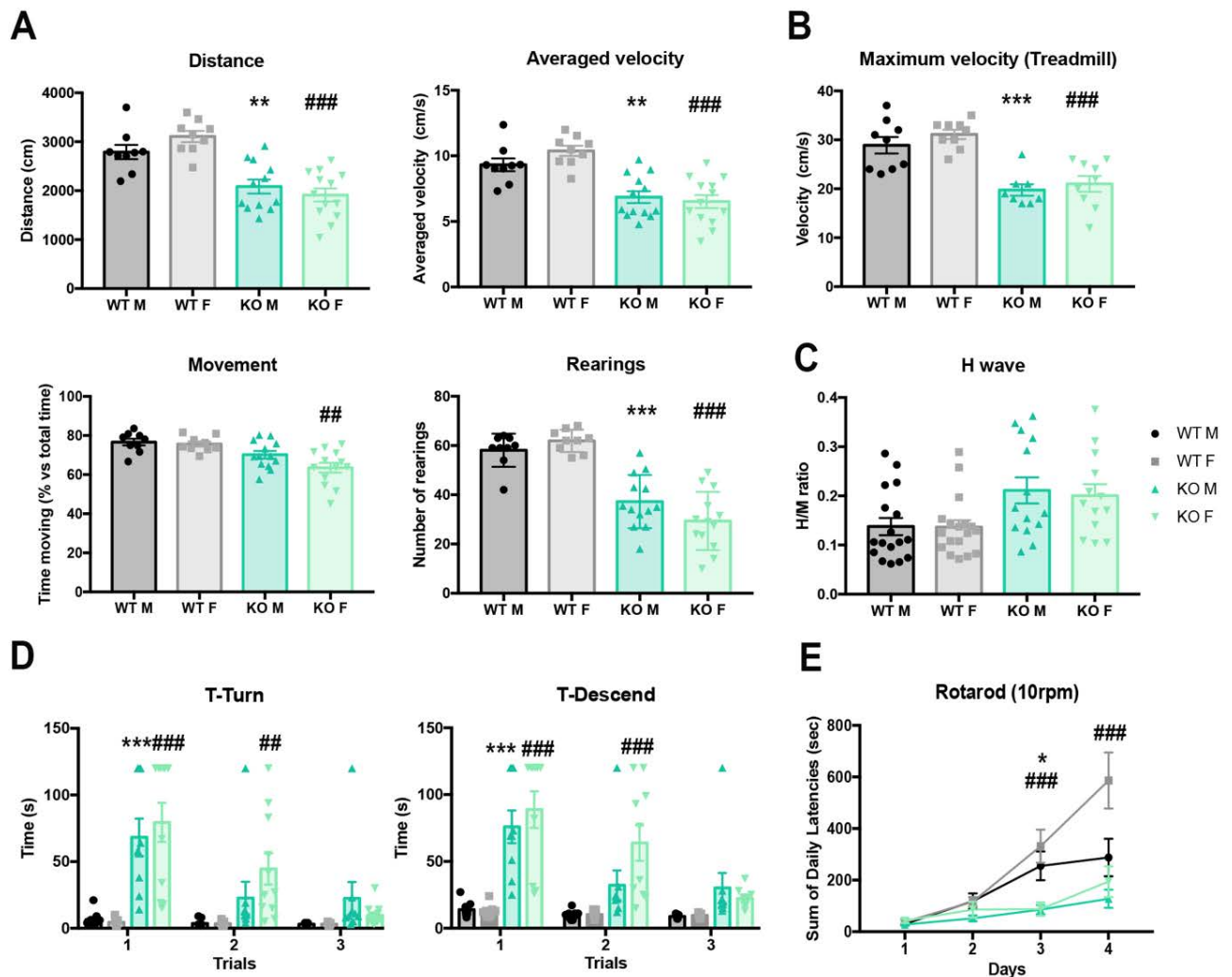
Conclusion

The present study demonstrates that aberrant PNNs enhance excitatory synapses and change the physiological properties of lumbar MNs, overall altering spinal circuits and producing motor impairment. This disorganization generates a permissive scenario for contralateral axons to sprout after SCI. Thus, new strategies to promote regeneration after injury require a more refined PNN modulation to strike an accurate balance between promoting plasticity and maintaining the beneficial properties of PNNs. In conclusion, PNNs' malleability makes them a potential therapeutic target to treat neural disorders in which plasticity and stability are key elements to consider.

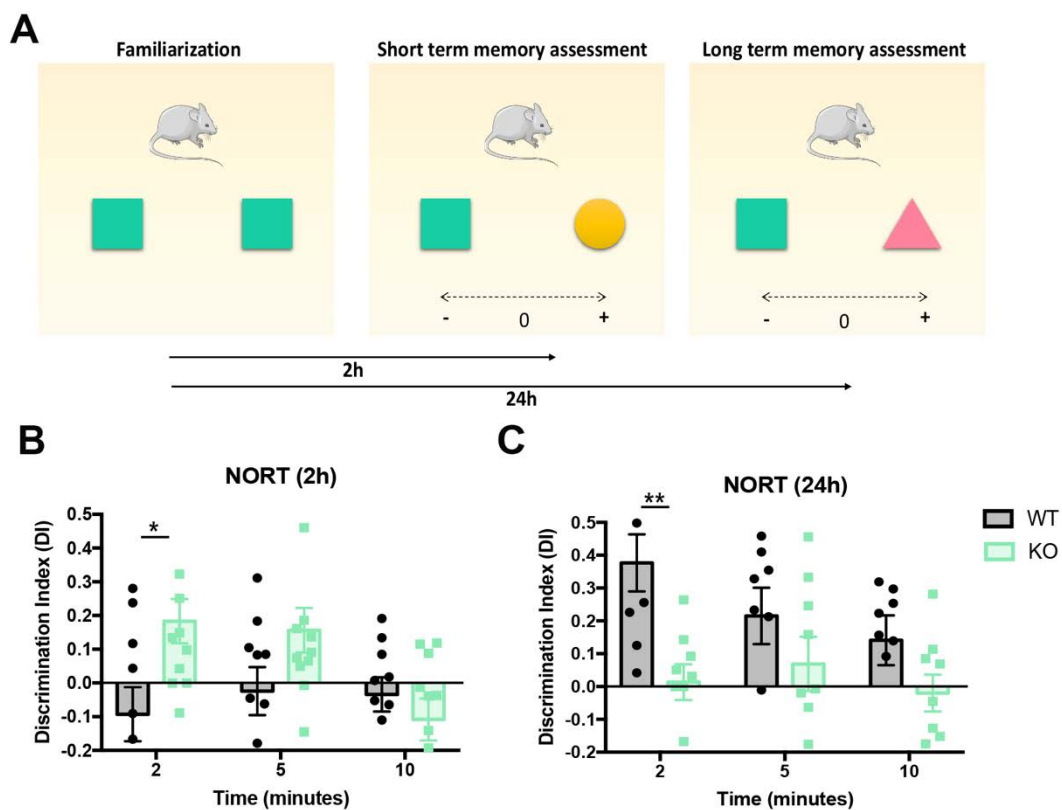
Supplementary figures



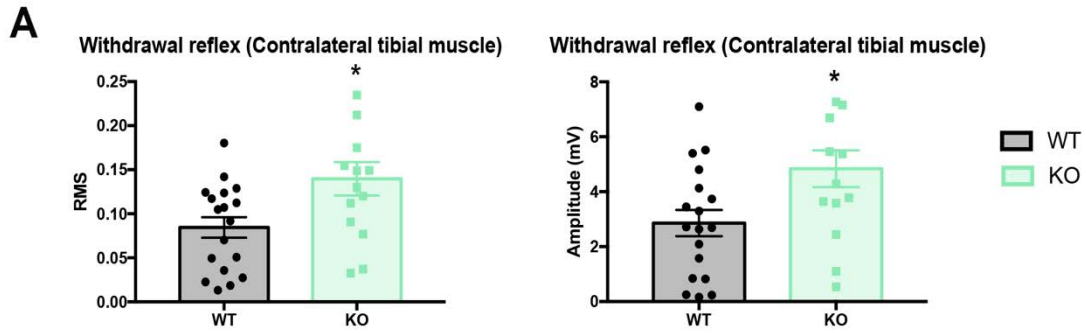
Supplementary figure 1. *Crtll* KO and WT mice show the same expression levels of the transgene in the cartilage. A. Cartilage samples (n=11; five WT and six *Crtll* KO mice) were homogenized, and the RNA was extracted using the RNeasy Mini Kit (QIAGEN) following the manufacturer's guidelines. Once the RNA was quantified using a spectrophotometer (NanoDrop Technologies), it was reverse transcribed using an Applied Biosystems kit (Thermo Fisher Scientific). Afterwards, the mRNA expression of the *Crtll* gene in the cartilage was quantified by RT-qPCR using SYBR Green QPCR Master Mix (Agilent Technologies) and the MC59 primer (Table 2). Glyceraldehyde-3-phosphate dehydrogenase (GAPDH) was used as a housekeeping gene. Bar graphs are representing the mean values \pm SEM; no significant differences were reported by unpaired t-test; WT: wild type; KO: knock-out.



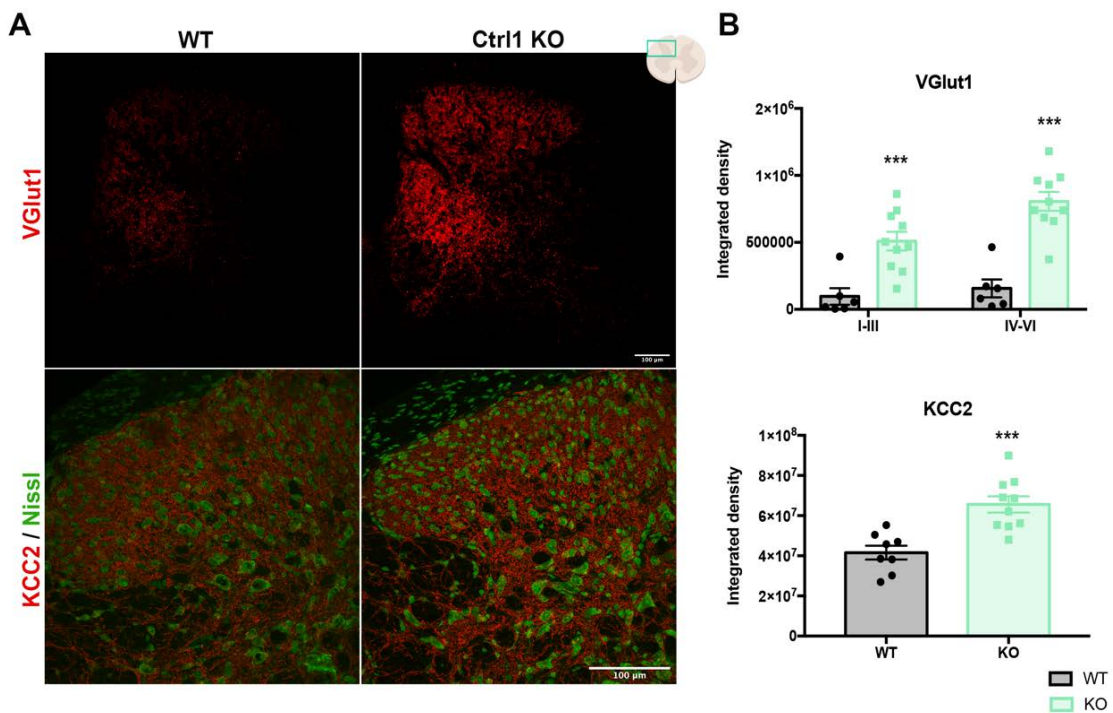
Supplementary figure 2. The lack of link protein 1 does not produce significant differences between *Crtll* KO male and female mice in functional tests such as the Open Field test (A), maximum velocity achieved (B), H/M ratio (C), Pole test (D) and adapted rotarod (E). Bar graphs are representing the mean value \pm SEM. * $p < 0.05$, ** $p < 0.01$, *** $p < 0.001$ WT M vs KO M; ### $p < 0.01$, ### $p < 0.001$ WT F vs KO F by one-way ANOVA (Distance: $F_{3,39} = 16.6$, $p < 0.001$; Averaged velocity: $F_{3,40} = 15.44$, $p < 0.001$; Movement: $F_{3,40} = 8.43$, $p < 0.001$; Rearings: $F_{3,40} = 29.72$, $p < 0.001$; Maximum velocity: $F_{3,31} = 15.95$, $p < 0.001$; H/M ratio: $F_{3,58} = 3.99$, $p = 0.011$) and two-way ANOVA (T-turn: time $F_{2,68} = 25.42$, $p < 0.001$; group $F_{3,34} = 8.87$, $p < 0.001$; interaction $F_{6,68} = 8.88$, $p < 0.001$; T-descend: time $F_{2,66} = 28.27$, $p < 0.001$; group $F_{3,33} = 12.81$, $p < 0.001$; interaction $F_{6,66} = 9.17$, $p < 0.001$; Adapted rotarod: time $F_{3,84} = 35.24$, $p < 0.001$; group $F_{1,28} = 19.38$, $p < 0.001$; interaction $F_{3,84} = 11.36$, $p < 0.001$) followed by post hoc test with Bonferroni correction. WT: wild type; KO: knock-out; M: male; F: female.



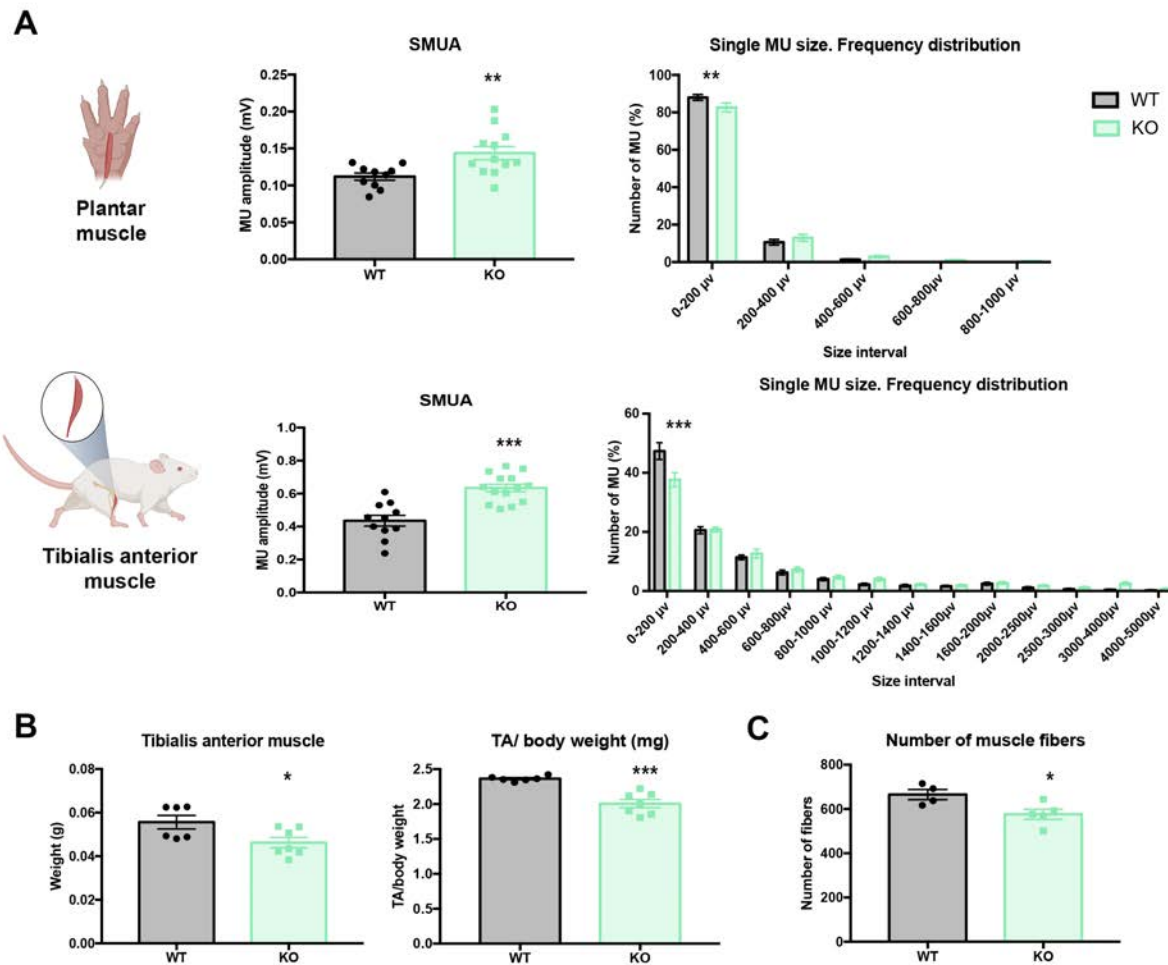
Supplementary figure 3. *Crtll* KO mice showed increased discriminatory ability but impaired long-term memory consolidation. A. Schematic diagram illustrating the timeline of the novel object recognition test. The time that the animal spent in each object is used to calculate the discriminatory index (DI) at 2, 5 and 10 minutes cumulatively to evaluate short-term memory (B) and long-term memory (C). Bar graphs are representing the mean values \pm SEM. * $p < 0.05$, ** $p < 0.01$ by two-way ANOVA (Short-term memory: time $F_{2,38} = 2.859$, $p = 0.069$; group $F_{1,19} = 4.312$, $df = 1$, $p = 0.051$; interaction $F_{2,38} = 4.277$, $p = 0.021$. Long-term memory: time $F_{2,30} = 2.923$, $p = 0.069$; group $F_{1,15} = 7.387$, $p = 0.016$; interaction $F_{2,30} = 2.328$, $p = 0.114$) followed by post hoc test with Bonferroni correction. WT: wild type; KO: knock-out; NORT: novel object recognition test.



Supplementary figure 4. *Crt11* KO mice presented increased excitability of spinal circuits observed in the contralateral withdrawal reflex (polysynaptic). A. Evaluation of the area under the curve (RMS) and maximum amplitude of the C3 component of the withdrawal reflex, recorded at the contralateral tibialis anterior muscle. Bar graphs are representing the mean values \pm SEM. * $p < 0.05$ by unpaired t-test. WT: wild type; KO: knock-out.



Supplementary figure 5. The VGlut1 increase observed in the ventral horn of the spinal cord is also observed in the dorsal horn of *Crt11* KO mice. A. Representative images of VGlut1 and KCC2 at the dorsal horn of the spinal cord. B. VGlut1 (above) and KCC2 (below) immunoreactivity quantification at the dorsal horn. Bar graphs are representing the mean values \pm SEM. Scale bar: 100 μ m. *** $p < 0.001$ by two-way ANOVA (time $F_{1,14} = 30.92$, $p < 0.001$; group $F_{1,14} = 28.94$, $p < 0.001$; interaction $F_{1,14} = 13.63$, $p = 0.002$) followed by post hoc test with Bonferroni correction (VGlut1) and by unpaired t-test (KCC2). WT: wild type; KO: knock-out.



Supplementary figure 6. *Crt1l* KO mice present altered MN recruitment and reduced muscle fibers. A. Electrophysiological estimation of the mean amplitude of SMUA and the frequency distribution of the MU size of the plantar and tibialis anterior muscle. B. Representation of the absolute value of the weight of the tibialis anterior muscle and the ratio with the body weight. C. Evaluation of the number of muscle fibers of the tibialis anterior muscle in the *Crt1l* KO and WT mice. Bar graphs are representing the mean values \pm SEM; * $p < 0.05$, ** $p < 0.01$, *** $p < 0.001$ by unpaired t-test, ** $p < 0.01$, *** $p < 0.001$ by two-way ANOVA (plantar muscle: time $F_{4,105}=2.91$, $p < 0.05$; group $F_{4,105}=1677$, $p < 0.001$; interaction $F_{1,105}=0$, $p > 0.999$; tibialis anterior muscle: time $F_{12,299}=4.844$, $p < 0.001$; group $F_{12,299}=311$, $p < 0.001$; interaction $F_{1,299}=0$, $p > 0.999$;) followed by post hoc test with Bonferroni correction. WT: wild type; KO: knock-out; SMUA: single motor unit action potential; MU: motor unit; TA: tibialis anterior muscle.

Chapter II

Voluntary wheel running preserves lumbar perineuronal nets,
enhances motor functions and prevents hyperreflexia after
spinal cord injury

Voluntary wheel running preserves lumbar perineuronal nets, enhances motor functions and prevents hyperreflexia after spinal cord injury

Authors

Sanchez-Ventura J¹, Giménez-Llort L², Penas C¹, Udina E^{1*}

Affiliation

¹Institute of Neurosciences, Department Cell Biology, Physiology and Immunology, Universitat Autònoma de Barcelona, and Centro de Investigación Biomédica en Red sobre Enfermedades Neurodegenerativas (CIBERNED), Bellaterra, Spain

²Institute of Neurosciences, Department of Psychiatry and Forensic Medicine, Universitat Autònoma de Barcelona, Bellaterra, Spain.

Abstract

Perineuronal nets (PNN) are a promising candidate to harness neural plasticity since their activity-dependent modulation allows to either stabilize the circuits or increase plasticity. Modulation of plasticity is the basis of rehabilitation strategies to reduce maladaptive plasticity after spinal cord injuries (SCI). Hence, it is important to understand how spinal PNN are affected after SCI and rehabilitation. Thus, this work aims to describe functional and PNN changes after thoracic SCI in mice, followed by different activity-dependent therapies: enriched environment, voluntary wheel and forced treadmill running. We found that the contusion provoked thermal hyperalgesia, hyperreflexia and locomotor impairment as measured by thermal plantar test, H wave recordings and the BMS score of locomotion, respectively. In the spinal cord, SCI reduced PNN density around lumbar motoneurons. In contrast, activity-based therapies increased motoneuron activity and reversed PNN decrease. The voluntary wheel group showed full preservation of PNN which also correlated with reduced hyperreflexia and better locomotor recovery. Furthermore, both voluntary wheel and treadmill running reduced hyperalgesia, but this finding was independent of lumbar PNN levels. In the brainstem sensory nuclei, SCI did not modify PNN whereas some activity-based therapies reduced them. The results of the present study highlight the impact of SCI on decreasing PNN at caudal segments of the spinal cord and the potential of physical activity-based therapies to reverse PNN disaggregation and to improve functional recovery. As modulating plasticity is crucial for restoring damaged neural circuits, regulating PNN by activity is an encouraging target to improve the outcome after injury.

Keywords: spinal cord injury, perineuronal nets, motoneurons, activity-dependent therapy, physical activity, hyperreflexia, neuropathic pain.

Introduction

One of the hallmarks of the central nervous system (CNS) is its potential to maintain the right balance between plasticity and stability. While plasticity prevails during development, stability predominates in the adult nervous system (Carulli et al., 2010). This fine plastic control is mediated, in part, by perineuronal nets (PNN). PNN are an aggregation of extracellular matrix molecules, among them chondroitin sulfate proteoglycans (CSPG), which are implicated in synaptic stabilization and plasticity inhibition (Wang and Fawcett, 2012). Their appearance temporally correlates with the maturation of the central synaptic circuitry and determines the end of the critical periods (Pizzorusso, 2002). As a dynamic structure, these nets are subjected to an activity-dependent modulation which varies depending on the anatomical localization (Smith et al., 2015). Hence, physical activity increases plasticity by means of reducing cerebellar (Foscarin et al., 2011) and cortical PNN (Smith et al., 2015). On the contrary, recent studies have pointed out that activity increases PNN around lumbar motoneurons (Arbat-Plana et al., 2015; Smith et al., 2015) and thus, it jeopardizes the statement that activity always increases plasticity in the nervous system. Understanding how physical activity or exercise regulates spinal PNN can have a huge impact, especially on spinal cord injury (SCI) models, since physical rehabilitation is currently one of the cornerstones for the treatment of SCI in humans.

SCI leads to devastating and non-reversible functional deficits due to the limited ability of central neurons to regenerate after injury. One main factor contributing to this regenerative failure is the upregulation of CSPGs (Silver and Miller, 2004). In fact, the application of chondroitinase ABC (chABC), an enzyme that degrades proteoglycans, at the injury site (Bradbury et al., 2002) or in distal regions where proteoglycans were also overexpressed (Massey et al., 2006; Alilain et al., 2011), promoted functional recovery. Despite an apparent contradiction, the combination of chABC treatment with specific rehabilitation further enhances functional recovery after injury, even if the applied rehabilitation increases the density of PNN (García-Álías et al., 2009; Wang et al., 2011). Thus, although spinal proteoglycan degradation is a potential strategy to boost plasticity, any approach must be mindful of plasticity-stability trade-off. In fact, maladaptive plastic changes can lead to the appearance of neuropathic pain and spasticity after SCI. Interestingly, physical exercise can attenuate both phenomena in experimental models of SCI (Côté et al., 2014; Detloff et al., 2014).

In the spinal cord, PNN are mainly found around lower motoneurons (Irvine and Kwok, 2018). Therefore, it is important to specifically evaluate the fate of spinal PNN after SCI, besides the generalized increase of proteoglycans related to reactive astrocytes (Silver and Miller, 2004). It is also worth pointing that despite their mesh-like appearance and their inhibitory role, their negatively charged net generates a microenvironment around neurons that contributes to the fine-tuning of neuron function regulating ionic buffering, neuroprotection, synaptic stabilization and neuronal development and plasticity (*reviewed in* (Sorg et al., 2016; Fawcett et al., 2019)).

Therefore, an optimal understanding of how spinal PNNs are modulated after SCI and which is the influence of activity-dependent therapies on these nets is still needed. The present study aims to evaluate the plastic changes induced by activity-based therapies after a thoracic spinal cord contusion and its relationship with PNN changes. Specifically, PNN around neurons denervated by the injury such as lumbar motoneurons and brainstem sensory neurons were studied. We hypothesized that reduced physical activity after a thoracic SCI would decrease PNN thickness around lumbar motoneurons, facilitating the disorganization of the circuitry, whereas the opposite effect would be observed in PNN of the sensory brainstem nuclei. Activity-dependent therapies might reverse those effects on PNN, through activating sensory and motor output and segmental reflexes such as the stretch reflex. To address these hypotheses, we used a contusion SCI in mice that were subjected to three different types of physical activities: an enriched environment, a voluntary and a forced exercise.

Material and methods

Experimental groups

All experimental procedures were conducted in accordance with the Universitat Autònoma de Barcelona Experimentation Ethical Committee (CEEAH I188R3-DMAH 6131) and followed the European Communities Council Directive 2010/63/EU. A total of 54 adult female mice (18-25g; 8 weeks, C57BL/6J, Charles River Laboratories) were housed at room temperature of 22 ± 2 °C and on a 12h light/dark cycle. Food and water were provided *ab libitum*.

Two sets of experiments were performed in this study for characterizing functional and histological outcomes produced at 5 weeks (Experiment 1) and at 11 weeks (Experiment 2) after the injury (Figure 1). The first experiment had five groups of mice. Initially, animals were divided in control (uninjured; $n=5$) or SCI ($n=23$) groups. Seven days after the injury, injured mice were further divided into four different treatment groups, a sedentary group (SED, $n=5$), and three groups submitted to activity-dependent therapies: enriched environment (EE, $n=6$), voluntary wheel (WR, $n=7$) and forced treadmill running (TR, $n=5$). The second experiment had three experimental groups: control (CTRL, $n=10$), SCI + sedentary (SED, $n=8$) and SCI + forced treadmill running (TR, $n=8$). All injured animals were randomly divided into the different

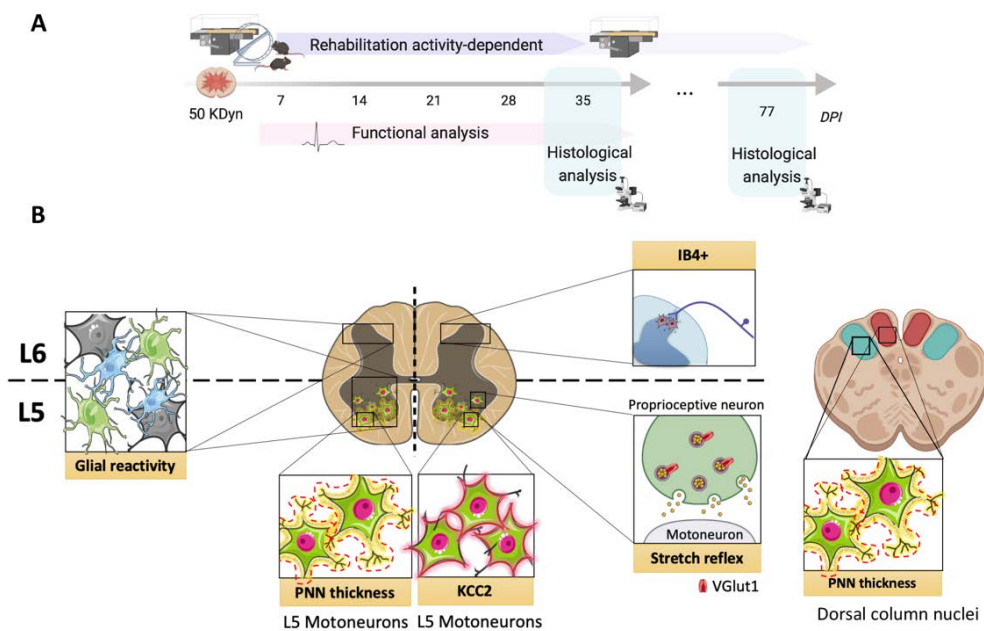


Figure 1. Schematic representation of the experimental procedure. (A) Diagram showing the timeline of the experiments. (B) Histological analysis from Experiment 1 at the spinal cord (L5 and L6) and the dorsal column nuclei. PNN: perineuronal net. Individual images were obtained from Biorender and Servier Medical Art.

experimental groups. In case unbalanced groups were generated, it was corrected using their tissue displacement and their Basso Mouse Scale (BMS) score at 7 dpi (days post-injury).

Spinal cord injury

Surgical procedures were performed under general anesthesia using an intraperitoneal injection (*i.p.*) of ketamine (90 mg/kg) and xylazine (10 mg/kg) in saline solution. After laminectomy, a moderate spinal cord contusion was performed at T11 using a force-controlled spinal cord impactor (Infinite Horizon Impactor Device). The applied force was set to 50 KDyn, which induced a tissue displacement around 300-490 μm . After surgery, animals received 1mL of saline subcutaneously to prevent dehydration. Postoperative care consisted of subcutaneous injections of buprenorphine (0.1 mg/kg) for three days and manual bladder voiding twice a day until voiding reflex returned.

Activity-based therapies protocol

Enriched environment (EE)

The enriched environment consisted of social housing (6 animals) in a cage (364 × 258 × 350mm³; Activity Wheel Cage System for mice, Tecniplast, Buguggiate, Italy) equipped with the wheel blocked and with tissue paper added as naturalistic bedding that stimulates fine-motor activity.

Voluntary wheel running (WR)

One week after injury, injured animals were housed in a cage equipped with a free-to-access running wheel (364 × 258 × 350mm³; Activity Wheel Cage System for mice, Tecniplast, Buguggiate, Italy). The wheels were connected to a wheel revolution count to daily calculate the running distance using the diameter of the wheel (21 cm) and a revolution correction. In order to avoid animal isolation, animals were housed in pairs, a group size that also ensured that both animals could run at the same time.

Forced treadmill running (TR)

Four days before the surgical procedure, all mice were familiarized with the treadmill (Treadmill LE 8706). The habituation protocol consisted of running for 15 min at a speed of 11 cm/s. The standard negative stimulus (a 0.1 mA low electric shock) was

used. Mice started the treadmill training one week after SCI and were exercised 5 days/week for 4 weeks (Experiment 1) or 10 weeks (Experiment 2). After surgery, the negative stimulus was replaced by a gentle tapping of the tail to encourage running when mice stopped. The training protocol consisted of running for 5 min at a speed of 11-14 cm/s and 15 min at an increasing velocity adapted to mice recovery. At the last training sessions, animals reached a maximum velocity of 24 cm/s.

Functional assessment

Basso Mouse Scale

Motor recovery was assessed in an open field using the Basso Mouse Scale (BMS) at 3, 7, 14, 21, 28 and 35 days after the injury. BMS is a nine-point scale that ranges from 0 to 9, which 0 means total paralysis and 9 reflects normal locomotion. The analysis was performed by two researchers which followed blinding procedures to establish the score of each animal. The score of each animal was the average score of each hind paw.

Algesimetry tests

Neuropathic pain was evaluated carrying out thermal algesimetry test, using a Plantar algesimeter device (Ugo Basile). Some days before the preoperative testing and the surgery, animals were acclimated to the testing chamber for three days (15 minutes/day). Then, tests were performed preoperatively to establish baseline values, at 14 and 28 days after the injury by a blinded researcher. A light beam (intensity=30 mW/cm²) was applied to the hind paw until the animal withdrew the paw (Hargreaves K, Dubner R, Brown F, Flores C, 1988). The paw withdrawal latency was recorded three times, with a resting time between trials, and averaged. Finally, values were normalized to those of control intact animals. To categorize animals with hyperalgesia, we first calculated the intra-group variability of control animals during the whole experiment (the average withdrawal latency of control animals was 8.95 ± 1.98 seconds, being 1.98 seconds the intra-group variability). Then, we establish an interval of normality of each injured animal based on their basal value (before the injury) and this intra-group variability. For example, if the basal value of an injured animal was of 8, its interval of normality would be 8 ± 1.98 seconds. This animal would be categorized with hyperalgesia whether at 28dpi presented a value < 6.02 seconds.

Electrophysiological tests

Electrophysiological tests were performed before SCI (basal values) and at 6, 21 and 32 days after injury with the animals under anesthesia (ketamine 90 mg/kg and xylazine 10 mg/kg), since it has negligible effects on the electrophysiological recording (Ho and Waite, 2002). During the tests, a heating pad was used to maintain body temperature and a microscope was used to ensure reproducibility of needle location on all animals.

Spasticity was analyzed by measuring the H wave and its rate-dependent depression (RDD) in the plantar muscle, assuming that the changes observed in that muscle are characteristic for the hindlimb musculature (Valero-Cabré et al., 2004). Firstly, we evaluated the maximum amplitudes of the M wave (M_{max} ; direct muscle response) and the H wave (H_{max} ; monosynaptic reflex) of the plantar interosseus muscle. Then, we calculated the ratio H_{max}/M_{max} (Thompson et al., 1992), as an index of the excitability of the Ia afferent synapse on spinal motoneurons. To assess the effect of activity in modulating hyperreflexia, only injured animals that presented hyperreflexia after the injury (6 dpi H_{max}/M_{max} ratio > basal H_{max}/M_{max} ratio) were included in the study. Then, we measured the changes in the H wave amplitude over consecutive stimulations, known as the rate-dependent depression (RDD) whose alteration is a hallmark of spastic animals (Thompson et al., 1992). For both measurements, we initially delivered single electrical pulses of 0.02 ms (Grass S88) by a needle inserted percutaneously at the sciatic notch. The recorded potentials were amplified and displayed on a digital oscilloscope (Tektronix 450S). While M_{max} was obtained with supramaximal stimulation, the H_{max} was elicited after trying a range of increasing stimulus intensities. The stimulation intensity that gave the H_{max} was then used for the RDD test. The RDD was measured performing trains of ten consecutive pulses at different frequencies (1, 5 and 10 Hz) with at least 30 seconds rest between each train. RDD values were expressed as the percentage of the ratio between the last (10th) and the first pulse. Then, in each experimental time-point, a curve expressing the % RDD (y-axis) at different frequencies (x-axis) was generated to further calculate the area under the curve for each animal.

Finally, we recorded the muscle evoked potentials (MEP) of the plantar interosseus, tibialis anterior and gastrocnemius muscles to evaluate descending pathways (Redondo-Castro et al., 2016). MEP values were presented as the percentage (%) of recovery using the basal value of each animal. Stimulation was delivered by means

of needle electrodes subcutaneously placed overlaying the sensorimotor cortex and applying pulses of 0.1 ms duration and supramaximal intensity.

Histological evaluation

Five (Experiment 1) or eleven (Experiment 2) weeks after the SCI, mice were euthanized with pentobarbital (*i.p.*; 200 mg/kg). Animals were transcardially perfused with cold 4% paraformaldehyde in 0.1M phosphate buffer (PB). Then, brains and spinal cords were dissected out and post-fixed in 4% paraformaldehyde in PB overnight and 2h, respectively. Tissues were cryoprotected in 30% sucrose solution in PB at 4°C until they sank.

For the spinal cord, the lesion site (T11) and the lumbar region (L4-L6) were serially cut on a cryostat (15 µm thick transverse sections) and collected onto gelatin-coated glass slides. Thoracic sections were used to evaluate demyelination with Luxol Fast Blue staining (LFB; Sigma-Aldrich) (Sánchez-Ventura et al., 2019). Briefly, after a dehydration phase, slides were placed in a 1mg/mL LFB solution in 95% ethanol and 0.05% acetic acid at 37°C overnight. Then, sections were washed in 95% ethanol and distilled water before being placed into a 0.05% Li₂CO₃ solution for 2:30 minutes at room temperature (RT). After another dehydration, sections were mounted in DPX mounting medium (Sigma-Aldrich).

A subset of cord sections was used to recognize the L5 and L6 segments after incubation in a cresyl-violet acetate solution for 3h at RT. L5 sections were used to analyze PNN, VGlut1 staining, the potassium chloride cotransporter KCC2 and glial reactivity (GFAP and Iba1), while L6 sections were used for glial reactivity and Isolectin IB4 biotin (IB4) afferences (Figure 1). For glial reactivity, PNN and VGlut1 staining, slides were blocked with 10% normal donkey serum (NDS) for 1h. For KCC2, sections were permeabilized with Phosphate Buffer saline Triton 0.3%- Bovine Serum Albumin 3% (PBST-BSA 3%) during 45 minutes at RT and then, nonspecific interactions were blocked with PBS-BSA 3% and 10% normal donkey serum for 1h at RT. In all cases, sections were then incubated overnight at 4°C with the primary antibody (Table 1). After washes, immunoreactive sites were revealed using species-specific secondary antibodies (1:200; Table 1). After 2h of incubation at RT, FluoroNissl Green (1:200) was added diluted in PBS in some immunohistochemical labeling. Sections were mounted in Fluoromount-G medium (Southern Biotech).

To analyze changes in the dorsal column nuclei, 3 mm of brainstem were serially cut on the cryostat (20 μm thick transverse sections). Then, PNN were immunostained using Aggrecan and the VGlut1 staining was used to identify the cuneatus nucleus (Niu et al., 2013). Only those sections containing the nuclei (Bregma -7.64 to -8.24) were quantified.

Table 1. List of antibodies used in the histological analysis

Primary antibodies				Secondary antibodies		
Antibody	Dilution	Host	Reference	Antibody	Host	Reference
GFAP	1:1000	Rabbit	AB5804- Millipore	Alexa Fluor 488	Donkey x Rabbit	A21206- Invitrogen
Ibal	1:400	Goat	AB5076- Abcam	Alexa 594	Donkey x Goat	A11058- Invitrogen
Aggrecan	1:250	Rabbit	AB1031- Millipore	Alexa Fluor 488	Donkey x Rabbit	A21206- Invitrogen
VGlut1	1:300	Guinea Pig	AB5905- Millipore	Cys 3	Donkey x Guinea Pig	706-165- 148- Jackson
KCC2	1:400	Rabbit	07-432- Millipore	Alexa Fluor 594	Donkey x Rabbit	A21207- Invitrogen
GSL-1*; Anti-GSL- I	10 $\mu\text{g}/\text{ml}$ 1:500	- Goat	L-1104- Vector AS2104- Vector	Alexa 488	Donkey x Goat	A 11055- Invitrogen

**Griffonia Simplicifolia* Lectin I

Histological analysis

Myelin sparing was calculated by delineating the spared LFB-stained tissue area as well as the whole spinal cord area from images taken at the epicenter of the injury and every 150 μm rostral and caudal to the lesion. Both areas were used to calculate the % of spared white matter.

For lumbar sections, grayscale microphotographs were captured at 40x in the ventral horn (L5) and at 20x in the dorsal horn (L6). The background was corrected, and the threshold was defined for all the microphotographs of the same marker. For glial reactivity quantification, integrated density of immunoreactivity was measured in the full image of the ventral horn, and in a region of interest (ROI) of 230 μm^2 of the dorsal horn. IB4+ area in laminae I-II was traced to quantify the intensity of labeling. KCC2 immunoreactivity was quantified measuring the integrated density of a band of 2 μm around FluoroNissl Green positive neurons in the ventral horn. At least five sections per

marker from each animal were used to calculate the mean value. In the KCC2 analysis, a minimum of 25 neurons was measured for each animal. Immunolabeled images were acquired with a digital camera Nikon DS-Ri2 attached to a Nikon Eclipse Ni-E microscope. Image analysis was performed by Fiji software.

To measure PNN expression and VGlut1 positive fibers on lumbar motoneurons, images were taken from four or five cord sections under a confocal laser-scanning microscope (around 30 steps, z-step size of 0.5 μm ; Leica TCS SP5) at 40x. To quantify PNN changes, a minimum of 30 motoneurons (identified by FluoroNissl Blue labeling, located within the ventral horn and presenting an area $>350\mu\text{m}^2$ (Friese et al., 2009) (Suppl Figure 1A)) were measured for each animal. After background correction, the maximal projection of the different z-stacks was done and then, a band of 4 μm around the selected neuron was calculated to measure the integrated density of that region. For measurements of VGlut1-positive fibers, the VGlut1-positive boutons present in a band of 4 μm around the selected motoneurons were counted. PNN thickness in the dorsal column nuclei were determined using the same method used to measure spinal PNN.

Statistical analysis

Data is reported as mean \pm standard error of the mean (SEM). Normality was assessed by Shapiro-Wilk test that showed that all quantitative data followed a normal distribution. Thus, the functional and electrophysiological results including motor and sensory tests were analyzed by two-way repeated-measures ANOVA with group and time after injury as factors, followed by Bonferroni *post-hoc* tests. Histological results were analyzed by one-way ANOVA with Bonferroni *post-hoc* test, except for Luxol fast blue analysis in which we used a two-way ANOVA (group \times distance in the spinal cord). Pearson's correlation and linear regression analysis were used to correlate H-reflex modulation with BMS score and the PNN thickness with the distance run/day in the WR group. Statistical analysis was done using GraphPad Prism 7 software. A p-value <0.05 was used to indicate significant differences between groups.

Results

Voluntary wheel running enhances functional recovery after SCI

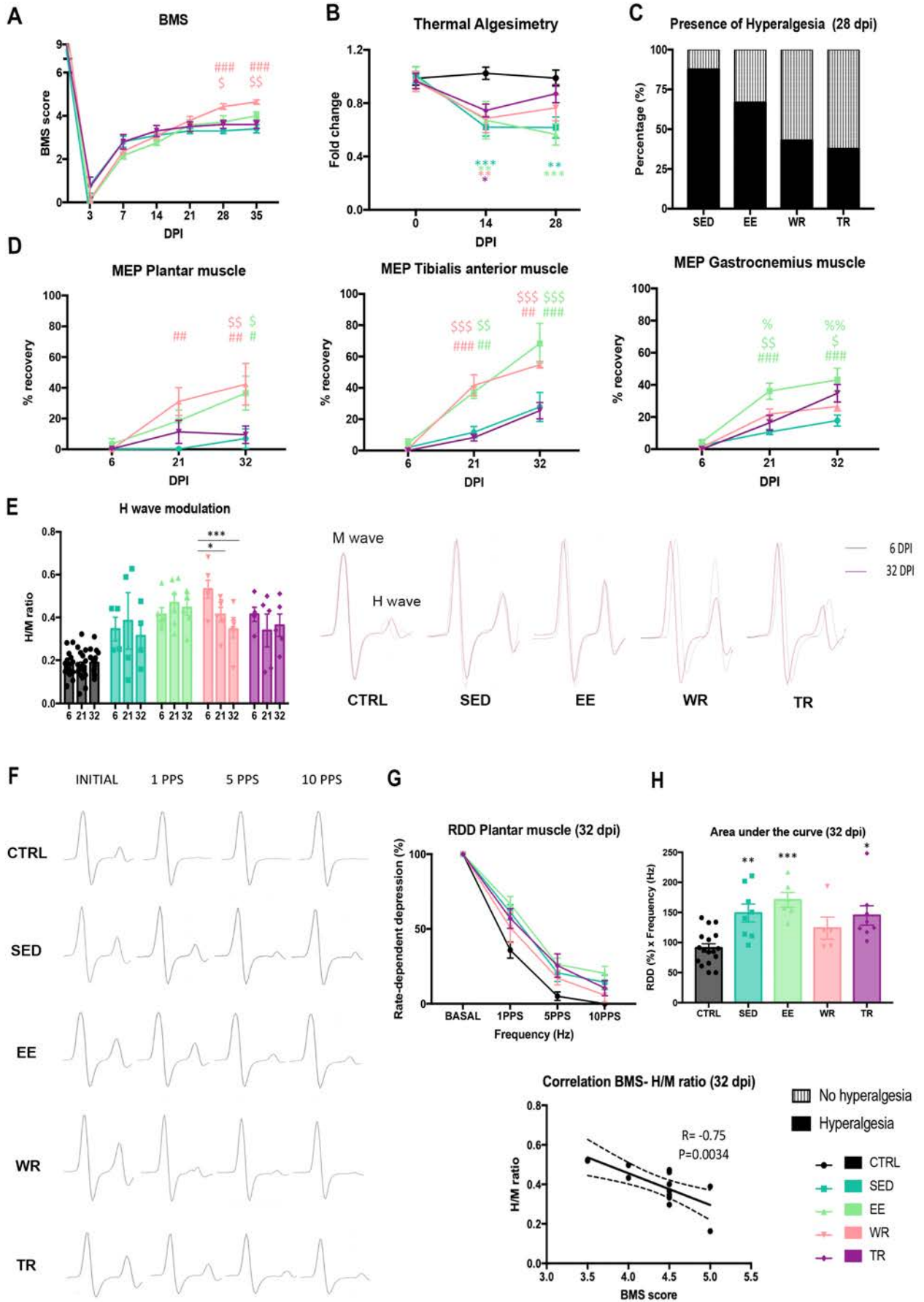
Locomotor function, evaluated as the BMS score, is shown in Figure 2A. All injured animals presented impaired hindlimb locomotion just after the injury and then, a gradual recovery during the following weeks. Only mice that voluntarily run on the wheel showed significant improvement of BMS score at 28 and 35 dpi compared to the SED ($p < 0.001$ at 28 and 35 dpi) and TR group ($p < 0.05$ at 28dpi; $p < 0.01$ at 35 dpi). In the WR group, the improvements of BMS score over time were also statistically significant ($p < 0.001$). Despite the EE group slightly increased the BMS score and a trend over time was observed, they did not reach statistical significance.

The results of the thermal algometry tests (Figure 2B) indicated that all SCI groups developed thermal hyperalgesia at 14 dpi as shown by a significant decrease in the withdrawal latency compared to the control intact group ($p < 0.001$ vs SED; $p < 0.01$ vs EE; $p < 0.01$ vs WR; $p < 0.05$ vs TR). At later time points, whereas the SED ($p < 0.01$) and EE ($p < 0.001$), the WR and TR groups increased their withdrawal latency towards control values. Figure 2C shows that the percentage of animals with thermal hyperalgesia at 28 dpi was considerably higher in the SED group than in the activity-treated groups (SED: 87.5%; EE: 66.67%; WR: 42.86%; TR: 37.5%).

The electrophysiological tests performed before SCI showed that MEPs elicited by brain stimulation were present in all mice (data not shown). Contrarily, six days after contusion, MEPs were abolished in the hindlimb muscles of all injured animals as the % of recovery at that time point is close to zero (Figure 2D). MEPs reappeared during the

(Figure in the next page)

Figure 2. Functional evaluation after SCI and activity-based therapies. (A) Open field locomotion assessed by BMS scale. (B) Neuropathic pain assessment by thermal algometry test recorded every two weeks. (C) Averaged percentage of the animals that presented hyperalgesia at the end of the experiment. (D) Representative recordings displaying the % of recovery of MEPs in plantar, tibialis anterior and gastrocnemius muscles during the experimental procedure. (E) Quantification of H_{max}/M_{max} changes before initiating the activity-based therapies (6dpi), at 21 dpi and at the end of the experiment (32 dpi). Representative electromyograms showing an initial M wave followed by the H wave at 6 and 32 dpi. (F) Paired-pulse depression profile of H wave after 10 consecutive stimulations at 1, 5 and 10 Hz. Increasing the frequency of stimulation leads to a dramatic decrease in the H wave amplitude in intact mice compared to injured ones. (G) Depression profile of the H wave at 32 dpi. Statistical differences are not shown. (H) Representation of the area under the curve of the recorded curve of each animal from figure 2G. (I) Relationship between BMS score and H wave recordings in the plantar muscle. * $p < 0.05$, ** $p < 0.01$, *** $p < 0.001$ vs control; ## $p < 0.01$, ### $p < 0.001$ vs SED; % $p < 0.05$, %% $p < 0.01$ vs WR, and \$ $p < 0.05$, \$\$ $p < 0.01$, \$\$\$ $p < 0.001$ vs TR; as calculated by two-way ANOVA followed by Bonferroni correction for the multiple comparison. MEP: motor evoked potentials, RDD: rate-dependent depression, BMS: Basso Mouse Scale, CTRL: control, SED: sedentary, EE: enriched environment, WR: voluntary wheel, TR: forced treadmill.



follow-up, but recovery was different in the three tested muscles. In the plantar and tibialis anterior muscles, the WR and EE groups presented a percentage of recovery higher than the SED and TR groups at the end of the experiment (WR: $p < 0.01$ vs SED plantar and tibialis; $p < 0.01$ and $p < 0.001$ vs TR plantar and tibialis, respectively; EE: $p < 0.05$ and $p < 0.001$ vs SED plantar and tibialis, respectively; $p < 0.05$ and $p < 0.001$ vs TR plantar and tibialis, respectively).

However, in the gastrocnemius muscle, this increased recovery was only observed in the EE group compared to the rest of groups ($p < 0.01$ vs WR, $p < 0.05$ vs TR, $p < 0.001$ vs SED). The higher recovery of MEPS in EE and WR groups could be related with a higher recuperation of supraspinal connections during the follow-up. However, we did not find increased white matter preservation in 1.2 mm around the epicenter of the injury in the EE nor WR groups as compared to the rest (Suppl Figure 2).

Regarding the H reflex (Figure 2E), control animals did not show noticeable changes in their H_{max}/M_{max} ratio during the follow-up, whereas the SCI produced hyperreflexia in 72% of the animals at 6 dpi (data not shown). At 21 and 32 dpi, H_{max}/M_{max} ratio was maintained at similar levels than at 6dpi in all the injured groups except the WR group, in which presented a significant decrease over time ($p < 0.05$ vs 21 dpi; $p < 0.001$ vs 32 dpi). However, the values obtained at the end of the experiment were similar between groups.

The RDD of the H reflex (Figure 2F) showed that while control animals had complete depression of their H wave after 10 consecutive stimuli at 5Hz, the SCI animals had less reduction. The area under the curve (Figure 2H) obtained from the depression profile of the plantar muscle (Figure 2G) showed that the SED, EE and TR groups area was significantly higher compared to control animals ($p < 0.01$ vs SED; $p < 0.001$ vs EE, $p < 0.05$ vs TR), indicating marked reduction of the H wave RDD due to the interruption of descending spinal pathways. In contrast, the WR group showed a slight reduction of the area under the curve at the end of the experiment, with values not significantly difference with respect to control animals.

We further questioned whether the locomotor improvement observed in the WR group was influenced by the reduction of hyperreflexia. To answer that question, we correlated the locomotion scores of animals from the groups with higher MEPs (EE and WR), as this parameter could also influence motor recovery, with their H_{max}/M_{max} ratio at 32 dpi. As shown in Figure 2I, there was a strong correlation between the H wave modulation and the BMS score ($R = -0.75$, $p = 0.0034$), indicating that a better modulation

of the spinal reflexes may be associated with improved locomotion in SCI mice subjected to voluntary wheel running.

Activity-based therapies contribute to maintain spinal PNN after SCI

To analyze changes in spinal cord PNN after SCI and the possible modulation by activity-based therapies, we evaluated the intensity of aggrecan labeling (Figure 3A, B). Aggrecan is a chondroitin-sulfate proteoglycan (CSPG) and the main constituent of PNN (Rowlands et al., 2018). In fact, it labels more PNN than the marker *Wisteria floribunda* agglutinin (WFA) in the spinal cord (Irvine and Kwok, 2018). Aggrecan immunostaining (Figure 3B) of the lumbar spinal cord revealed that PNN around motoneurons were significantly reduced 5 weeks after SCI in the injured-SED group ($p < 0.001$). In contrast, we found that WR and TR significantly prevented PNN reduction, whereas the EE group did not ($p < 0.05$). Comparatively, PNN preservation was greater in the WR group than the rest of the treated groups. This effect seems related to the amount of physical activity since the WR group run much more than the TR group during the 4 weeks of follow-up ($p < 0.001$; Figure 3C). In addition, within the WR group, there were also differences in the distance run per day, which positively correlated ($R = 0.79$) with PNN preservation.

Next, we assessed the proprioceptive contacts on the lumbar motoneurons using the VGlut1 marker, which is specific for Ia sensory afferents from the muscle spindle (Todd et al., 2003) (Figure 3A, E). We found that all activity-treated groups presented increased VGlut1 staining compared to sedentary animals ($p < 0.01$), but only the WR group presented more VGlut1 staining than control mice ($p < 0.05$).

Lastly, to examine the progression of PNN and VGlut1 preservation over time, a second experiment was conducted with two SCI groups which were followed-up for 11 weeks and one of them was submitted to the treadmill protocol (Suppl Figure 1B). At 10 weeks after the injury, no significant differences were observed neither in PNN integrity nor in VGlut1 staining.

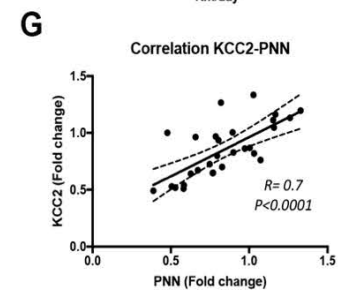
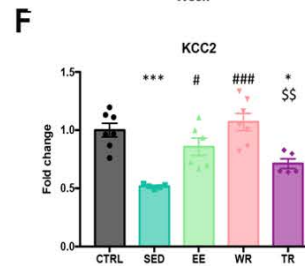
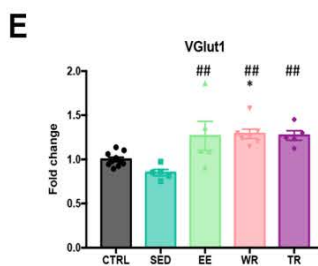
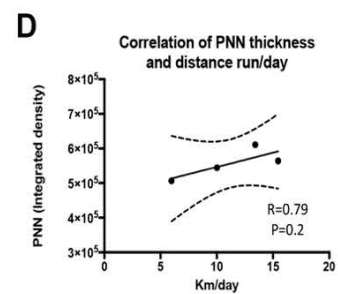
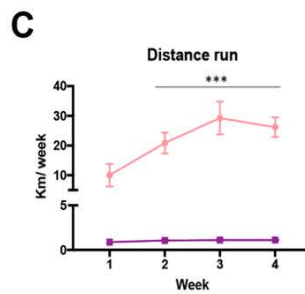
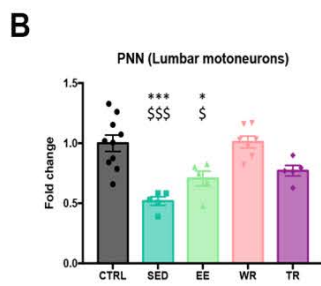
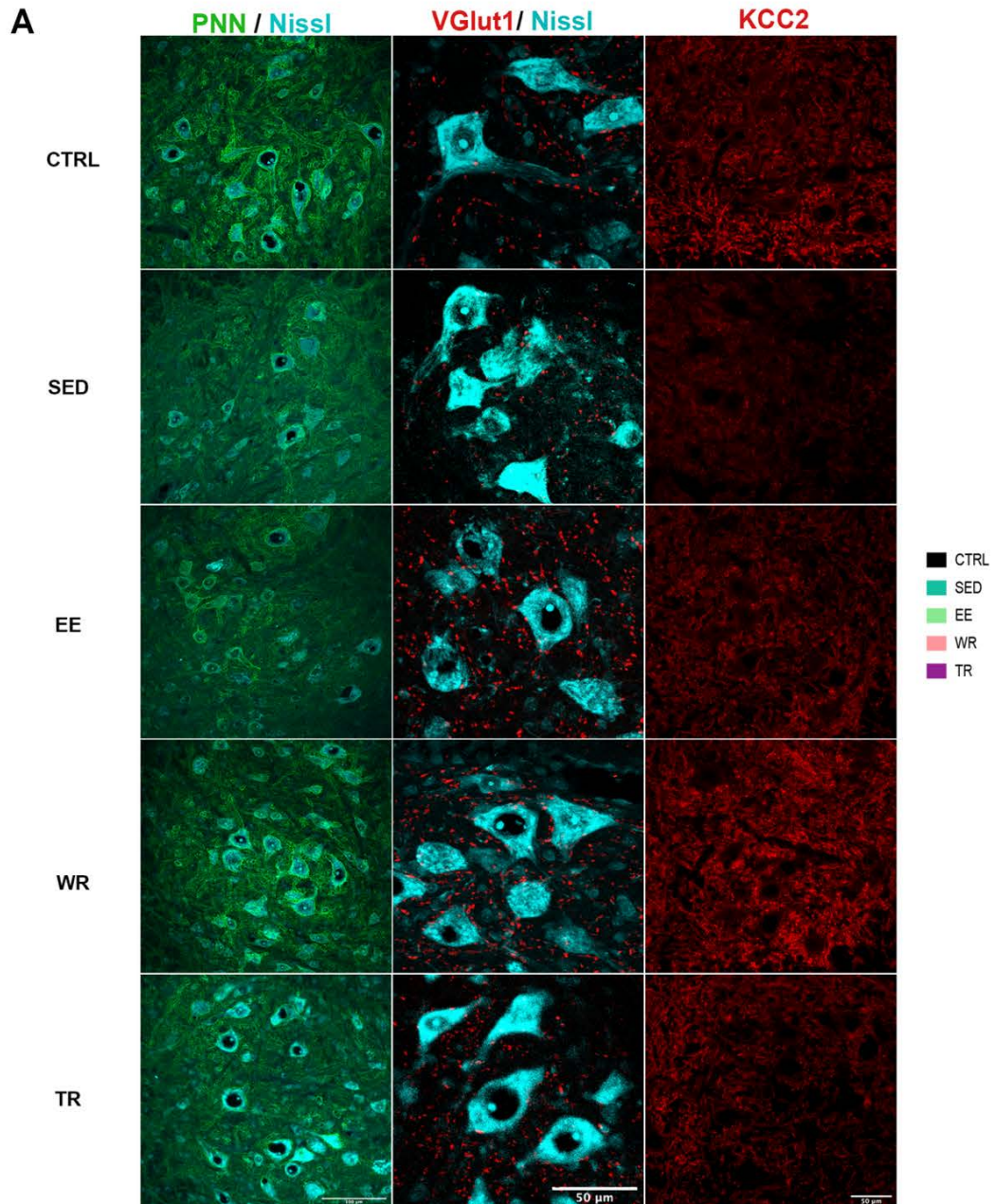


(Figure in the previous page)

Figure 3. Histological changes in the lumbar spinal cord after SCI and activity-based therapies. (A) Representative images of lumbar ventral horn of different histological parameters after SCI and activity-dependent activities. (B) Quantification of PNN labelled with aggrecan (green) around lumbar motoneurons, labelled with FluoroNissl (blue). (C) Average distance run per week over the training period (4 weeks) of the WR and TR groups. (D) Relationship between PNN intensity and distance run per day in the WR group. Each dot represents a cage in which a couple of mice freely run in the wheel. (E) Quantification of proprioceptive fibers, labelled with VGlut1 (red) in 4 μ m around lumbar motoneurons, labelled with FluoroNissl (blue). (F) Quantification of the potassium-chloride cotransporter KCC2 (red) around lumbar motoneurons. (G) Relationship between KCC2 and PNN expression in the lumbar spinal motoneurons. Each dot represents one single animal. * $p < 0.05$, *** $p < 0.001$ vs control; ## $p < 0.01$, ### $p < 0.001$ vs SED; and \$ $p < 0.05$, \$\$ $p < 0.01$, \$\$\$ $p < 0.001$ vs WR; as calculated by one-way ANOVA with Bonferroni multiple comparison (PNN $F_{4,27} = 11.32$, $p < 0.0001$; VGlut1: $F_{4,27} = 7.76$, $p = 0.0003$; KCC2: $F_{4,25} = 12.43$, $p < 0.0001$). Data are expressed as mean \pm SEM normalized to control group. Scale bar: 100 μ m (PNN), 50 μ m (VGlut1 and KCC2). CTRL: control, SED: sedentary, EE: enriched environment, WR: voluntary wheel, TR: forced treadmill.

Activity-based therapies modulate the expression of KCC2 after SCI

In order to assess whether PNN reduction by the SCI could alter the physiological properties of lumbar motoneurons, we evaluated the expression of KCC2, which is necessary to maintain the inhibitory GABAergic tone (D'Amico et al., 2014). We found that the SCI significantly reduced KCC2 staining in the ventral horn ($p < 0.001$ vs SED, Figure 3F). We further observed that mice of the TR group, similar to sedentary ones, presented significantly decreased KCC2 immunoreactivity compared to control animals ($p < 0.05$ vs TR). On the other hand, the EE and WR groups showed a preserved expression of KCC2 with similar values to control animals, and significantly higher than sedentary animals ($p < 0.05$ vs EE $p < 0.0001$ vs WR). Interestingly, linear regression analysis showed a significant correlation between PNN and KCC2 expression ($R = 0.7$, $p < 0.0001$, Figure 3G).

Activity-based therapies modify the glial reactivity and nociceptive nonpeptidergic C-fibers after SCI

To assess the role of activity-dependent therapies in the modulation of the inflammatory response after SCI, we analyzed the expression of two hallmarks of inflammation: GFAP, to label astrocytes and Iba1, a marker of microglia/macrophages (Figure 4A, B, C). As expected, there was a significant increase in astroglial reactivity in the ventral horn (Figure 4B) in all injured animals compared to control ones ($p < 0.05$ vs SED); $p < 0.001$ vs EE; $p < 0.01$ vs WR; $p < 0.01$ vs TR), without changes in the groups receiving activity-based strategies. In contrast, we found that levels of Iba1 microglial marker presented a slight but not significant increase in SCI sedentary mice compared to control

mice. However, enriched environment and voluntary wheel treatments induced a significant increase in the expression of Iba1 in the ventral horn ($p < 0.001$ vs EE; $p < 0.001$ vs WR). This marked increase could be attributed to changes in microglial morphology more than an increase in the number of microglia. These changes were not observed in the treadmill group.

Next, we wanted to ascertain whether the differences in pain sensitivity were related to changes in glial reactivity in the dorsal horn at L6 (Figure 4C). The absence of differences between groups in both immunostainings might indicate that the inflammatory milieu generated by the thoracic injury did not reach level L6. In fact, only the EE group presented a significant increase of astrogliosis compared to the other groups ($p < 0.001$ vs CTRL, $p < 0.05$ vs SED, $p < 0.05$ vs WR). Finally, nociceptive nonpeptidergic C-fibers were labelled by IB4 marker (Figure 4D). IB4+ staining was found in the lamina II of the dorsal horn, which was unaffected by the injury. In contrast, WR and TR groups presented a significant reduction on IB4+ staining ($p < 0.05$ vs WR; $p < 0.01$ vs TR). However, this reduction was not observed in the EE group.

PNN in the dorsal column nuclei are differently modulated by activity-dependent therapies than spinal PNN after SCI

Given the importance of sensory input in regulating PNN, we hypothesized that the dorsal column nuclei, which receives sensory information from the hindlimbs, could present altered PNN integrity after SCI (Figure 5A). Considering the gracile nucleus (Figure 5B), quantitative analysis of aggrecan staining showed that the SCI did not produce changes in PNN expression. However, some activity-dependent therapies could modulate PNN since EE and WR groups showed significantly reduced expression of PNN compared to control ($p < 0.0001$) and SED groups ($p < 0.01$ vs. EE and $p < 0.05$ vs. WR). TR group did not show significant differences either between control or sedentary animals. Regarding the cuneatus nucleus (Figure 5C), the injury did not modify aggrecan staining. Moreover, in this nucleus, all the activity-based therapies reduced the expression of PNN compared to the SED group ($p < 0.01$ vs EE, $p < 0.01$ vs WR, $p < 0.05$ vs TR).

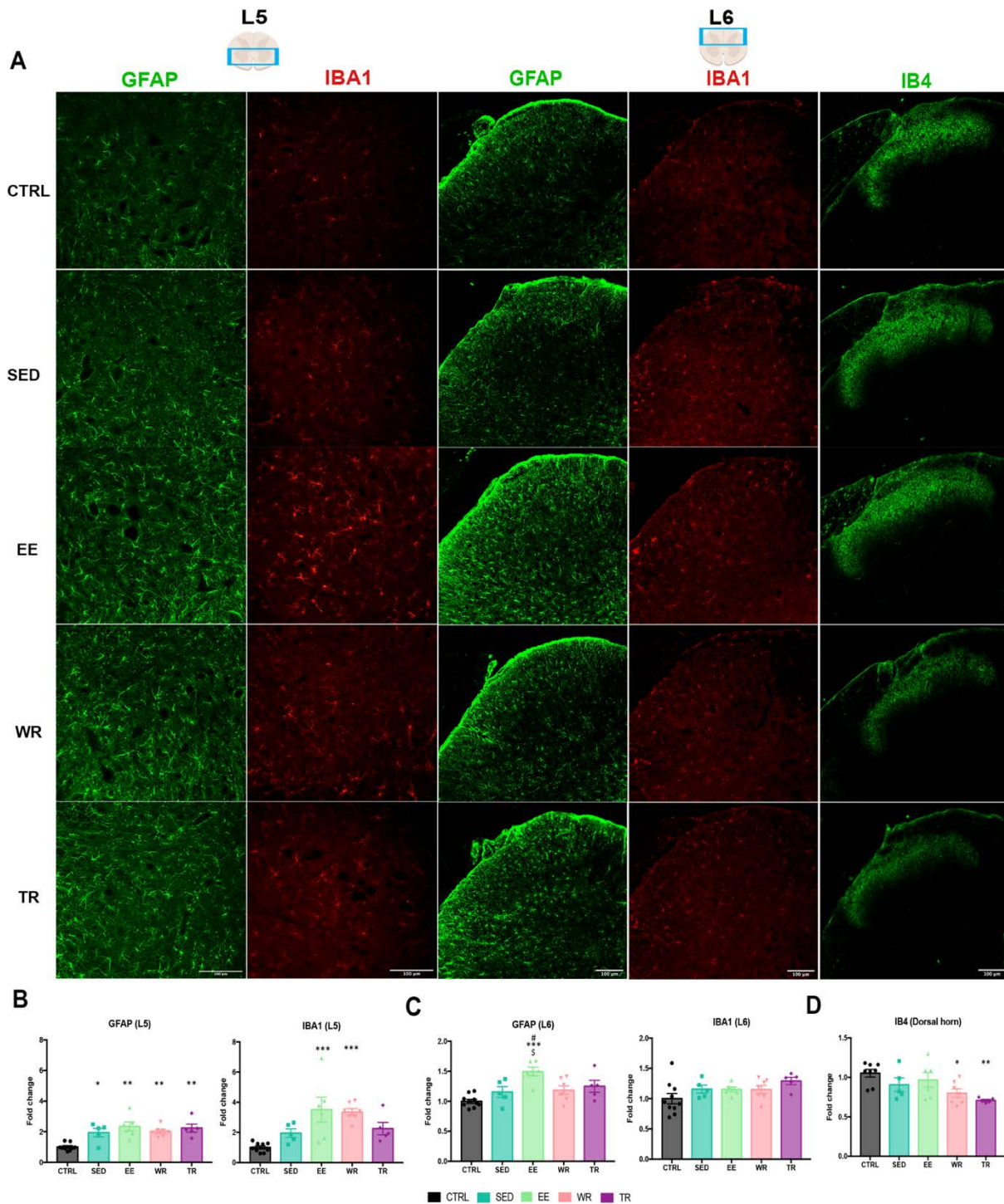


Figure 4. Inflammation and neuropathic pain assessment after SCI and activity-dependent therapies. (A) Representative images of lumbar L5 ventral and L6 dorsal horn of different histological markers after SCI and activity-based therapies. (B) Quantification of astrocytes and microglia labelled with GFAP (green) and Iba1 (red) at the ventral horn of L5 spinal cord. (C) Quantification of the intensity of glial markers labelled with GFAP (green) and Iba1 (red) at the dorsal horn of L6 spinal cord. (D) Quantification of IB4+ afferences in the dorsal horn of L6 spinal cord. * $p < 0.05$, ** $p < 0.01$, *** $p < 0.001$ vs control; # $p < 0.05$ vs SED; \$ $p < 0.05$ vs WR; as calculated by two-way ANOVA followed by Bonferroni correction for multiple comparisons (GFAP L5: $F_{4,27} = 8.88$, $p = 0.0001$; Iba1 L5: $F_{4,27} = 7.73$, $p = 0.0003$, GFAP L6: $F_{4,28} = 8.05$, $p = 0.0002$; Iba1 L6: $F_{4,28} = 2.1$, $p = 0.11$). Data are expressed as mean \pm SEM normalized to control group. Scale bar: 100 μm . CTRL: control, SED: sedentary, EE: enriched environment, WR: voluntary wheel, TR: forced treadmill.

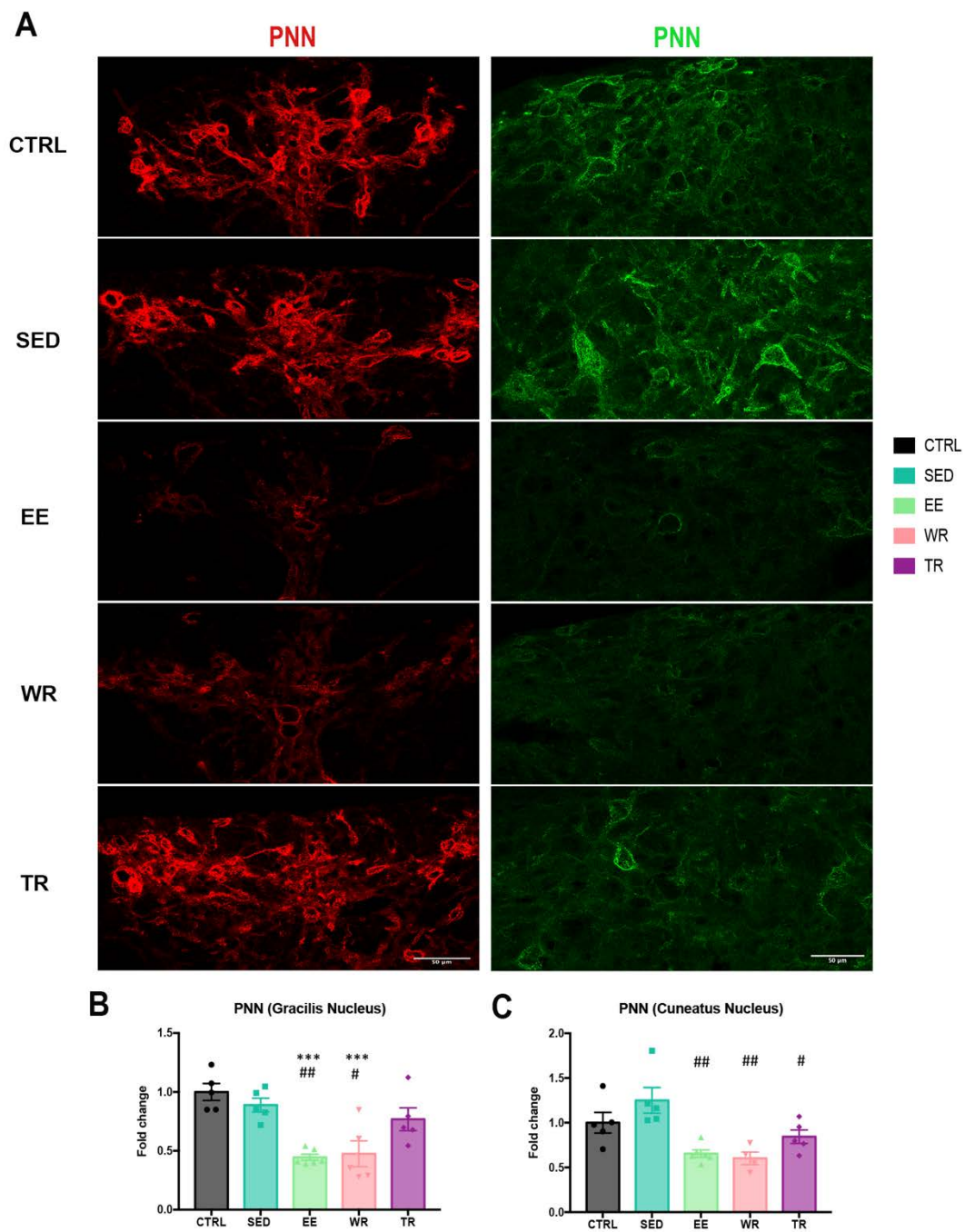


Figure 5. Modulation of PNN in the dorsal column nuclei after SCI and activity-dependent therapies. (A) Confocal images of PNN labelled with aggrecan (red in the gracile nucleus and green in the cuneatus nucleus) at 35 dpi. Quantitative analysis of PNN in the gracile (B) and cuneatus nuclei (C) in all groups. Quantitative analysis of *** $p < 0.001$ vs control; # $p < 0.05$, ### $p < 0.01$ vs SED, as calculated by one-way ANOVA with Bonferroni multiple comparison (Gracilis: $F_{4,21} = 10.82$, $p < 0.0001$; Cuneatus: $F_{4,20} = 7.63$, $p = 0.0007$). Data are expressed as mean \pm SEM normalized to control group. Scale bar: Scale bar: 50 μm . CTRL: control, SED: sedentary, EE: enriched environment, WR: voluntary wheel running, TR: forced treadmill running.

Discussion

During the past decades, intense research has focused on overcoming the inhibitory influence of proteoglycans after SCI, mainly by a general application of chABC. This approach, although very promising, could have masked the specific role of spinal PNN after injury. Here, we wanted to evaluate how a SCI and different types of physical activity could affect PNN around spinal motoneurons caudal to the injury and thus, to further understand the role of these nets in the functionality of spinal circuits. Finally, the fate of PNN in dorsal column nuclei in the brainstem after SCI was also evaluated.

Effects of SCI and activity-based therapies on lumbar PNN

We found that the contusion on the thoracic spinal cord produced a reduction of lumbar PNN after the injury. The partial disappearance of PNN could be explained by a decreased activity in motoneurons (Dityatev A, Brückner G, Dityateva G, Grosche J, Kleene R, 2007) produced not only by the interruption of descending inputs but also by the reduced sensory input from the muscle spindles caused by the paresis of the hindlimb. Indeed, a reduction of aggrecan expression around motoneurons was reported after paralyzing hindlimb muscles with botulinus toxin A (Kalb and Hockfield, 1994). Complementary, metalloproteases, the proteolytic enzymes that degrade PNN, become upregulated after SCI which could also contribute to PNN reduction (Zhang et al., 2011).

In contrast to our findings, a previous work pointed out that after a cervical spinal cord hemisection, there is a fast increase of proteoglycans at the phrenic motor nuclei (Alilain et al., 2011) although no quantification of PNN was performed. In contrast, we specifically measured PNN, by analyzing aggrecan intensity, around lumbar motoneurons. Phrenic motoneurons are related with breathing motor control, whereas lumbar motoneurons are mainly locomotor, therefore activity could differentially affect their PNN, as differentially affects encephalic and lumbar ones (Foscarin et al., 2011). In fact, it is not surprising that the hindlimb paralysis caused by the SCI decreased PNN in the lumbar spinal cord since previous works have already demonstrated that neural activity increases lumbar PNN (Arbat-Plana et al., 2015; Smith et al., 2015). In our study, the application of the different activity-dependent therapies reverted the decrease of PNN induced by the injury, being the voluntary wheel running the most effective protocol preserving these nets.

To understand the differential effect of the three types of activities is important to note that, in our study, the enriched environment did not favor intense physical

activity, as the wheel was blocked, whereas the paper tissue elicited fine-motor activity to build the nest. However, the WR group included both an enriched environment and full access to a wheel during all the follow-up. In contrast, animals submitted to a forced and ruled physical activity were kept in standard cages and physical exercise was limited to 20 minutes per day in a treadmill, with an intensity adapted to the locomotor capabilities of each mouse. This fact could explain the weaker effect of the TR group on spinal PNN compared to previous works (Arbat-Plana et al., 2015). Altogether, our results suggest that the quantity and intensity of physical activity performed may be crucial in determining the degree of PNN modulation. In fact, previous work in our laboratory already pointed out that the amount and not the type of physical activity is important for the maintenance of spinal PNN after neural injuries (Arbat-Plana et al., 2017).

The potential of physical rehabilitation to favor motor recovery after SCI has been related with increased expression of neurotrophic factors (Vaynman et al., 2003; Hutchinson et al., 2004) and activation of the spinal circuits, which integrate sensory information to generate appropriate motor responses without supraspinal inputs (de Leon et al., 1998). In addition, segmentary sensory inputs are crucial for the maintenance of spinal PNN mediated by physical activity (Arbat-Plana et al., 2015).

On the one hand, during exercise, activation of motoneurons either by segmentary reflexes or spare descending motor tracts could mediate PNN formation through AMPA receptors (AMPAr) activation. In fact, in cortical interneurons, calcium influx via AMPAr and L-type channels is necessary for the activity-dependent formation of PNN (Dityatev et al., 2007).

On the other hand, several works have highlighted the potential of enriching activities to modulate cortical (Sale et al., 2007; Madinier et al., 2014; O'Connor et al., 2019) and cerebellar PNN (Foscarin et al., 2011). However, to our knowledge, there are no previous studies analyzing the impact of enriching stimuli on spinal PNN. Regardless of the anatomical location, enriched stimuli produce epigenetic changes in the neuron transcription machinery affecting genes involved in synaptic signaling and plasticity (Rampon et al., 2000; Fischer et al., 2007). These changes in chromatin remodeling are tightly related to PNN since were first described in the visual cortex during the critical period (Putignano et al., 2007). Exposure to an enriched environment, with free access to a wheel, had beneficial effects on the sensorimotor functions of adult mice, with improved equilibrium, motor coordination and muscular strength (García-Mesa et al.,

2011). In a recent study, it enhanced the activity of proprioceptive neurons and increased their regenerative potential in an experimental model of SCI (Hutson et al., 2019). These effects were also mediated by epigenetic reprogramming in proprioceptive neurons. Therefore, similar to cerebellar PNN (Foscarin et al., 2011), regulation of spinal PNN could be mediated by a synergistic effect between intrinsic and extrinsic factors.

It is important to note that the improvements of BMS score over time observed in the WR group and slightly shown also in EE talk in favor of a time-dependent progression that may be facilitated by these treatments. However, the effects of activity on PNN observed at 35 dpi were not found in the long-term experiment, in which there were no differences in PNN levels between the studied groups. Probably, the spontaneous recovery and the increased locomotor activity observed after this mild injury, progressively provided the necessary input to increase spinal PNN and consequently neutralized the effect of activity-dependent therapies.

Effects of activity-based therapies on functional and electrophysiological outcomes after SCI

SCI does not only lead to loss of motor and sensory function but also facilitates the appearance of spasticity and neuropathic pain, which are related to maladaptive plasticity after the injury. We observed that SCI mice developed hyperreflexia and hyperalgesia. Activity-dependent therapies reduced them, although with variable effects depending on the type of activity applied. Voluntary wheel running was able to modulate both alterations, whereas treadmill running only attenuated hyperalgesia after SCI. Previous works have already demonstrated that physical exercise can modulate both neuropathic pain and hyperreflexia after SCI (Côté et al., 2014; Detloff et al., 2014).

Considering hyperreflexia, the H-wave, typically altered after SCI, was recovered by bike-training in SCI animals, and these changes were related with normalized levels of KCC2 in the lumbar spinal cord (Côté et al., 2014), similarly to what we described in the WR group. In contrast, our forced exercise protocol had no effects on these parameters, probably due to the lower amount of activity performed compared to the WR group. In fact, we found a relationship between the functionality of spinal circuits and lumbar spinal PNN. Hence, changes in PNN may directly contribute to the development of hyperreflexia or indirectly through alterations in the KCC2 cotransporter. A reduction of the inhibitory responses of motoneurons has been attributed to changes in the intracellular $[Cl^-]$ balance due to a reduction of cation-

chloride cotransporters (CCC). In fact, the reduction in the KCC2 transporter found in the SCI mice has been linked to the excitatory state of motoneurons and contribute to the development of hyperreflexia (Boulenguez et al., 2010). However, recent work points out that proteoglycan sulfates found in PNN determine the homeostatic set point of Cl⁻ and hence, neuron polarity of GABA signaling (Glykys et al., 2014). Thus, the reduction of negative extracellular charges may modify the transmembrane Cl⁻ gradient (De Luca and Papa, 2016), altering the inhibitory synaptic potentials and impairing network excitability (Glykys et al., 2014; Miao et al., 2014; Tewari et al., 2018). In addition, the positive and strong correlation between PNN and KCC2 levels suggest a possible relation between both markers. Actually, immature motoneurons found during development are characterized by reduced level of KCC2 and an absence of PNN. At P14, there is a robust increase of KCC2 which coincides with an increased synthesis of PNN components (Galtrey et al., 2008; Ben-Ari et al., 2012). Thus, it seems that after SCI, motoneurons turned into an immature phenotype which is reversed by activity-based therapies. Moreover, our hypothesis is also supported by the electrophysiological tests. Mice submitted to wheel running had significant preservation of spinal PNN and, in parallel, showed electrophysiological H-reflex parameters closer to control animals. Besides, our findings give support to the previous suggestion that optimal neuronal excitability provided by PNN preservation together with modulation of stretch reflex by proprioceptive afferent activation may contribute to locomotion recovery (Takeoka et al., 2014).

We also found that activity-based therapies significantly increased the density of glutamatergic VGlut1⁺ terminals around spinal motoneurons, even above control levels. A previous study demonstrated that there is a competition between proprioceptive terminals and corticospinal descending inputs to contact spinal motoneurons (Jiang et al., 2016). Thus, the increased activity of proprioceptive fibers together with a reduced descending input due to the SCI, increases primary afference inputs to motoneurons from injured animals exposed to activity. However, besides the number of contacts, other factors determine the effectiveness of these synapses. Similar to GABA responses, the effectiveness of glutamatergic signaling through AMPAR is also related to this net-like extracellular matrix (Sylantsev et al., 2008; Frischknecht et al., 2009). In fact, in immature neurons, a higher diffusion of AMPAR has been described compared to mature neurons (Frischknecht et al., 2009). Hence, it is feasible that proprioceptive neurons and PNN present mutual and positive feedback: while proprioceptive activation might

participate in the synthesis of PNN components, the presence of PNN would be essential for the functionality of the mature synapses and thus, to reinforce the circuit.

Regarding neuropathic pain, a thoracic SCI produced thermal allodynia which was reversed by therapies that increased physical activity, such as treadmill running or voluntary running in a wheel, but not when animals were just kept in an enriched environment. In the literature, different protocols of exercise have been able to revert mechanical and sometimes thermal hyperalgesia after diverse SCI models (Detloff et al., 2014; Sliwinski et al., 2018). In our model, the reduction in neuropathic pain was not related with changes in microglia reaction, since we did not find microgliosis at the L5-L6 segments where nociceptive afferents from the hind paw enter in the spinal cord. A previous study also found that activation of mechanosensory afferents did not induce microglial proliferation in the dorsal horn of the spinal cord (Hathway et al., 2009).

Strikingly, sensorimotor activity induces structural changes in the nociceptive system, as we observed that those animals with reduced pain presented less IB4+ staining. During the painful state, there is a process mediated by IB4+ cells called hyperalgesic priming, that drives the progression of acute pain into a chronic state (Joseph and Levine, 2010; Alvarez et al., 2012). Besides, the reduction of thermal hyperalgesia and decrease of IB4+ staining in the dorsal horn by physical exercise has also been observed in a SCI model of chronic neuropathic pain (Sliwinski et al., 2018).

Since enriched environment and treadmill groups presented similar levels of PNN but not similar latency withdrawal in the thermal test, it seems clear that PNN do not contribute to neuropathic pain in this model. However, our study focuses on PNN around motoneurons. It would be interesting to study the implications of the fewer PNN located in the dorsal horn (Galtrey et al., 2008), as overexpressing Sema3A, one of the plasticity inhibitors in the PNN (Vo et al., 2013), in injured animals prevented pain development (Tang et al., 2004).

Differential effects of SCI and activity-based therapies on PNN in spinal cord and brainstem

A current challenge in the PNN field is to understand why PNN are differently regulated by activity depending on the anatomical localization. In this study, we also evaluated how SCI affected PNN in the dorsal column nuclei, the brainstem centers that process limb sensory information (Gordon and Grant, 1982). The gracile nucleus is classically considered the sensory relay of fine sensation from the hindlimb, being the cuneate nucleus the equivalent for the forelimb (Watson, 2012). *Massey et al (2006)*. had

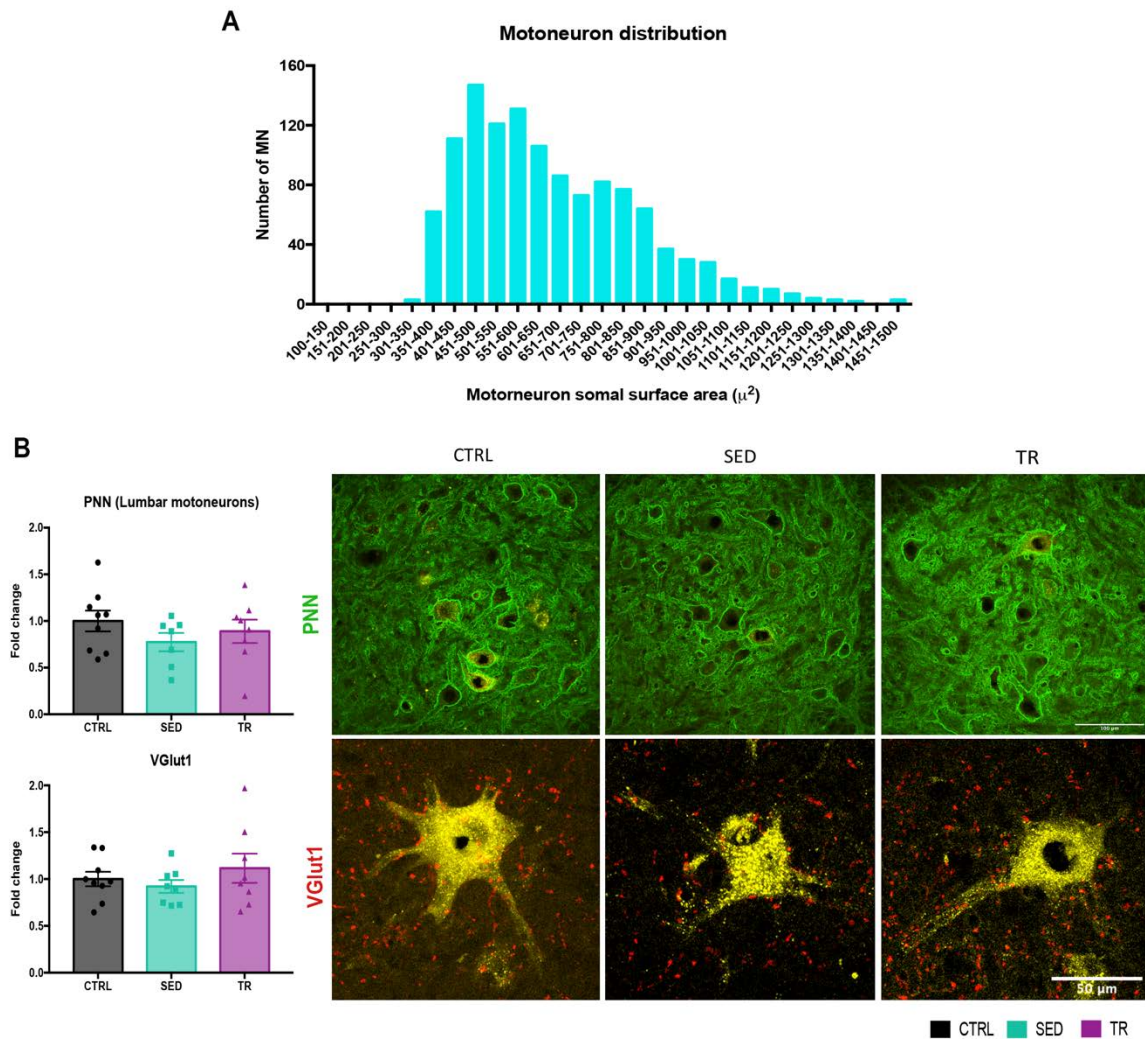
already shown that a cervical SCI increased PNN in the cuneatus nucleus, although no quantification was presented in the paper (Massey et al., 2006). In contrast, we found that the thoracic injury did not modify PNN around denervated gracile neurons at 35 dpi. Since a recent work points out that while the gracile nucleus only processes the hindlimb fine tactile information, cuneate nucleus integrates the forelimb fine tactile and the fore and hindlimb proprioceptive information (Niu et al., 2013), we therefore, analyzed PNN of the cuneate nucleus, too. PNN in these nuclei were also non affected by the thoracic injury.

Considering the effect of activity on both brain stem nuclei, we could observe a clear reduction of PNN by the enriched environment and voluntary exercise, whereas the treadmill protocol only reduced PNN in the cuneate nucleus. Probably, the maintenance of PNN on these nuclei could be also mediated by descending inputs from higher somatosensory centers (Watson, 2012) and not just by direct projections from peripheral neurons. In fact, several works have already demonstrated that enriching activities reduces PNN from sensory cortices (Hutchinson et al., 2004; Sale et al., 2007).

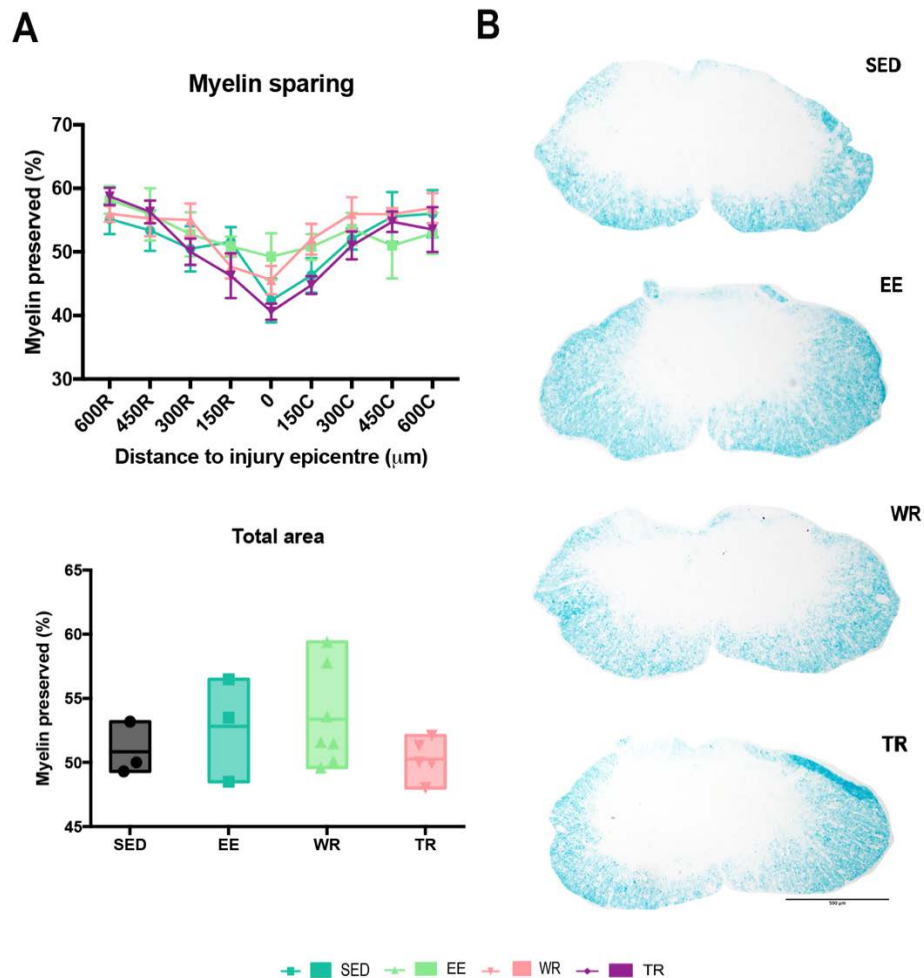
Conclusion

In conclusion, this study evidences that SCI has a direct impact on PNN around spinal motoneurons caudal to the injury, and that different types of activity can modulate the expression of PNN, together with beneficial effects on functional outcome after the injury. We propose that these PNN have a relevant influence on motoneuron excitability and synaptic connectivity. Altogether, the modulation of PNN expression emerges as a versatile target to treat neuronal disorders that either need to boost plasticity or protect synaptic integrity.

Supplementary figures



Supplemental Figure 1. Lumbar PNN and VGlut1 modulation 11 weeks after SCI. (A) Representative distribution of motoneurons selected to quantify PNN. (B) Confocal images of PNN, labelled with aggrecan (green) and proprioceptive contacts, labelled by VGlut1 (red) around lumbar motoneurons, labelled with Nissl (yellow) in the lumbar spinal cord at 77 dpi, preceded by the quantitative analyses of aggrecan and VGlut1 immunostaining. No significant differences were found by one-way ANOVA with Bonferroni multiple comparison (PNN: $F_{2,21} = 0.98$, $p = 0.39$; VGlut1: $F_{2,22} = 0.82$, $p = 0.46$). Data are expressed as mean \pm SEM normalized to control group. CTRL: control, SED: sedentary, TR: forced treadmill running.



Supplemental Figure 2. Tissue damage evaluation after SCI and activity-based therapies. (A) Quantification of white matter sparing from the injury epicentre to 600 µm rostral and caudal. Total white matter sparing in 1.2mm spinal cord samples of different mice groups. (B) Representative micrographs showing white matter sparing at the epicentre of the injury in sections stained against LFB from all experimental groups. No significant differences were found as calculated by two-way (myelin sparing; distance $F_{8,110} = 7.62$, $p < 0.0001$; group $F_{3,110} = 2.22$, $p = 0.09$; interaction $F_{24,110} = 0.67$, $p = 0.87$) and one-way (total area; $F_{3,21} = 1.84$; $p = 0.17$) ANOVA with Bonferroni multiple comparison. SED: sedentary, EE: enriched environment, WR: voluntary wheel running, TR: forced treadmill running.

Chapter III

Link protein 1 is involved in the activity-dependent modulation of perineuronal nets in the spinal cord

Link protein I is involved in the activity-dependent modulation of perineuronal nets in the spinal cord

Sánchez-Ventura J¹, Lago N¹, Penas C¹, Navarro X¹, Udina E^{1*}

Author affiliations:

¹Institute of Neuroscience, Department Cell Biology, Physiology and Immunology, Universitat Autònoma de Barcelona, and Centro de Investigación Biomédica en Red sobre Enfermedades Neurodegenerativas (CIBERNED), Bellaterra, Spain

Abstract

One of the challenges of the mature nervous system is to maintain the stability of neural networks while providing a degree of plasticity to generate experience-dependent modifications. This dynamic plasticity-stability balance is regulated by perineuronal nets (PNNs) and is crucial for the proper functioning of the system. In previous studies, we found a relation between spinal PNNs reduction and maladaptive plasticity after spinal cord injury (SCI), which was attenuated by maintaining PNNs with activity-dependent therapies. Moreover, transgenic mice lacking the cartilage link protein 1 (*Crtl1* KO mice) showed aberrant spinal PNNs and increased spinal plasticity as observed just after SCI. Therefore, the aim of this study is to evaluate the role of link protein 1 in the activity-dependent modulation of spinal PNNs, and its impact on the maladaptive plasticity observed following SCI. We first studied the activity-dependent modulation of spinal PNNs using a voluntary wheel-running protocol for two weeks in *Crtl1* KO and WT mice. This training protocol increased spinal PNNs in WT mice but did not modify PNN components in *Crtl1* KO mice, suggesting that link protein 1 mediates the activity-dependent modulation of PNNs. Secondly, *Crtl1* KO and WT mice received a thoracic cord contusion, and functional outcomes were evaluated for 35 days. Interestingly, hyperreflexia and hyperalgesia found at the end of the experiment in WT-injured mice were already present at basal levels in *Crtl1* KO mice and remained unchanged after the injury. These findings demonstrated that link protein 1 plays a dual role in the correct formation and in activity-dependent modulation of PNNs, turning it into an essential element for the proper function of PNN in spinal circuits.

Keywords: perineuronal nets, spinal cord injury, link protein 1, activity-dependent therapy, maladaptive plasticity.

Introduction

The extracellular matrix (ECM) is a crucial part of the central nervous system (CNS) that provides structural and biochemical support to cells. While most of the ECM is diffuse and fills all the intercellular space, there are also specialized and highly condensed pericellular coats of ECM, named perineuronal nets (PNNs), that just surrounds some neurons in the CNS (Tewari et al., 2022). Perineuronal nets are primarily known for their role in synaptic stabilization and plasticity control (Pizzorusso, 2002). However, other roles have been recently attributed such as ionic buffering, neuroprotection, and neural maturation (Fawcett et al., 2019). PNNs are mainly composed of hyaluronan, chondroitin sulfate proteoglycans (CSPGs; including aggrecan, versican, neurocan and brevican), link proteins and the glycoprotein Tenascin-R (Kwok et al., 2011). Among all of them, link proteins are the most important elements since they are crucial for the formation and maintenance of PNNs structure (Carulli et al., 2010). *In vitro*, the lack of the gene *Crtll*, which encodes the link protein 1, prevents PNNs formation around PNN-bearing cells (Kwok et al., 2010). *In vivo*, it generates attenuated PNNs in the visual cortex (Carulli et al., 2010) the deep cerebellar nuclei (Foscarin et al., 2011), and aberrant PNNs in the spinal cord, with an altered proportion of their components (Sánchez-Ventura et al., 2022).

Although PNNs structure is quite stable, it can be rearranged by the activity of neurons, facilitating, or restricting plasticity (Dityatev et al., 2007). *Smith et al* demonstrated that this activity-dependent regulation differs depending on the anatomical location; while physical activity reduced cortical PNNs, the same activity increased spinal PNNs (Smith et al., 2015). Likewise, a protocol of voluntary running reduced PNNs in the brainstem sensory nuclei but increased spinal PNNs around lumbar motoneurons (Sánchez-Ventura et al., 2021).

Changes in PNN structure can be also observed after traumatic spinal cord injury (SCI), when alterations in the ECM break the plasticity-stability balance of the mature nervous system. Indeed, spared neurons below the injury level increase their plastic capability and create new connections that enhance spontaneous recovery or lead to maladaptive symptoms such as neuropathic pain and spasticity (Finnerup, 2017). Activity-dependent therapies are one of the most successful strategies to rewire and stabilize synapses in a functional manner and thus, reduce maladaptive symptoms after SCI (Torres-Espín et al., 2018). In a recent study, we showed that after a thoracic SCI

there is a reduction in the thickness of PNNs around lumbar motoneurons, and the application of activity-dependent therapies counteracts this reduction promoting functional recovery (Sánchez-Ventura et al., 2021). These findings highlight the link between maladaptive plasticity, activity-dependent therapies and spinal PNN, and situate spinal PNNs in the spotlight of the pathophysiology and recovery after SCI.

Thus, the goal of this study was to evaluate the role of link protein 1 in the activity-dependent modulation of PNNs, and its importance for a proper function of spinal PNNs. For this purpose, transgenic mice lacking the link protein 1 (*Crtll* KO) were used. We previously reported that these mice had aberrant spinal PNNs, increased spinal excitability and presented motor disfunctions (Sánchez-Ventura et al., 2022). In the present study, we investigated whether absence of link protein 1 affects the increase of PNNs observed after physical activity, and the decrease of PNNs observed after the inactivity produced by SCI. Thus, functional, and histological outcomes produced by a thoracic SCI were compared between *Crtll* KO and WT mice.

Material and methods

Experimental groups

Transgenic mice used in the present work were provided by Dr. Pizzorusso and maintained in the Animal Facility of the Universitat Autònoma de Barcelona (UAB). Their generation and phenotype were described previously (Czipri et al., 2003; Sánchez-Ventura et al., 2022).

Adult (8-10 weeks) female and male mice were used in this study. Two different experiments were carried out to determine the activity-dependent modulation of spinal PNNs of WT and *Crt11* KO mice (Figure 1). In the first experiment, four groups were generated to evaluate changes of spinal PNNs after exposing mice to a voluntary wheel-running protocol for 15 days. Thus, the groups were: WT sedentary (n=8), WT wheel (n=9), *Crt11* KO sedentary (n=6); *Crt11* KO wheel (n=10). For the second experiment, four groups were generated to evaluate the effect of inactivity, produced by SCI, on PNNs.

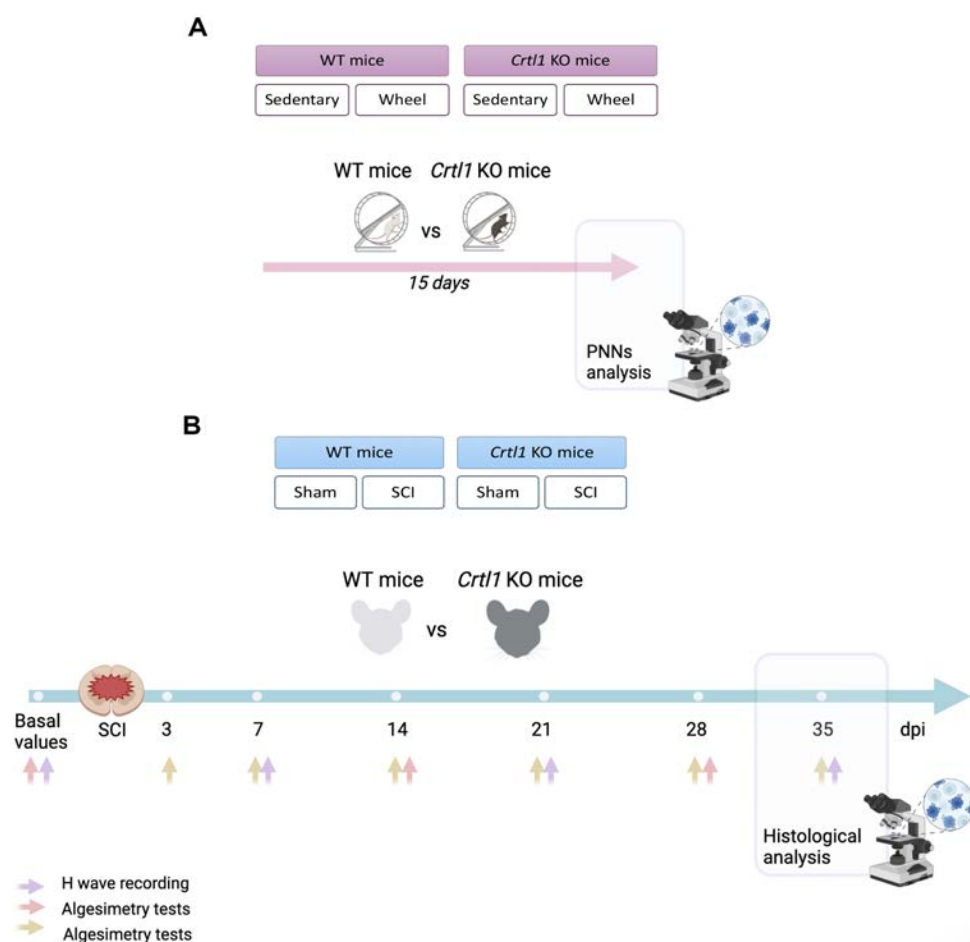


Figure 1. Schematic representation of the experimental design. A. Diagram showing the experimental groups and the timeline of the activity-dependent modulation experiment. B. Schematic diagram of the experimental groups and the timeline of the SCI experiment. Individual images were obtained from Biorender. WT: wild-type; *Crt11*: cartilage link protein 1; *Crt1*: cartilage link protein 1; KO: knock-out; PNNs: perineuronal nets; SCI: spinal cord injury; DPI: days post-injury.

Thus, WT and *Crtll* KO mice were subdivided in: WT sham (n=10), WT SCI (n=8), *Crtll* KO sham (n=10), *Crtll* KO SCI (n=6). Experimenters were blinded to genotype during behavioral and histological evaluations.

The experimental procedures were approved by the Experimental Ethical Committee (CEAAH) of our institution and conducted following the animal welfare guidelines of the European Communities Council Directive 2010/63/EC. Mice were housed in groups, at 22 °C (\pm 2 °C), kept on a 12:12 light/dark cycle and received water and food *ad libitum*.

Spinal cord injury

Mice were anesthetized with an intraperitoneal injection of ketamine (90 mg/kg) and xylazine (10 mg/kg) in saline solution. Then, a longitudinal incision was made in the skin of the dorsum, the vertebrae was accessed, and laminectomy was performed to expose the dura at the low thoracic level. After laminectomy, a moderate contusion was performed at T11 using the Infinite Horizon Impactor device (50 KDyn, tissue displacement between 300-490 μ m). After the surgery, animals were kept on a thermostatically regulated heating pad until completely awake and received 1 ml of saline solution subcutaneously to prevent dehydration. Postoperative care consisted of subcutaneously injections of buprenorphine (0.1 mg/kg) during the following three days and bladder expression twice a day until the voiding reflex was reestablished. For the sham group, only laminectomy was performed.

Activity-based therapy protocol

WT and *Crtll* KO mice of the wheel groups were housed in a cage equipped with a free-to-access running wheel (364 × 258 × 350 mm; Activity Wheel Cage System for mice, Tecniplast, Buguggiate, Italy). The wheels were connected to a wheel lap counter to daily calculate the running distance using the diameter of the wheel (21 cm) and a revolution correction. Animals were housed alone to determine the running distance of each animal.

Functional assessment

Locomotion assessment

Motor recovery was studied in an open field using the Basso Mouse Scale (BMS), a nine-point scale where 0 means total paralysis and 9 normal locomotion. The test was

performed at 3, 7, 14, 21, 28 and 35 days post-injury (DPI). The evaluation was performed by two researchers blinded to the mice genotype. The score of each paw was averaged for each animal each testing day.

As an exclusion criterion, those mice that showed a BMS >3 the day after the contusion, were excluded from the experiment.

Algesimetry tests

Thermal and mechanical algesimetry tests were performed preoperatively to determine baseline values and at 14 and 28 days after the injury, for assessing appearance of hyperalgesia. Before testing sessions, mice were acclimatized to the room and habituated to the testing chambers for 15 minutes. Then, tests were performed by a blinded researcher.

Mechanical allodynia was assessed using an electronic Von Frey device (Bioseb). Mice were placed in individual compartments with grid base and Von Frey metal tip was applied to the plantar surface of the hindpaw. An increasing mechanical force was applied until a paw withdrawal response resulted. Thermal hyperalgesia was evaluated with the Plantar Algesimeter device (Ugo Basile). Briefly, a light beam (intensity= 30 mW/cm²) was pointed to the hindpaw until the animal withdrew the paw. The temperature reached to the response was measured. The cut of time was defined in 20 seconds. In both tests, three values were obtained for each paw, and the mean values of both paws were averaged for each animal.

Electrophysiological tests

Hyperreflexia was evaluated prior to the injury and at 7, 21 and 35 days after the injury with electrophysiological tests. Tests were conducted under general anesthesia with ketamine 90 mg/kg and xylazine 10 mg/kg, since it has negligible effects on electrophysiological recordings (Ho and Waite, 2002). During the electrophysiological evaluation, a heating pad was used to maintain the body temperature, and a dissection microscope was used to ensure reproducibility of needle location between mice.

Recorded signals were amplified and visualized on a digital oscilloscope (Tektronix 450S), then fed to a PowerLab 4ST unit, and LabChart software used for signal analysis.

Hyperreflexia was studied measuring the H wave response, the electrical counterpart of the stretch monosynaptic reflex. Specifically, we measured the amplitude

ratio of the H wave and its rate-dependent depression (RDD) in the interosseous plantar muscle.

Firstly, the sciatic nerve was stimulated by delivering single electrical pulses of 0.01 ms (Grass S88 stimulator) with monopolar needles inserted in the sciatic notch. The compound muscle action potential (CMAP) of the plantar muscle was recorded using microneedles inserted in the belly of the muscle as active electrode and on the fourth toe as reference. The maximal baseline to peak amplitude of the M wave (M_{\max} : direct muscle response), and the maximum amplitude of the H wave (H_{\max} : monosynaptic reflex) were measured. Then, the H_{\max}/M_{\max} ratio was calculated as an index of excitability of the afferent inputs on spinal efferent motoneurons. M wave values were obtained at supramaximal stimulation, whereas the H_{\max} was elicited by progressively increasing the intensity of the electrical stimuli until reaching the maximum amplitude of the H wave.

The RDD of the H wave consists of measuring the changes in the amplitude of the H wave with repetitive stimulations. Alterations in this parameter are a hallmark of hyperreflexia. Trains of ten consecutive pulses, using the stimulation intensity that produced the H_{\max} , were delivered at different frequencies (1, 5, 10 and 20 Hz), with at least 30 seconds rest between each train. RDD values were expressed as the percentage of the ratio between the last and the first pulse. Then, a curve expressing the % RDD (y-axis) at different frequencies (x-axis) was generated.

Histological evaluation

In the voluntary-wheel experiment, mice were euthanized 15 days after the beginning of the experiment, whereas in the SCI experiment, mice were euthanized 35 days after the contusion. In both cases, mice were deeply anesthetized (200 mg/kg of pentobarbital) and were transcardially perfused with cold 4% paraformaldehyde (PFA) in 0.1M phosphate buffer (PB). Spinal cords were harvested and post-fixed in 4% PFA over 2h. Then, they were cryopreserved in 30% sucrose solution in PB at 4°C.

Lumbar spinal cords (L4-L6) were transversally cut on a cryostat (20 μ m thick sections) and collected onto gelatin-coated glass slides. L4-L5 sections were used to analyze PNN components (aggrecan, Tenascin-R), proprioceptive afferents (VGlut1: vesicular glutamate transporter 1) and glial reactivity (astrocytes, stained with GFAP, and microglia stained with Ibal) in the ventral horn. L6 sections were used to evaluate glial reactivity in the dorsal horn. For immunofluorescence staining, sections were permeabilized with phosphate buffer saline Triton 0.3% (PBST 0.3%) and nonspecific

interactions were blocked with 10% normal donkey serum for 1h at room temperature (RT). Then, sections were incubated overnight (ON) at 4°C with primary antibodies (Table 1). After washes, immunoreactive sites were revealed using species-specific secondary antibodies (1:200; Table 1). After 2h of incubation at RT, sections were washed and mounted with Fluoromount medium (Southern Biotech).

Table 1. List of primary and secondary antibodies.

Primary antibodies				Secondary antibodies			
Name	Dilution	Host	Reference	Name	Dilution	Host	Reference
Aggrecan	1:250	Rabbit	AB1031- Millipore	Alexa 488	1:200	Donkey x Rabbit	A21206- Invitrogen
Tenascin- R	1:200	Goat	AF3865- R&D systems	Alexa Fluor 594	1:200	Donkey x Goat	A11058- Invitrogen
VGlut1	1:300	Guinea Pig	AB5905- Millipore	Cys3	1:200	Donkey x Guinea Pig	706-165- 148- Jackson
GFAP	1:1000	Rabbit	AB5804- Millipore	Alexa 488	1:200	Donkey x Rabbit	A21206- Invitrogen
Ibal	1:300	Goat	AB5076- Abcam	Alexa 594	1:200	Donkey x Goat	A11058- Invitrogen

Histological analysis

For PNN components and glutamatergic synaptic markers, images were taken with a confocal laser-scanning microscope (around 30 steps, z-step size of 0.5 μm , Leica TCS SP5) at 40x. For each mouse, 4 images of the spinal cord were taken in which a minimum of 30 MNs (located within the ventral horn and presenting an area $> 350 \mu\text{m}^2$ (Friese et al., 2009)) were measured. PNN and VGlut1 analysis were performed following the next steps: the maximal projection of the z-stacks was performed and then, the background was corrected. Afterwards, a band of 4 μm around the cell body of MNs was delimited to measure the integrated density of that region.

For glial reactivity, grayscale microphotographs were captured at 20x in the ventral and dorsal horn. After background correction, the threshold was defined for all the microphotographs of each marker. Then, the integrated density of immunoreactivity was measured in a region of interest (ROI) of 302,141 μm^2 in the ventral horn, and a ROI of 301,692 μm^2 in the dorsal horn. At least eight sections per marker from each mouse

were used to calculate the averaged value. Images were acquired with a digital camera Nikon DS-Ri2 attached to a Nikon Eclipse Ni-E microscope. Image analysis was performed by Fiji software.

Statistical analysis

Statistical analysis was done using GraphPad Prism 7 software and data was expressed as mean \pm standard error of the mean (SEM). A normal distribution was confirmed using a Shapiro-Wilk test. For the voluntary-wheel experiment, the distance run during the 15 days was analyzed with a two-way repeated measures ANOVA, whereas the total distance run was studied with a Student's t-test. Functional tests in the SCI experiment were analyzed by two-way repeated-measures ANOVA with group and time after injury as factors, followed by Bonferroni post-hoc correction. All histological results were analyzed with one-way ANOVA. Differences were considered significant when $p < 0.05$.

Results

Link protein 1 is involved in the activity-dependent changes of PNNs in the spinal cord

Our first goal was to determine whether the activity-dependent modulation of PNNs, produced by two weeks of free access to a running wheel, is mediated by the link protein 1. There were not significant differences in the distance run during the 15 days

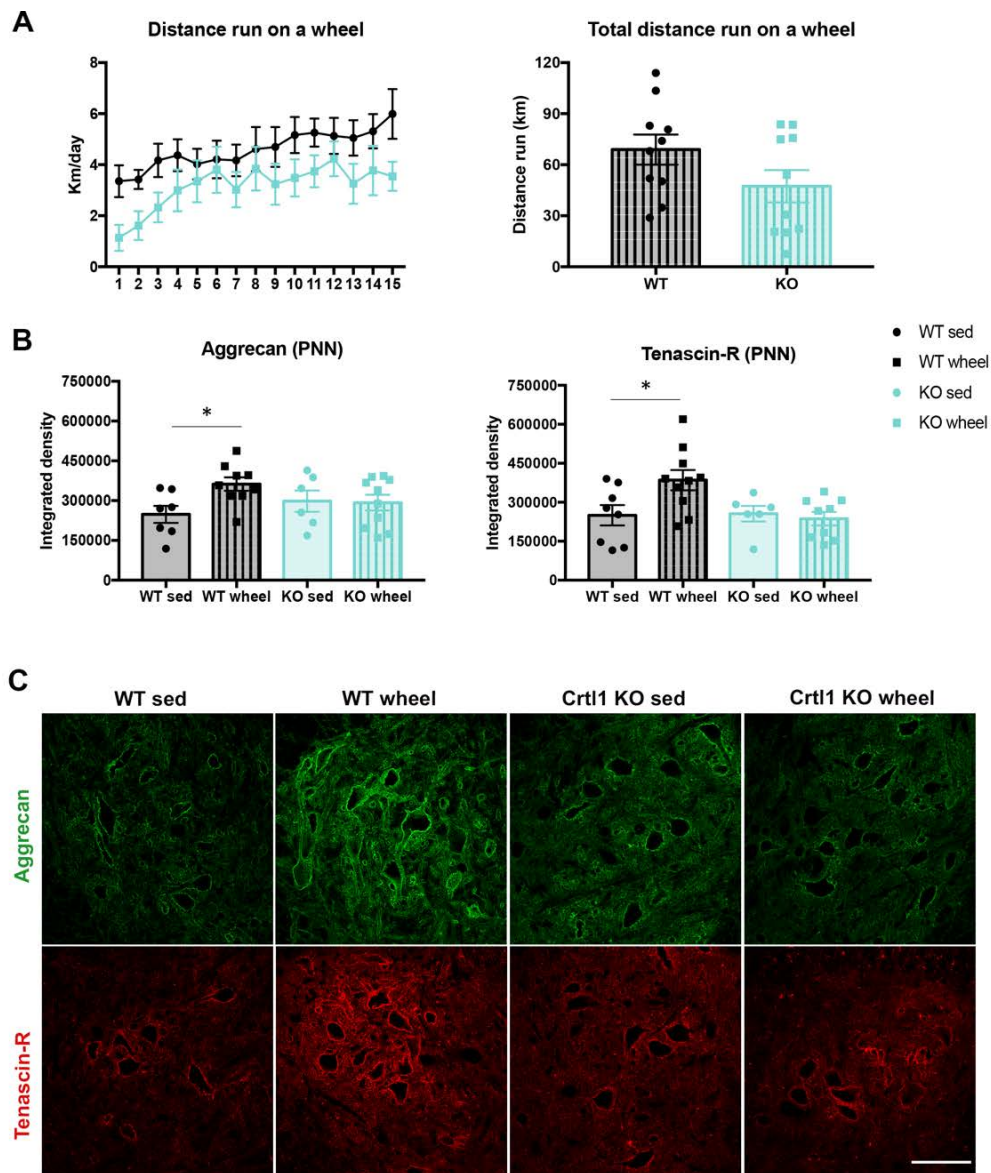


Figure 2. Link protein 1 is implicated in the activity-dependent modulation of PNNs. A. Averaged distance run on the wheel during each day of the follow-up and the total distance run during the 15 days. B. Quantification of the immunolabelling of the PNN components aggrecan and tenascin-R. C. Maximal projection of confocal images from the ventral horn of the lumbar spinal cord of WT and *Crt11* KO mice, showing the expression of aggrecan (green) and tenascin-R (red). $N_{\text{total}} = 33$ mice. Bar graphs are representing the mean values \pm SEM. Scale bar: 100 μm . * $p < 0.05$ by one-way ANOVA (Aggrecan: $F_{3,28} = 2.31$, $p = 0.09$; Tenascin-R: $F_{3,29} = 4.408$, $p < 0.05$) followed by post hoc test with Bonferroni correction. WT: wild-type; *Crt11*: cartilage link protein 1; KO: knock-out; sed: sedentary; PNN: perineuronal net.

nor in the total distance between WT and *Crtll* KO mice, despite the latter tended to run less distance (Figure 2A). However, the activity protocol induced changes in PNN components (Figures 2B, C). Specifically, WT mice that ran in a wheel showed a significant increase in the integrated intensity of the markers aggrecan and tenascin-R ($p < 0.05$ vs WT sed). However, *Crtll* KO mice that ran in a wheel had the same intensity levels of aggrecan and tenascin-R than the *Crtll* sedentary group (Figure 2B, C).

Uninjured *Crtll* KO mice mimic the functional outcomes observed in the injured WT mice

The thoracic spinal cord contusion produced similar motor impairment in WT and *Crtll* KO mice. All injured mice initially presented hindlimb paralysis, followed by a gradual and spontaneous recovery over the next days. No significant differences were found between groups in the BMS scale during follow-up (Figure 3A).

When mechanical and thermal sensitivity were assessed before the injury, we observed a significant decrease in the withdrawal force and in the heating latency in *Crtll* KO mice compared to WT mice ($p < 0.05$ and $p < 0.001$, respectively) (Figure 3B). These findings suggested that these transgenic mice already presented thermal and mechanical pain sensitivity before the injury. After SCI, WT mice developed thermal hyperalgesia (Figure 3B), which was manifested by a significant decrease in the withdrawal latency over time ($p < 0.05$ basal vs 14 dpi; $p < 0.001$ basal vs 28 dpi and 14 vs 28 dpi $p > 0.05$). However, the same injury did not produce mechanical allodynia in these mice, since they maintained the same withdrawal force at 14 and 28 dpi (Figure 3B).

In contrast, *Crtll* KO mice maintained their withdrawal threshold values, that were already reduced throughout the experiment, suggesting that the injury had no further effect on their pain sensitivity (Figure 3B).

Regarding hyperreflexia (Figure 4A, B), the electrophysiological tests performed before the injury showed that *Crtll* KO mice presented a higher H_{\max}/M_{\max} ratio compared to WT mice ($p < 0.05$). After SCI, *Crtll* KO mice maintained the same basal levels during the follow-up period. In contrast, 7 and 21 days after the contusion, WT mice presented a significant increase in their H_{\max}/M_{\max} ratio compared to their basal values ($p < 0.05$ basal vs 7 dpi; $p < 0.05$ basal vs 21 dpi), reaching the same levels of hyperreflexia than *Crtll* KO mice at 7, 21 and 35 dpi.

The RDD of the H reflex showed that both groups had almost complete depression of the H wave after 10 consecutive stimuli at 1 Hz (87.5% and 82.5% of depression in *Crtll* KO and WT mice, respectively) before SCI. After SCI, the depression profile changed similarly in both groups, with a significant increase in the % of depression of the H wave at 1 Hz at 7, 21 and 35 dpi in WT ($p<0.05$) and at 7 and 35 dpi in *Crtll* KO mice ($p<0.05$) (Figure 4C).

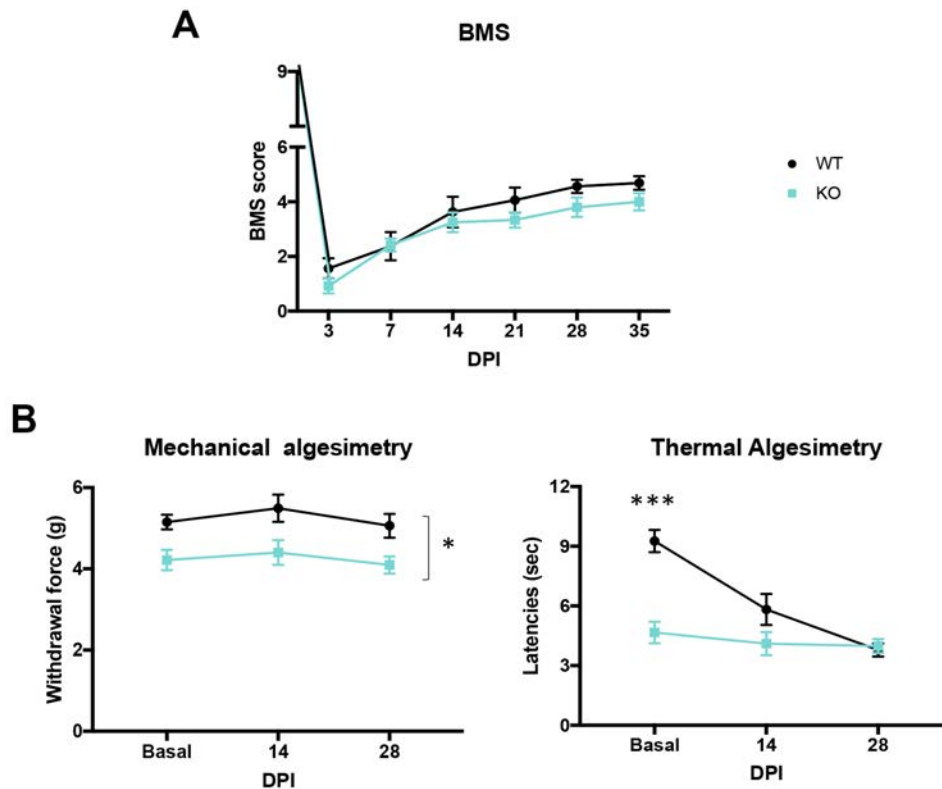


Figure 3. The neuropathic pain produced by the spinal cord contusion was already present in *Crtll* KO mice before the injury. A. Open field locomotion assessed by the BMS scale. B. Neuropathic pain assessment by thermal and mechanical algesimetry tests performed every two weeks. $N_{\text{total}}=14$ mice. Data are representing the mean values \pm SEM. * $p<0.05$, *** $p<0.001$ vs WT injured mice as calculated by two-way ANOVA (BMS: time $F_{5,60}=74.51$, $p<0.0001$; group $F_{1,12}=1.146$, $p=0.3$; interaction $F_{5,60}=1.273$, $p=0.28$; Mechanical algesimetry: time $F_{2,26}=1.031$, $p=0.37$; group $F_{1,13}=18.27$, $p<0.001$; interaction $F_{2,26}=0.049$, $p=0.95$; Thermal algesimetry: time $F_{2,26}=13.86$, $p<0.0001$; group $F_{1,13}=28.57$, $p=0.0001$, interaction $F_{2,26}=8.28$, $p=0.0017$) followed by Bonferroni correction for the multiple comparison. BMS: Basso Mouse Scale; DPI: days post-injury; WT: wild-type; KO: knock-out.

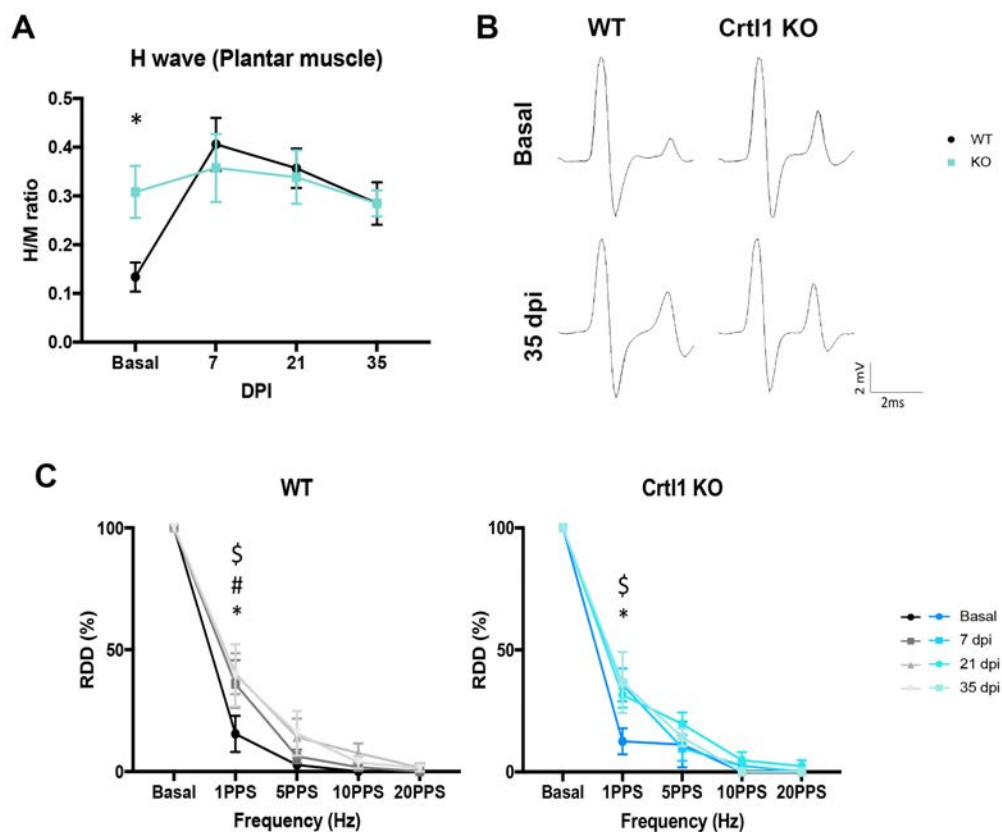


Figure 4. The hyperreflexia produced by the SCI was already observed in *Crt11* KO mice before the injury. A. Quantification of the H_{max}/M_{max} changes in the plantar muscle before the injury and at 6, 21 and 35 days after the injury. B. Representative electromyograms showing the initial M wave, resulting from the direct activation of motor axons, and a small wave with longer latency, the H wave, resulting from the monosynaptic activation of lumbar motoneurons by Ia afferences before the injury and at the end of the experiment. C. Depression profile of the H wave after 10 consecutive stimulations at 1, 5, 10 and 20 PPS at the beginning of the experiment, at 6, 21 and 35 days after the injury. $N_{total}=14$ mice. Data are representing the mean values \pm SEM. * $p<0.05$ vs WT (A) or 7 dpi (C); # $p<0.05$ vs 21 dpi; \$ $p<0.05$ vs 35 dpi as calculated by two-way ANOVA (*H wave recordings*: time $F_{3,39}=5.69$, $p=0.003$; group $F_{1,13}=0.38$, $p=0.551$; interaction $F_{3,39}=2.84$, $p=0.051$; RDD WT: frequency $F_{4,28}=201.4$, $p<0.0001$; time $F_{3,21}=2.63$, $p=0.077$, interaction $F_{12,84}=1.479$, $p=0.148$; RDD KO: frequency $F_{4,24}=591.7$, $p<0.0001$; time $F_{3,18}=1.39$, $p=0.28$; interaction $F_{12,72}=1.23$, $p=0.28$) followed by Bonferroni correction for multiple comparison. RDD: rate-dependent depression. WT: wild-type; *Crt11*: cartilage link protein 1; KO: knock-out; DPI: days post-injury; PPS: paired-pulse per second.

Lack of modulation of PNNs after SCI in *Crt11* KO mice

Changes of spinal PNNs were studied after SCI in both groups. Aggrecan immunostaining at the lumbar spinal cord revealed that the contusion significantly decreased the thickness of spinal PNNs in injured WT mice compared to the sham group (Figure 5A, $p<0.05$). In contrast, we did not find differences in the aggrecan immunolabeling of spinal PNNs between sham and injured *Crt11* KO mice.

Then, we studied the proprioceptive inputs to lumbar MNs with the VGlut1 marker (Figure 5B), that is specific for Ia sensory afferents from the muscle spindle (Todd et al., 2003). Despite uninjured *Crt11* KO mice showed increased values of VGlut1 on MNs, this increase did not reach significance. Besides, the SCI did not modify VGlut1 immunolabeling at 35 days after the injury neither in WT nor in *Crt11* KO mice.

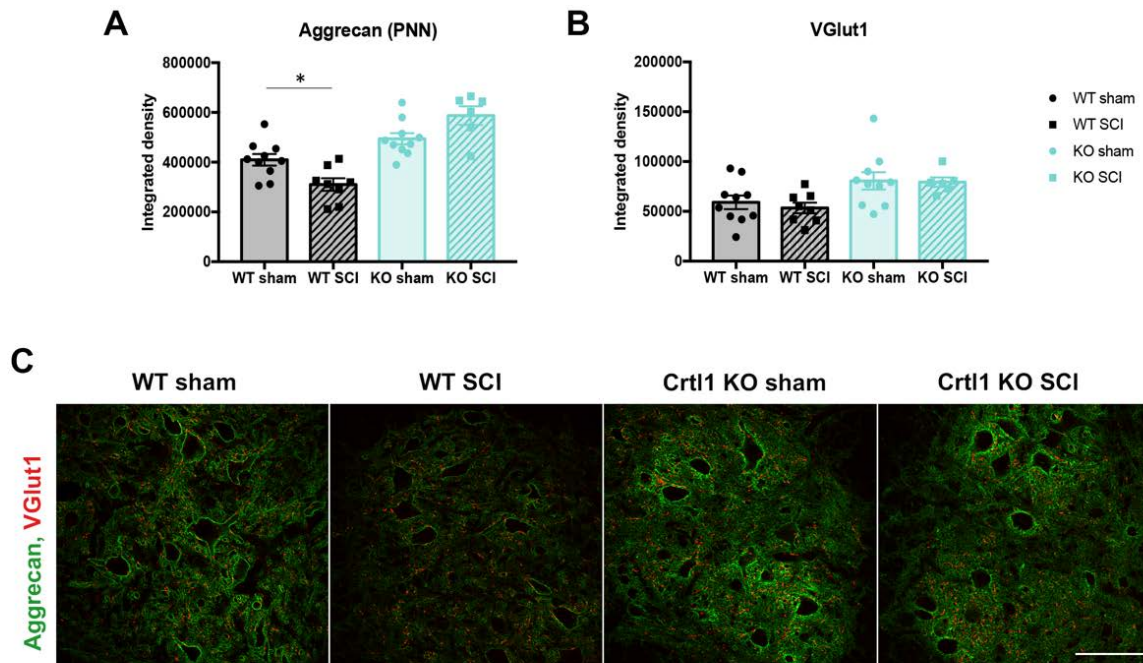


Figure 5. The spinal cord injury reduced lumbar perineuronal nets in WT but not in *Crt11* KO mice. A. Quantification of PNNs labelled with aggrecan (green) around lumbar motoneurons. B. Quantification of the proprioceptive afferents found in $4\mu\text{m}$ around lumbar motoneurons, labelled with VGlut1 (red). C. Confocal images representing PNN and the proprioceptive afferents around lumbar motoneurons found in the ventral horn. $N_{\text{total}} = 34$ mice. Scale bar: $100\mu\text{m}$; Bar graphs are representing the mean values \pm SE. $*p < 0.05$ as calculated by one-way ANOVA (Aggrecan: $F_{3,30} = 16,48$, $p < 0.0001$; Tenascin-R: $F_{3,30} = 3,68$, $p = 0.023$) with Bonferroni comparison. PNN: perineuronal nets; WT: wild-type; *Crt11*: cartilage link protein 1; KO: knock-out; SCI: spinal cord injury; VGlut1: vesicular glutamate transporter 1.

Lack of link protein 1 modifies glial reactivity after SCI

Astroglial and microglial reactivity was studied at the ventral and dorsal horns of the lumbar spinal cord. Before the injury, *Crt11* KO sham mice showed a significant increase in the intensity of the markers GFAP and Iba1 at the ventral horn (GFAP: $p < 0.05$; Iba1: $p < 0.01$; Figures 6B, C) and the dorsal horn ($p < 0.001$; Figures 6D, E) compared to WT sham mice. At 35 dpi, astroglial reactivity in the ventral horn of WT mice tended to increase compared to the sham group but without reaching significance ($p = 0.07$). In contrast, SCI did not modify astroglial reactivity in the *Crt11* KO injured mice (Figure 6B).

The same finding was observed in microglia reactivity since neither WT nor *Crtll* KO injured mice showed a significant increase with respect to the respective sham group (Figure 6C).

At the dorsal horn, no differences of both glial markers were found in WT mice, indicating that the inflammatory milieu generated below the injury did not reach L6 segment, or it was already subsided. Remarkably, glial immunoreactivity was higher in *Crtll* KO sham mice than in WT mice, and unexpectedly, SCI produced a significant reduction of GFAP (Figure 6D) and Iba1 (Figure 6E) intensity compared to the *Crtll* KO sham group ($p < 0.01$ and $p < 0.001$, respectively).

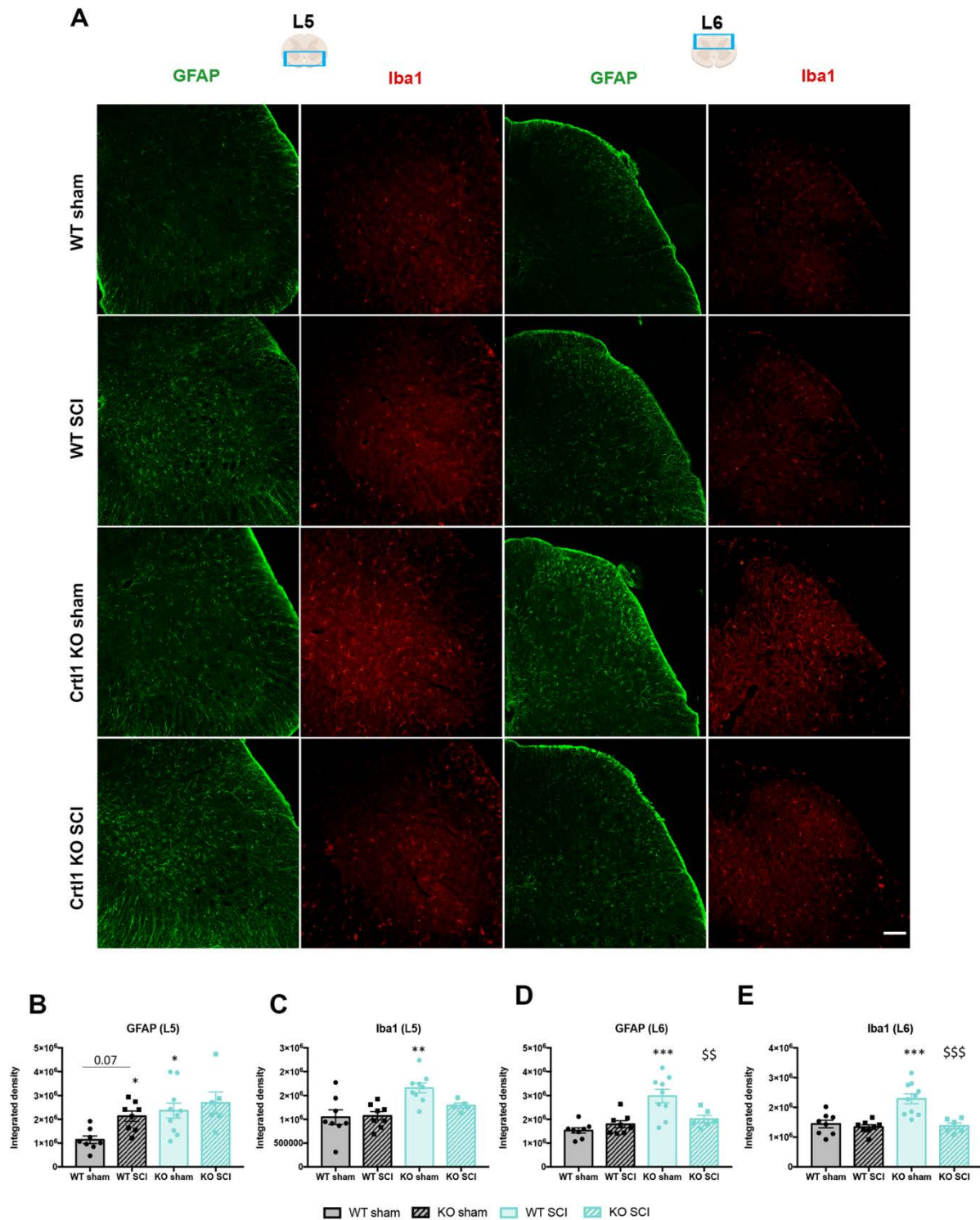


Figure 6. The lack of link protein 1 and the spinal cord injury produce different changes in glial reactivity. **A.** Representative microphotographs of the ventral (L5 region) and dorsal horn (L6 region) of the lumbar spinal cord in which astrocytes (GFAP; in green) and microglia (Iba1; in red) are shown. **B.** Quantification of astrocytes and microglia labelled with GFAP and Iba1 at the ventral horn of L5 spinal cord. **C.** Quantification of the intensity of the glial markers GFAP and Iba1 at the dorsal horn of L6 spinal cord. Scale bar: 100 μ m; Bar graphs are representing the mean values \pm SEM. * p <0.05, ** p <0.01, *** p <0.001 by one-way ANOVA (GFAP L5: $F_{3,28}$ = 4.88, p =0.008; Iba1 L5: $F_{3,26}$ = 7.09, p =0.001; GFAP L6: $F_{3,27}$ = 10.9, p <0.0001; Iba1 L6: $F_{3,28}$ = 12.83, p <0.0001) followed by post hoc test with Bonferroni correction. WT: wild-type; Crt1: cartilage link protein 1; KO: knock-out; SCI: spinal cord injury.

Discussion

The developmental formation of PNNs is activity-dependent and coexists with the end of the critical period of plasticity and maturation of the CNS (Kalb and Hockfield, 1988; Kalb and Hockfield, 1994; Dityatev et al., 2007). Once condensed PNNs are formed, they still present an activity-dependent dynamism that is crucial for CNS function (Carulli et al., 2020). However, the mechanisms involved in PNN modulation are not well understood. Here, we have demonstrated that link protein 1 participates in the activity-dependent remodeling of spinal PNNs. Our data provide evidence that link protein 1 not only contributes to PNN structure but also participates in the modulation of PNN structure by activity. This dual role is reflected in the following findings: (1) neither activity-dependent therapy nor SCI produce significant changes in spinal PNNs components and thickness in *Crtll* KO mice, although they respectively increase and reduce spinal PNNs thickness in WT mice; (2) aberrant PNNs in *Crtll* KO mice produce maladaptive changes in spinal circuits that result in hyperreflexia and hyperalgesia, as observed after SCI in WT mice, a condition that also alters PNN integrity.

Link protein 1 mediates the activity-dependent remodeling of PNNs

The importance of link protein 1 in the appearance of mature PNN was proved a decade ago *in vitro* and *in vivo* (Carulli et al., 2010; Kwok et al., 2010). Now, we have reported that link protein 1 not only orchestrates the developmental activity-dependent formation of PNN but also its activity-dependent remodeling in adulthood.

Link proteins are comprised of four members, three of them expressed in the CNS (*Crtll* or *Hapln1*, *Hapln2* and *Bral2* or *Hapln4* genes) (Ogawa et al., 2004) but just two in PNNs (*Crtll* and *Bral2* genes) (Oohashi et al., 2015). The latter ones regulate the micro-organization of PNNs by interacting with lecticans and hyaluronan. The *Crtll* gene allows the capture of aggrecan into the hyaluronan backbone, whereas the *Bral2* links brevican with hyaluronan (Bekku et al., 2003, 2012). Although both link proteins are considered organizers of PNNs, link protein 1 triggers the activity-dependent formation of the net since its expression reaches a peak that coincides with the onset of PNNs appearance (Carulli et al., 2010). Dark-rearing experiments were the first to assess this activity-dependent formation: early sensory deprivation prevents PNN formation and reduces *Crtll* gene expression in the visual cortex. The subsequent light exposure returned link protein 1 expression and, thus, PNN formation (Pizzorusso, 2002; Carulli

et al., 2010). In the present study, PNN remodeling was assessed in the mature spinal cord using transgenic mice lacking the link protein 1 (*Crtll* KO mice) and submitting them to two different activity-dependent conditions that enhance (locomotor activity) or reduce (SCI) neuronal activity.

Remodeling of spinal PNNs after a locomotor activity

Wang et al. were the first to demonstrate that activity increases spinal PNNs (Wang et al., 2011). This finding was initially overlooked despite demonstrating that activity modulates spinal and cortical PNN in opposite directions. In fact, it was not until 2015, that the differential activity-dependent modulation of spinal and encephalic PNNs was clearly reported (Smith et al., 2015).

We have observed that WT mice that run on a wheel significantly increase their spinal PNN components after the two-week protocol compared to sedentary WT mice. The voluntary wheel protocol was chosen considering previous works that described that an intense duration and intensity were necessary to increase spinal PNNs (Arbat-Plana et al., 2017; Sánchez-Ventura et al., 2021). In contrast, *Crtll* KO mice that run on the wheel did not modify their PNN components, indicating the importance of link protein 1 on PNN remodeling. Although transgenic mice seem to run less distance than WT mice, probably because their motor problems (Sánchez-Ventura et al., 2022), these differences did not reach significance and thus, cannot fully explain the differential PNN modulation between WT and transgenic mice. Besides, while WT trained mice showed a positive, although not significant, correlation between the distance run and PNN thickness, this correlation was absent in *Crtll* KO mice (data not shown). Thus, link protein 1 is implicated in modulating PNN in the mature nervous system. *Foscarin et al.* (2011) found similar results in which exposure to an enriched environment significantly decreased the mRNA expression of PNN components in WT mice but not in *Crtll* KO mice (Foscarin et al., 2011).

Remodeling of spinal PNNs after SCI

Prior studies have already described changes in PNN remodeling following SCI in WT mice (Alilain et al., 2011; Takeda et al., 2018; Sánchez-Ventura et al., 2021). In agreement with our previous results analyzing the changes of PNN structure after a thoracic cord contusion (Sánchez-Ventura et al., 2021), we observed a reduced PNN thickness around disconnected lumbar motoneurons. However, in the present study,

PNN reduction was less pronounced, probably due to a faster spontaneous recovery that resulted in more propriospinal inputs on denervated neurons, which eventually offset PNN reduction.

Considering PNNs reduction after SCI, similar findings were detected after a spinal hemisection in goldfish. In particular, it was observed that SCI produced an alteration in the sulphation pattern of CSPGs, specifically a downregulation of the CS-C around MNs (Takeda et al., 2018). Other works did not report a reduction in lumbar PNNs after a thoracic SCI (Al'joboori et al., 2020). This difference could be explained by the use of the marker Wisteria Floribunda lectin (WFA), which only stains 30% of α -MN compared to the 80% stained with aggrecan (Galtrey et al., 2008; Irvine and Kwok, 2018). Thus, these differences could have masked a possible change in PNNs after injury.

In contrast to WT mice, aberrant PNNs in *Crtll* KO remained unchanged after the spinal cord contusion, suggesting that the lack of the link protein I impairs the activity-dependent modulation of PNNs after the injury. The mechanisms implicated in PNNs remodeling around disconnected neurons are probably the same endogenous mechanisms involved in the regular turnover of PNNs. In this process and following the quadripartite synapse concept (Dityatev and Rusakov, 2011), neurons and glial cells participate either synthesizing or digesting PNN components through the release of metalloproteases (MMP) or ADAMTs (A Disintegrin and Metalloproteinase with Thrombospondin motifs) (Cawston and Young, 2010; Liu et al., 2021). After SCI, the equilibrium between synthesis and degradation may be disrupted and tipped toward degradation. In fact, different researchers have described an upregulation of MMPs and ADAMTs after SCI (de Castro et al., 2000; Zhang et al., 2011). In our study, we did not observe significant changes in the gliosis after the lesion, suggesting that the reduction of lumbar PNN is not directly caused by microglia digestion, but rather by a reduction of the synthesis of PNN components, or the release of neural proteinases.

Contrarily, the *Crtll* KO mice presented an increased astrogliosis in both ventral and dorsal horns before the injury. Since during the first postnatal weeks there is a robust proliferation of astrocytes (Ge et al., 2012; Felix et al., 2021), which may allow plasticity at these early stages of development, the astrogliosis observed in *Crtll* KO mice may contribute to the maintenance of spinal circuits in an immature state in the adulthood, mimicking those in the critical period, before condensed PNNs emerged.

Link protein 1 plays a role in neural excitability

Many studies have tried to investigate the functional role of spinal PNNs by applying the enzyme Chondroitinase ABC (chABC), which digests the glycosaminoglycans (GAGs) found in their CSPGs (Bradbury et al., 2002; Prabhakar et al., 2005). Nevertheless, chABC application cannot determine the extent to which PNNs contribute to post-SCI maladaptive symptoms, as this enzyme indiscriminately digests both diffuse ECM and PNNs, and only 2% of CSPGs are found in PNNs (Fawcett, 2015). Thus, harnessing the strengths of transgenic mice with aberrant PNNs is a good alternative to elucidate the functional implication of PNNs and PNN remodeling in the healthy and injured spinal cord.

In the present study, we have observed that *Crtll* KO mice presented hyperreflexia and hyperalgesia, mimicking the same phenomena observed in WT mice after SCI. Such maladaptive symptoms remained unchanged after the lesion in the *Crtll* KO mice, indicating that the SCI did not affect the already disorganized spinal networks of the transgenic mice. Thus, alterations in PNN integrity, either produced by the lack of the link protein 1 or by reduction of aggrecan after injury, may contribute to disorganize spinal circuits and trigger maladaptive changes. *Tansley et al.* described that the appearance of neuropathic pain after a peripheral nerve injury was caused by the digestion of spinal PNNs in the dorsal horn (Tansley et al., 2022). Similarly, development of excessive pain sensitivity in *Crtll* KO mice may be caused by alterations of PNNs rather than changes in glial cells. In fact, hyperalgesia was manifested at baseline and persisted throughout the follow-up after SCI, whereas microglial cells were overactivated already before the injury and downregulated afterwards. Regarding hyperreflexia, we have previously described an increased excitability in monosynaptic and polysynaptic reflex circuits in *Crtll* KO mice compared to WT mice (Sánchez-Ventura et al., 2022). Thus, we hypothesize that the spinal disorganization produced by changes in PNN integrity turns those PNN-bearing neurons, and their respective circuits, into an immature state. This explanation is supported by the similarities between immature neurons without PNN during the critical period, neurons with immature PNN in *Crtll* KO mice, and reduced PNN thickness in denervated neurons after a SCI. During the critical period, excitatory circuits prevail over inhibitory ones, as the high intracellular Cl^- levels favor depolarizing responses. The increase in excitatory synapses was also observed in the spinal cord of *Crtll* KO mice (Sánchez-Ventura et al., 2022), and the increased intracellular $[\text{Cl}^-]$ in

denervated neurons after a SCI due to KCC2 downregulation (Boulenguez et al., 2010; Sánchez-Ventura et al., 2021). In fact, KCC2 cotransporter and PNNs are tightly related since their developmental expression in the spinal cord coincides at P14 (Galtrey et al., 2008; Ben-Ari et al., 2012). Besides, the juvenile levels of plasticity observed in both the visual cortex and the spinal cord of *Crtll* KO mice (Carulli et al., 2010; Sánchez-Ventura et al., 2022) resemble the boost of plasticity observed in spared neurons after injury (Raineteau and Schwab, 2001), and in immature neurons during the refinement of synaptic wiring (Cameron and Núñez-Abades, 2000).

When link protein 1 is present, PNN alterations and their functional consequences can be counteracted by the activity-dependent remodeling of PNN orchestrated by this protein. This is observed in the dark/light exposure experiments and in SCI experiments followed by physical rehabilitation (Pizzorusso, 2002; Sánchez-Ventura et al., 2021). Since maturation of PNN is activity-dependent, the lack of the link protein 1 might impede maturation of spinal circuits which remain immature in adulthood.

Altogether, this work has demonstrated the implication of the link protein 1 and thus, PNNs, in the proper function of the spinal cord. Alterations in this net have a clear impact on the pathophysiology of a SCI.

Conclusion

PNNs malleability maintains the nervous system in homeostatic equilibrium. In the present study we have shown that this equilibrium is possible due to the dual role of the link protein 1: it organizes PNN structure, and it contributes to remodeling PNNs in an activity-dependent manner. Once spinal PNNs are altered, spinal circuits become disorganized, generating maladaptive changes that resemble those observed after SCI. Since activity has the opposite effect on encephalic PNN, further studies should address how this link protein differentially modulate cortical and spinal PNNs.

Chapter IV

Perineuronal net changes reveal a distinct right and left spinal
phrenic circuit

Perineuronal nets changes reveal a distinct right and left spinal phrenic circuit

Sánchez-Ventura J¹, Schardien KA², Fortino TA², Zholudeva LV³, Lane MA², Udina E^{1*}

Author affiliations:

¹Institute of Neuroscience, Department Cell Biology, Physiology and Immunology, Universitat Autònoma de Barcelona, and Centro de Investigación Biomédica en Red sobre Enfermedades Neurodegenerativas (CIBERNED), Bellaterra, Spain

²Department of Neurobiology and Anatomy, College of Medicine, Drexel University, Philadelphia, PA 19129, United States of America; The Marion Murray Spinal Cord Research Center, College of Medicine, Drexel University, Philadelphia, PA 19129, United States of America.

³Gladstone Institutes, San Francisco, CA, United States of America

Abstract

Respiratory failure is one of the greatest causes of mortality and mobility after spinal cord injury (SCI). It occurs after cervical lesions which are the most common type of SCI. Fortunately, several experimental and clinical studies have reported some spontaneous recovery after injury that has increased the interest of scientists to further evaluate and potentiate neuroplasticity in the phrenic system. However, many questions are still unanswered regarding the plastic potential of this circuitry. Thus, the aim of this study is to evaluate the structural plasticity of the right and left phrenic network by analyzing perineuronal net (PNN) changes after a C2 hemisection (Hx C2). For this purpose, the right and left phrenic systems were retrogradely traced with a pseudorabies virus (PRV), a transsynaptic retrotracer. Before the injury, we found that most PNN-bearing neurons were found in the ventral horn, coating phrenic motoneurons (PhMNs), whereas spinal interneurons presented very few PNNs. When the right phrenic circuit was injured, we observed a significant increase in PNNs and glutamatergic synapses around ipsilateral PhMNs, but no changes when the left side was injured. According to these findings, the injury to the right phrenic circuitry severely reduced ipsilateral PhMN activity compared to injuring the left circuit. Consequently, the right-side injury required a marker plastic reorganization to overcome respiratory dysfunction. These findings, together with the fact that the right phrenic circuit contained more motoneurons in naïve mice, indicate that the right and left respiratory circuits exhibited different anatomy. As a result, they contribute differently after injury to compensate dysfunctional breathing. These results provide a novel insight into respiratory plasticity although further research is needed to extrapolate this histological data into a functional framework.

Keywords: perineuronal nets, phrenic motoneurons, spinal cord injury, interneurons, plasticity

Introduction

Neuroplasticity is defined as the anatomical and functional changes produced in the nervous system in response to stimuli or injury. In the spinal cord, plasticity has been mainly studied in the locomotor system to promote recovery after a spinal cord injury (SCI) (reviewed in (Loy & Bareyre, 2019)). Nevertheless, other spinal circuits such as the phrenic motor system has also shown spontaneous recovery after injury (Golder and Mitchell, 2005; Fuller et al., 2006). Phrenic motoneurons (PhMNs) are located around spinal cervical levels 3 to 6 (C3-C6) and are responsible for the innervation of the most important muscle for respiration, the diaphragm (Lane, 2011). Thus, high and mid-cervical injuries disconnect PhMNs from upper centers, generating dysfunctional respiration, which is one of the leading causes of mortality and morbidity in SCI patients (Garshick et al., 2005). Despite this devastating outcome, clinical and experimental research has shown some spontaneous plasticity that promotes limited, but promising, functional recovery after cervical SCI (Nantwi et al., 1999). The model of hemisection at the C2 level (HxC2) has become the preclinical standard lesion to study respiratory plasticity. Specifically, the hemisection interrupts descending bulbospinal pathways and immediately silences the activity of the ipsilateral diaphragm. However, within minutes to hours after the injury, anatomical plasticity occurs and leads to functional recovery weeks or months later (Goshgarian and Rafols, 1989; Lindsay et al., 1993; Nantwi et al., 1999). In this ipsilateral recovery process, spinal interneurons seem to play a key role. It is reported that they can anatomically reorganize the injured network and modulate PhMNs excitability (Bareyre et al., 2004; Lane et al., 2009; Sandhu et al., 2009; Alilain et al., 2011). However, it is poorly understood the plastic potential of these neurons and PhMNs after injury.

Perineuronal nets are structures rich in chondroitin sulfate proteoglycans (CSPGs) that control plasticity processes of neurons ensheathed by them, in an activity-dependent manner (reviewed in (Fawcett et al., 2019)). Thus, changes in neural activity can rearrange PNN structure, and consequently promote stability or plasticity in the central nervous system (CNS). The reduction of PNNs opens a window of plasticity that favors the reorganization of circuits, whereas the increase of PNNs closes this plasticity period, stabilizing the synaptic contacts previously generated (Pizzorusso, 2002). Thus, PNN analysis around neurons in the CNS can appraise the plastic or stability events produced in a specific neural circuit and moment. In previous works, we observed that 5 weeks after a thoracic SCI, PNN decreased their thickness around lumbar motoneurons,

which favored plasticity. After eleven weeks, PNN recovered normal values, closing the plasticity period, and stabilizing the newly formed synapses (Sánchez-Ventura et al., 2021). Although locomotor and respiratory circuits share some similarities, their window of plasticity might differ. The neural networks controlling breathing must be more flexible to any physiological or environmental challenge, due to their biological significance. Hence, the aim of this study is to analyze PNN changes around neurons that take part in the phrenic motor circuit after a HxC2. This evaluation was possible due to the aid of the transsynaptic retrotracer pseudorabies virus (PRV) that stained the left and right phrenic motor circuit. Thus, harnessing PNN dynamics in the intact and injured spinal cord can be crucial to elucidate the contribution of these neural populations in the spontaneous plasticity that mediates respiratory recovery.

Materials and methods

Experimental design

Fifty-one adult female mice (C56BL6/J) were used for the present study. To assess the changes of PNNs in the phrenic spinal circuit after a spinal cord injury (SCI), mice were separated into a sham (n=7) and injured group (n=36), which suffered a spinal cord hemisection at the cervical 2 level (HxC2). Some of the injured mice received the cervical hemisection on their left side, while others on their right side. In the left side group, animals were followed for 7 (n=16) and 14 days post-injury (dpi) (n=14). However, mice injured on the right side were followed only at 7 dpi (n=6) since most of them died within the first days after the HxC2 (Figure 1).

Then, another set of mice (n=8) were used to estimate the number of motoneurons contained in the left and right phrenic motor pool.

Some mice were housed at the animal care facility at Drexel University College of Medicine, whereas others were maintained in the animal care facility of the Universitat Autònoma de Barcelona (UAB). Mice were kept on a 12:12 light/dark cycle and received food and water *ab libitum* in any case.

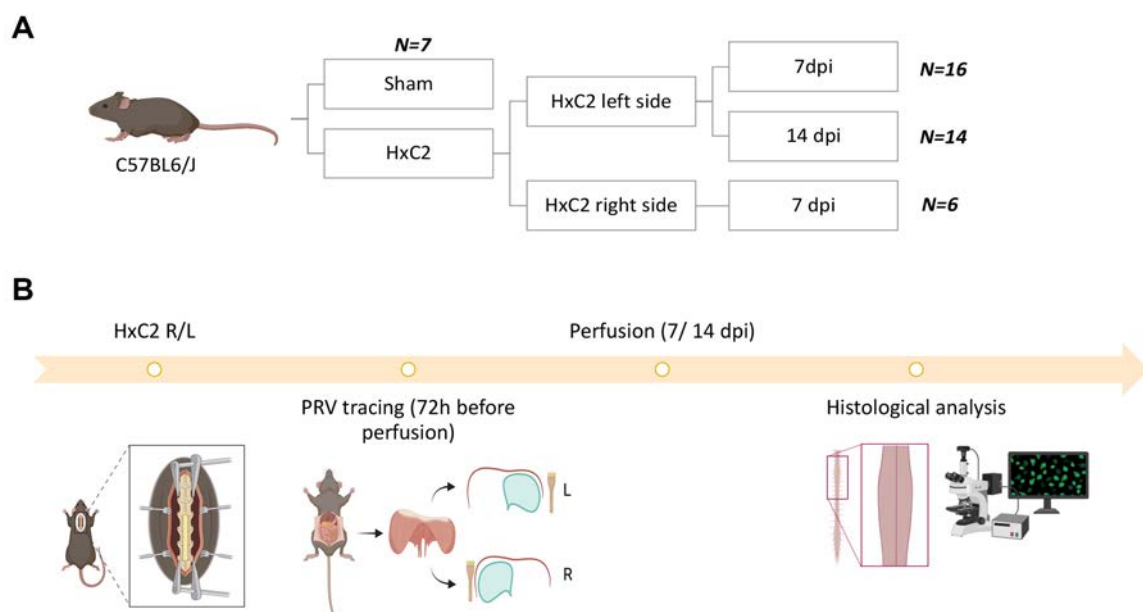


Figure 1. Schematic representation of the experimental groups and design. (A) Scheme of the different experimental groups. (B) Diagram showing the timeline of the HxC2 experiment. HxC2: hemisection at the C2 level. PRV: pseudorabies virus; L: left; R: right; dpi: days post-injury. Individual images were obtained from Biorender.

Experimental procedures were conducted with approval from the Institutional Animal Care and Use Committee of Drexel University and the UAB Experimental Ethical Committee (CEEAA). These procedures followed the National Research Council Guidelines for the Care and Use of Laboratory Animals (USA) and the animal welfare guidelines of the European Communities Council Directive (2010/63/EC).

Spinal cord injury

Cervical cord hemisection at C2 level was performed under isoflurane anesthesia (induction 4%, maintenance 1-2%) and on a water-circulating heating pad. The skin of the dorsal part of the neck was shaved and an incision was made from the base of the skull to the shoulder blades. A partial laminectomy was performed at the C2 vertebral level. Then, a C2 hemisection (HxC2) was made immediately caudal to C2 roots, from the middle to lateral edge of the spinal cord using a scalpel blade. To ensure a complete and reproducible hemisection, the scalpel was applied three times. Surrounding muscles were sutured and skin was closed using wound clips. Postoperatively, lactated ringers' solution (3 ml) and buprenorphine (0.03 mg/ml; 0.05 ml) were provided.

Neuronal tracing

Sham and injured mice were traced with a transsynaptic retrograde pseudorabies virus (PRV) to study the spinal phrenic motor circuit (Fortino et al., 2022). Different PRVs tracers used were: PRV614 (8×10^8 plaque-forming units [pfu]/ml; expressing red fluorescent protein), PRV152 (5×10^9 [pfu]/ml; expressing green fluorescence protein) and PRV Bartha (1×10^9 [pfu]/ml; without a fluorescence protein).

Animals were first anesthetized with isoflurane anesthesia (induction 4%, maintenance 0.5-2%). Then, a laparotomy was performed to expose the diaphragm and the lateral lobes of the liver was gently moved. Afterwards, a total volume of 40 μ l the pseudorabies virus was topically applied on the inferior surface of the hemidiaphragm of interest (left or right) as described in mouse (Qiu et al., 2010) and rat (Lane et al., 2008). Finally, the abdominal muscles were sutured, and the skin was closed. Postoperatively, lactated ringers' solution (1 ml) and buprenorphine (0.03 mg/ml; 0.05 ml) were provided. Animals were euthanized 72h after the neuronal tracing (Lane et al., 2008).

To count the number of phrenic motoneurons that innervate the left and right hemidiaphragm, mice were retrogradely traced with True-Blue Chloride (1%; TB, Setareh Biotech). In this case, mice were anesthetized with ketamine (90 mg/kg) and xylazine

(10 mg/kg). Similarly, a laparotomy was performed to expose the diaphragm and a total volume of 9 μ l of TB were applied topically in the left and right hemidiaphragm. Once the abdominal muscles and skin were sutured, analgesia was provided subcutaneously with buprenorphine (0.1 mg/kg). Animals were euthanized 6 days after the tracing.

Histological evaluation

In the HxC2 experiment, seven or fourteen days after the injury, mice were euthanized and transcardially perfused with physiological saline solution (0.9% NaCl in water) and paraformaldehyde (4% PFA in 0.1 M phosphate buffer saline (PBS); pH 7.4). Brains and spinal cords were collected and post-fixed in 2% PFA at 4°C. Two days prior to sectioning, tissue was cryoprotected by sequentially soaking it in 15% and 30% sucrose (in 0.1 M PBS) until it sinks.

For the motoneuron counting experiment, mice were perfused with 4% PFA in 0.1 M phosphate buffer (PB) and the cervical spinal cords were harvested and post-fixed in 4% PFA over 2h. Then, they were cryoprotected in 30% sucrose solution in PB (4°C).

The cervical spinal cords of both experiments were longitudinally cut on a cryostat (20 μ m thick) and collected onto serial gelatin-coated glass slides.

For PNN and synaptic changes evaluation, sections separated 60 μ m each were rehydrated for 15 min in PBS (0.1 M), blocked against endogenous peroxidase activity (30% methanol, 0.6% hydrogen peroxide in PBS, incubated for 1h) and blocked against nonspecific protein labeling (10% normal donkey serum (NDS) in PBS incubated for 1h). Primary antibodies (Table 1) were incubated overnight (ON) at room temperature in a blocking solution (5% NDS in PBS containing 0.03% Triton X-100). After several washes, sections were incubated with secondary antibodies at room temperature for 2h. Immunolabeled sections were washed, and cover-slipped with fluorescence mounting medium (Fluoromount medium; Southern Biotech).

Histological analysis

For motoneuron (MN) counting, cervical sections separated 40 μ m each were used to count the number of MN traced by the TB retrotracer in both sides of the spinal cord. Images were taken at 10x.

For PNN components and synaptic markers, images were captured in a confocal laser-scanning microscope (around 30 steps, z-step size of 0.5 μ m, Leica TCS SP5) at

20x. For each animal, all the neurons traced from rostral to caudal were imaged. To analyze the staining, the maximal projection of the z-stacks was performed and then, the background was corrected. For aggrecan and VGlut2, a band of 4 μm around the PRV stained cell body was delimited to measure the integrated density of that region. For 5-HT staining, the immunolabeling intensity of the whole picture was quantified. Then, the data obtained was clustered in spinal cord regions (dorsal horn, intermediate region, and ventral horn).

Table 1. List of primary and secondary antibodies

Primary antibodies			
Antigen	Dilution	Host	Reference
Aggrecan	1:250	Rabbit	AB1031- Millipore
VGlut2	1:1000	Guinea Pig	AB2251-I Sigma
5HT	1:400	Rabbit	AB_572263
PRV	1:10000	Goat	NIH Virus Center grant n ^o P40 OD010996
Secondary antibodies			
Alexa 594	1:200	Donkey x Rabbit	Jackson immunoresearch- 711-585-152
Alexa 488	1:200	Donkey x Goat	Jackson immunoresearch- 705-545-147
Alexa 647	1:200	Donkey x Guinea Pig	Jackson immunoresearch – 706-605-148
Alexa 488	1:200	Donkey x Rabbit	Jackson immunoresearch- 711-545-152
Alexa 594	1:200	Donkey x Goat	Jackson immunoresearch- 705-585-003

Statistical analysis

Data is analyzed using GraphPad prism 7 software and reported as mean \pm standard error of the mean (SEM). Differences between groups were considered significant when $p\text{-value} < 0.05$. Normal distribution was confirmed using Shapiro-Wilk test for each variable/group. The expression of aggrecan before the injury in the different spinal cord regions was assessed by ordinary one-way ANOVA followed by Bonferroni's multiple comparison test. The changes in PNNs and synaptic markers (VGlut2 and 5-HT) at 7 and 14 dpi were evaluated with one-way ANOVA with same post-hoc as above. However, the number of MN found in the left and right phrenic MN pool was analyzed by Student's t-test (unpaired), since variables present equal variances.

Results

The presence of PNNs in the spinal phrenic circuit increases from dorsal to ventral

To characterize the changes that PNNs suffer after a high cervical hemisection, we first describe the expression of PNNs, stained with aggrecan, before the injury, in the different spinal cord regions (Figure 2A, B). Data was normalized to dorsal horn levels since was the spinal cord area where less PNN-bearing neurons were found. Comparatively, the intermediate region showed higher levels of PNNs than the dorsal horn, although without reaching significance. In contrast, PhMNs showed a significant increase in PNN levels compared with the dorsal horn ($p < 0.01$), indicating that they are the neuronal type in the spinal phrenic system with more PNNs.

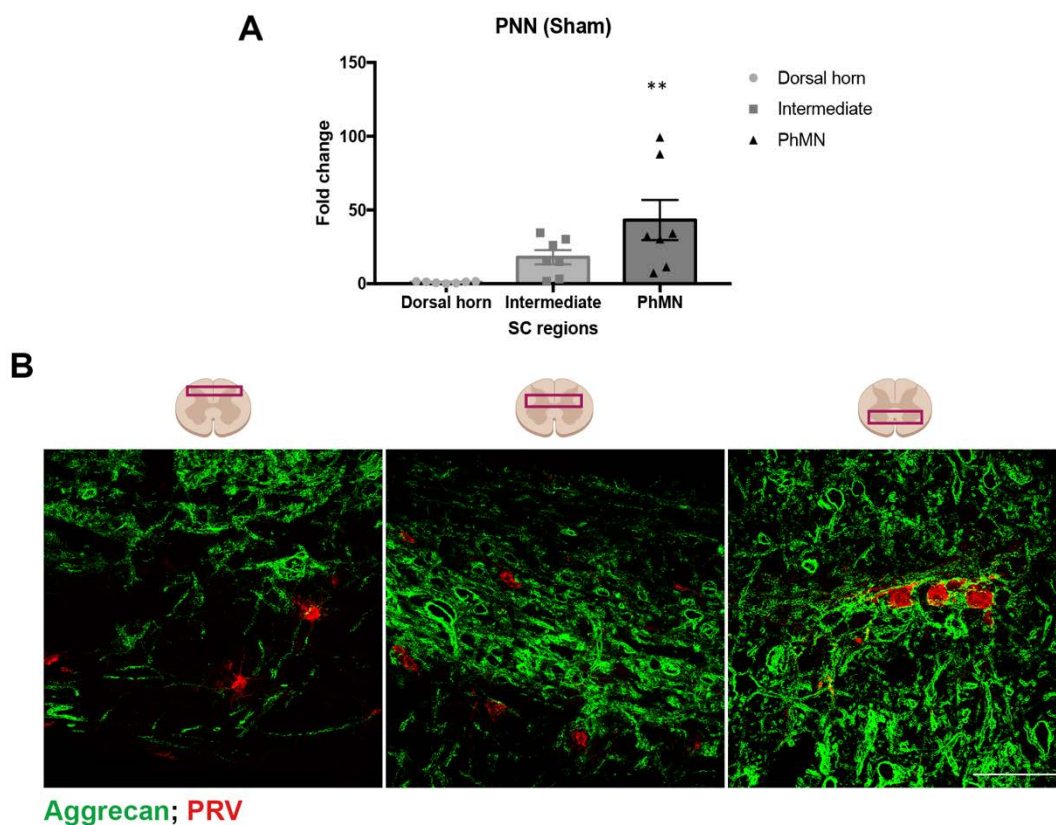


Figure 2. PNN are mainly found around PhMN, whereas very few spinal interneurons are coated by them. (A) Quantification of the integrated intensity of PNNs around neurons from the phrenic circuitry. The analysis was performed separating the different spinal cord regions. (B) Representative images from PNNs, stained with aggrecan (green) surrounding spinal interneurons in the dorsal and intermediate region and PhMNs from the ventral horn, stained with PRV (red). Scale bar: 100 μ m. Bar graphs are representing the mean value \pm SEM. ** $p < 0.01$, by one-way ANOVA ($F_{2,18} = 6.47$, $p < 0.01$) followed by post hoc test with Bonferroni correction. PNN: perineuronal nets; PRV: pseudorabies virus; SC: spinal cord; PhMN: phrenic motoneuron.

PNN are differently regulated depending on the side of the injury

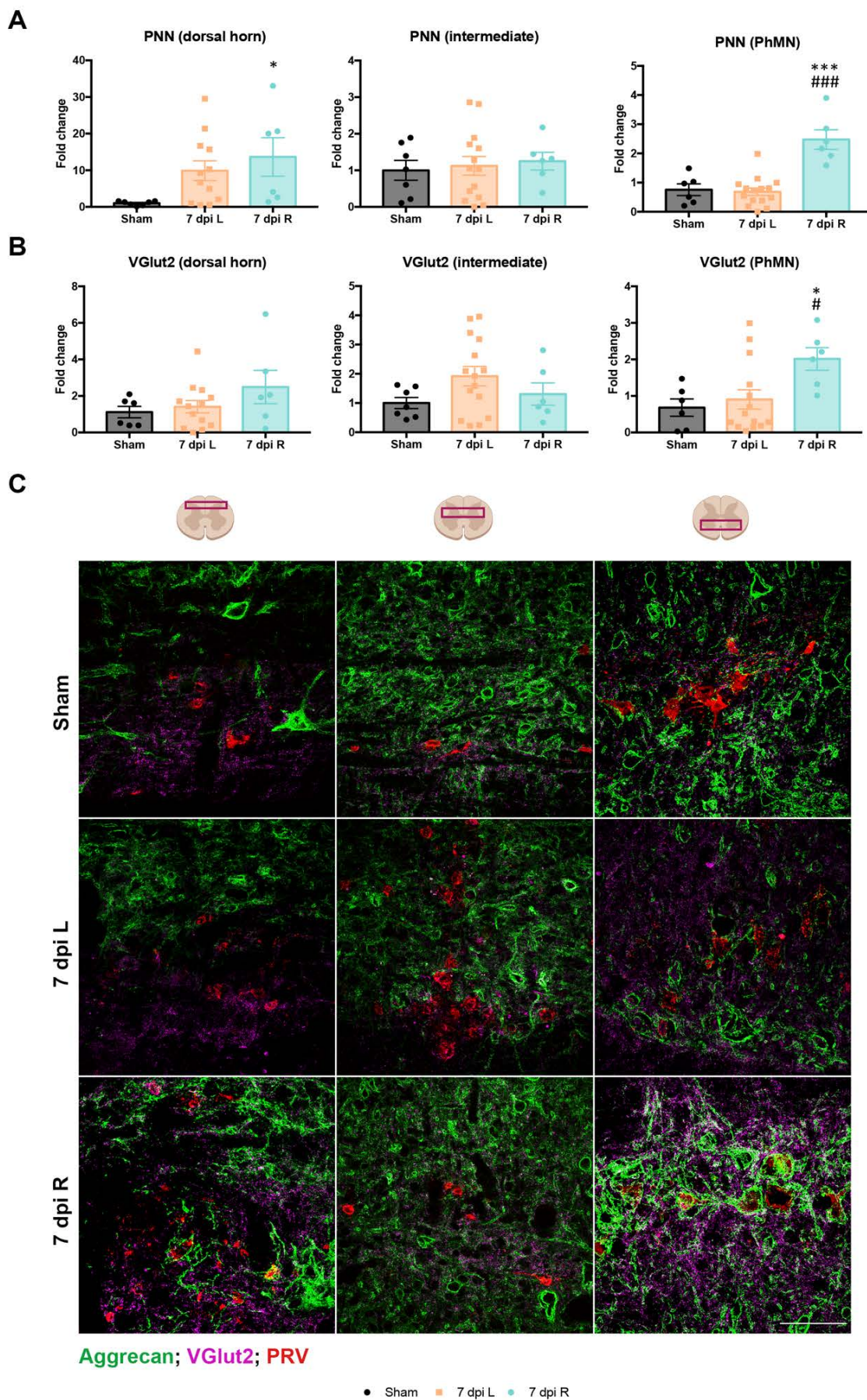
At 7 dpi, the different injured sides were compared. Interestingly, significant changes in PNNs and glutamatergic synapses were reported between the left and right side. Specifically, after injuring the right C2 level, PNN surrounding neurons in the dorsal horn significantly increased their thickness compared to the sham group ($p < 0.05$, Figure 3A, C). In contrast, in the left side, this increase did not reach significance. Similarly, ipsilateral PhMNs after right-side hemisection significantly increase their PNN thickness, compared to sham and left-injured group ($p < 0.001$ vs sham and 7dpi left). However, the injury did not significantly modify PNN in the intermediate region.

Glutamatergic synapses found in the spinal phrenic circuit were studied with the VGlut2 marker (Figure 3B, C). Remarkably, the high cervical injury in the right side significantly increased VGlut2 intensity around ipsilateral right PhMNs compared to the sham and left-injured group ($p < 0.05$ vs sham and 7 dpi left). Thus, at 7 dpi, the left HxC2 did not modify PNN nor glutamatergic levels around neurons within the spinal phrenic system. In fact, all the changes observed were found in the group injured in the right spinal cord.

Considering serotonergic fibers (Figure 4A, B), the cervical hemisection did not significantly modify their levels in none of the spinal cord regions studied. However, the injury in the left cervical spinal cord tended to decrease serotonergic inputs in the ventral horn. This tendency reach significance at 14 days dpi compared to the sham group (Suppl. Figure 1).

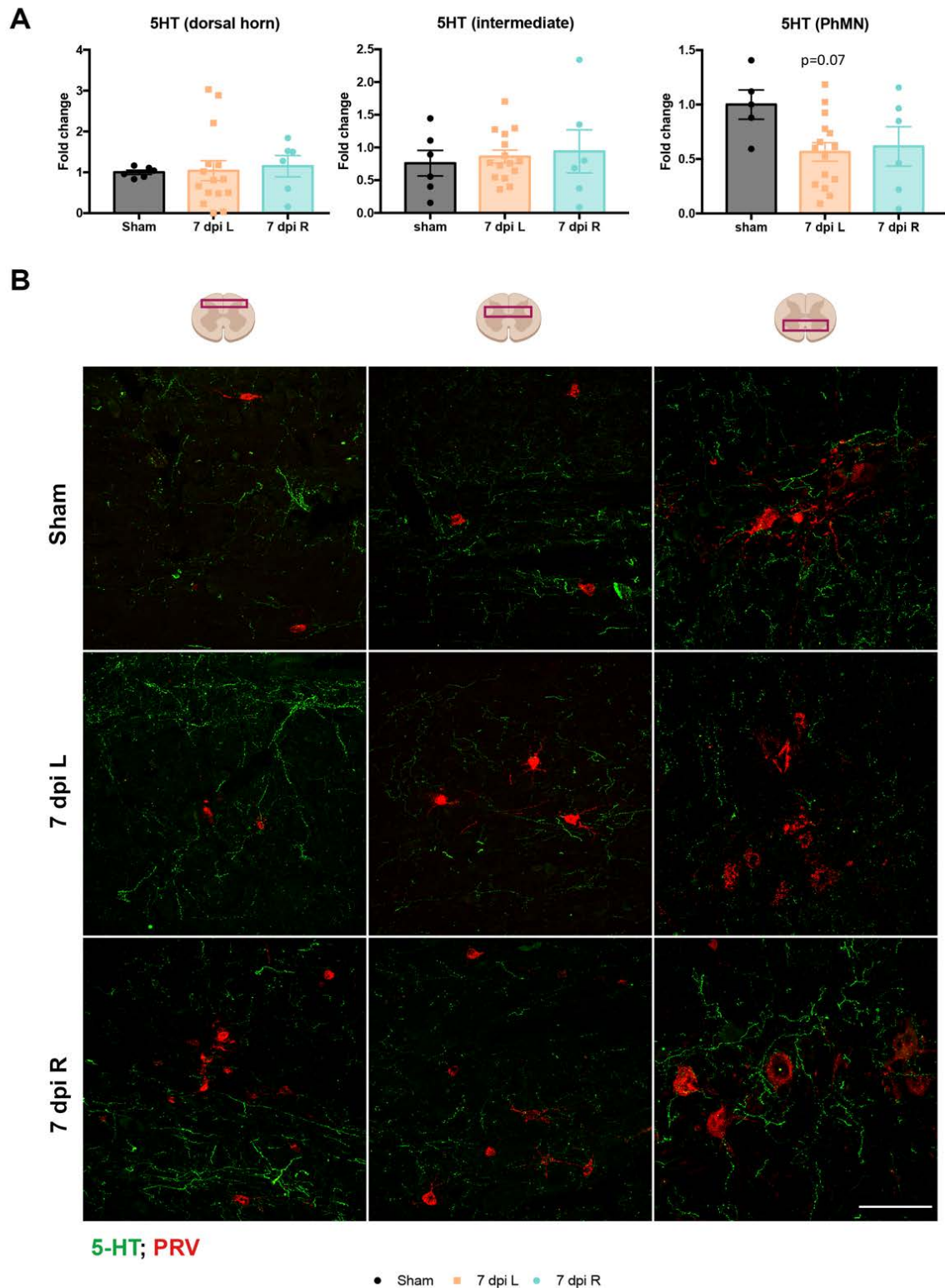
(Figure in the next page)

Figure 3. PNNs and VGlut2 are differently regulated depending on the side of the HxC2. Quantification of the intensity of PNNs (A) and glutamatergic synapses (B) around neurons within the spinal phrenic circuitry. The analysis was performed separating the different spinal cord regions at 7 dpi. (C) Representative confocal images of PNNs (stained with aggrecan (green)), glutamatergic synapses (stained with VGlut2 (purple)) around neurons within the spinal phrenic circuitry (stained with PRV (red)) in the left and right dorsal horn, intermediate region, and ventral horn. Scale bar: 100 μ m. Bar graphs are representing the mean value \pm SEM. * $p < 0.05$ *** $p < 0.001$ vs sham; # $p < 0.05$, ### $p < 0.001$ vs left side by one-way ANOVA (PNN dorsal horn: $F_{2,22} = 3.56$, $p < 0.05$; PNN intermediate region: $F_{2,24} = 0.14$, $p = 0.87$; PNN PhMNs: $F_{2,24} = 22.08$, $p < 0.0001$; VGlut2 dorsal horn: $F_{2,22} = 1.58$, $p = 0.23$; VGlut2 intermediate region: $F_{2,25} = 1.92$, $p = 0.17$; VGlut2 PhMNs: $F_{2,23} = 4.42$, $p < 0.05$) followed by post hoc test with Bonferroni correction. PNN: perineuronal nets; VGlut2: vesicular glutamate transporter 2; PRV: pseudorabies virus; PhMN: phrenic motoneuron; L: left; R: right; dpi: days post-injury.



The right phrenic motor pool presented more phrenic motoneurons

To explain the differences in PNN and excitatory synaptic contacts between sides after the injury, PhMNs were counted in the left and right phrenic circuit of naïve mice (Figure 5A, B). Interestingly, the right phrenic motor pool showed 23% more MNs than in the left side ($p < 0.01$).



(Figure in the previous page)

Figure 4. No significant changes in 5-HT were found at 7 dpi. (A) Quantification of serotonergic fibers in the dorsal horn, intermediate region, and ventral horn at 7 dpi in the left and right spinal phrenic network. (B) Confocal images representing serotonergic fibers (in green) and neurons within the spinal phrenic network (in red) in the different experimental conditions. Scale bar: 100 μm . Bar graphs are representing the mean value \pm SEM. No significant differences were found by one-way ANOVA (5-HT dorsal horn: $F_{2,24} = 0.06$, $p=0.94$; 5-HT intermediate region: $F_{2,24} = 0.18$, $p=0.83$; 5-HT PhMNs: $F_{2,23} = 2.94$, $p=0.07$) followed by post hoc test with Bonferroni correction. 5-HT: 5-hydroxytryptamine; PRV: pseudorabies virus; PhMN: phrenic motoneuron; L: left; R: right; dpi: days post-injury.

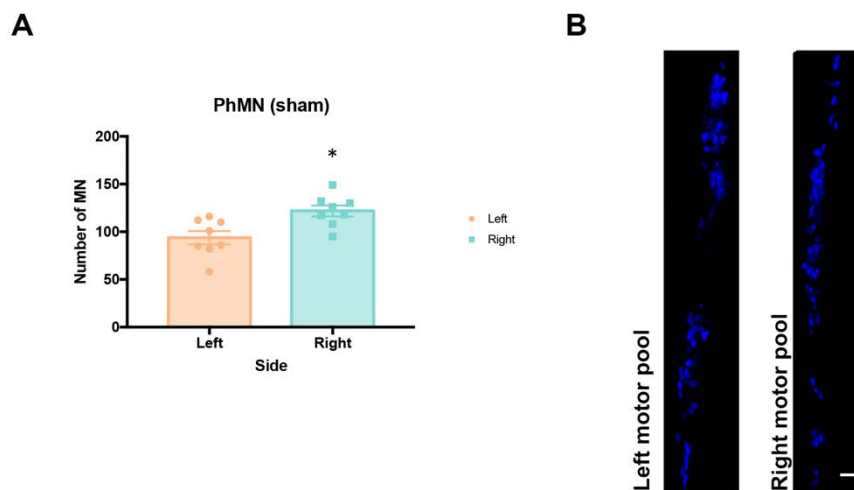


Figure 5. The right phrenic network presented more PhMNs. (A) Quantification of the number of PhMNs retrotraced with True Blue in the right and left phrenic circuit. (B) Representative microphotographs of the MN pool traced at the C3-C6 spinal cord level. Bar graphs are representing the mean values \pm SEM. * $p < 0.05$ by unpaired t -test. One sample from the left side was removed due to a reduced tracing. Scale bar: 100 μm . PhMN: phrenic motoneurons. MN: motoneurons.

Discussion

Structure and function are closely tied. Thus, understanding structural plasticity within the phrenic circuit and its progressive variations after SCI is crucial to predict its role post-injury. In this study, structural plasticity was assessed by analyzing PNN changes around interneurons and PhMN after a HxC2. Since most HxC2 data comes from injuring the left phrenic circuit (Minor et al., 2006; Boulenguez et al., 2007; Buttry and Goshgarian, 2014; Zholudeva et al., 2017; Bezdudnaya et al., 2018; Dougherty et al., 2018), here we have also described the plastic changes produced after injuring the right phrenic circuit.

PNN expression confirms the plastic potential of the phrenic motor system

To get a better understanding of PNN dynamics, it is important to first evaluate the basal state of PNNs around the phrenic neural population. In normal conditions, PNNs are rarely expressed around neurons in the dorsal horn. Similarly, interneurons located in the intermediate region showed faint PNNs. In contrast, PhMNs are the neural population with thicker PNNs, being significantly higher than interneurons from the dorsal horn. These findings reinforce the idea that interneurons present a plastic phenotype and thus, can be rapidly recruited under specific physiological and environmental demands (Lane et al., 2009; Sandhu et al., 2009; Zholudeva et al., 2017; Satkunendrarajah et al., 2018). Contrarily, PhMNs are more static cells since they provide stable and synchronized motor output to activate the diaphragm (George and Ghali, 2018). The phrenic motor system, when it is compared with other spinal circuits, can be considered an extremely malleable circuit. In the lumbar spinal cord, we previously observed more PNN-bearing neurons in the ventral horn and intermediate region than in the phrenic network. This fact highlights the biological significance of phrenic circuitry flexibility in comparison with other spinal circuits.

Differential structural plasticity appears depending on the injured side

Insults in the spinal cord rearrange the previously known circuits into new anatomy. In our work, we have observed that the HxC2 produced different plastic outcomes depending on the side of the injury at 7 dpi. Interestingly, while the HxC2 at the left side of the cord did not modify PNNs, the same injury at the right side significantly increased PNN thickness around interneurons in the dorsal horn and PhMNs. Similarly, glutamatergic inputs also significantly increase around right

ipsilateral PhMNs compared to sham and the left-injured group. PNN increase around cervical denervated neurons was unexpected since we formerly observed a reduction around lumbar disconnected neurons after thoracic SCI (Sánchez-Ventura et al., 2021). PNNs have an activity-dependent modulation that follows the classical Hebbian synaptic strengthening concept of “either use it or lose it” (Hebb, 1949). Briefly, the loss of synaptic contacts reduces PNN and leads to neuronal pruning, whereas the return of these inputs increases PNNs, which strengthens synaptic connections. Considering this statement, denervated PhMNs should have reduced their PNNs due to the decline of inputs received after hemisection. However, activity-dependent plasticity does not follow the same rules in all neural systems and consequently, PNNs expression cannot always predict the activity of the neuron surrounded. In constitutive active systems such as the respiratory one, plasticity is regulated by other activity-independent mechanisms that guard the system against inactivity (since the consequence of failure is death). This compensatory mechanism is called “inactivity-induced phrenic motor facilitation (iPMF)” and consists of a burst of inputs around PhMNs after a period of activity deprivation (Mahamed et al., 2011; Strey et al., 2013). Thus, the HxC2 declined ipsilateral PhMN activity, which initiate a compensatory mechanism that increased glutamatergic synapses, and consequently increase PNNs. Surprisingly, this fact was just observed after injuring the right side of the cervical spinal cord. Since the boost of synaptic contacts is proportional to the magnitude of inactivity (Mahamed et al., 2011), it is possible that lesioning the right or left phrenic circuit had a distinct impact on PhMN activity. Remarkably, diaphragm innervation is not symmetric. In fact, the right phrenic nerve presents 20% more axons than the left nerve, innervating a larger area of the diaphragm (Song et al., 1999). This fact coincides with our MN counting in which we observed 23% more PhMNs on the right side compared to the left in naïve mice. Consequently, our hemisection did not paralyze 50% of the diaphragm in each case, but rather 30% or 70% when we injured the left or right side, respectively. The differential denervated states can be extrapolated into PNN changes. Since the left-side injury did not have a huge impact on respiratory rate, little spinal reorganization was needed and thus, PNN remained unchanged. However, after the right-side injury, just 30% of the diaphragm remained active, activating the iPFM and increasing PNNs around disconnected PhMNs. This histological finding was corroborated at the functional level, since the right-side injury had an extremely high mortality rate within the first days after the injury, compared to the left-side injury.

Neuronal circuits mediating this respiratory recovery after injury are challenging to identify. The activation of latent, crossed, and monosynaptic projections from the ventral respiratory column (VRC), although possibly being the most effective route to enhance the excitatory drive to PhMN (Goshgarian, 2003), hardly contributes to the spontaneous recovery found after HxC2 (Alilain et al., 2011). Instead, retrograde and transsynaptic tracing experiments have revealed an increased number of labeled interneurons connecting the ipsilateral phrenic network after injury (Lane et al., 2008, 2009, 2012; Sandhu et al., 2009). This observation indicates a role of spinal interneurons in the spontaneous respiratory function after cervical SCI. Among spinal interneurons' diversity, excitatory interneurons seem to be recruited within the first weeks after the injury and thus, participates in respiratory recovery (Satkunendrarajah et al., 2018). Specifically, glutamatergic V2a interneurons are a promising candidate for facilitating breathing after SCI (Zholudeva et al., 2017). In naïve mice, they are not integrated into the phrenic motor circuit. However, after HxC2, they ipsilaterally project glutamatergic inputs to PhMNs. Therefore, the significant increase of glutamatergic contacts around PhMNs after the right-side injury compared to left side could be due to the stronger activation of this type of plastic events when the right spinal phrenic system is affected by a lesion. Besides, V2a interneurons receive serotonergic (5-HT) inputs (Zholudeva et al., 2017). It has been reported that 5-HT plays a neuromodulator role in contributing to respiratory recovery through enhancing neuroplasticity in the phrenic system (White and Neuman, 1980; Lindsay et al., 1993). In fact, at 7 dpi, 5-HT tend to decrease, and become significant at 14 dpi on the left side. Instead, on the right side, 5-HT marker remained unchanged at 7dpi, fact that may facilitate plasticity on the right side.

Finally, one of the limitations of the study is the lack of samples of mice injured on the right side at 14 dpi, mainly due to the high mortality rate produced by injuring the right phrenic circuit. In the left-side injured group, since few changes were observed at 7 dpi, it is not surprising that at 14 dpi, the same markers remain unchanged. Functional plasticity starts to be observed in the second-week post-injury (Zholudeva et al., 2017; Bezdudnaya et al., 2018). Thus, structural, and anatomical plasticity should have appeared before.

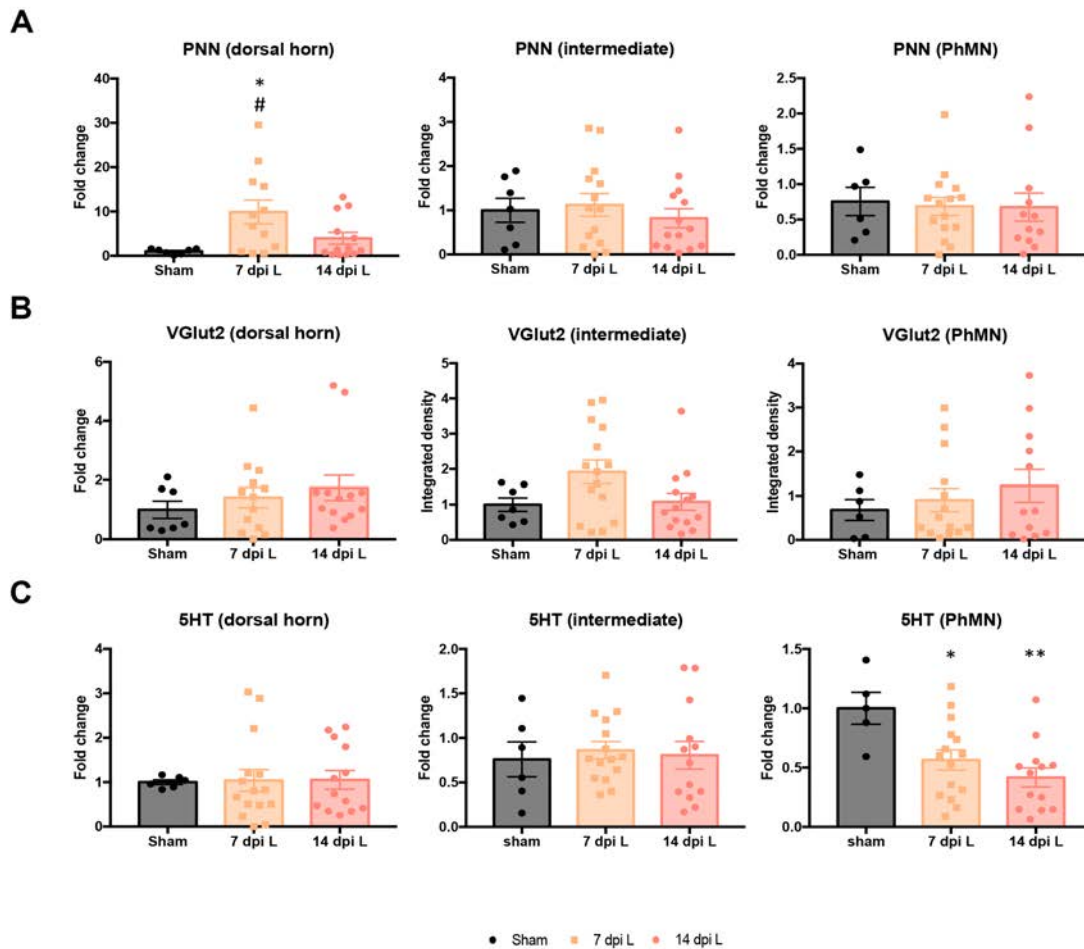
Hence, our data have demonstrated an asymmetrical distribution of phrenic motoneurons between spinal sides, and a differential PNN modulation after injuring the right or left spinal cord at the cervical level. These anatomical findings suggest a

predominant phrenic circuitry in the right side, that would undergo a stronger plastic reorganization after injury.

Conclusion

This study has demonstrated differences between the right and left phrenic circuitry that directly affects the plastic outcomes after SCI. This data provides a new perspective on phrenic network functionality in naïve and injured conditions and encourages further research into the functional implications of affecting both phrenic circuits. A better understanding of phrenic circuitry would be beneficial in harnessing the spontaneous and limited recovery observed in this system and potentiating it through therapeutic interventions.

Supplementary figures



Supplementary figure 1. Serotonergic fibers significantly decreased around left PhMNs whereas PNN and VGlut2 contacts remain unchanged 2 weeks after injury. Quantification of the integrated density of PNN (A), glutamatergic synapses (B) and serotonergic fibers (C) at 7 and 14 dpi in the different spinal cord regions. Bar graphs are representing the mean value \pm SEM. * $p < 0.05$ ** $p < 0.01$ vs sham by one-way ANOVA (PNN dorsal horn: $F_{2,29} = 4.8$, $p < 0.05$; PNN intermediate region: $F_{2,32} = 0.44$, $p = 0.65$; PNN PhMNs: $F_{2,30} = 0.04$, $p = 0.96$; VGlut2 dorsal horn: $F_{2,30} = 0.76$, $p = 0.48$; VGlut2 intermediate region: $F_{2,33} = 3.03$, $p = 0.06$; VGlut2 PhMNs: $F_{2,29} = 0.59$, $p = 0.56$; 5-HT dorsal horn: $F_{2,31} = 0.01$, $p = 0.99$; 5-HT intermediate region: $F_{2,31} = 0.11$, $p = 0.89$; 5-HT PhMNs: $F_{2,30} = 6.45$, $p < 0.01$) followed by post hoc test with Bonferroni correction. PNN: perineuronal net; VGlut2: vesicular glutamate transporter 2; 5-HT: 5-hydroxytryptamine; PhMN: phrenic motoneuron; L: left; R: right; dpi: days post-injury.

Annex

Do spinal perineuronal nets participate in motoneuron degeneration?

Do spinal perineuronal nets participate in motoneuron degeneration?

Sánchez-Ventura J¹, Badia C¹, Herrando-Grabulosa M¹, Udina E^{1*}

Author affiliations:

¹Institute of Neuroscience, Department Cell Biology, Physiology and Immunology, Universitat Autònoma de Barcelona, and Centro de Investigación Biomédica en Red sobre Enfermedades Neurodegenerativas (CIBERNED), Bellaterra, Spain

Abstract

Motoneuron (MN) loss is a hallmark of neurodegenerative diseases and traumatic injuries in the spinal cord, that produce important deficits in patients. Thus, during the last decades, several studies have identified many therapeutic targets to promote MN survival. Among the list of targets, perineuronal nets (PNNs), a specialized and condensed extracellular matrix, have been recently included. Although they are mainly known for their role in restricting plasticity in the central nervous system, PNNs also show neuroprotective properties. This feature has been mainly studied in the brain and specifically in the context of degenerative diseases such as Alzheimer's and Parkinson's disease. However, the role of spinal PNNs in neuroprotection has been unexplored. Hence, the aim of this study is to elucidate the role of PNNs in the survival of MNs in a model of spinal root avulsion. For this purpose, WT and transgenic mice with immature PNNs (*Crtll* KO mice) received a brachial-plexus injury and different histological markers were evaluated 21 days after the injury. The injury significantly increased spinal PNNs around injured MN in WT mice and produced a huge MN loss. In contrast, it did not significantly modify spinal PNNs, and produce less MN death in *Crtll* KO mice. The differences between PNNs, together with a distinct glial reactivity between groups could explain the differential MN loss. The present data suggests that spinal PNNs could be involved in MN death rather than MN survival. However, further research is needed to better understand their role.

Introduction

Perineuronal nets (PNNs) are reticular structures composed of hyaluronan, chondroitin sulfate proteoglycans (CSPGs), Tenascin-R and link proteins (Deepa et al., 2006; Irvine and Kwok, 2018). The interaction between these components forms a condensed scaffold that coats specific populations of neurons in the central nervous system (CNS) (*reviewed in* (van 't Spijker & Kwok, 2017)). PNN's composition and function are closely related. The highly negative charge of CSPGs creates a polyanionic milieu around PNN-ensheathed neurons that contributes to many PNN functions, in addition to the widely known plasticity inhibition (Gama et al., 2006). For instance, this environment serves as a local buffering system for physiologically relevant cations (Brückner et al., 1993). From a pathological point of view, this anionic shield also provides a neuroprotective environment around PNN-bearing neurons against excitotoxicity and oxidative stress (Okamoto et al., 1994). More specifically, PNNs generate a physical and chemical barrier that protects and isolates neurons from oxidative stress and inflammatory cytokine activity (Cabungcal et al., 2013; Suttkus et al., 2014). These observations have been mainly reported in the cortex and specifically, in neurodegenerative diseases such as Alzheimer's and Parkinson's disease (Morawski et al., 2010). In these pathologies, cortical neurons surrounded by PNNs were less affected by degeneration than neurons without PNNs, suggesting that neural vulnerability depends on PNNs (Suttkus et al., 2016).

Akin to the brain, neurodegenerative processes are also observed in the spinal cord. The spinal root avulsion is an excellent model to study the phenomena of neuronal death after spinal cord injuries (Ruven et al., 2014). The brachial-plexus avulsion model produces a cascade of events including an inflammatory response, oxidative stress and glial scar formation that contributes to the massive death of motoneurons (MNs) at the corresponding spinal segment (Guo et al., 2019). Consequently, sensory and motor functions in the innervated region are seriously affected. Considering the data provided by cortical PNN studies, it is feasible that spinal PNNs are a crucial factor for neural protection too. Nevertheless, the neuroprotective function of PNNs in the spinal cord has been overlooked, until now. Hence, in this work we have evaluated MN survival in WT and transgenic mice (*Crtll* KO) with aberrant PNNs after a brachial plexus injury. These mutant mice lack for the cartilage link protein 1 (*Crtll*), a crucial element of PNNs function and structure (Carulli et al., 2010). A better understanding of the involvement

of the link protein 1 in the neuroprotective effect of spinal PNNs might improve the progression of pathologies that affect motoneuron survival in the spinal cord.

Materials and methods

Experimental design

The experiment was carried out on WT and *Crtll* KO female and male mice (C57BL6J background). *Crtll* KO mice were provided by Dr. Pizzorusso and bred in the Animal Facility of the Universitat Autònoma de Barcelona (UAB). The generation, genotype and phenotype were described by *Czipri et al.* (Czipri et al., 2003) and in our previous work (Sánchez-Ventura et al., 2022).

A total of 21 adult (8-12 weeks) mice were used in this study. WT and transgenic mice were divided into a sham and injured group, which suffered a brachial plexus injury (BPI). The groups were: WT sham (n=6), WT BPI (n=5), *Crtll* KO sham (n=4), *Crtll* KO BPI (n=6). All of them were housed in groups of two to five per cage, at 22 °C (\pm 2 °C) and kept on a 12:12 light/dark cycle. Food and water were provided *ad libitum*.

All the experimental procedures and protocols were approved by UAB Experimental Ethical Committee (CEAAH) and performed in accordance with the animal welfare guidelines 2010/63/EC of the European Communities Council Directive.

Brachial plexus injury

Mice were anesthetized with an intraperitoneal injection (i.p.) of ketamine (90 mg/kg) and xylazine (10mg/kg). After placing the mice in a prone position, an incision was made in the skin near the clavicle. Then, the superficial and deep neck muscles were separated to expose the left brachial plexus. Specifically, superior (C5-C6), middle (C7) and inferior (C8-T1) nerve trunks were exposed and cut. The distal part of the nerves was separated to avoid axon regeneration. Finally, the incision was sutured, and mice were kept on a thermostatically regulated heating pad until completely awake. Analgesia was provided subcutaneously with buprenorphine (0.1 mg/kg) during the following two days.

Retrograde labelling

The motoneuron pools that innervate the left triceps muscle were retrogradely labeled using the True-Blue Chloride retrotracer (1,25%; TB, Setareh Biotech). Under general anesthesia with ketamine (90 mg/kg) and xylazine (10 mg/kg), a small incision was made along the skin to expose the muscle. 5 μ l of retrotracer were applied topically

(i.e., “painted” onto the muscle surface) in the whole extension of the triceps muscle. Then, the wound was sutured. Animals were traced 5 days before the injury.

Histological evaluation

Twenty-one days after the injury, WT and *Crtll* KO mice were euthanized with an intraperitoneal injection of pentobarbital (200 mg/kg) and transcardially perfused with cold paraformaldehyde in 0.1 M phosphate buffer (PB). Then, cervical spinal cords were harvested and post-fixed in 4% PFA over 2h. Afterwards, they were cryopreserved in 30% sucrose solution in PB until they sank (4°C).

Cervical spinal cords were transversally cut on a cryostat (20 µm thick). Each cervical section was sequentially collected onto 10 separate gelatin-coated glass slides. The region of interest was localized with the aid of the retrotracer, which was mainly observed from C5-C8.

For MN survival evaluation, C5-C8 sections separated 100 µm of each other were rehydrated and stained for 3h with an acidified solution of cresyl violet 3.1 mM. The slides were dehydrated with different concentrations of ethanol, cleared with xylol, and mounted with DPX.

The rest of sections were used to evaluate PNNs (aggrecan, Tenascin-R) and glial reactivity (microglia stained with Iba1 and astrocytes with GFAP). To do so, sections were permeabilized with phosphate buffer saline Triton 0.3% (PBST 0.3%) and nonspecific interactions were blocked with 10% Normal Donkey Serum for 1h at room temperature (RT). Then, sections were incubated ON at 4°C with primary antibodies (Table 1). After washes, immunoreactive sites were revealed using species-specific secondary antibodies (Table 1). After 2h of incubation at RT, sections were washed and mounted with Fluoromount medium (Southern Biotech).

Histological analysis

For cresyl violet sections, the number of MNs (identified by a polygonal shape, a diameter larger than 20 µm and a prominent nucleolus) per each section was counted. Images were taken at 40x in the ventral horn.

For PNN's components, images were captured in a confocal laser-scanning microscope (around 30 steps, z-step size of 0.5 µm, Leica TCS SP5) at 40x. For each animal, 4 images from the ventral horn were taken and a minimum of 30 MNs were measured. To analyze aggrecan and tenascin-R staining, the maximal projection of the z-

stacks was performed and then, the background was corrected. Finally, a band of 4 mm around the cell body of MNs was delimited to measure the integrated density of that region. From this analysis, we also obtained the area of each MN, information that was also used to compare the MN size between WT and *Crtll* KO mice before and after the injury.

Inflammatory markers were studied taking grayscale microphotographs at 20x in the ventral horn. For glial reactivity quantification, the background was corrected, and the threshold was defined for all the photographs of the same marker. Images were acquired with a digital camera Nikon DS-Ri2 attached to a Nikon Eclipse Ni-E microscope. Image analysis was performed by Fiji software.

Table 1. List of primary and secondary antibodies.

Primary antibodies				Secondary antibodies			
Name	Dilution	Host	Reference	Name	Dilution	Host	Reference
Aggrecan	1:250	Rabbit	AB1031-Millipore	Alexa 488	1:200	Donkey x Rabbit	A21206-Invitrogen
Tenascin-R	1:200	Goat	AF3865-R&D systems	Alexa Fluor 594	1:200	Donkey x Goat	All058-Invitrogen
GFAP	1:1000	Rabbit	AB5804-Millipore	Alexa 488	1:200	Donkey x Rabbit	A21206-Invitrogen
Iba1	1:300	Goat	AB5076-Abcam	Alexa 594	1:200	Donkey x Goat	All058-Invitrogen

Statistical analysis

Data is reported as mean \pm standard error of the mean (SEM). Normality was confirmed using the Shapiro-Wilk test for each variable/group. A Student's t-test (unpaired) was used to compare MN survival and glial reactivity between sides since variables presented equal variances. However, ipsilateral glial reactivity comparison between groups was evaluated by Welch t-test since variables did not present equal variance. PNN markers, MN size and distribution were analyzed by two-way ANOVA followed by pairwise post-hoc contrast with Bonferroni adjustment of p values. Statistical analysis was done using GraphPad Prism 7 software. A p-value <0.05 was used to indicate significant differences between groups.

Results

Crt11 KO mice showed enhanced motoneuron survival after brachial plexus injury

The brachial plexus injury (BPI) caused a severe MN loss (42%) in the ipsilateral side of WT mice, 21 days after the injury. However, this loss was significantly reduced (24%) in *Crt11* KO mice ($p < 0.01$; Figure 1A, B). A slight, although not significant, reduction of MNs in the contralateral side of WT mice was also observed compared to uninjured animals (data not shown). Thus, *Crt11* KO mice showed a MN protective effect after the proximal axotomy.

The injury did not affect the size of surviving MNs on the ipsilateral side (Figure 2A), despite generating a differential MN distribution between groups (Figure 2B, C). Before the injury (Figure 2B), WT mice showed a MN distribution peaking between 410-450 μm^2 , whereas *Crt11* KO mice showed a flatter distribution with a peak ranging from 351 to 500 μm^2 . After the BPI (Figure 2C), the marked MN peak in WT mice tended to the left ranging from 351-400 μm^2 . However, the distribution of MN in the *Crt11* KO mice still maintained its peak in the same range, although slightly displacing the distribution to the right (peak between 451-500 μm^2).

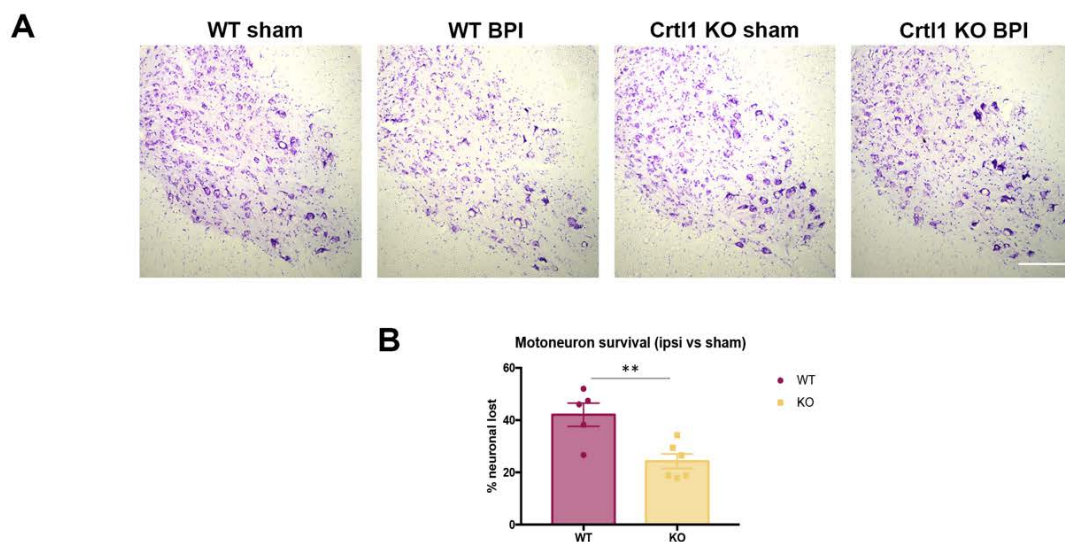


Figure 1. *Crt11* KO mice present enhanced motoneuron survival following brachial plexus injury. **A.** Representative microphotographs of cresyl violet staining corresponding to ventral horns of C7-C8 spinal segments at 21 days after the brachial plexus injury. **B.** Quantification of the survival of α -MNs in C5-C8 spinal segments. Data are representing the mean values \pm SEM. $N_{\text{total}} = 21$ mice. ** $p < 0.01$ by unpaired t-test. Scale bar: 100 μm . WT: wild-type; *Crt11*: cartilage link protein 1; KO: knock-out; BPI: brachial plexus injury.

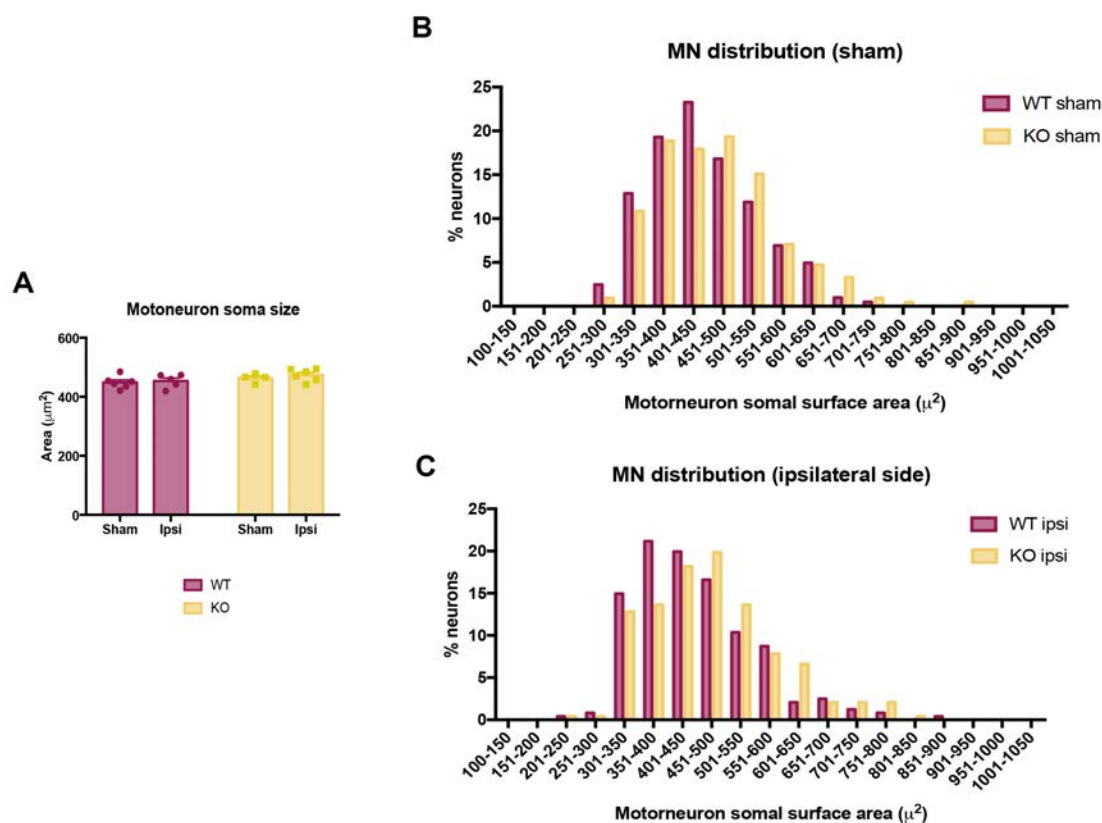


Figure 2. The brachial plexus injury slightly changed the distribution of spared MNs between WT and *Crtll* KO mice. A. Bar graphs representing the area of surviving spinal MNs at 21 dpi in WT and transgenic mice. B. Distribution of spared MNs in sham WT and *Crtll* KO mice. C. Distribution of spared MNs in the ipsilateral side of WT and *Crtll* KO mice 21 days after the spinal root avulsion. $N_{\text{total}} = 21$ mice. Significant differences were not found by two-way ANOVA. WT: wild-type; KO: knock-out; Ipsi: ipsilateral side. MN: motoneuron.

The spinal root avulsion generated an increase of PNN around injured neurons

The BPI produced a significant increase of the PNN marker aggrecan in the ipsilateral side of WT injured mice ($p < 0.01$ vs sham; Figure 3A, B). This significant upregulation was not observed in the *Crtll* KO mice, although a slight and not significant increase was observed too ($p = 0.08$). Interestingly, the thickening of PNN in the WT mice resembled extracellular matrix deposits rather than a condensed and thick PNN (Figure 3B). No significant changes were found in the tenascin-R marker between experimental groups and conditions (Figure 3A).

As is observed in the scatter graph, bigger MNs present thicker PNN compared to smaller MNs before and after the injury. Although this finding was found in both WT and transgenic groups, they were more pronounced in the WT group (Figure 3C, D).

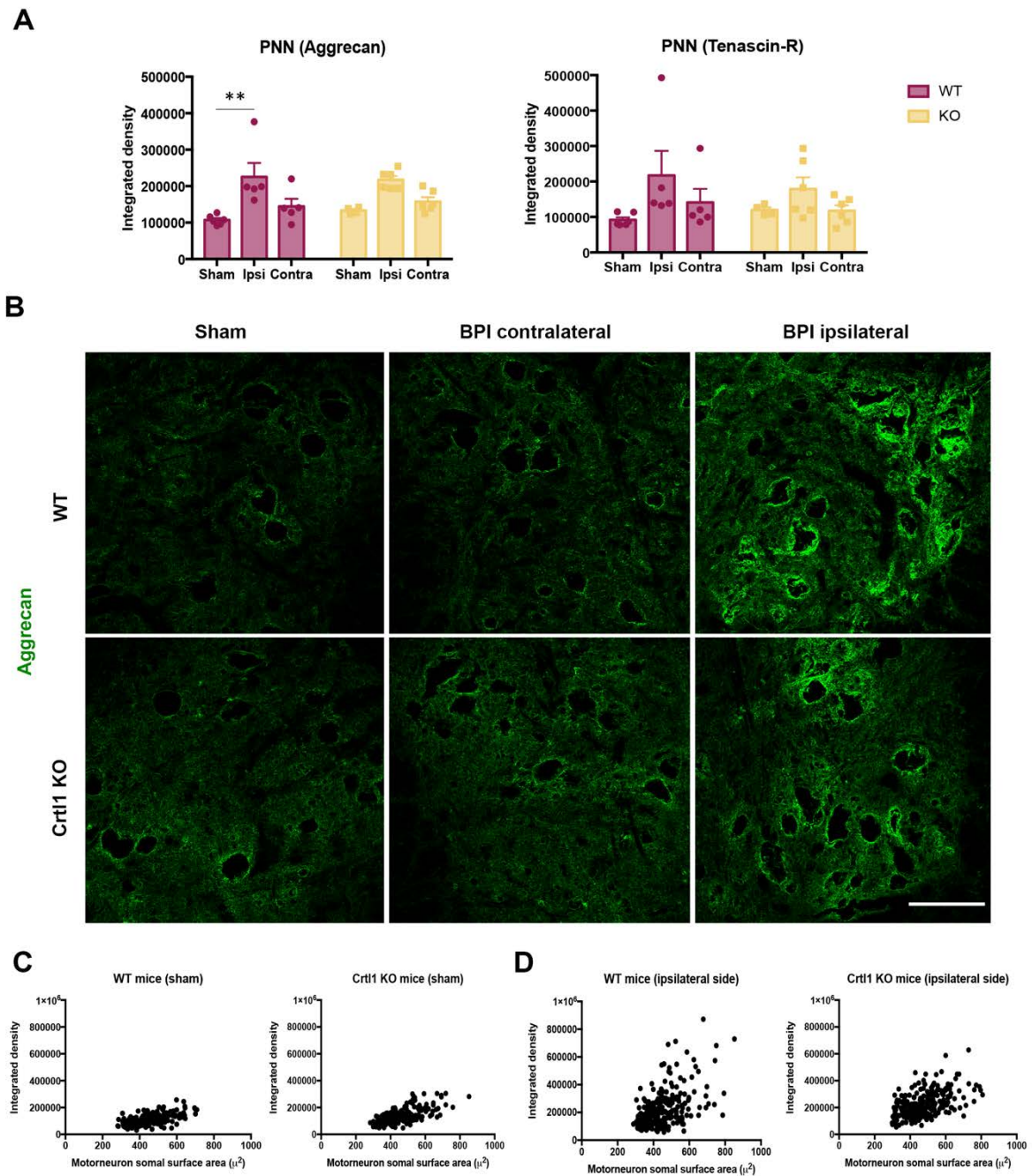


Figure 3. The brachial plexus injury produced an aberrant increase of PNNs around WT-injured neurons. A. Quantification of the immunolabeling (integrated density) of PNN components (aggrecan and tenascin-R) around neurons. B. Maximal projection of confocal images showing aggrecan staining in both sham and injured WT and *Crt11* KO mice (ipsilateral and contralateral side). C. Scatter graph representing the relationship between PNN intensity and the area of MNs in WT and *Crt11* KO sham mice. D. Scatter graph representing the relationship between PNN intensity and the area of spared MNs in the ipsilateral side of WT and *Crt11* KO injured mice. Bar graphs are representing the mean values \pm SEM. Scale bar: 100 μ m. $N_{\text{total}} = 21$ mice. ****** $p < 0.01$ vs sham WT as calculated by two-way ANOVA (*aggrecan*: side $F_{2,26} = 15.59$, $p < 0.0001$; groups $F_{1,26} = 0.47$, $p = 0.4990$, interaction $F_{2,26} = 0.43$, $p = 0.66$; *Tenascin-R*: side $F_{2,26} = 3.71$, $p < 0.05$; groups $F_{1,26} = 0.15$, $p = 0.69$; interaction $F_{2,26} = 0.46$, $p = 0.63$) followed by Bonferroni correction for the multiple comparison. WT: wild-type; *Crt11*: cartilage link protein 1; KO: knock-out; BPI: brachial plexus injury.

The brachial plexus injury produced a different inflammatory response between WT and *Crt11*KO mice

After the brachial plexus injury, there was a differential activation of microglia and astrocytes in the ipsilateral ventral horn between groups. While the mean value of GFAP intensity was similar between WT and *Crt11* KO mice on the ipsilateral side, *Crt11* KO mice showed a more variable response (Figure 4A). In fact, the astroglial reactivity in the ipsilateral side compared to the contralateral one tended to be higher in the *Crt11* KO mice than in WT mice, although not significant (Figure 4B, C; $p=0.06$). Regarding microglia, the BPI produce a slight microglial reaction at 21 dpi. In the *Crt11* KO mice, the Iba1 reactivity found in the ipsilateral side tended to decrease compared to WT mice and remained unchanged compared to the contralateral side (Figure 4D, E, F).

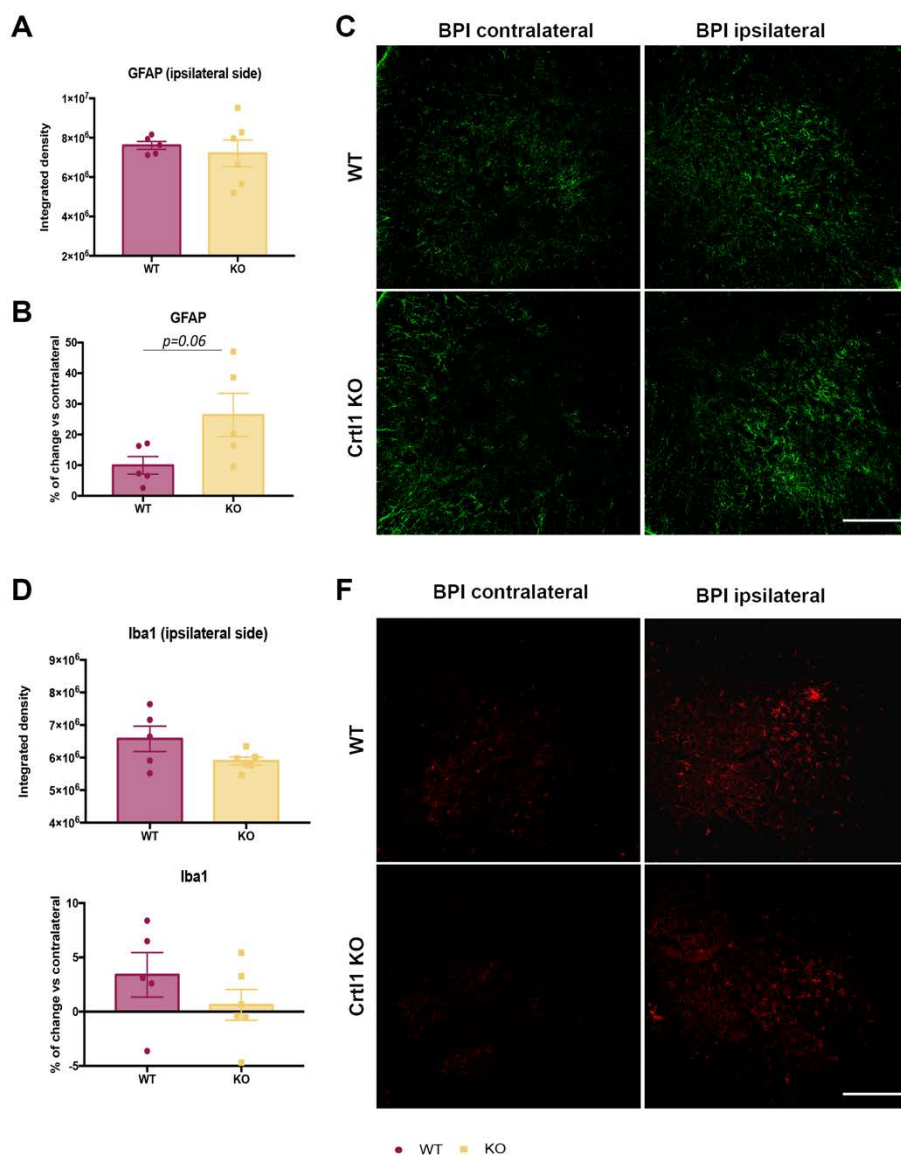


Figure 4. *Crtll* KO mice showed an altered inflammatory response after the injury. A. Quantification of the GFAP immunolabeling in the ventral horn of C5-C8 sections, in which the ipsilateral sides of both groups are compared. B. Bar graphs representing the percentage of change between the ipsilateral and contralateral side of the GFAP marker in both WT and *Crtll* KO mice. C. Representative microphotographs of astroglia (stained with the GFAP marker) in both sides of injured WT and *Crtll* KO mice. D. Quantification of the Ibal immunolabeling in the ventral horn of C5-C8 spinal sections, in which the ipsilateral sides of both groups are compared. E. Bar graphs representing the percentage of change between the ipsilateral and contralateral side of the Ibal marker in both WT and *Crtll* KO mice. F. Representative microphotographs of microglia (stained with the Ibal marker) of both sides of the injured WT and *Crtll* KO mice. Bar graphs are representing the mean values \pm SEM. Scale bar: 200 μ m. $N_{\text{total}}= 21$ mice. Significant differences were not found by student's t-test (ipsilateral vs contralateral side) nor Welch t-test (ipsilateral side between groups). WT: wild-type; *Crtll*: cartilage link protein I; KO: knock-out; BPI: brachial plexus injury.

Discussion

Research on PNNs is mostly based on studies in the brain. As a result, spinal PNNs and their therapeutic potential are still poorly understood. Possibly, it was assumed for many years, that all PNNs within the CNS operated equally. Nevertheless, recent works have revealed differences between cortical and spinal PNNs (Vitellaro-Zuccarello et al., 2007; Smith et al., 2015; Irvine and Kwok, 2018), that have raised concern about the assumption that PNNs play similar roles in both anatomical locations. Thus, we believe it is crucial to further study some of the already attributed functions of cortical PNN in the spinal cord. Specifically, this work pretends to evaluate the neuroprotective potential of spinal PNNs using a model of MN degeneration, the spinal root avulsion in the brachial plexus.

In this context, MN survival was evaluated and compared between WT mice and transgenic mice with disorganized and immature PNNs. In detail, these mutant mice (*Crtll* KO mice) lack the cartilage link protein 1 (*Crtll*), a gene that encodes for the link protein 1 which is relevant for triggering PNN formation (Carulli et al., 2010).

PNNs upregulation triggered by the injury increases MN death

The brachial plexus injury (BPI) is characterized by a massive MN death produced by the disconnection of MN cell bodies with their axons (Ruven et al., 2014). Throughout the first weeks, there is a progressive loss of MN that eventually leads to a dramatic MN death (Wu, 1993; Wu and Li, 1993). Thus, in our study, injured animals were followed for three weeks to observe enough MN degeneration. In WT mice, the BPI produced a loss of 42% of MNs around C5-C8 spinal segments. Surprisingly, *Crtll* KO mice showed only 24% of MN death in the same spinal region.

To investigate why MN survival differed between WT and *Crtll* KO mice, we analyzed PNNs around spared neurons. We observed that the injury significantly increased the thickness of PNNs in the ipsilateral side of WT mice. However, this significant increase was not observed in the *Crtll* KO mice, which just presented a slight upregulation of the PNN marker aggrecan. The increase in PNN triggered by the proximal axotomy was unexpected. Prior works in rats described that a distal axotomy in the sciatic nerve induced a marked reduction of PNN around axotomized MNs (Arbat-Plana et al., 2015). Similarly, after a SCI, denervated lumbar MNs below the injury also suffered a reduction in their PNNs (Sánchez-Ventura et al., 2021). In fact, different

studies have related a decreased activity with a decrease in spinal PNN, being this PNN reduction reversed by physical exercise (Arbat-Plana et al., 2015; Sánchez-Ventura et al., 2021). Therefore, a proximal axotomy, in which afferent inputs are also disrupted, would reduce PNN too. However, the BPI also triggers an important MN death not seen following a distal axotomy. Some researchers have described the formation of a glial scar after this type of injury (Guo et al., 2019). Similarly, the increase of the CSPG aggrecan could be caused by a mechanism that isolates injured MN, that eventually may die, rather than an activity-dependent modulation. Indeed, the morphology of PNNs in this model is completely different from the one induced by physical exercise. While activity-dependent therapies produce a regular and bright thickening around lumbar PNNs (Arbat-Plana et al., 2015; Sánchez-Ventura et al., 2021), the avulsion generated deposits of aggrecan that formed a coarse coat around cervical neurons. Hence, PNNs thickening observed 3 weeks after a BPI could be the result of mechanisms triggered by the injury. Interestingly, this increase was not significant in *Crtll* KO mice, despite observing some aberrant staining around PNNs. If these depositions are related to death mechanisms, the reduced increase of PNNs in *Crtll* KO mice could be linked to the lower MN loss reported. Since we have already demonstrated that link protein 1 is necessary for the activity-dependent modulation of spinal PNN (chapter 3), it could also mediate their injury-dependent modulation. Thus, the lack of this protein in these transgenic animals attenuated PNN depositions after BPI. Overall, the aberrant increase of PNNs might trigger a neuronal death program that is prevented in the absence of the link protein 1.

In the literature, it has been described a programmed cell death initiated once the extracellular matrix is separated from the cellular membrane (Sater et al., 2018), the so-called anoikis. In this process, integrins are implicated (Attwell et al., 2000) which in turn, interact with CSPGs (Orlando et al., 2012). Remarkably, this type of death has been also described in the context of lumbar plexus injury (Casas et al 2015). Therefore, it is possible that the disorganized PNN found in *Crtll* KO mice hinders this death mechanism. Nevertheless, further studies are needed to corroborate this hypothesis.

Moreover, it is interesting to note that after the injury, WT mice displaced their MN size distribution to the left, suggesting that intermediate and larger MNs were more vulnerable to death. This specific neural susceptibility, in which PNNs participate, is reported in cortical neurons after oxidative stress and excitotoxicity. More specifically, those cortical regions where neurons are not coated by PNNs showed an increased MN loss compared to brain areas rich in PNN-bearing neurons (Morawski et al., 2010;

Cabungcal et al., 2013). In contrast, according to the scatter plot of our study, the most vulnerable MNs (the largest ones) showed thicker PNNs. However, in *Crtll* KO mice, a similar MN distribution was found before and after the injury indicating that a preferential loss of larger neurons was not observed. This fact suggests that the immaturity of PNN observed in *Crtll* KO mice is protecting this type of MNs after a BPI.

***Crtll* KO mice showed an altered inflammatory response**

The massive MN loss produced after the BPI is mainly caused by a huge inflammatory response and an upregulation of reactive oxygen species (Wu and Li, 1993; Guo et al., 2019). Thus, the differential inflammatory response between WT and *Crtll* KO mice could also contribute to the differential MN survival, specifically the reduced microglial reactivity in *Crtll* KO mice.

In this study, no significant changes in glial reactivity were found between groups, although clear tendencies were observed. This could be explained by the time-point analyzed. It is described in the literature that the inflammatory response starts one day after the injury and reaches a peak within the following 4 days. After that, a decline in inflammatory markers is reported (Yuan et al., 2003). Since our data was obtained 21 days after the injury, a marked inflammatory response was not expected. Nevertheless, a relationship between neural survival, ECM and glial cells exists. In fact, the proper neural function depends on the interaction of neurons, glial cells and the extracellular matrix (Dityatev and Rusakov, 2011). Specifically, PNN components share receptors and ligands with these inflammatory cells (Dityatev and Fellin, 2008). Thus, it is possible that the disorganized structure of PNNs in *Crtll* KO mice in basal conditions already disturbed the interaction and communication with glial cells. The reduced microglia reaction after injury was also observed in our previous work in which *Crtll* KO mice received a thoracic SCI (chapter 3). This fact confirms the idea that a dysregulation of the microglial reaction is occurring in *Crtll* KO mice.

Overall, although the information provided is insufficient to reach tough conclusions, it seems that the lack of link protein 1, by preventing a marked deposit of aggrecan around axotomized MN after a BPI, would have protective effects. Future research is needed to complement this data and decipher the implication of spinal PNN in motoneuron death programs after injury.

VIII. General discussion

Over the past few decades, growing evidence has shed light on the potential of PNNs in controlling the proper function of the CNS. Most of the literature mainly describes the formation (Pizzorusso, 2002; Carulli et al., 2010; Cornez et al., 2018), modulation (Balmer et al., 2009; Foscarin et al., 2011), and function of cortical PNNs in various brain areas (Nadine et al., 2009; Romberg et al., 2013; Carulli et al., 2020). Indeed, several brain disorders have been linked to alterations in cortical PNNs too (Morawski et al., 2010; Mcrae et al., 2012; Brandenburg and Blatt, 2022). In contrast, spinal PNNs are poorly understood. Thus, this work pretended to expand the focus of PNNs beyond the brain to the overlooked spinal cord. The results of this thesis dissertation provide novel information about the role and modulation of PNNs in the healthy and injured spinal cord. Our data demonstrate that subtle changes in PNN structure had a huge impact on the functionality of spinal circuits, turning spinal PNNs from neglected structures into challenging ones in the field of neurophysiology.

PNNs in the healthy spinal cord

The spinal cord is composed of many interconnected circuits, whose functionality relies on the orchestration of their individual components. Perineuronal nets are interesting candidates to mediate their dynamic control, since different studies have linked them to the regulation of plasticity and stability processes in an activity-dependent manner (reviewed in (Wang and Fawcett, 2012)). Nevertheless, no studies have directly evaluated the involvement of PNNs in the function of the spinal cord, until now. For many years, the role of spinal PNN have been inferred from studies that have been used chABC in specific CNS regions. However, chABC digests the CSPGs of both loose ECM and PNNs (Fawcett, 2015) and therefore, its application does not exclusively target PNNs. Transgenic mice could be a good alternative to specifically study the role of PNNs. The absence of one or more PNN components in these mice can give a boarder vision of PNNs role, informing about the similarities and divergences of PNNs from different CNS regions and neural populations. Link protein 1 is an interesting candidate for the study of PNN functionality since it is responsible for PNN assembly during development (Carulli et al., 2010). Transgenic mice lacking the cartilage link protein 1 were initially used to evaluate PNNs in the visual cortex (Carulli et al., 2010) and the cerebellum (Foscarin et al., 2011). Here, we have harnessed these mice model to decipher the role of PNNs in the spinal cord.

In the first chapter, we found that the lack of link protein 1 produced aberrant PNNs in the lumbar spinal cord and the motor cortex. In the lumbar spinal cord, these altered PNNs disrupted excitatory synapses and changed the physiological properties of lumbar motoneurons, switching them into a more excitable phenotype. These two outcomes increased the excitability of spinal circuits and lead to motor impairment. We believed that the lack of link protein 1 impaired the final condensation of PNNs and kept them in an immature form. Since PNNs and CNS maturation coexist (Pizzorusso, 2002; Galtrey et al., 2008), immature PNNs might also maintain the spinal cord of *Crtll* KO mice in a permanently immature plastic state. This plasticity is corroborated by the increased sprouting of the corticospinal tract in these transgenic mice. Similarly, other features of the early development like more excitable motoneurons and a higher ratio of excitatory-inhibitory synapses are also observed in *Crtll* KO mice (chapter 1). The lack of the link protein 1 has also impeded the acquisition of one of the most important qualities that defined PNNs: their activity-dependent malleability. In the third chapter, we demonstrated that link protein 1 is implicated in the activity-dependent remodeling of PNNs in adulthood. In normal conditions, spinal PNNs present an activity-dependent modulation based on the Hebbian synaptic strengthening concept (Arbat-Plana et al., 2015; Smith et al., 2015). Thus, inactivity reduces PNN thickness and enhances plasticity, whereas increased activity enlarges PNN thickness and promotes the stability of the circuit. However, the absence of link protein 1 kept the same PNN thickness after exposing *Crtll* KO mice to conditions that increase and decrease neural activity.

Overall, our study shows that link protein 1 is crucial for PNN functionality, not only participating in the assembly of mature PNNs but also ensuring their malleability, which is one of the qualities that define PNNs. This activity-dependent remodeling is essential to regulate two opposite actions: plasticity and stability. In the spinal cord, these opposite functions are both necessary to maintain spinal reflexes stable but also provide a degree of synaptic flexibility after possible physiological or environmental challenges.

PNNs in the injured spinal cord

After a SCI, there are alterations in the ECM that consequently break the plasticity-stability balance. The most evident changes in ECM following SCI are related to the formation of the fibro-glial scar at the injury site, mainly produced by astrocytes and fibroblasts (Fawcett and Asher, 1999). However, little is known about the changes

that spinal PNNs suffer due to the injury and their implication in the spinal circuits. Hence, this thesis pretended to elucidate the impact of SCI on spinal PNNs and its functional implication.

The fate of PNNs located below the level of the injury is controversial since different studies have reported a reduction (Lemons et al., 2001), no changes (YD et al., 2020) or an increase (Alilain et al., 2011) in PNNs thickness. These disputed results were also observed in the second and fourth chapters of this thesis in which we assessed the structural alterations of lumbar PNNs after a thoracic SCI and cervical PNNs after a cervical SCI, respectively.

PNN reduction: lumbar locomotor circuit

In the second chapter, reduced staining of aggrecan around lumbar MNs was reported 35 days after a thoracic SCI, recovering normal levels at later stages. Similar findings were described after hemisection in goldfish (Takeda et al., 2018). A study evaluating aggrecan synthesis and degradation found a significant decline in aggrecan levels after SCI too (Lemons et al., 2001). In our experiment (Figure 14), we hypothesized that the thoracic SCI reduced lumbar PNNs in an activity-dependent manner. Spinal motoneurons below the injury become denervated from higher centers due to the disruption of descending inputs. Moreover, the muscle paresia associated to the injury lead to a reduction of proprioceptive signals, eventually reducing PNNs around these motoneurons. This histological outcome was accompanied by maladaptive symptoms such as hyperalgesia and hyperreflexia. In fact, we demonstrated a correlation between the reduced levels of PNNs and the hyperreflexia assessed electrophysiologically. Contrarily, we were unable to relate hyperalgesia with that reduction in PNN, in contrast to others (Tansley et al., 2022), because we did not evaluate PNNs from the dorsal horn, just around motoneurons. Nevertheless, the relationship between PNN decline and maladaptive symptoms after SCI was reinforced when the increase of PNNs after an activity-dependent therapy could counterpart both hyperalgesia and hyperreflexia (Arbat-Plana et al., 2015, 2017). Specifically, the highly intense activity of the voluntary wheel running significantly increased the proprioceptive afferents around lumbar motoneurons which enlarged PNN thickness. Overall, these results provide a clear correlation between PNN reduction and maladaptive plasticity. However, a cause-effect relationship was not established until the third chapter. There, we observed that the uninjured *Crtll* KO mice mimicked the maladaptive plasticity assessed in WT mice

35 days after SCI. The neuropathic pain and hyperreflexia observed in the *Crtll* KO before the injury remained unchanged after the thoracic contusion, indicating that the SCI did not further alter the already disorganized spinal circuits produced by aberrant PNNs. Thus, we eventually conclude that PNN integrity is affected after a SCI and that alteration is directly implicated in the development of the maladaptive symptoms that characterized this pathologic condition.

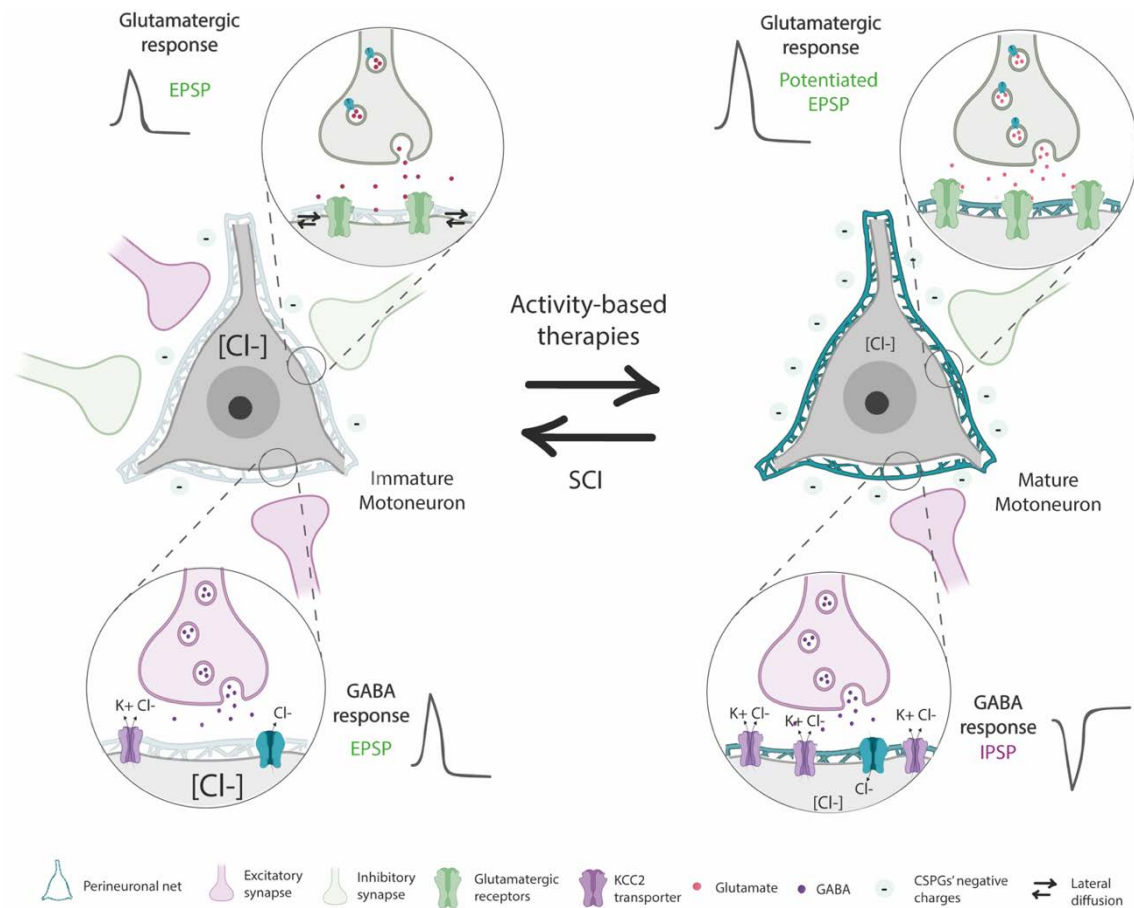


Figure 14. Developmentally immature neurons and denervated neurons post-SCI share similarities in PNN integrity and neuronal properties. Mature neurons present stable PNN, which generate a high density of negative charges around neurons that maintain ionic homeostasis necessary for proper synapse functioning. Besides, the physical barrier provided by PNNs, maintain receptors in the cell surface and stabilize synapses. However, after SCI, denervated neurons reduced PNNs thickness, shifting the GABAergic response of inhibitory neurons due to a reduction of the KCC2 co-transporter and a decrease of their negative charges around the neuron. Besides, PNNs decline facilitates the mobility of receptors, generating inefficient excitatory synapses. These characteristics resemble those seen in developmentally immature neurons. The application of activity-dependent therapies prevents PNNs reduction and restores mature neuron properties.

Considering that statement, is the restoration of PNN structure a strategy to treat SCI? We previously confirmed that physical activity restored PNN levels and reduced

maladaptive symptoms in the SCI mice model. It has been extensively studied that rehabilitation can rewire and stabilize synapses in a functionally meaningful manner, therefore, reducing hyperreflexia and neuropathic pain after SCI (*reviewed in* (Torres-Espín et al., 2018)). Nevertheless, many questions remain unanswered regarding the mechanisms involved. Since this synaptic stabilization is comparable to that found at the end of the critical period, in which PNNs contribute, it is plausible that these nets participate in the recovery promoted by rehabilitation after SCI. At the spinal level, physical activity prevented PNNs decline caused by the injury (Wang et al., 2011; Arbat-Plana et al., 2015; Smith et al., 2015), which probably contribute to the synaptic stabilization of the newly formed connections and hence, promote functional recovery (García-Alías et al., 2009; Wang et al., 2011; Zhang et al., 2014). Remarkably, the blockage of MMP-9 and MMP-2 in the spinal cord inhibits the early and late phases of neuropathic pain, respectively (Kawasaki et al., 2008).

Paradoxically, the most famous strategy to preclinically treat SCI is the application of the enzyme chABC, which can indirectly digest spinal PNNs and entail deleterious effects on the physiology of spinal neurons (Chu et al., 2018). This method has been mostly used to digest the fibro-glia scar and promote regeneration (Barritt et al., 2006). Nevertheless, although regeneration or sprouting is important for recovery, it is not always sufficient. The plasticity promoted by this enzyme needs an appropriate interaction with its target to make functional networks (García-Alías et al., 2009; Tom et al., 2009; Harris et al., 2010; Alilain et al., 2011; Wang et al., 2011). Combinatory strategies seem to be the most effective approach to solving that problem. In this regard, the plasticity achieved by therapies that widen the window of plasticity and modify the fibro-glia scar, such as chABC, only establishes meaningful connections when they are combined with rehabilitation. However, in the context of promoting regeneration in human spinal cords, chABC has some limitations, not only in its nonspecific nature but also in the multiple injections or large volumes needed. Thus, a more precise and selective manipulation is needed. Transgenic mice expressing chABC under the GFAP promoter, that limited chABC expression on astrocytes, showed enhanced corticospinal regeneration at the injury site (Cafferty et al., 2007). However, given that astrocytes can also contribute to PNNs' turnover, this type of approach can also indirectly act on spinal PNNs. Similarly, targeting the mRNA of critical enzymes in CSPGs' glycosylation and elongation have been tested *in vitro* (Grimpe and Silver, 2004; Laabs et al., 2007) and *in vivo* (Grimpe and Silver, 2004) with encouraging results in regeneration around the

lesion site. However, the selectivity of these molecules in the glial scar is unclear. To solve this non-specificity, antibodies against specific structures are found in the literature. Antibodies that neutralize the CSPG NG2 have demonstrated effectiveness in increasing the regeneration of sensory axons after injecting them into the dorsally transected spinal cord (Tan et al., 2006). Considering that, as far as we know, no work has previously described the presence of the lectican NG2 in spinal PNNs, the application of this neutralizing antibody could offer an alternative way to specifically target the glial scar (Galtrey et al., 2008; Irvine and Kwok, 2018).

PNN increase: spinal respiratory circuit

Smith et al. described that PNNs present a different activity-dependent modulation depending on their anatomical location (Smith et al., 2015), demonstrating that activity modulates cortical and spinal PNNs in opposite directions. In the second chapter, we corroborate this fact as activity-dependent therapies increase lumbar PNNs but reduced PNNs from the brainstem. Nevertheless, this statement indirectly suggests that within the spinal cord, all PNNs are modulated equally. Instead, controversial literature regarding the fate of spinal PNNs after SCI has questioned whether anatomical location actually determines PNN modulation or other factors may be considered such as neural function and innervation.

In the fourth chapter, we evaluated PNN changes after SCI in a different spinal circuit, the respiratory one. Although the locomotor and respiratory spinal circuits share some characteristics, they differ in their function (breathing vs. locomotion) and innervation (low vs. high proprioceptive Ia afferents (Alvarez et al., 2004; Nair et al., 2017)). Interestingly, we observed that after a right-side hemisection, PNNs around PhMNs increase their thickness. Similarly, *Alilain et al.* (Alilain et al., 2011) also showed an upregulation of CSPGs, labelled by WFA, around phrenic MNs after a cervical SCI. The different PNN modulation between the respiratory and locomotor circuits can be explained by the biological significance of each circuit. The phrenic system, unlike the locomotor one, can jeopardize survival when its response is impaired. Thus, an urgent mechanism called “inactivity-induced phrenic motor facilitation (iPMF)” generates a boost of synaptic inputs around disconnected PhMNs that ensure a motor output to the diaphragm (Strey et al., 2013). In contrast, the disconnection of lumbar motoneurons increases their plastic capacity to form new connections that not necessarily will be functional, unless an activity-dependent therapy shapes them properly. Thus, while

activity-dependent therapies are necessary to generate appropriate motor responses in the locomotor system, they are not essential to generate a spontaneous respiratory recovery. The amount of inputs that neurons received in each situation is observed by PNN morphology. Hence, the boost of inputs after the cervical injury eventually increased PNNs but the plastic state of denervated lumbar motoneurons decreased PNN thickness.

Remarkably, no significant changes were reported around PhMNs after injuring the left phrenic system. Since the left phrenic circuit has a smaller contribution to diaphragm innervation (Song et al., 1999), the left hemisection did not severely affect the respiratory rate and little structural plasticity was required.

Overall, these data demonstrated that not all spinal PNNs are modulated equally. The characteristics of each neuron and the circuit involved are important factors to understand PNN integrity. Indeed, assessing the basal PNN structure and its dynamics after injury or any physiological demands can be useful to better understand how each circuit works.

Limitations of the study

Transgenic mice used in this thesis have some limitations. One could expect that the lack of link protein 1 would generate naked neurons, without any PNN component around them. However, *Crtll* KO mice still had PNNs with an altered proportion of their components that were distributed in an aberrant morphology. Although the interaction of all PNN components is required to generate functional PNNs, the individual charge and function of each component also participate in the final role. Thus, although the differences between the PNNs from WT and *Crtll* KO mice were enough to elucidate the function of spinal PNNs, their absence would likely produce more conclusive results.

A possible alternative gene to know out could be aggrecan. Since it is considered the most abundant PNN component in the spinal cord, its lack might result in fainter PNNs.

Future considerations

Based on the findings of the present thesis, PNNs play an important role in spinal cord physiology. However, many questions are still unanswered. Are spinal PNNs also implicated in neural protection? Why spinal PNNs are differently modulated from cortical PNNs? For a comprehensive understanding of PNNs, further research and new

techniques that allow an *in vivo* analysis are required. Once PNNs are fully characterized, they could be used as potential therapeutic targets to treat SCI and other disorders. Interestingly, altered spinal PNNs are not only observed after SCI but rather in other pathologies that affect the spinal cord such as amyotrophic lateral sclerosis (ALS) and spinal muscular atrophy (SMA). Indeed, disorganized and vestigial PNNs are found in the ventral horn of terminal SOD1 mice (Forostyak et al., 2014), an experimental model of ALS. *In vitro* and *in vivo* studies revealed that SMA patients present a downregulation of the *Crtll* gene, altering their PNNs (Dayangac-Erden et al., 2018).

Besides, considering that PNNs are key regulating plasticity and stability of circuits, they can also be useful in treating pathologies that either need to boost plasticity or potentiate the stability. However, PNN remodeling must strike an accurate balance. A possible strategy to modulate PNNs without severely affecting their structure is with the application of physical rehabilitation or selective antibodies against 4- or 6-sulfated GAG chains which can improve (Yang et al., 2017) or reduce (Gilbert et al., 2005) plasticity.

IX. Conclusions

Chapter I. Aberrant perineuronal nets alter spinal circuits, impair motor function, and increase plasticity

- The lack of link protein 1 generates immature PNNs characterized by an altered proportion of their components.
- These aberrant PNNs disrupt excitatory synapses and alter the physiological properties of motoneurons, thereby producing hyperreflexia and motor impairments.
- The disorganized spinal circuits generate a permissive scenario for contralateral corticospinal axons to sprout after injury.

Chapter II. Voluntary wheel running preserves lumbar perineuronal nets, enhances motor functions and prevents hyperreflexia after spinal cord injury

- The thoracic SCI produces motor impairment, thermal hyperalgesia, and hyperreflexia as well as reduces PNN around lumbar motoneurons.
- The voluntary wheel running enhances motor function, reduces hyperalgesia, and hyperreflexia as well as increases PNN around lumbar motoneurons.
- PNN values show a positive correlation with the KCC2 cotransporter, which is important in controlling the excitability of motoneurons.
- Activity-dependent therapies increase PNNs in the lumbar spinal cord and decrease them in the gracilis nucleus.

Chapter III. Link protein 1 is involved in the activity-dependent modulation of perineuronal nets in the spinal cord

- The link protein 1 is implicated in the activity-dependent remodeling of mature PNNs.
- At basal levels, transgenic mice lacking the link protein 1 show the same maladaptive outcomes observed in WT mice after a thoracic SCI

Chapter IV. Perineuronal net changes reveal a distinct right and left spinal phrenic circuit

- The spinal respiratory circuit presents few PNN-ensheathed neurons, compatible with a very plastic circuit.

Conclusions

- The high cervical hemisection at the right side of the cord increases PNNs around ipsilateral phrenic motoneurons whereas the same hemisection at the left side does not modify PNNs.
- There is a higher number of phrenic motoneurons in the right side compared to the left side, thus spinal respiratory circuits show anatomical differences between sides that have an impact after injury.

X. References

- Ahuja CS, Wilson JR, Nori S, Kotter MRN, Druschel C, Curt A, Fehlings MG (2017) Traumatic spinal cord injury. *Nat Rev Dis Primers* 3.
- Alilain WJ, Horn KP, Hu H, Dick TE, Silver J (2011) Functional regeneration of respiratory pathways after spinal cord injury. *Nature* 475:196–200.
- Alizadeh A, Dyck SM, Karimi-Abdolrezaee S (2019) Traumatic spinal cord injury: An overview of pathophysiology, models and acute injury mechanisms. *Front Neurol* 10.
- Al'joboori YD, Edgerton VR, Ichiyama RM (2020) Effects of rehabilitation on perineural nets and synaptic plasticity following spinal cord transection. *Brain Sci* 10:1–13.
- Alpár A, Gärtner U, Härtig W, Brückner G (2006) Distribution of pyramidal cells associated with perineuronal nets in the neocortex of rat. *Brain Res* 1120:13–22.
- Alvarez FJ, Villalba RM, Zerda R, Schneider SP (2004) Vesicular Glutamate Transporters in the Spinal Cord, with Special Reference to Sensory Primary Afferent Synapses. *Journal of Comparative Neurology* 472:257–280.
- Alvarez P, Gear RW, Green PG, Levine JD (2012) IB4-saporin attenuates acute and eliminates chronic muscle pain in the rat. *Exp Neurol* 233:859–865.
- Anjum A, Yazid MD, Daud MF, Idris J, Hwei Ng AM, Naicker AS, Rashidah Ismail OH, Kumar RKA, Lokanathan Y (2020) Spinal cord injury: Pathophysiology, multimolecular interactions, and underlying recovery mechanisms. *Int J Mol Sci* 21:1–35.
- Arbat-Plana A, Navarro X, Udina E (2017) Effects of forced, passive, and voluntary exercise on spinal motoneurons changes after peripheral nerve injury. *European Journal of Neuroscience* 46:2885–2892.
- Arbat-Plana A, Torres-Espín A, Navarro X, Udina E (2015) Activity dependent therapies modulate the spinal changes that motoneurons suffer after a peripheral nerve injury. *Exp Neurol* 263:293–305.
- Atoji Y, Yamamoto Y, Suzuki Y, Matsui F, Oohira A (1997) Immunohistochemical localization of neurocan in the lower auditory nuclei of the dog. *Hear Res* 110:200–208.
- Attwell S, Roskelley C, Dedhar S (2000) The integrin-linked kinase (ILK) suppresses anoikis. *Oncogene* 19:3811–3815.
- Balmer TS, Carels VM, Frisch JL, Nick TA (2009) Modulation of perineuronal nets and parvalbumin with developmental song learning. *Journal of Neuroscience* 29:12878–12885.
- Bareyre FM, Kerschensteiner M, Raineteau O, Mettenleiter TC, Weinmann O, Schwab ME (2004) The injured spinal cord spontaneously forms a new intraspinal circuit in adult rats. *Nat Neurosci* 7:269–277.
- Barritt AW, Davies M, Marchand F, Hartley R, Grist J, Yip P, McMahon SB, Bradbury EJ (2006) Chondroitinase ABC promotes sprouting of intact and injured spinal systems after spinal cord injury. *Journal of Neuroscience* 26:10856–10867.
- Battistuzzo CR, Rank MM, Flynn JR, Morgan DL, Callister R, Callister RJ, Galea MP (2016) Gait recovery following spinal cord injury in mice: Limited effect of treadmill training. *Journal of Spinal Cord Medicine* 39:335–343.
- Battistuzzo CR, Rank MM, Flynn JR, Morgan DL, Callister R, Callister RJ, Galea MP (2017) Effects Of treadmill training on hindlimb muscles of spinal cord-injured mice. *Muscle Nerve* 55:232–242.
- Bekku Y, Oohashi T (2011) Neurocan contributes to the molecular heterogeneity of the perinodal ECM. *Arch Histol Cytol* 73:95–102.

- Bekku Y, Saito M, Moser M, Fuchigami M, Maehara A, Nakayama M, Kusachi S, Ninomiya Y, Oohashi T (2012) Bral2 is indispensable for the proper localization of brevican and the structural integrity of the perineuronal net in the brainstem and cerebellum. *Journal of Comparative Neurology* 520:1721–1736.
- Bekku Y, Su WD, Hirakawa S, Fässler R, Ohtsuka A, Kang JS, Sanders J, Murakami T, Ninomiya Y, Oohashi T (2003) Molecular cloning of Bral2, a novel brain-specific link protein, and immunohistochemical colocalization with brevican in perineuronal nets. *Molecular and Cellular Neuroscience* 24:148–159.
- Bekku Y, Vargová L, Goto Y, Vorísek I, Dmytrenko L, Narasaki M, Ohtsuka A, Fässler R, Ninomiya Y, Syková E, Oohashi T (2010) Bral1: Its role in diffusion barrier formation and conduction velocity in the CNS. *Journal of Neuroscience* 30:3113–3123.
- Belichenko P V, Miklossy J, Celio MR (1997) HIV-1 Induced Destruction of Neocortical Extracellular Matrix Components in AIDS Victims. *Neurobiol Dis* 4:301–310.
- Ben-Ari Y, Khalilov I, Kahle KT, Cherubini E (2012) The GABA excitatory/inhibitory shift in brain maturation and neurological disorders. *Neuroscientist* 18:467–486.
- Berardi N, Pizzorusso T, Maffei L (2000) Critical periods during sensory development. *Curr Opin Neurobiol* 10:138–145.
- Beurdeley M, Spatazza J, Lee HHC, Sugiyama S, Bernard C, Di Nardo AA, Hensch TK, Prochiantz A (2012) Otx2 binding to perineuronal nets persistently regulates plasticity in the mature visual cortex. *Journal of Neuroscience* 32:9429–9437.
- Bevins RA, Besheer J (2006) Object recognition in rats and mice: a one-trial non-matching-to-sample learning task to study “recognition memory.” *Nat Protoc* 1:1306–1311.
- Bezdudnaya T, Hormigo KM, Marchenko V, Lane MA (2018) Spontaneous respiratory plasticity following unilateral high cervical spinal cord injury in behaving rats. *Exp Neurol* 305:56–65.
- Boulenguez P, Gauthier P, Kastner A (2007) Respiratory neuron subpopulations and pathways potentially involved in the reactivation of phrenic motoneurons after C2 hemisection. *Brain Res* 1148:96–104.
- Boulenguez P, Liabeuf S, Bos R, Bras H, Jean-Xavier C, Brocard C, Stil A, Darbon P, Cattaert D, Delpire E, Marsala M, Vinay L (2010) Down-regulation of the potassium-chloride cotransporter KCC2 contributes to spasticity after spinal cord injury. *Nat Med* 16:302–307.
- Bradbury EJ, Moon LDF, Popat RJ, King VR, Bennett GS, Patel PN, Fawcett JW, McMahon SB (2002) Chondroitinase ABC promotes functional recovery after spinal cord injury. *Nature* 416.
- Brakebusch C, Seidenbecher CI, Asztely F, Rauch U, Matthies H, Meyer H, Krug M, Böckers TM, Zhou X, Kreutz MR, Montag D, Gundelfinger ED, Fässler R (2002) Brevican-Deficient Mice Display Impaired Hippocampal CA1 Long-Term Potentiation but Show No Obvious Deficits in Learning and Memory. *Mol Cell Biol* 22:7417–7427.
- Brandenburg C, Blatt GJ (2022) Region-Specific Alterations of Perineuronal Net Expression in Postmortem Autism Brain Tissue. *Front Mol Neurosci* 15.
- Brückner G, Brauer K, Hart W, Joachim Wolff GR, Rickma MJ, Derouiche A, Delpech B, Girard N, Oertel WH, Reichenbach A (1993) Perineuronal Nets Provide a Polyanionic, Glia-Associated Form of Microenvironment Around Certain Neurons in Many Parts of the Rat Brain.
- Brückner G, Grosche J, Schmidt S, Härtig W, Margolis RU, Delpech B, Seidenbecher CI, Czaniara R, Schachner M (2000) Postnatal development of perineuronal nets

- in wild-type mice and in a mutant deficient in tenascin-R. *Journal of Comparative Neurology* 428:616–629.
- Brückner G, Härtig W, Kacza J, Seeger J, Welt K, Brauer K (1996) Extracellular matrix organization in various regions of rat brain grey matter. *J Neurocytol* 25:333–346.
- Burke RE, Levine DN, Tsairis P, Zajac FE (1973) Physiological types and histochemical profiles in motor units of the cat gastrocnemius. *J Physiol* 234:723–748.
- Buss A, Pech K, Kakulas BA, Martin D, Schoenen J, Noth J, Brook GA (2009) NG2 and phosphacan are present in the astroglial scar after human traumatic spinal cord injury. *BMC Neurol* 9:1–15.
- Buttry JL, Goshgarian HG (2014) Injection of WGA-Alexa 488 into the ipsilateral hemidiaphragm of acutely and chronically C2 hemisectioned rats reveals activity-dependent synaptic plasticity in the respiratory motor pathways. *Exp Neurol* 261:440–450.
- Cabungcal JH, Steullet P, Morishita H, Kraftsik R, Cuenod M, Hensch TK, Do KQ (2013) Perineuronal nets protect fast-spiking interneurons against oxidative stress. *Proc Natl Acad Sci U S A* 110:9130–9135.
- Cafferty WBJ, Bradbury EJ, Lidieth M, Jones M, Duffy PJ, Pezet S, McMahon SB (2008) Chondroitinase ABC-mediated plasticity of spinal sensory function. *Journal of Neuroscience* 28:11998–12009.
- Cafferty WBJ, Yang SH, Duffy PJ, Li S, Strittmatter SM (2007) Functional axonal regeneration through astrocytic scar genetically modified to digest chondroitin sulfate proteoglycans. *Journal of Neuroscience* 27:2176–2185.
- Caggiano AO, Zimber MP, Ganguly A, Blight AR, Gruskin EA (2005) Chondroitinase ABCI improves locomotion and bladder function following contusion injury of the rat spinal cord. *J Neurotrauma* 22:226–239.
- Cameron WE, Núez-Abades PA (2000) Physiological changes accompanying anatomical remodeling of mammalian motoneurons during postnatal development. *Brain Res Bull* 53:523–527.
- Carstens KE, Phillips ML, Pozzo-Miller L, Weinberg RJ, Dudek SM (2016) Perineuronal nets suppress plasticity of excitatory synapses on CA2 pyramidal neurons. *Journal of Neuroscience* 36:6312–6320.
- Carulli D, Broersen R, De Winter F, Muir EM, Meškovi M, De Waal M, De Vries S, Boele H-J, Canto CB, De Zeeuw CI, Verhaagen J (2020) Cerebellar plasticity and associative memories are controlled by perineuronal nets. *Proc Natl Acad Sci U S A* 117:6855–6865.
- Carulli D, Pizzorusso T, Kwok JCF, Putignano E, Poli A, Forostyak S, Andrews MR, Deepa SS, Glant TT, Fawcett JW (2010) Animals lacking link protein have attenuated perineuronal nets and persistent plasticity. *Brain* 133:2331–2347.
- Carulli D, Rhodes KE, Brown DJ, Bonnert TP, Pollack SJ, Oliver K, Strata P, Fawcett JW (2006) Composition of perineuronal nets in the adult rat cerebellum and the cellular origin of their components. *J Comp Neurol* 494:559–577.
- Cawston TE, Young DA (2010) Proteinases involved in matrix turnover during cartilage and bone breakdown. *Cell Tissue Res* 339:221–235.
- Celio MR, Spreafico R, De Biasi S, Vitellaro-Zuccarello L (1998) Perineuronal nets: past and present. *Trends Neurosci* 21:510–515.
- Chu P, Abraham R, Budhu K, Khan U, de Marco Garcia N, Brumberg JC (2018) The Impact of Perineuronal Net Digestion Using Chondroitinase ABC on the Intrinsic Physiology of Cortical Neurons. *Neuroscience* 388:23–35.
- Clarke RW, Harris J (2004) The organization of motor responses to noxious stimuli. In: *Brain Research Reviews*, pp 163–172.

- Corda M, Von Euler C, Lennerstrand AG (1965) Proprioceptive innervation of the diaphragm P. *J Physiol* 178:161–177.
- Cornez G, Jonckers E, ter Haar SM, van der Linden A, Cornil CA, Balthazart J (2018) Timing of perineuronal net development in the zebra finch song control system correlates with developmental song learning. *Proceedings of the Royal Society B: Biological Sciences* 285.
- Costigan M, Woolf CJ (2000) Pain: Molecular mechanisms. *Journal of Pain* 1:35–44.
- Côté MP, Gandhi S, Zambrotta M, Houlé JD (2014) Exercise modulates chloride homeostasis after spinal cord injury. *Journal of Neuroscience* 34:8976–8987.
- Côté MP, Murray LM, Knikou M (2018) Spinal control of locomotion: Individual neurons, their circuits and functions. *Front Physiol* 9.
- Cregg JM, Chu KA, Hager LE, Maggard RSJ, Stoltz DR, Edmond M, Alilain WJ, Philippidou P, Landmesser LT, Silver J (2017) A Latent Propriospinal Network Can Restore Diaphragm Function after High Cervical Spinal Cord Injury. *Cell Rep* 21:654–665.
- Czipri M, Otto JM, Cs-Szabó G, Kamath R V., Vermes C, Firneisz G, Kolman KJ, Watanabe H, Li Y, Roughley PJ, Yamada Y, Olsen BR, Glant TT (2003) Genetic rescue of chondrodysplasia and the perinatal lethal effect of cartilage link protein deficiency. *Journal of Biological Chemistry* 278:39214–39223.
- D'Amico JM, Condliffe EG, Martins KJB, Bennett DJ, Gorassini MA (2014) Recovery of neuronal and network excitability after spinal cord injury and implications for spasticity. *Front Integr Neurosci* 8.
- Dauth S, Grevesse T, Pantazopoulos H, Campbell PH, Maoz BM, Berretta S, Parker KK (2016) Extracellular matrix protein expression is brain region dependent. *Journal of Comparative Neurology* 524:1309–1336.
- Dayangac-Erden D, Gur-Dedeoglu B, Eskici FN, Oztemur-Islakoglu Y, Erdem-Ozdamar S (2018) Do Perineuronal Net Elements Contribute to Pathophysiology of Spinal Muscular Atrophy? *in Vitro and Transcriptomics Insights. OMICS* 22:598–606.
- de Castro RJr, Burns CL, McAdoo DJ, Romanic AM (2000) Metalloproteinase increases in the injured rat spinal cord. *Neuroreport* 11.
- de Leon RD, Hodgson JA, Roy RR, Edgerton VR, Leon D, Rossignol VRE (1998) Locomotor Capacity Attributable to Step Training Versus Spontaneous Recovery After Spinalization in Adult Cats.
- De Luca C, Papa M (2016) Looking Inside the Matrix: Perineuronal Nets in Plasticity, Maladaptive Plasticity and Neurological Disorders. *Neurochem Res* 41:1507–1515.
- Deepa SS, Carulli D, Galtrey C, Rhodes K, Fukuda J, Mikami T, Sugahara K, Fawcett JW (2006) Composition of perineuronal net extracellular matrix in rat brain: A different disaccharide composition for the net-associated proteoglycans. *Journal of Biological Chemistry* 281:17789–17800.
- Detloff MR, Quiros-Molina D, Javia AS, Daggubati L, Nehlsen AD, Naqvi A, Ninan V, Vannix KN, McMullen MK, Amin S, Ganzer PD, Houlé JD (2016) Delayed Exercise Is Ineffective at Reversing Aberrant Nociceptive Afferent Plasticity or Neuropathic Pain after Spinal Cord Injury in Rats. *Neurorehabil Neural Repair* 30:685–700.
- Detloff MR, Smith EJ, Quiros Molina D, Ganzer PD, Houlé JD (2014) Acute exercise prevents the development of neuropathic pain and the sprouting of non-peptidergic (GDNF- and artemin-responsive) c-fibers after spinal cord injury. *Exp Neurol* 255:38–48.
- Deuchars SA, Brooke RE, Frater B, Deuchars J (2001) I. Deuchars SA, Brooke RE, Frater B, Deuchars J. Properties of interneurons in the intermediolateral cell column of the rat spinal cord: role of the potassium channel subunit Kv3.1. *Neuroscience*.

- 2001;106(2):433–46. Properties of interneurons in the int. *Neuroscience* 106:433–446.
- Devinney MJ, Nichols NL, Mitchell GS (2016) Sustained hypoxia elicits competing spinal mechanisms of phrenic motor facilitation. *Journal of Neuroscience* 36:7877–7885.
- Dick G, Liktan C, Alves JN, Ehlert EME, Miller GM, Hsieh-Wilson LC, Sugahara K, Oosterhof A, van Kuppevelt TH, Verhaagen J, Fawcett JW, Kwok JCF (2013) Semaphorin 3A binds to the perineuronal nets via chondroitin sulfate type E motifs in rodent brains. *Journal of Biological Chemistry* 288:27384–27395.
- Dityatev A, Brückner G, Dityateva G, Grosche J, Kleene R, Schachner M (2007) Activity-dependent formation and functions of chondroitin sulfate-rich extracellular matrix of perineuronal nets. *Dev Neurobiol* 67:570–588.
- Dityatev A, Fellin T (2008) Extracellular matrix in plasticity and epileptogenesis. *Neuron Glia Biol* 4:235–247.
- Dityatev A, Rusakov DA (2011) Molecular signals of plasticity at the tetrapartite synapse. *Curr Opin Neurobiol* 21:353–359.
- Dityatev A, Schachner M (2003) Extracellular matrix molecules and synaptic plasticity. *Nat Rev Neurosci* 4:456–468.
- Dougherty BJ, Terada J, Springborn SR, Vinit S, MacFarlane PM, Mitchell GS (2018) Daily acute intermittent hypoxia improves breathing function with acute and chronic spinal injury via distinct mechanisms. *Respir Physiol Neurobiol* 256:50–57.
- Ellenberger HH, Feldman JL (1988) Monosynaptic Transmission of Respiratory Drive to Phrenic Motoneurons From Brainstem Bulbosplinal Neurons in Rats.
- Engesser-Cesar C, Anderson AJ, Basso DM, Edgerton VR, Cotman CW (2005) Voluntary Wheel Running Improves Recovery from a Moderate Spinal Cord Injury.
- Engesser-Cesar C, Ichiyama RM, Nefas AL, Hill MA, Edgerton VR, Cotman CW, Anderson AJ (2007) Wheel running following spinal cord injury improves locomotor recovery and stimulates serotonergic fiber growth. *European Journal of Neuroscience* 25:1931–1939.
- Erschbamer MK, Pham TM, Zwart MC, Baumans V, Olson L (2006) Neither environmental enrichment nor voluntary wheel running enhances recovery from incomplete spinal cord injury in rats. *Exp Neurol* 201:154–164.
- Faist M, Mazevet D, Dietz V, Pierrot-Deseilligny E (1994) A quantitative assessment of presynaptic inhibition of Ia afferents in spastics Differences in hemiplegics and paraplegics.
- Favuzzi E, Marques-Smith A, Deogracias R, Winterflood CM, Sánchez-Aguilera A, Mantoan L, Maeso P, Fernandes C, Ewers H, Rico B (2017) Activity-Dependent Gating of Parvalbumin Interneuron Function by the Perineuronal Net Protein Brevican. *Neuron* 95:639–655.
- Fawcett JW (2015) The extracellular matrix in plasticity and regeneration after CNS injury and neurodegenerative disease. Elsevier B.V.
- Fawcett JW, Asher RA (1999) The glial scar and central nervous system repair. *Brain Res Bull* 49:377–391.
- Fawcett JW, Oohashi T, Pizzorusso T (2019) The roles of perineuronal nets and the perinodal extracellular matrix in neuronal function. *Nat Rev Neurosci* 20:451–465.
- Felix L, Stephan J, Rose CR (2021) Astrocytes of the early postnatal brain. *European Journal of Neuroscience* 54:5649–5672.
- Finnerup NB (2017) Neuropathic pain and spasticity: intricate consequences of spinal cord injury. *Spinal Cord*:1–5.

- Fischer A, Sananbenesi F, Wang X, Dobbin M, Tsai LH (2007) Recovery of learning and memory is associated with chromatin remodelling. *Nature* 447:178–182.
- Forostyak S, Homola A, Turnovcova K, Svitil P, Jendelova P, Sykova E (2014) Intrathecal delivery of mesenchymal stromal cells protects the structure of altered perineuronal nets in SOD1 rats and amends the course of ALS. *Stem Cells* 32:3163–3172.
- Fortino TA, Randelman ML, Hall AA, Singh J, Bloom DC, Engel E, Hoh DJ, Hou S, Zholudeva L v., Lane MA (2022) Transneuronal tracing to map connectivity in injured and transplanted spinal networks. *Exp Neurol* 351.
- Foscarin S, Ponchione D, Pajaj E, Leto K, Gawlak M, Wilczynski GM, Rossi F, Carulli D (2011) Experience-dependent plasticity and modulation of growth regulatory molecules at central synapses. *PLoS One* 6.
- Fouad K, Metz GAS, Merkler D, Dietz V, Schwab ME (2000) Treadmill training in incomplete spinal cord injured rats. *Behavioural Brain Research* 115:107–113.
- Fouad K, Tetzlaff W (2012) Rehabilitative training and plasticity following spinal cord injury. *Exp Neurol* 235:91–99.
- Freitag S, Schachner M, Morellini F (2003) Behavioral alterations in mice deficient for the extracellular matrix glycoprotein tenascin-R. *Behavioural Brain Research* 145:189–207.
- Friese A, Kaltschmidt JA, Ladle DR, Sigrist M, Jessell TM, Arber S (2009) Gamma and alpha motor neurons distinguished by expression of transcription factor *Err3*. *The Proceedings of the National Academy of Sciences* 106:13588–13593.
- Frischknecht R, Heine M, Perrais D, Seidenbecher CI, Choquet D, Gundelfinger ED (2009) Brain extracellular matrix affects AMPA receptor lateral mobility and short-term synaptic plasticity. *Nat Neurosci* 12:897–904.
- Fuller DD, Golder FJ, Olson Jr EB, Mitchell GS (2006) Recovery of phrenic activity and ventilation after cervical spinal hemisection in rats. *J Appl Physiol* 100:800–806
- Gaál B, Rác É, Juhász T, Holló K, Matesz C (2014) Distribution of extracellular matrix macromolecules in the vestibular nuclei and cerebellum of the frog, *Rana esculenta*. *Neuroscience* 258:162–173.
- Galtrey CM, Kwok JCF, Carulli D, Rhodes KE, Fawcett JW (2008) Distribution and synthesis of extracellular matrix proteoglycans, hyaluronan, link proteins and tenascin-R in the rat spinal cord. *European Journal of Neuroscience* 27:1373–1390.
- Gama CI, Tully SE, Sotogaku N, Clark PM, Rawat M, Vaidehi N, Goddard WA, Nishi A, Hsieh-Wilson LC (2006) Sulfation patterns of glycosaminoglycans encode molecular recognition and activity. *Nat Chem Biol* 2:467–473.
- Gandevia SC, Rothwell JC (1987) Knowledge of motor commands and the recruitment of human motoneurons. *Brain* 110:1117–1130.
- García-Álías G, Barkhuysen S, Buckle M, Fawcett JW (2009) Chondroitinase ABC treatment opens a window of opportunity for task-specific rehabilitation. *Nat Neurosci* 12:1145–1151.
- García-Mesa Y, López-Ramos JC, Giménez-Llort L, Revilla S, Guerra R, Gruart A, LaFerla FM, Cristòfol R, Delgado-García JM, Sanfeliu C (2011) Physical Exercise Protects Against Alzheimer's Disease in 3xTg-AD Mice. *Journal of Alzheimer's Disease* 24:421–454.
- Garshick E, Kelley A, Cohen SA, Garrison A, Tun CG, Gagnon D, Brown R (2005) A prospective assessment of mortality in chronic spinal cord injury. *Spinal Cord* 43:408–416.
- Ge WP, Miyawaki A, Gage FH, Jan YN, Jan LY (2012) Local generation of glia is a major astrocyte source in postnatal cortex. *Nature* 484:376–380.

- Geissler M, Gottschling C, Aguado A, Rauch U, Wetzel CH, Hatt H, Faissner A (2013) Primary hippocampal neurons, which lack four crucial extracellular matrix molecules, display abnormalities of synaptic structure and function and severe deficits in perineuronal net formation. *Journal of Neuroscience* 33:7742–7755.
- George M, Ghali Z (2018) Phrenic motoneurons: output elements of a highly organized intraspinal network. *J Neurophysiol* 119:1057–1070.
- Ghali MGZ (2018) Phrenic motoneurons: Output elements of a highly organized intraspinal network. *J Neurophysiol* 119:1057–1070.
- Giamanco KA, Morawski M, Matthews RT (2010) Perineuronal net formation and structure in aggrecan knockout mice. *Neuroscience* 170:1314–1327.
- Gilbert RJ, McKeon RJ, Darr A, Calabro A, Hascall VC, Bellamkonda R V (2005) CS-4,6 is differentially upregulated in glial scar and is a potent inhibitor of neurite extension. *Molecular and Cellular Neuroscience* 29:545–558.
- Glykys J, Dzhalala V, Egawa K, Balena T, Saponjian Y, Kuchibhotla K V, Bacskai BJ, Kahle KT, Zeuthen T, Staley KJ (2014) Local impermeant anions establish the neuronal chloride concentration. *Science* (1979) 343:670–675.
- Golder FJ, Mitchell GS (2005) Spinal synaptic enhancement with acute intermittent hypoxia improves respiratory function after chronic cervical spinal cord injury. *Journal of Neuroscience* 25:2925–2932.
- Gómez-Pinilla F, Ying Z, Roy RR, Molteni R, Reggie Edgerton V (2002) Voluntary exercise induces a BDNF-mediated mechanism that promotes neuroplasticity. *J Neurophysiol* 88:2187–2195.
- Gordon G, Grant G (1982) Dorsolateral spinal afferents to some medullary sensory nuclei. An anatomical study in the cat. *Exp Brain Res* 46:12–23.
- Goshgarian HG (2003) The crossed phrenic phenomenon: a model for plasticity in the respiratory pathways following spinal cord injury. *J Appl Physiol* 94:795–810.
- Goshgarian HG, Rafols JA (1989) Newonal and Glial Changes in the Rat Phrenic Nucleus Occurring Within Hours After Spinal Cord Injury. *J Comp Neurol*:284519–284533.
- Gottschling C, Wegrzyn D, Denecke B, Faissner A (2019) Elimination of the four extracellular matrix molecules tenascin-C, tenascin-R, brevican and neurocan alters the ratio of excitatory and inhibitory synapses. *Sci Rep* 9.
- Grillner S (2006) Biological Pattern Generation: The Cellular and Computational Logic of Networks in Motion. *Neuron* 52:751–766.
- Grimpe B, Silver J (2004) A Novel DNA Enzyme Reduces Glycosaminoglycan Chains in the Glial Scar and Allows Microtransplanted Dorsal Root Ganglia Axons to Regenerate beyond Lesions in the Spinal Cord. *Journal of Neuroscience* 24:1393–1397.
- Guo WL, Qi ZP, Yu L, Sun TW, Qu WR, Liu QQ, Zhu Z, Li R (2019) Melatonin combined with chondroitin sulfate ABC promotes nerve regeneration after root-avulsion brachial plexus injury. *Neural Regen Res* 14:328–338.
- Hargreaves K, Dubner R, Brown F, Flores C JJ (1988) A new and sensitive method for measuring thermal nociception in cutaneous hyperalgesia. *Pain* 32:77–88.
- Hargreaves K, Hargreaves K, Dubner R, Dubner R, Brown F, Brown F, Flores C, Flores C, Joris J, Joris J (1988) A new and sensitive method for measuring thermal nociception in cutaneous hyperalgesia. *Pain* 32:11.
- Harris NG, Mironova YA, Hovda DA, Sutton RL (2010) Chondroitinase ABC enhances pericontusion axonal sprouting but does not confer robust improvements in behavioral recovery. *J Neurotrauma* 27:1971–1982.
- Härtig W, Brauer K, Brückner G (1992) Wisteria floribunda agglutinin-labelled nets surround parvalbumin-containing neurons. *Neuroreport* 3:869–872.

- Hartig W, Derouiche A, Welt K, Brauer K, Grosche J, Mader M, Reichenbach A, Brückner G (1999) Cortical neurons immunoreactive for the potassium channel Kv3.1b subunit are predominantly surrounded by perineuronal nets presumed as a buffering system for cations.
- Hartig W, Derouiche A, Welt K, Brauer K, Grosche J, Mader M, Reichenbach A, Brückner G (1999) Cortical neurons immunoreactive for the potassium channel Kv3.1b subunit are predominantly surrounded by perineuronal nets presumed as a buffering system for cations. *Brain Res* 842:15–29.
- Hartig W, Mages B, Aleithe S, Nitzsche B, Altmann S, Barthel H, Krueger M, Michalski D (2017) Damaged neocortical perineuronal nets due to experimental focal cerebral ischemia in mice, rats and sheep. *Front Integr Neurosci* 11:1–16.
- Hathway GJ, Vega-Avelaira D, Moss A, Ingram R, Fitzgerald M (2009) Brief, low frequency stimulation of rat peripheral C-fibres evokes prolonged microglial-induced central sensitization in adults but not in neonates. *Pain* 144:110–118.
- Haussoø A, Ibrahim M, Bartsch U, Letiembre M, Celio MR, Menoud PA (2000) Morphology of perineuronal nets in tenascin-R and parvalbumin single and double knockout mice. *Brain Res* 864:142–145.
- Hausen D, Brückner G, Drlicek M, Hartig W, Brauer K, Bigl V (1996) Pyramidal cells ensheathed by perineuronal nets in human motor and somatosensory cortex. *Neuroreport* 7:1725–1729.
- Hausmann ON (2003) Post-traumatic inflammation following spinal cord injury. *Spinal Cord* 41:369–378.
- Hayani H, Song I, Dityatev A (2018) Increased excitability and reduced excitatory synaptic input into fast-spiking CA2 interneurons after enzymatic attenuation of extracellular matrix. *Front Cell Neurosci* 12:1–13.
- Hebb D O (1949) *The Organization of Behavior. A Neuropsychological theory.*
- Hirono M, Watanabe S, Karube F, Fujiyama F, Kawahara S, Nagao S, Yanagawa Y, Misonou H (2018) Perineuronal nets in the deep cerebellar nuclei regulate GABAergic transmission and delay eyeblink conditioning. *Journal of Neuroscience* 38:6130–6144.
- Ho SM, Waite PME (2002) Effects of different anesthetics on the paired-pulse depression of the H reflex in adult rat. *Exp Neurol* 177:494–502.
- Hobohm C, Günther A, Grosche J, Roßner S, Schneider D, Brückner G (2005) Decomposition and long-lasting downregulation of extracellular matrix in perineuronal nets induced by focal cerebral ischemia in rats. *J Neurosci Res* 80:539–548.
- Hockfield S, McKay RDG (1983) A surface antigen expressed by a subset of neurons in the vertebrate central nervous system. *Proc Natl Acad Sci U S A* 80:5758–5761.
- Hoh DJ, Mercier LM, Hussey SP, Lane MA (2013) Respiration following spinal cord injury: Evidence for human neuroplasticity. *Respir Physiol Neurobiol* 189:450–464.
- Hsieh TH, Cheong Lee HH, Hameed MQ, Pascual-Leone A, Hensch TK, Rotenberg A (2017) Trajectory of parvalbumin cell impairment and loss of cortical inhibition in traumatic brain injury. *Cerebral Cortex* 27:5509–5524.
- Hubel DH, Wiesel TN (1970) The period of susceptibility to the physiological effects of unilateral eye closure in kittens. *J Physiol* 206:419–436.
- Hussein RK, Mencia CP, Katagiri Y, Brake AM, Geller HM (2020) Role of Chondroitin Sulfation Following Spinal Cord Injury. *Front Cell Neurosci* 14:1–12.
- Hutchinson KJ, Gómez-Pinilla F, Crowe MJ, Ying Z, Basso DM (2004) Three exercise paradigms differentially improve sensory recovery after spinal cord contusion in rats. *Brain* 127:1403–1414.

- Hutson TH et al. (2019) Cbp-dependent histone acetylation mediates axon regeneration induced by environmental enrichment in rodent spinal cord injury models. *Sci Transl Med* 11.
- Hylin MJ, Orsi SA, Moore AN, Dash PK (2013) Disruption of the perineuronal net in the hippocampus or medial prefrontal cortex impairs fear conditioning. *Learning and Memory* 20:267–273.
- Ichiyama R, Potuzak M, Balak M, Kalderon N, Edgerton VR (2009) Enhanced motor function by training in spinal cord contused rats following radiation therapy. *PLoS One* 4.
- Ira Fox S (2003) *Human Physiology, Seventh*. Mc Graw Hill- interamerica.
- Irvine SF, Kwok JCF (2018) Perineuronal nets in spinal motoneurons: Chondroitin sulphate proteoglycan around alpha motoneurons. *Int J Mol Sci* 19.
- Iseda T, Okuda T, Kane-Goldsmith N, Mathew M, Ahmed S, Chang YW, Young W, Grumet M (2008) Single, high-dose intraspinal injection of chondroitinase reduces glycosaminoglycans in injured spinal cord and promotes corticospinal axonal regrowth after hemisection but not contusion. *J Neurotrauma* 25:334–349.
- Jäger C, Lendvai D, Seeger G, Brückner G, Matthews RT, Arendt T, Alpár A, Morawski M (2013) Perineuronal and perisynaptic extracellular matrix in the human spinal cord. *Neuroscience* 238:168–184.
- Jammes Y, Arbogast S, De Troyer AA (2000) Response of the rabbit diaphragm to tendon vibration. *Neurosci Lett*:85–88.
- Jiang YQ, Zaaimi B, Martin JH (2016) Competition with primary sensory afferents drives remodeling of corticospinal axons in mature spinal motor circuits. *Journal of Neuroscience* 36:193–203.
- Jones LL, Margolis RU, Tuszynski MH (2003) The chondroitin sulfate proteoglycans neurocan, brevican, phosphacan, and versican are differentially regulated following spinal cord injury. *Exp Neurol* 182:399–411.
- Jordan LM, Sławińska U (2014) The Brain and Spinal Cord Networks Controlling Locomotion. In: *Neuronal Networks in Brain Function, CNS Disorders, and Therapeutics*, pp 215–233. Elsevier Inc.
- Joseph EK, Levine JD (2010) Hyperalgesic priming is restricted to IB4-positive nociceptors. *Neuroscience* 169:431–435.
- Kakinohana O, Hefferan MP, Nakamura S, Kakinohana M, Galik J, Tomori Z, Marsala J, Yaksh TL, Marsala M (2006) Development of GABA-sensitive spasticity and rigidity in rats after transient spinal cord ischemia: A qualitative and quantitative electrophysiological and histopathological study. *Neuroscience* 141:1569–1583.
- Kalb RG, Hockfield S (1988) Molecular Evidence for Early Activity-Dependent Development of Hamster Motor Neurons.
- Kalb RG, Hockfield S (1994) Electrical Activity in the Neuromuscular Unit Can Influence the Molecular Development of Motor Neurons. :539–548.
- Kaplan A, Spiller KJ, Towne C, Kannng K, Choe G, Geber A, Akay T, Aebischer P, Henderson C (2014) Neuronal matrix metalloproteinase-9 is a determinant of selective neurodegeneration. *Neuron* 81:333–348.
- Kawasaki Y, Xu ZZ, Wang X, Park JY, Zhuang ZY, Tan PH, Gao YJ, Roy K, Corfas G, Lo EH, Ji RR (2008) Distinct roles of matrix metalloproteases in the early- and late-phase development of neuropathic pain. *Nat Med* 14:331–336.
- Kommenov D, Solarewicz JZ, Afzal F, Nantwi KD, Kuhn DM, Mateika JH (2016) Intermittent hypoxia promotes recovery of respiratory motor function in spinal cord-injured mice depleted of serotonin in the central nervous system. *J Appl Physiol* 121:545–557.

- Kwok JCF, Carulli D, Fawcett JW (2010) In vitro modeling of perineuronal nets: Hyaluronan synthase and link protein are necessary for their formation and integrity. *J Neurochem* 114:1447–1459.
- Kwok JCF, Dick G, Wang D, Fawcett JW (2011) Extracellular matrix and perineuronal nets in CNS repair. *Dev Neurobiol* 71:1073–1089.
- Kwon M, Altin M, Duenas H, Alev L (2014) The role of descending inhibitory pathways on chronic pain modulation and clinical implications. *Pain Practice* 14:656–667.
- Laabs TL, Wang H, Katagiri Y, McCann T, Fawcett JW, Geller HM (2007) Inhibiting glycosaminoglycan chain polymerization decreases the inhibitory activity of astrocyte-derived chondroitin sulfate proteoglycans. *Journal of Neuroscience* 27:14494–14501.
- Lane MA (2011) Spinal respiratory motoneurons and interneurons. *Respir Physiol Neurobiol* 179:3–13.
- Lane MA, Lee KZ, Fuller DD, Reier PJ (2009) Spinal circuitry and respiratory recovery following spinal cord injury. *Respir Physiol Neurobiol* 169:123–132.
- Lane MA, Lee KZ, Salazar K, O'Steen BE, Bloom DC, Fuller DD, Reier PJ (2012) Respiratory function following bilateral mid-cervical contusion injury in the adult rat. *Exp Neurol* 235:197–210.
- Lane MA, White TE, Coutts MA, Jones AL, Sandhu MS, Bloom DC, Bolser DC, Yates BJ, Fuller DD, Reier PJ (2008) Cervical prephrenic interneurons in the normal and lesioned spinal cord of the adult rat. *Journal of Comparative Neurology* 511:692–709.
- Lang B, JM C, DePaul M, Tran A, Xu K, Dyck S, Madalena K, Brown B, Weng Y, Li S, Karimi-Abdolrezaee S, Busch S, Shen Y, Silver J (2015) Modulation of the proteoglycan receptor PTP σ promotes recovery after spinal cord injury. *518:404–408*.
- Lee H, Leamey CA, Sawatari A (2012) Perineuronal nets play a role in regulating striatal function in the mouse. *PLoS One* 7.
- Lee H, McKeon RJ, Bellamkonda R V. (2010) Sustained delivery of thermostabilized chABC enhances axonal sprouting and functional recovery after spinal cord injury. *Proc Natl Acad Sci U S A* 107:3340–3345.
- Lee-Kubli C, Marshall AG, Malik RA, Calcutt NA (2018) The H-Reflex as a Biomarker for Spinal Disinhibition in Painful Diabetic Neuropathy. *Curr Diab Rep* 18.
- Lemons ML, Sandy JD, Anderson DK, Howland DR (2001) Intact aggrecan and fragments generated by both aggrecanase and metalloproteinase-like activities are present in the developing and adult rat spinal cord and their relative abundance is altered by injury. *Journal of Neuroscience* 21:4772–4781.
- Lima R, Monteiro A, Salgado AJ, Monteiro S, Silva NA (2022) Pathophysiology and Therapeutic Approaches for Spinal Cord Injury. *Int J Mol Sci* 23:13833.
- Lindsay AD, Feldman JL, Lindsa AD, Feldman JL (1993) Modulation of respiratory activity of neonatal rat phrenic motoneurons by serotonin. *Journal of Physiology* 461:213–233.
- Liu YJ, Spangenberg EE, Tang B, Holmes TC, Green KN, Xu X (2021) Microglia elimination increases neural circuit connectivity and activity in adult mouse cortex. *Journal of Neuroscience* 41:1274–1287.
- Lorenzo Bozzelli P, Alaiyed S, Kim E, Villapol S, Conant K (2018) Proteolytic Remodeling of Perineuronal Nets: Effects on Synaptic Plasticity and Neuronal Population Dynamics. *Neural Plast* 2018.
- Loy K, Bareyre FM (2019) Rehabilitation following spinal cord injury: How animal models can help our understanding of exercise-induced neuroplasticity. *Neural Regen Res* 14:405–412.

- Lundell A, Olin AI, Mörgelin M, Al-Karadaghi S, Aspberg A, Logan DT (2004) Structural basis for interactions between tenascins and lectican C-type lectin domains: Evidence for a crosslinking role for tenascins. *Structure* 12:1495–1506.
- Madinier A, Quattromani MJ, Sjölund C, Ruscher K, Wieloch T (2014) Enriched housing enhances recovery of limb placement ability and reduces aggrecan-containing perineuronal nets in the rat somatosensory cortex after experimental stroke. *PLoS One* 9.
- Mahamed S, Strey KA, Mitchell GS, Baker-Herman TL (2011) Reduced respiratory neural activity elicits phrenic motor facilitation. *Respir Physiol Neurobiol* 175:303–309.
- Mancuso R, Oliván S, Osta R, Navarro X (2011) Evolution of gait abnormalities in SOD1 G93A transgenic mice. *Brain Res* 1406:65–73.
- Manuel M, Zytnicki D (2019) Molecular and electrophysiological properties of mouse motoneuron and motor unit subtypes. *Curr Opin Physiol* 8:23–29.
- Manzanares G, Brito-Da-Silva G, Gandra PG (2019) Voluntary wheel running: Patterns and physiological effects in mice. *Brazilian Journal of Medical and Biological Research* 52.
- Martínez-Silva M de L, Imhoff-Manuel RD, Sharma A, Heckman CJ, Shneider NA, Roselli F, Zytnicki D, Manuel M (2018) Hypoexcitability precedes denervation in the large fast-contracting motor units in two unrelated mouse models of ALS. *Elife* 7:1–26.
- Massey JM, Hubscher CH, Wagoner MR, Decker JA, Amps J, Silver J, Onifer SM (2006) Chondroitinase ABC Digestion of the Perineuronal Net Promotes Functional Collateral Sprouting in the Cuneate Nucleus after Cervical Spinal Cord Injury. *The Journal of Neuroscience* 26:4406–4414.
- Matthews RT, Kelly GM, Zerillo CA, Gray G, Tiemeyer M, Hockfield S (2002) Aggrecan glycoforms contribute to the molecular heterogeneity of perineuronal nets. *Journal of Neuroscience* 22:7536–7547.
- McKeon RJ, Jurynek MJ, Buck CR (1999) The chondroitin sulfate proteoglycans neurocan and phosphacan are expressed by reactive astrocytes in the chronic CNS glial scar. *Journal of Neuroscience* 19:10778–10788.
- McKeon RJ, Schreiber RC, Rudge JS, Silver J (1991) Reduction of neurite outgrowth in a model of glial scarring following CNS injury is correlated with the expression of inhibitory molecules on reactive astrocytes. *Journal of Neuroscience* 11:3398–3411.
- Mcrae PA, Baranov E, Rogers SL, Porter BE (2012) Persistent decrease in multiple components of the perineuronal net following status epilepticus. *European Journal of Neuroscience* 36:3471–3482.
- Meyer OA, Tilson HA, Byrd WC, Riley MT (1979) A method for the routine assessment of fore- and hindlimb grip strength of rats and mice. *Neurobehav Toxicol* 1:233–236.
- Miao QL, Ye Q, Zhang XH (2014) Perineuronal net, CSPG receptor and their regulation of neural plasticity. *Acta physiologica Sinica* 66:387–397.
- Minor KH, Akison LK, Goshgarian HG, Seeds NW (2006) Spinal cord injury-induced plasticity in the mouse-The crossed phrenic phenomenon. *Exp Neurol* 200:486–495.
- Miyata S, Kitagawa H (2017) Formation and remodeling of the brain extracellular matrix in neural plasticity: Roles of chondroitin sulfate and hyaluronan. *Biochim Biophys Acta Gen Subj* 1861:2420–2434.
- Miyata S, Komatsu Y, Yoshimura Y, Taya C, Kitagawa H (2012) Persistent cortical plasticity by upregulation of chondroitin 6-sulfation. *Nat Neurosci* 15:414–422.

- Molteni R, Zheng J-Q, Ying Z, Gó mez-Pinilla F, Twiss JL (2004) Voluntary exercise increases axonal regeneration from sensory neurons.
- Montag-Sallaz M, Montag D (2003) Severe cognitive and motor coordination deficits in tenascin-R-deficient mice. *Genes Brain Behav* 2:20–31.
- Moon LDF, Asher RA, Rhodes KE, Fawcett JW (2001) Regeneration of CNS axons back to their target following treatment of adult rat brain with chondroitinase ABC. 4:465–466.
- Morawski M, Alpár A, Brückner G, Fiedler A, Jäger C, Gati G, Stieler JT, Arendt T (2009) Chondroitin sulfate proteoglycan-based extracellular matrix in chicken (*Gallus domesticus*) brain. *Brain Res* 1275:10–23.
- Morawski M, Brückner G, Jäger C, Seeger G, Arendt T (2010) Neurons associated with aggrecan-based perineuronal nets are protected against tau pathology in subcortical regions in Alzheimer's disease. *Neuroscience* 169:1347–1363.
- Morikawa S, Ikegaya Y, Narita M, Tamura H (2017) Activation of perineuronal net-expressing excitatory neurons during associative memory encoding and retrieval. *Sci Rep* 7:1–9.
- Mueller AL, Davis A, Sovich S, Carlson SS, Robinson FR (2016) Distribution of N-Acetylgalactosamine-Positive Perineuronal Nets in the Macaque Brain: Anatomy and Implications. *Neural Plast* 2016.
- Multon S, Franzen R, Poirrier A-L, Scholtes F, Schoenen J (2003) The Effect of Treadmill Training on Motor Recovery after a Partial Spinal Cord Compression-Injury in the Adult Rat.
- Murakami F, Song WJ, Katsumaru H (1992) Plasticity of neuronal connections in developing brains of mammals. *Neurosci Res* 15:235–253.
- Murray M (2014) General Overview of Spinal Anatomy and Physiology Organization. In: *Encyclopedia of Computational Neuroscience*, pp 1–15. Springer New York.
- Nadanaka S, Miyata S, Yaqiang B, Tamura JI, Habuchi O, Kitagawa H (2020) Reconsideration of the semaphorin-3a binding motif found in chondroitin sulfate using galnac4s-6st-knockout mice. *Biomolecules* 10:1–16.
- Nadine G, Pico C, Andreas L, Cyril H (2009) Perineuronal Nets Protect Fear Memories from Erasure. *Science* (1979) 325:1258–1261.
- Nair J, Streeter KA, Turner SMF, Sunshine MD, Bolser DC, Fox EJ, Davenport PW, Fuller DD (2017) Anatomy and physiology of phrenic afferent neurons. *J Neurophysiol* 118:2975–2990.
- Nantwi KD, El-Bohy AA, Schrimsher GW, Reier PJ, Goshgarian HG (1999) Spontaneous Functional Recovery in a Paralyzed Hemidiaphragm Following Upper Cervical Spinal Cord Injury in Adult Rats. *Neurorehabil Neural Repair*:225–234.
- Navarro X, Udina B (2009) Neurofisiología de la espasticidad. In: *Evaluación Clínica y Tratamiento de la Espasticidad*, pp 1–15. Panamericana.
- Nees TA, Finnerup NB, Blesch A, Weidner N (2017) Neuropathic pain after spinal cord injury. *Pain* 158:371–376.
- Nees TA, Tappe-Theodor A, Sliwinski C, Motsch M, Rupp R, Kuner R, Weidner N, Blesch A (2016) Early-onset treadmill training reduces mechanical allodynia and modulates calcitonin gene-related peptide fiber density in lamina III/IV in a mouse model of spinal cord contusion injury. *Pain* 157:687–697.
- Nithianantharajah J, Hannan AJ (2006) Enriched environments, experience-dependent plasticity and disorders of the nervous system. *Nat Rev Neurosci* 7:697–709.
- Niu J, Ding L, Li JJ, Kim H, Liu J, Li H, Moberly A, Badea TC, Duncan ID, Son YJ, Scherer SS, Luo W (2013) Modality-based organization of ascending

- somatosensory axons in the direct dorsal column pathway. *Journal of Neuroscience* 33:17691–17709.
- O'Connor AM, Burton TJ, Mansuri H, Hand GR, Leamey CA, Sawatari A (2019) Environmental Enrichment From Birth Impacts Parvalbumin Expressing Cells and Wisteria Floribunda Agglutinin Labelled Peri-Neuronal Nets Within the Developing Murine Striatum. *Front Neuroanat* 13:1–14.
- Ogawa H, Oohashi T, Sata M, Bekku Y, Hirohata S, Nakamura K, Yonezawa T, Kusachi S, Shiratori Y, Ninomiya Y (2004) Lp3/Hapl3, a novel link protein that co-localizes with versican and is coordinately up-regulated by platelet-derived growth factor in arterial smooth muscle cells. *Matrix Biology* 23:287–298.
- Ogawa N, Hirose Y, Ohara S, Ono T, Watanabe Y (1985) A simple quantitative bradykinesia test in MPTP-treated mice. *Res Commun Chem Pathol Pharmacol* 50:435–441.
- Okamoto M, Mori S, Endo H (1994) A protective action of chondroitin sulfate proteoglycans against neuronal cell death induced by glutamate.
- Olson CB, Swett Jr. CP (1969) Speed of Contraction of Skeletal Muscle: The Effect of Hypoactivity and Hyperactivity. *Arch Neurol* 20:263–270.
- Oohashi T, Edamatsu M, Bekku Y, Carulli D (2015) The hyaluronan and proteoglycan link proteins: Organizers of the brain extracellular matrix and key molecules for neuronal function and plasticity. *Exp Neurol* 274:134–144.
- Orlando C, Ster J, Gerber U, Fawcett JW, Raineteau O (2012) Perisynaptic chondroitin sulfate proteoglycans restrict structural plasticity in an integrin-dependent manner. *Journal of Neuroscience* 32:18009–18017.
- Oyinbo CA (2011) Secondary injury mechanisms in traumatic spinal cord injury: A nugget of this multiply cascade. *Acta Neurobiol Exp (Wars)* 71:281–299.
- Pearson KG (2004) Generating the walking gait: role of sensory feedback. *Prog Brain Res* 143:123–129.
- Perreau VM, Adlard PA, Anderson AJ, Cotman CW (2005) Exercise-Induced Gene Expression Changes in the Rat Spinal Cord.
- Pizzorusso T (2002) Reactivation of Ocular Dominance Plasticity in the Adult Visual Cortex. *Science* (1979) 298:1248–1251.
- Pizzorusso T, Medini P, Landi S, Baldini S, Berardi N, Maffei L (2006) Structural and functional recovery from early monocular deprivation in adult rats. *Proc Natl Acad Sci U S A* 103:8517–8522.
- Prabhakar V, Raman R, Capila I, Bosques CJ, Pojasek K, Sasisekharan R (2005) Biochemical characterization of the chondroitinase ABC I active site. *Biochemical Journal* 390:395–405.
- Putignano E, Lonetti G, Cancedda L, Ratto G, Costa M, Maffei L, Pizzorusso T (2007) Developmental Downregulation of Histone Posttranslational Modifications Regulates Visual Cortical Plasticity. *Neuron* 54:177.
- Pyka M, Wetzel C, Aguado A, Geissler M, Hatt H, Faissner A (2011) Chondroitin sulfate proteoglycans regulate astrocyte-dependent synaptogenesis and modulate synaptic activity in primary embryonic hippocampal neurons. *European Journal of Neuroscience* 33:2187–2202.
- Qiu K, Lane MA, Lee KZ, Reier PJ, Fuller DD (2010) The phrenic motor nucleus in the adult mouse. *Exp Neurol* 226:254–258.
- Raineteau O, Schwab ME (2001) Plasticity of motor systems after incomplete spinal cord injury. *Nat Rev Neurosci*:263–273
- Rampon C, Jiang CH, Dong H, Tang YP, Lockhart DJ, Schultz PG, Tsien JZ, Hu Y (2000) Effects of environmental enrichment on gene expression in the brain. *Proc Natl Acad Sci U S A* 97:12880–12884.

- Randelman M, Zholudeva L v., Vinit S, Lane MA (2021) Respiratory Training and Plasticity After Cervical Spinal Cord Injury. *Front Cell Neurosci* 15.
- Redondo-Castro E, Navarro X, García-Álías G (2016) Longitudinal evaluation of residual cortical and subcortical motor evoked potentials in spinal cord injured rats. *J Neurotrauma* 33:907–916.
- Rexed B (1954) A cytoarchitectonic atlas of the spinal cord in the cat. *J Comp Neurol* 100:297–379.
- Rivera C, Voipio J, Payne JA, Ruusuvoori E, Lahtinen H, Lamsa K, Pirvola U, Saarma M, Kaila K (1999) The K⁺/Cl⁻ co-transporter KCC2 renders GABA hyperpolarizing during neuronal maturation. *Nature* 397:251–255.
- Romberg C, Yang S, Melani R, Andrews MR, Horner AE, Spillantini MG, Bussey TJ, Fawcett JW, Pizzorusso T, Saksida LM (2013) Depletion of perineuronal nets enhances recognition memory and long-term depression in the perirhinal cortex. *Journal of Neuroscience* 33:7057–7065.
- Ronnevi L-O, Conradi S (1974) Ultrastructural evidence for spontaneous elimination of synaptic terminals on spinal motoneurons in the kitten. *Brain Res* 80:335–339.
- Rossignol S, Dubuc J, Gossard J-P (2006) Dynamic Sensorimotor Interactions in Locomotion.
- Rossignol S, Frigon A (2011) Recovery of locomotion after spinal cord injury: Some facts and mechanisms. *Annu Rev Neurosci* 34:413–440.
- Rowlands D, Lensjø KK, Dinh T, Yang S, Andrews MR, Hafting T, Fyhn M, Fawcett JW, Dick G (2018) Aggrecan directs extracellular matrix-mediated neuronal plasticity. *Journal of Neuroscience* 38:10102–10113.
- Rudy B, McBain CJ (2001) Kv3 channels: Voltage-gated K⁺ channels designed for high-frequency repetitive firing. *Trends Neurosci* 24:517–526.
- Ruven C, Chan TK, Wu W (2014) Spinal root avulsion: An excellent model for studying motoneuron degeneration and regeneration after severe axonal injury. *Neural Regen Res* 9:117–118.
- Saghatelian AK, Gorissen S, Albert M, Hertlein B, Schachner M, Dityatev A (2000) The extracellular matrix molecule tenascin-R and its HNK-1 carbohydrate modulate perisomatic inhibition and long-term potentiation in the CA1 region of the hippocampus. *Eur J Neurosci* 12:3331–3342.
- Sale A, Maya Vetencourt JF, Medini P, Cenni MC, Baroncelli L, De Pasquale R, Maffei L (2007) Environmental enrichment in adulthood promotes amblyopia recovery through a reduction of intracortical inhibition. *Nat Neurosci* 10:679–681.
- Sánchez-Ventura J, Amo-Aparicio J, Navarro X, Penas C (2019) BET protein inhibition regulates cytokine production and promotes neuroprotection after spinal cord injury. *J Neuroinflammation* 16:1–12.
- Sánchez-Ventura J, Canal C, Hidalgo J, Penas C, Navarro X, Torres-Espin A, Fouad K, Udina E (2022) Aberrant perineuronal nets alter spinal circuits, impair motor function, and increase plasticity. *Exp Neurol* 358.
- Sánchez-Ventura J, Giménez-Llort L, Penas C, Udina E (2021) Voluntary wheel running preserves lumbar perineuronal nets, enhances motor functions and prevents hyperreflexia after spinal cord injury. *Exp Neurol* 336.
- Sandhu MS, Dougherty BJ, Lane MA, Bolser DC, Kirkwood PA, Reier PJ, Fuller DD (2009) Respiratory recovery following high cervical hemisection. *Respir Physiol Neurobiol* 169:94–101.
- Sater AP, Rael LT, Tanner AH, Lieser MJ, Acuna DL, Mains CW, Bar-Or D (2018) Cell death after traumatic brain injury: Detrimental role of anoikis in healing. *Clinica Chimica Acta* 482:149–154.

- Satkunendrarajah K, Karadimas SK, Laliberte AM, Montandon G, Fehlings MG (2018) Cervical excitatory neurons sustain breathing after spinal cord injury. *Nature* 562:419–422.
- Seibenhener ML, Wooten MC (2015) Use of the open field maze to measure locomotor and anxiety-like behavior in mice. *Journal of Visualized Experiments*:1–6.
- Shen Y, Tenney AP, Busch SA, Horn KP, Fernando X, Liu K, He Z, Silver J, Flanagan JG (2009) PTP σ is a receptor for Chondroitin Sulfate Proteoglycan, an inhibitor of neural regeneration. *Science* (1979) 326:592–596.
- Shields LBE, Zhang YP, Burke DA, Gray R, Shields CB (2008) Benefit of chondroitinase ABC on sensory axon regeneration in a laceration model of spinal cord injury in the rat. *Surg Neurol* 69:568–577.
- Shiotsuki H, Yoshimi K, Shimo Y, Funayama M, Takamatsu Y, Ikeda K, Takahashi R, Kitazawa S, Hattori N (2010) A rotarod test for evaluation of motor skill learning. *J Neurosci Methods* 189:180–185.
- Silva NA, Sousa N, Reis RL, Salgado AJ (2014) From basics to clinical: A comprehensive review on spinal cord injury. *Prog Neurobiol* 114:25–57.
- Silver J, Miller JH (2004) Regeneration beyond the glial scar. *Nat Rev Neurosci*:146–156.
- Slaker M, Churchill L, Todd RP, Blacktop JM, Zuloaga DG, Raber J, Darling RA, Brown TE, Sorg BA (2015) Removal of perineuronal nets in the medial prefrontal cortex impairs the acquisition and reconsolidation of a cocaine-induced conditioned place preference memory. *Journal of Neuroscience* 35:4190–4202.
- Sliwinski C, Nees TA, Puttagunta R, Weidner N, Blesch A (2018) Sensorimotor activity partially ameliorates pain and reduces nociceptive fiber density in the chronically injured spinal cord. *J Neurotrauma* 35:2222–2238.
- Smith CC, Mauricio R, Nobre L, Marsh B, Wüst RCI, Rossiter HB, Ichiyama RM (2015) Differential regulation of perineuronal nets in the brain and spinal cord with exercise training. *Brain Res Bull* 111:20–26.
- Sofroniew M V (2010) Molecular dissection of reactive astrogliosis and glial scar formation. *Trends in Neuroscience* 32:638–647.
- Song A, Tracey DJ, Ashwell KWS (1999) Development of the rat phrenic nerve and the terminal distribution of phrenic afferents in the cervical cord. *Anat Embryol (Berl)* 200:625–643.
- Sorg BA, Berretta S, Blacktop JM, Fawcett JW, Kitagawa H, Kwok JCF, Miquel M (2016) Casting a wide net: Role of perineuronal nets in neural plasticity. *Journal of Neuroscience* 36:11459–11468.
- Spicer AP, Joo A, Bowling RA (2003) A hyaluronan binding link protein gene family whose members are physically linked adjacent to chondroitin sulfate proteoglycan core protein genes. The missing links. *Journal of Biological Chemistry* 278:21083–21091.
- Starkey ML, Bartus K, Barritt AW, Bradbury EJ (2012) Chondroitinase ABC promotes compensatory sprouting of the intact corticospinal tract and recovery of forelimb function following unilateral pyramidotomy in adult mice. *European Journal of Neuroscience* 36:3665–3678.
- Stifani N (2014) Motor neurons and the generation of spinal motor neuron diversity. *Front Cell Neurosci* 8.
- Strey KA, Baertsch NA, Baker-Herman TL (2013) Inactivity-induced respiratory plasticity: Protecting the drive to breathe in disorders that reduce respiratory neural activity. *Respir Physiol Neurobiol* 189:384–394.

- Sugiyama S, Di Nardo AA, Aizawa S, Matsuo I, Volovitch M, Prochiantz A, Hensch TK (2008) Experience-Dependent Transfer of Otx2 Homeoprotein into the Visual Cortex Activates Postnatal Plasticity. *Cell* 134:508–520.
- Sunshine MD, Sutor TW, Fox EJ, Fuller DD (2020) Targeted activation of spinal respiratory neural circuits. *Exp Neurol* 328:113256.
- Suttkus A, Morawski M, Arendt T (2016) Protective Properties of Neural Extracellular Matrix. *Mol Neurobiol* 53:73–82.
- Suttkus A, Rohn S, Weigel S, Glöckner P, Arendt T, Morawski M (2014) Aggrecan, link protein and tenascin-R are essential components of the perineuronal net to protect neurons against iron-induced oxidative stress. *Cell Death Dis* 5.
- Svensson M, Rosvall P, Boza-Serrano A, Andersson E, Lexell J, Deierborg T (2016) Forced treadmill exercise can induce stress and increase neuronal damage in a mouse model of global cerebral ischemia. *Neurobiol Stress* 5:8–18.
- Sylantsev S, Savtchenko LP, Niu YP, Ivanov AI, Jensen TP, Kullmann DM, Xiao MY, Rusakov DA (2008) Electric fields due to synaptic currents sharpen excitatory transmission. *Science* (1979) 319:1845–1849.
- Takeda A, Shuto M, Funakoshi K (2018) Chondroitin sulfate expression in perineuronal nets after goldfish spinal cord lesion. *Front Cell Neurosci* 12.
- Takeoka A, Vollenweider I, Courtine G, Arber S (2014) Muscle spindle feedback directs locomotor recovery and circuit reorganization after spinal cord injury. *Cell* 159:1626–1639.
- Takesian AE, Hensch TK (2013) Balancing plasticity/stability across brain development. Elsevier B.V.
- Takiguchi M, Morinobu S, Funakoshi K (2021) Chondroitin sulfate expression around spinal motoneurons during postnatal development in rats. *Brain Res* 1752.
- Tan AM, Colletti M, Rorai AT, Skene JHP, Levine JM (2006) Antibodies against the NG2 proteoglycan promote the regeneration of sensory axons within the dorsal columns of the spinal cord. *Journal of Neuroscience* 26:4729–4739.
- Tang XQ, Tanelian DL, Smith GM (2004) Semaphorin3A Inhibits Nerve Growth Factor-Induced Sprouting of Nociceptive Afferents in Adult Rat Spinal Cord. *Journal of Neuroscience* 24:819–827.
- Tansley S et al. (2022) Microglia-mediated degradation of perineuronal nets promotes pain. *Science* (1979) 377:80–86.
- Tewari BP, Chaunsali L, Campbell SL, Patel DC, Goode AE, Sontheimer H (2018) Perineuronal nets decrease membrane capacitance of peritumoral fast spiking interneurons in a model of epilepsy. *Nat Commun* 9.
- Tewari BP, Chaunsali L, Prim CE, Sontheimer H (2022) A glial perspective on the extracellular matrix and perineuronal net remodeling in the central nervous system. *Front Cell Neurosci* 16.
- Thompson FJ, Reier PJ, Lucas CC, Parmer R (1992) Altered patterns of reflex excitability subsequent to contusion injury of the rat spinal cord. *J Neurophysiol* 68:1473–1486.
- Todd AJ, Hughes DI, Polgár E, Nagy GG, Mackie M, Ottersen OP, Maxwell DJ (2003) The expression of vesicular glutamate transporters VGLUT1 and VGLUT2 in neurochemically defined axonal populations in the rat spinal cord with emphasis on the dorsal horn. *European Journal of Neuroscience* 17:13–27.
- Tom VJ, Kadakia R, Santi L, Houlé JD (2009) Administration of chondroitinase ABC rostral or caudal to a spinal cord injury site promotes anatomical but not functional plasticity. *J Neurotrauma* 26:2323–2333.
- Torres-Espín A, Beaudry E, Fenrich K, Fouad K (2018) Rehabilitative Training in Animal Models of Spinal Cord Injury. *J Neurotrauma* 35:1970–1985.

- Tsien RY (2013) Very long-term memories may be stored in the pattern of holes in the perineuronal net. *Proc Natl Acad Sci U S A* 110:12456–12461.
- Valero-Cabré A, Forés J, Navarro X (2004) Reorganization of reflex responses mediated by different afferent sensory fibers after spinal cord transection. *J Neurophysiol* 91:2838–2848.
- van Praag H, Kempermann G, Gage FH (2000) Neural consequences of environmental enrichment. *Nat Rev Neurosci* 1:191–198.
- van 't Spijker HM, Kwok JCF (2017) A Sweet Talk: The Molecular Systems of Perineuronal Nets in Controlling Neuronal Communication. *Front Integr Neurosci* 11:1–10.
- Vaynman S, Ying Z, Gomez-Pinilla F (2003) Interplay between brain-derived neurotrophic factor and signal transduction modulators in the regulation of the effects of exercise on synaptic-plasticity. *Neuroscience* 122:647–657.
- Vitellaro-Zuccarello L, Bosisio P, Mazzetti S, Monti C, De Biasi S (2007) Differential expression of several molecules of the extracellular matrix in functionally and developmentally distinct regions of rat spinal cord. *Cell Tissue Res* 327:433–447.
- Vo T, Carulli D, Ehlert EME, Kwok JCF, Dick G, Mecollari V, Moloney EB, Neufeld G, de Winter F, Fawcett JW, Verhaagen J (2013) The chemorepulsive axon guidance protein semaphorin3A is a constituent of perineuronal nets in the adult rodent brain. *Molecular and Cellular Neuroscience* 56:186–200.
- Wang D, Fawcett J (2012) The perineuronal net and the control of CNS plasticity. *Cell Tissue Res* 349:147–160.
- Wang D, Ichiyama RM, Zhao R, Andrews MR, Fawcett JW (2011) Chondroitinase combined with rehabilitation promotes recovery of forelimb function in rats with chronic spinal cord injury. *Journal of Neuroscience* 31:9332–9344.
- Wang H, Katagiri Y, Mccann TE, Unsworth E, Yu Z, Tan F, Santiago L, Mills EM, Wang Y, Aviva J, Geller HM (2009) Chondroitin-4-sulfation negatively regulates axonal guidance and growth. *J Neurosci* 29:3083–3091.
- Watson C (2012) Chapter 21 - The Somatosensory System. In (Watson C, Paxinos G, Puelles LBT-TMNS, eds), pp 563–570. San Diego: Academic Press.
- Watson C, Kayalioglu G (2009) Chapter 1 - The Organization of the Spinal Cord. In: The Spinal Cord (Watson C, Paxinos G, Kayalioglu G, eds), pp 1–7. San Diego: Academic Press.
- Weber P, Bartsch U, Rasband MN, Czaniera R, Lang Y, Bluethmann H, Margolis RU, Levinson SR, Shrager P, Montag D, Schachner M (1999) Mice deficient for tenascin-R display alterations of the extracellular matrix and decreased axonal conduction velocities in the CNS. *Journal of Neuroscience* 19:4245–4262.
- White SR, Neuman RS (1980) Facilitation of spinal motoneuron excitability by 5-hydroxytryptamine and noradrenaline.
- Witts EC, Zagoraiou L, Miles GB (2014) Anatomy and function of cholinergic C-bouton inputs to motor neurons. *J Anat* 224:52–60.
- Wolfe JM, Kluender KR, Levi DM (2006) Touch. In: *Sensation & Perception*, pp 288–313. Sinauer Associates Inc.
- Woolf CJ, Shortland P, Coggeshall RE (1992) Peripheral nerve injury triggers central sprouting of myelinated afferents. *Nature* 355:75–78.
- Wu W (1993) Expression of Nitric-Oxide Synthase (NOS) in Injured CNS Neurons as Shown by NADPH Diaphorase Histochemistry. *Exp Neurol* 120:153–159.
- Wu W, Li L (1993) Inhibition of nitric oxide synthase reduces motoneuron death due to spinal root avulsion. *Neurosci Lett* 153:121–124.

- Xiao ZC, Ragsdale DS, Malhotra JD, Mattei LN, Braun PE, Schachner M, Isom LL (1999) Tenascin-R is a functional modulator of sodium channel β subunits. *Journal of Biological Chemistry* 274:26511–26517.
- Yamaguchi Y (2000) Lecticans: Organizers of the brain extracellular matrix. *Cellular and Molecular Life Sciences* 57:276–289.
- Yang S, Hilton S, Alves JN, Saksida LM, Bussey T, Matthews RT, Kitagawa H, Spillantini MG, Kwok JCF, Fawcett JW (2017) Antibody recognizing 4-sulfated chondroitin sulfate proteoglycans restores memory in tauopathy-induced neurodegeneration. *Neurobiol Aging* 59:197–209.
- YD A, Edgerton VR, Ichiyama RM (2020) Effects of Rehabilitation on Perineural Nets and Synaptic Plasticity Following Spinal Cord Transection. *Brain Sci* 10.
- Yuan Q, Xie Y, So KF, Wu W (2003) Inflammatory response associated with axonal injury to spinal motoneurons in newborn rats. *Dev Neurosci* 25:72–78.
- Zhang H, Chang M, Hansen CN, Basso DM, Noble-Haeusslein LJ (2011) Role of Matrix Metalloproteinases and Therapeutic Benefits of Their Inhibition in Spinal Cord Injury. *Neurotherapeutics* 8:206–220.
- Zhang L, Kaneko S, Kikuchi K, Sano A, Maeda M, Kishino A, Shibata S, Mukaino M, Toyama Y, Liu M, Kimura T, Okano H, Nakamura M (2014) Rewiring of regenerated axons by combining treadmill training with semaphorin3A inhibition. *Mol Brain* 7:1–17.
- Zholudeva L v., Abraira VE, Satkunendrarajah K, McDevitt TC, Goulding MD, Magnuson DSK, Lane MA (2021) Spinal interneurons as gatekeepers to neuroplasticity after injury or disease. In: *Journal of Neuroscience*, pp 845–854. Society for Neuroscience.
- Zholudeva L V., Karliner JS, Dougherty KJ, Lane MA (2017) Anatomical Recruitment of Spinal V2a Interneurons into Phrenic Motor Circuitry after High Cervical Spinal Cord Injury. *J Neurotrauma* 34:3058–3065.
- Zholudeva L v, Qiang L, Marchenko V, Dougherty KJ, Sakiyama-Elbert SE, Lane MA (2018) The Neuroplastic and Therapeutic Potential of Spinal Interneurons in the Injured Spinal Cord. *Trends Neurosci* 41:625–639.
- Zhou X, He X, Ren Y (2014) Function of microglia and macrophages in secondary damage after spinal cord injury. *Neural Regen Res* 9:1787.
- Zhou X-H, Brakebusch C, Matthies H, Oohashi T, Hirsch E, Moser M, Krug M, Seidenbecher CI, Boeckers TM, Rauch U, Buettner R, Gundelfinger ED, Fässler R (2001) Neurocan Is Dispensable for Brain Development. *Mol Cell Biol* 21:5970–5978.